UNIVERSITY OF NAPLES FEDERICO II

FACULTY OF MATHS, PHYSICS AND NATURAL SCIENCES

PHD IN CHEMISTRY
XXII CYCLE

STRUCTURE AND BIOACTIVITY OF BACTERIAL GLYCOLIPIDS AS TARGETS FOR BIOMEDICAL APPLICATIONS

TERESA IERANÒ

TUTOR
Prof. Antonio Molinaro
CO-TUTOR
Dr. Alba Silipo

SUPERVISOR
prof. Orlando Crescenzi

UNIVERSITÀ DEGLI STUDI DI NAPOLI FEDERICO II

FACOLTA' DI SCIENZE MATEMATICHE, FISICHE E NATURALI

DOTTORATO IN SCIENZE CHIMICHE
XXII CICLO

STRUTTURA E ATTIVITÀ DI GLICOCONIUGATI DI ORIGINE BATTERICA QUALI PRINCIPI ATTIVI PER APPLICAZIONI IN CAMPO BIOMEDICO

TERESA IERANÒ

TUTORE
Ch.mo Prof. Antonio Molinaro
CO-TUTORE
Dott.ssa Alba Silipo

RELATORE
Ch.mo prof. Orlando Crescenzi

Riassunto

Il presente progetto di dottorato è stato incentrato sull'indagine strutturale di una particolare classe di glicoconiugati di origine batterica: i lipopolisaccaridi (LPS). Tali macromolecole biologiche sono presenti esclusivamente sulla superficie cellulare dei batteri Gram negativi e sono indispensabili per la sopravvivenza e l'adattamento del batterio.[1-3] I LPS sono noti anche con il nome di endotossine batteriche in quanto costituiscono i principali fattori di virulenza attraverso i quali il batterio espleta la propria patogenicità. Più specificatamente il lipide A, la porzione più conservata dei LPS, viene immediatamente riconosciuto dal sistema immunitario innato dell'ospite mentre il core e l' O-chain mediano la risposta immunitaria specifica. Variazioni strutturali anche minime hanno come conseguenza marcate differenze dell'attività tossica di queste molecole *in vivo*. La caratterizzazione dei LPS è finalizzata dunque alla comprensione della relazione struttura-attività biologica di tali molecole.

Una prima tematica affrontata ha previsto la caratterizzazione dell' endotossina estratta da una particolare classe di batteri Gram negativi, quella del *Burkholderia cepacia complex (Bcc)*.[4] Il progetto è in collaborazione con il gruppo del professor De Soyza che lavora presso l'Università del Newcastle (UK), il quale ha fornito gli isolati clinici del Bcc. Questi microorganismi sono patogeni opportunisti e sono oggetto di notevole interesse in quanto responsabili di gravi infezioni a danno di individui immunocompromesi affetti da Fibrosi Cistica (FC). Non tutti i membri del *Bcc* hanno lo stesso grado di patogenicità ma la tossicità di questi batteri è intimamente correlata ai fattori di virulenza che essi esprimono. Il progetto ha avuto come finalità la caratterizzazione strutturale dell'LPS isolato per la prima volta da *B. multivorans* (genomovar II) e *Burkholderia vietnamensis* (genomovar V). In entrambi i casi l'endotossina è stata estratta da due strain clonali del batterio, isolati da uno stesso paziente FC prima e dopo il trapianto polmonare. L'analisi effettuata ha dunque consentito di studiare la stessa molecola isolata in due momenti diversi in modo da mettere in evidenza il ruolo dell'endotossina nei meccanismi di interazione patogeno-ospite che consentono l'adattamento e la sopravvivenza del batterio.[5]

Gli strain pre e post trapianto di *B. multivorans* producono entrambi un lipooligosaccaride (LOS). In tutti e due i casi i LOS sono stati sottoposti ad una blanda idrolisi acida al fine di scindere la porzione glicolipidica (lipide A) da quella glicidica (core) e di studiarle separatamente.

In base ai risultati ottenuti dalle analisi chimiche, da analisi di massa MALDI e da indagini spettroscopiche NMR mono e bidimensionali (COSY, TOCSY, HSQC, HMBC, NOESY, ROESY, HSQC-TOCSY) è stata ricavata la seguente struttura oligosaccaridica che risulta essere la stessa per entrambi i LOS con l'unica eccezione di un ulteriore residuo di 4-ammino-4-desossi-arabinosio

(Ara4N) legato in posizione 8 al Ko presente esclusivamente nel LOS estratto dallo strain post-trapianto polmonare:

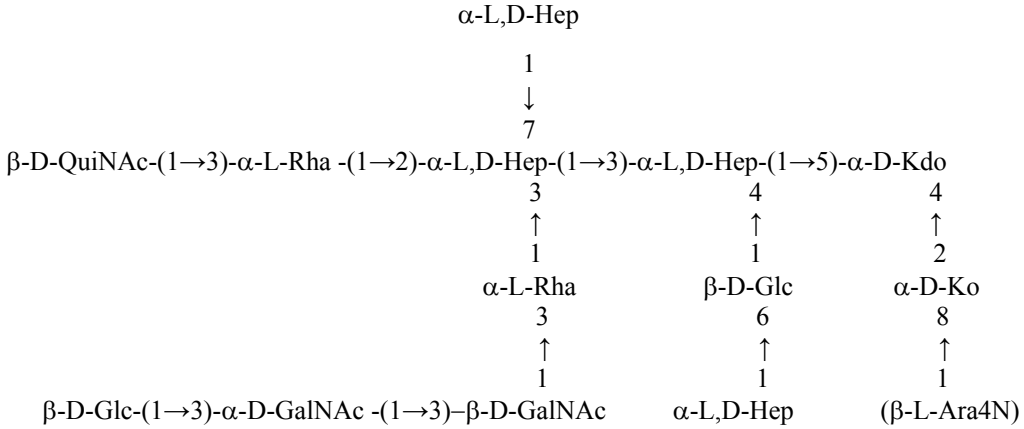

Le principali differenze tra i LOS estratti pre e post trapianto polmonare sono invece relative alla porzione glicolipidica e altamente conservata di tali macromolecole (lipide A). Mediante analisi chimiche e di massa (MALDI) è stata analizzata la struttura del lipide A di *B. multivorans* il quale risulta essere costituito dallo scheletro [P→4-β-D-Glc*p*N-(1→6)-α-D-Glc*p*N-1→P→Ara4N] già trovato precedentemente in altri LPS di *Burkholderia.*[1] Dagli studi condotti è emerso che la differenza tra gli isolati clinici consiste nell'abbondanza relativa delle specie di lipide A presenti in miscela nei campioni analizzati. La specie pre trapianto risulta essere costituita in eguale misura da lipide A tetraacilato e pentaacilato recante fino a due residui di Ara4N legati mediante ponti fosfodiesterei al disaccaride di GlcN. La specie post-trapianto risulta invece prevalentemente costituita da Lipide A tetraacilato e bis-fosforilato, mentre le specie pentaacilate sono espresse a bassi livelli, ed è esigua l'abbondanza di specie recanti due residui di Ara4N.[6]

Lo stesso approccio chimico e metodologico è stato eseguito sui LOS estratti dai due strain clonali *B. vietnamiensis*. Di seguito è riportata la porzione oligosaccaridica del core che risulta la stessa per entrambi gli due strain clonali esaminati:

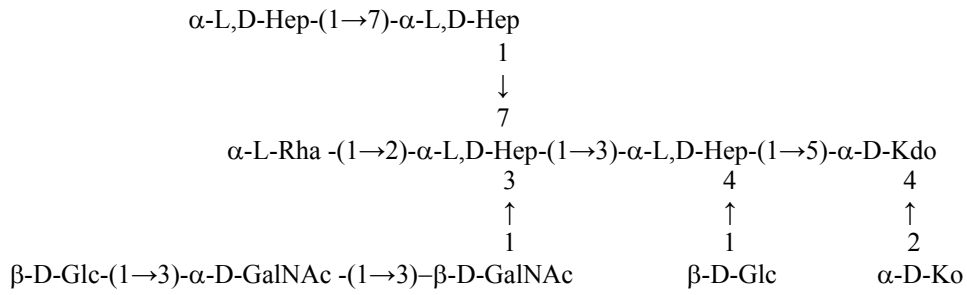

Anche in questo caso le principali differenze tra i LOS estratti pre e post trapianto polmonare sono relative alla porzione glicolipidica di tali macromolecole (lipide A). La specie pre trapianto è costituita da lipide A tetraacilato e pentaacilato recante fino a due residui di Ara4N in ponti

fosfodiesterei; la specie post-trapianto è invece prevalentemente costituita da lipide A pentaacilato. [7]

Un'ultima parte del progetto in collaborazione con il gruppo di Newcastle ha previsto invece la caratterizzazione dell'endotossina estratta da un isolato clinico di *B. cenocepacia* (genomovar III), prelevato da un paziente FC dopo trapianto polmonare al fine di confrontarla con quella dello strain più virulento di *B. cenocepacia*, il clone ET-12, già caratterizzata nel nostro laboratorio.[8]

Dagli studi effettuati risulta che l'endotossina caratterizzata è formata da una porzione glicolipidica (lipide A), costituita principalmente dalla specie recante quattro residui di acidi grassi come quello isolato da *B. cenocepacia* ET-12. La porzione oligosaccaridica del core è riportata di seguito: [9]

α-L,D-Hep-(1→7)-α-L,D-Hep-(1→3)-α-L,D-Hep-(1→5)-α-D-Kdo

3	4	4
↑	↑	↑
1	1	2
α-D-Glc	β-D-Glc	α-D-Ko
6	6	8
↑	↑	↑
1	1	1
α-D-Gal	α-D-Glc	β-L-Ara4N

La differenza ritrovata tra questa endotossina ed l' LOS già caratterizzato [8] sta nella mancanza di ramificazioni della porzione del core, che risulta quindi considerevolmente ridotta in lunghezza.

Nell'ambito della caratterizzazione delle endotossine batteriche da isolati clinici FC, si inserisce inoltre lo studio dell' LPS isolato dal più virulento degli strain di *B. multivorans* C1576 (genomovar II), affrontato il terzo anno di tesi. Sono state studiate la porzione glicolipidica del lipide A e quella polisaccaridica dell' O-chain ottenute mediante idrolisi acida sull' endotossina purificata ed estratta dal liofilizzato cellulare. Il lipide A, analizzato mediante spettrometria di massa ESI, risulta costituito principalmente da una miscela di specie dove prevale quella tetraacilata e monofosforilata a differenza del lipide A di *B. multivorans* isolato dal LOS pre e post trapianto caratterizzato in precedenza (vedi sopra). Si può quindi ipotizzare che la de-fosforilazione del lipide A, modifica post-biosintetica, sia dipendente alla lunghezza della porzione saccaridica dell'endotossina espressa dal batterio.[10] L'O-chain isolata è stata analizzata mediante spettroscopia NMR mono e bidimensionale (COSY, TOCSY, HSQC, HMBC, NOESY, ROESY) ed è risultata costituita da due polisaccaridi in miscela, ciascuno caratterizzato dalle unità ripetitive riportate di seguito, con un'abbondanza relativa differente:

I polisaccaride (40%)

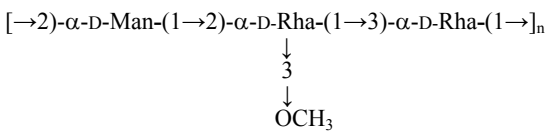

II polisaccaride (60%)

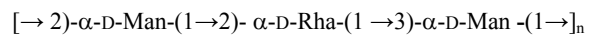

E' stata condotta un' analisi conformazionale su entrambi i polimeri al fine di determinarne l'arrangiamento supra-molecolare mediante analisi NMR, meccanica e dinamica molecolare. Le distanze *inter*-protone sono state valutate attraverso l'analisi dei contatti NOE *inter*-residuo, sono state calcolate le regioni energeticamente favorevoli per ogni coppia di angoli di torsione, phi (Φ) e psi (Ψ), del legame glicosidico di ciascun disaccaride. Infine, l'analisi di dinamica molecolare, effettuata con Macro Model utilizzando il campo di forza MM3*, in acqua implicita, ha consentito di esplorare tutte le possibili conformazioni.[11] Dall'analisi risulta che la diversa sequenza saccaridica caratterizzante i due polisaccaridi, si traduce in un diverso arrangiamento supra-molecolare. Entrambi le catene assumono una conformazione non estesa ma, mentre la catena contenente il polisaccaride I assume un arrangiamento più compatto, l'altra è caratterizzata da una struttura tridimensionale più allungata. Considerando il ruolo indispensabile dell'O-chain nel riconoscimento del batterio da parte dell'anticorpo, si quindi può ipotizzare che una così complessa articolazione strutturale dell'antigene batterico garantisca un'alta specificità nel riconoscimento.

L' aspetto dell'analisi conformazionale dei LPS è stato ulteriormente approfondito attraverso uno studio di modeling molecolare effettuato presso il gruppo di ricerca della dott.ssa Anne Imberty e del prof. Serge Perez che ha sede nel Centre de Recherche sur les Macromolécules Végétales (CERMAV) di Grenoble, Francia. Tale progetto è consistito nell'analisi conformazionale del core oligosaccaridico isolato dall' endotossina estratta dal più virulento degli strain del *Bcc*: *B. cenocepacia* ET-12 caratterizzata nel nostro laboratorio.[8] Attraverso l'uso del programma SYBYL è stato costruito un database contenente i monomeri costituenti la molecola in esame. Dall'analisi di meccanica molecolare sono state ricavate le mappe adiabatiche relative ad ogni coppia di descrittori phi (Φ) e psi (Ψ) del legame glicosidico di ciascun disaccaride. Attraverso l'uso dell' AMBER package è stata eseguita una simulazione in acqua esplicita che ha consentito di esplorare le conformazioni possibili della molecola oggetto di studio. Le distanze *inter*-protone ottenute tramite la simulazione sono risultate in accordo con le distanze sperimentali ricavate dall'analisi dei contatti NOE. Dall'analisi effettuata sono emersi alcuni aspetti conformazionali interessanti riguardanti l'estrema rigidità della porzione dell'inner core, L,D-Hep-(1→3)-[β-D-Glc-(1→4)]-α-L,D-Hep-(1→5)-α- D-Kdo, estremamente conservata all'interno delle specie batteriche, e l'esposizione del trisaccaride α-L,D-Hep-(1→7)-α-L,D-Hep-α-L,D-Hep,

legato all'outer core, che risulta probabilmente implicato nei meccanismi di riconoscimento molecolare.

La questione dell' adattamento del batterio all'ambiente esterno, affrontato attraverso lo studio della modifica strutturale a cui vanno incontro i LPS conseguentemente al trapianto polmonare, è stato approfondito attraverso l'analisi di un altro fenomeno, quello della persistenza dell'infezione. E' stata effettuata l'analisi dell' endotossina isolata da *Pseudomonas aeruginosa*, al fine di rilevare modifiche strutturali indicanti il coinvolgimento delle endotossine batteriche nei meccanismi di cronicizzazione delle infezioni batteriche a danno degli individui FC. *P. aeruginosa* è uno dei principali patogeni opportunisti isolati dai pazienti FC. L'endotossina è stata estratta da tre strain clonali di *P. aeruginosa* isolati da uno stesso paziente FC in momenti diversi dell'infezione: dopo sei mesi (strain AA2) e dopo 7,5 anni di infezione (strain mucoide AA43 e strain non mucoide AA44). I tre LPS sono stati estratti e purificati dal liofilizzato cellulare e sottoposti ad idrolisi acida. Da un' analisi preliminare è emerso che la porzione polisaccaridica dell'O-chain presentava lo stesso profilo negli spettri ^{1}H NMR eseguiti su tutti e tre gli LPS isolati. Pertanto, studi più approfonditi, mediante spettrometria di massa MALDI, sono stati eseguiti sulle porzioni glicolipidiche (Il lipide A) e sono state riscontrate differenze sostanziali nel grado di acilazione dei tre strain esaminati. Lo strain isolato dopo sei mesi di infezione e quello mucoide isolato dopo 7,5 anni di colonizzazione sono caratterizzati dalla stessa miscela di specie, vale a dire lipide A recanti cinque catene di acidi grassi e quelli recanti sei catene distribuite in maniera asimmetrica. Il lipide A dello strain non mucoide, invece, risulta costituito principalmente da specie esa-acilate, caratterizzate da una distribuzione simmetrica delle catene aciliche, e da specie epta-acilate. Il lipide A, dunque, sembra avere un ruolo chiave nella persistenza dello *Pseudomonas* durante l'infezione cronica. Il batterio infatti sembra avere l'esigenza di apportare un cambiamento chimico nella struttura del lipide A, a favore di specie meno tossiche, solo nel caso in cui non ci sia il biofilm a mascherare i segnali molecolari responsabili della virulenza. L'over-acilazione dello strain persistente non mucoide è realizzata attraverso l'inibizione di una lipasi, PagL, costitutivamente espressa.[12]

In conclusione, i risultati ottenuti da ogni lavoro in cui è articolato l'intero progetto di tesi, ha consentito uno screening strutturale delle macromolecole direttamente coinvolte nella patogenesi batterica. Le analisi strutturali condotte rappresentano dunque una base fondamentale che consentirà di comprendere i meccanismi molecolari attraverso i quali il batterio riesce ad adattarsi all'ospite causando infezioni persistenti o sopravvivendo a bruschi cambi ambientali, come nel caso del trapianto polmonare. Le analisi conformazionali condotte possono inoltre chiarire i determinanti molecolari coinvolti nel meccanismo di riconoscimento delle porzioni antigeniche delle endotossine

(core o O-chain) che consentiranno l' individuazione di nuovi target per terapie farmacologiche mirate.

[1] De Soyza A, Silipo A, Lanzetta R, Govan JR, Molinaro A.. Chemical and biological features of *Burkholderia cepacia* complex lipopolysaccharides. *Innate Immun*. (2008) 14: 127-144.

[2] Raetz, C.R., Whitfield, C. Lipopolysaccharide endotoxins. *Annu. Rev. Biochem.* (2002) 71: 635-700

[3] Alexander C, Rietschel ET. Bacterial lipopolysaccharides and innate immunity. *J. Endotoxin Res.* (2001) 7: 167-20.

[4] Mahenthiralingam E, Coenye T, Chung JW, Speert DP, Govan JRW, Taylor P, Vandamme P. Diagnostically and Experimentally Useful Panel of Strains from the *Burkholderia cepacia* Complex. *J. Clin. Microbiol*. (2000) 38: 910-913.

[5] De Soyza A, Corris PA. Lung transplantation and the *Burkholderia cepacia* complex. *The Journal of Heart and Lung Transplantation* (2003) 22: 954-958 .

[6] Ieranò T, Silipo A, Sturiale L, Garozzo D, Brookes H, Khan CM, Bryant C, Gould FK, Corris PA, Lanzetta R, Parrilli M, De Soyza A, Molinaro A. "The structure and pro-inflammatory activity of the lipopolysaccharide from *Burkholderia multivorans* and the differences between clonal strains colonizing pre- and post-transplanted lungs". *Glycobiology* (2008), 18: 871-81.

[7] Ieranò T, Silipo A, Sturiale L, Garozzo D, Bryant C, Lanzetta R, Parrilli M, Aldrige C, Gould FK, Corris PA, Khan CM, De Soyza A, Molinaro A. "First structural characterization of *Burkholderia vietnamiensis* lipooligosaccharide from Cystic Fibrosis associated lung transplantation strains". *Glycobiology* (2009), 19: 1214-1223.

[8] Silipo A, Molinaro A, Ieranò T, De Soyza A, Sturiale L, Garozzo D, Aldridge C, Corris PA, Khan CMA, Lanzetta R, Parrilli M. 2007. The complete structure and pro-inflammatory activity of the lipooligosaccharide of the highly epidemic and virulent gram-negative bacterium *Burkholderia cenocepacia* ET-12 (strain J2315). *Chemistry.* 13: 3501– 3511.

[9] Ieranò T, Silipo A, Sturiale L, Garozzo D, Corris PA, Perry J, Lanzetta R, Parrilli M, De Soyza A, Molinaro A. Structural elucidation of a novel *B. cenocepacia* ET-12 lipooligosaccharide isolated from a cystic fibrosis patient after lung transplantation. *Eur. J. Org. Chem.* (2009) accepted for publication.

[10] Ieranò T, Cescutti P, Leone MR, Luciani A, Rizzo R, Raia V, Lanzetta R, Parrilli M, Maiuri L, Silipo A, Molinaro A. "The lipid A of *Burkholderia multivorans* C1576 smooth-type lipopolysaccharide and its pro-inflammatory activity in a cystic fibrosis airways model " *Innate Immunity* (2009), accepted for publication.

[11] Ieranò T, Silipo A, Cescutti P, Leone MR, Rizzo R, Lanzetta R, Parrilli M, Molinaro A. "Structural study and conformational behavior of the two different lipopolysaccharide O-antigens produced by the cystic fibrosis pathogen *Burkholderia multivorans*. " *Chemistry-A European Journal* (2009), 15: 7156-66.

[12] Cigana C, Curcuru'L, Leone MR, Ieranò T, Lorè NI, Bianconi I, Silipo A, Cozzolino F, Lanzetta R, Molinaro A, Bernardini ML, Bragonzi A. "*Pseudomonas aeruginosa* exploits lipid A and muropeptides modification as a strategy to lower innate immunity during chronic lung infection in cystic fibrosis" *Plos Pathogens* (2009) accepted for publication

Summary

This thesis is focused on the characterization of Gram negative endotoxin as they play a key role in bacterial pathogenesis. Gram negative endotoxins or lipopolysaccharides (LPS) are glycoconjugates molecules exposed toward the external environment as they are the major components of Gram negative external leaflet. They have a structural role since they contribute to the cellular rigidity increasing the strength of cell wall and mediate the contacts with the external environment. Moreover, LPS can modulate the host immune response as they are recognised by immune mechanisms of defence. Structural elucidation of these molecules is an essential pre requisite in the comprehension of chemical structures that are responsible for bacterial pathogenesis. Lipopolysaccharides are build up according to a common structural architecture. They are composed of a hydrophilic hetero-polysaccharide (formed by *core oligosaccharide* and *O-specific polysaccharide* or *O-chain*) covalently linked to a lipophilic domain termed *lipid A*, which is embedded in the outer leaflet and anchors these macromolecules to the membrane through electrostatic and hydrophobic interactions. These three major domains are genetically, biologically and chemically distinct.

The endotoxins analysed in this work are extracted from opportunistic Cystic Fibrosis pathogens. These bacteria are responsible for feared infections that reduce life expectancy in CF patients.

The first part of the project was centred on the study of LPS involvement in bacterial adaptation after lung transplantation to a healthy not CF tissue. LPS were extracted from the most representative and problematic group of CF pathogens, the *Burkholderia cepacia* complex (Bcc). *Burkholderia multivorans* (genomovar II) and *Burkholderia vietnamiensis* (genomovar V) were respectively isolated from CF patients that underwent lung transplantation. For each clinical isolated, two paired clonal strains were recovered: one pre and the other post transplantation. Thus, in order to investigate the possible structural changes that possible occurred during the adaptation, for the first time LPSs from each strain, isolated in two different moments of the infection, were extracted and characterized. *B. multivorans* LPS isolated pre and post transplantation lacking the polysaccharidic moiety of the O-chain, revealed to be a lipooligosaccharide (LOS). The differences between the LOSs isolated from the two clonal strains were mainly found in the lipid A moiety, even though in the post transplantation strain there was an additional residue of Ara4N on the core portion. These chemical differences were responsible for the different

biological activities found for LOSs. Generally, it was found a loss of inflammatory activity after lung transplantation when the two purified LOSs were tested as elicitors of TNF-alpha induction in human myelomonocytic U937 cells and of NF-KB induction in transfected TLR 4/MD2/CD 14 HEK cell lines. Even *B. vietnamiensis*, producing in both pre- and post transplantation strains LOSs, showed substantial differences in the lipid A moieties that justified an increased inflammatory activity for post transplantation strain when it was tested for TNF-alpha and NF-KB inductions. The features found in both studies revealed that lipid A moiety changes during bacterial adaptation. These data are not surprising since this LPS portion accounts for endotoxin virulence as it is recognized by the innate immune system of the host.

Further, from a post transplanted allograft, *B. cenocepacia* (genomovar III) the most virulent of Bcc members, was also collected, and its endotoxin characterized. This structural investigation constituted a complementary work to the previous study on *B. cenocepacia* ET-12 endotoxin already performed in this laboratory. Thus, it gives a clear aspect of the endotoxin phenotype produced by the most pathogenic strain of Bcc, when it colonized a survived CF patient.

An additional structural investigation was also performed on the second most pathogenic Bcc member, namely *B. multivorans*. The endotoxin was recovered from the most virulent strain of genomovar II, the C1576, that was responsible of a fatal outbreak in Glasgow, when only few children survived to adulthood. This strain produces a smooth type LPS, and its lipid A and O-chain moieties were characterized. In this case, differently from the other *Burkholderia* lipid A analyzed, bacteria produced a less phosphorylated blend of lipid A species. Even though lipid A is the highest conserved portion of LPS, little changes, as the presence or absence of charged residues or the number and the distribution of fatty acids, may occur in response to bacterial exigencies of adaptation. The O-chain portion was instead constituted by two polysaccharides characterized by two different repeating units. Moreover, a conformational study was executed on these polysaccharides in order to investigate about their supra molecular arrangements.

A conformational study and a MD simulation was also performed on the oligosaccharidic region of the LOS molecule extracted from the clinical isolated strain of *B. cenocepacia* ET-12, previously characterized. This analysis was performed with AMBER package in a solvent explicit model, thus mimicking real conditions. The investigation on three dimensional structure adopted by the most exposed moiety of *B. cenocepacia* endotoxin better clarified its spatial orientation. Moreover, data obtained give a real idea of the

residues that are exposed toward the external environment, thus playing a key role in molecular recognition. The results carried out also gave information about the relative orientation of sugar rings and the conformational spaces energetically permitted for glycosidic bond rotations. These data can also contribute to justify and explain LPS role in increasing membrane rigidity and cell-wall strength.

The last part of this project was focused on the investigation of whether and, possibly, how *P. aeruginosa* genetic adaptation resulted in a bacterial strategy to evade the host immune sensing. With this aim, the impact of lipopolysaccharide, purified by *P. aeruginosa* strains isolated from acute and chronic infection of a CF patient, was analysed. Typically, *P. aeruginosa* infections are followed by a chronic persistence of the disease that cause permanent respiratory symptoms and decline in lung functions. The long term colonization of CF airways selects pathoadaptive variants with several features which differentiate late *P. aeruginosa* isolates from the initially acquired strain. Even though *P. aeruginosa* strains that initiates infections are characterized by a large arsenal of virulence factors, CF chronic infection are characterized by less virulent but more persistent phenotypes. LPS modification appears to be one of the main factors in the adaptation of this pathogen during chronic infections but no conclusive information were present so far on the putative lipid A changes in the acute to chronic evolution of the infection. The results obtained emphasize the reduced immunopotential of LPS extracted from late colonizer *P. aeruginosa* strains, demonstrating the lost of large arsenal of virulence factors during chronic infection.

Abbreviations

ASL	Airway surface liquid
Bcc	*Burkholderia cepacia* complex
CF	Cystic fibrosis
CFTR	Cystic fibrosis transmembrane conductance regulator
COSY	Correlation Spectroscopy
DQF COSY	Double-quantum filtered COSY
ENaC	Epithelia Na^+ channel
ESI	Electrospray Ionization
GC-MS	Gas chromatography-Mass spectrometry
HMBC	Heteronuclear multiple-bond correlation
HSQC	Heteronuclear single-quantum correlation
LBP	Lipopolysaccharide binding protein
LOS	Lipooligosaccharide
LPS	Lipopolysaccharide
MALDI	Matrix assisted laser desorption
MCC	Mucociliary clearance system
MD	Molecular Dynamics
MD2	Myeloid differentiation factor 2
MM	Molecular Mechanics
NMR	Nuclear magnetic resonance
NOESY	Nuclear Overhauser effect spectroscopy
PAMP	Pathogen associated molecular pattern
PCL	Periciliary liquid layer
PRR	Pattern recognition receptor
ROESY	Rotating frame Overhauser effect spectroscopy
ROS	Reactive oxygen species
TLR	Toll like receptor
TOCSY	Total correlation spectroscopy
t-ROESY	Transverse ROESY

Index

SECTION II

SECTION III

SECTION I

INTRODUCTION

Chapter 1

GRAM NEGATIVE CELL ENVELOPE

1.1 Bacterial cell wall structure

Bacteria, *Archea* and *Eukaryotes* are the three macro-groups in which are classified all living organisms. *Bacteria* and *Archea* are also identified as Prokaryotes.[1] They possess a simple cellular structure lacking membrane-enclosed organelles and nucleus, that contains genome in eukaryotic organisms. Typically, *Archea* include all the extremophiles prokaryotic organisms that live in habitat conditions unusual for the other microorganisms as high salinity or pressure, extreme temperatures or critic pH values. *Bacteria* is a wide group of microorganisms that also encloses pathogenic species. They are divided into two sub-classes, Gram negative and Gram positive, depending on the different response to the colorimetric Gram test. This further classification arises from a substantial diversity in cell-wall structure between the two class of microorganisms (figure 1). Both Gram positive and Gram negative cells possess a cytoplasmic membrane, a phospholipidic bilayer surrounding the cytosol, that constitutes a physical semi-permeable barrier that regulates the flux of endogenous and exogenous substances in and out the cell. This membrane is in turn enclosed by a layer named peptidoglycan or murein, responsible for the shape and the strength of the cell. This is a polymer composed by a network of saccharidic backbones of N-acetyl-glucosamine e N-acetylmuramic acid cross-linked by peptide chains. In Gram positive bacteria the external portion of the cell is composed by 90% of peptidoglycan. In Gram negative bacteria there is a thin layer of peptidoglycan followed by an additional asymmetric phospholipidic bilayer, the outer membrane (OM). This is the first barrier that protects Gram negative cell from the environment, essential for bacterial survival. Substances trafficking throughout the outer membrane are regulated by molecular size. The inner surface of this membrane is constituted by glycerophospholipids while the external leaflet is composed by trans-membrane proteins and, for the 75%, by lipopolysaccharides (LPS).[2]

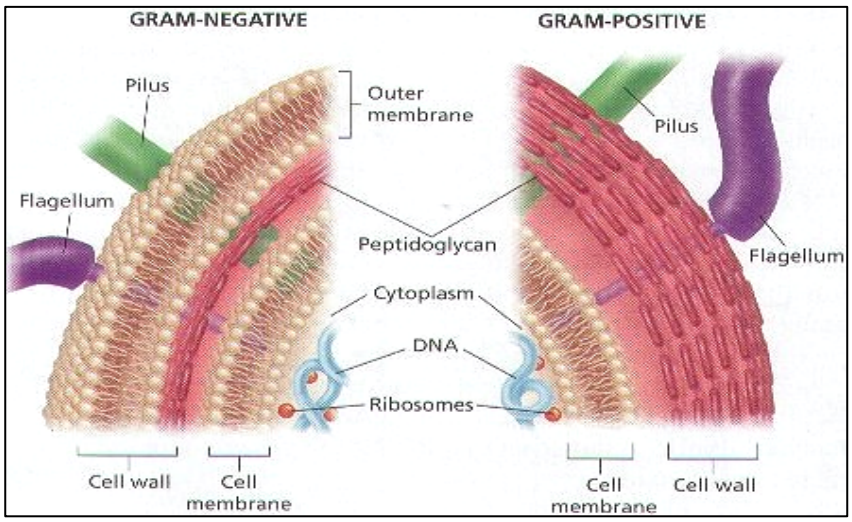

Figure 1. Structural differences between Gram negative and Gram positive cell envelope

1.2 Lipopolysaccharides (LPS)

Lipopolysaccharides are heat-stable amphiphilic molecules, markers for Gram-negative organisms, essential for bacterial survival. They are intercalated into the outer membrane forming hydrophobic interactions between the phospholipid bilayer and the lipid A that is the highest conserved glycolipidic portion of LPS. All the LPS molecules are interconnected through ionic bridges due to electrostatic interactions of divalent cations (as Mg^{2+} and Ca^{2+}) with negatively charged groups present on LPS molecules. Thus, they form a high structured barrier against the external environment increasing cell rigidity and strength. In addition, since they are the cellular components exposed toward the external habitat, they are involved in bacterial mechanisms of adaptation and in Gram-negative viability in host environment. Moreover, LPS are also known as bacterial *endotoxins* since they are potent immunostimulators used as specific indicators of Gram negative infection in a wide range of eukariotic organisms.[2]

Lipopolysaccharides have a common structural motifs in which three distinct regions can be distinguished since they are encoded by different gene clusters (figure 2). They are composed of a lipophilic domain, named lipid A, that is the highest conserved region of LPS even among different species of the same bacterial genus. This is covalently linked to a saccharidic portion named core oligosaccharide, that can be divided into inner core and outer core, followed by a polysaccharidic moiety named O-specific chain. The O-chain is characterized by a highly variable structure which constitutes the chemical basis for the

serological classification of bacterial strains. Bacteria can also biosynthesize LPS without O-specific chain and in this case LPS is defined of R-type (Rough type) or lipooligosaccharide (LOS) and confers a rough appearance to the colony morphology; LPSs with O-chain are of S-type (Smooth type) and provide a smooth aspect to the bacterial colonies.

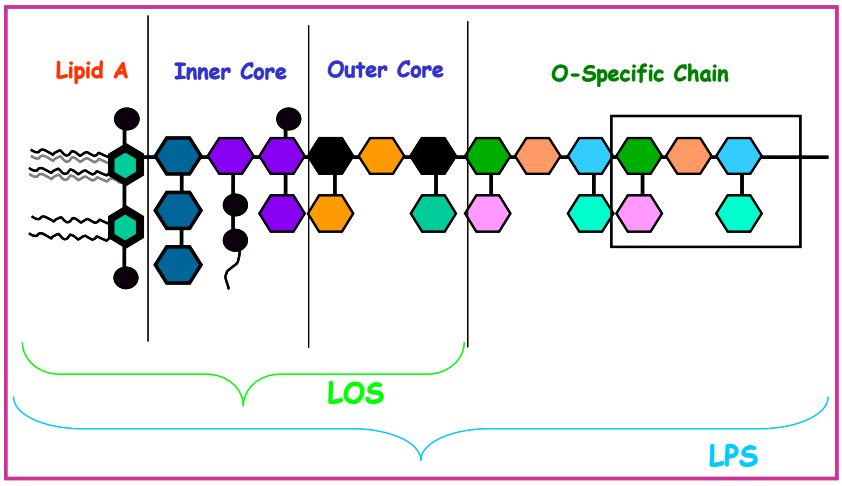

Figure 2. Structure of Gram negative bacteria LPS and LOS.

1.2.1 Structure and biological activity of lipid A

Lipid A represents the endotoxic principle of LPS since it is the primary immunoreactive centre of these molecules promptly recognised by numerous components of the host innate immune system. It possesses a high conservative structure consisting of a backbone of β-(1→6) linked D-glucosamine disaccharide α-phosphorylated at positions 1 of reducing residue (GlcN I) and at 4' of the non-reducing glucosamine (GlcN II). Both GlcN residues are acylated with primary 3-hydroxy fatty acids at positions 2 and 3 and the hydroxyl groups of the primary fatty acids can be further acylated by secondary acyl moieties (figure 3).

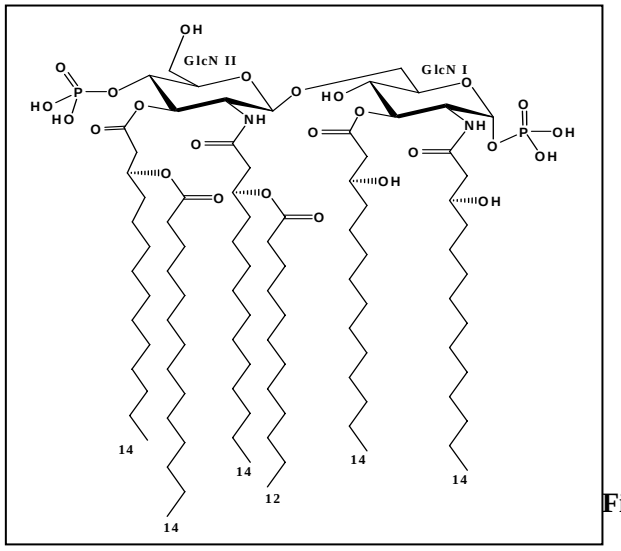

Figure 3. Structure of *Escherichia coli* lipid A

The lipid A biosynthesis has been fully elucidated for *Escherichia coli* (figure 4).[3] All the steps are catalysed by an enzyme which is present in a single copy in the whole genome. The most conserved among bacteria are LpxA and LpxC. The former is an UDP-GlcN acyltranferase that has an active site, located between two adiacent subunits, highly selective. It is an accurate hydrocarbon ruler: for *E. coli,* it is set for the incorporation of 14-carbon acyl chain, while a 10-carbon acyl chain is add in *Pseudomonas aeruginosa* lipid A. LpxC is a zinc metalloenzyme that acts as a deacetylase whose action allows the biosynthesis equilibrium moving towards the incorporation of the second acyl chain on the UDP-3-*O*-acyl-GlcNAc. This has been demonstrated as a potential target for the synthesis of specific antibiotics. [4]

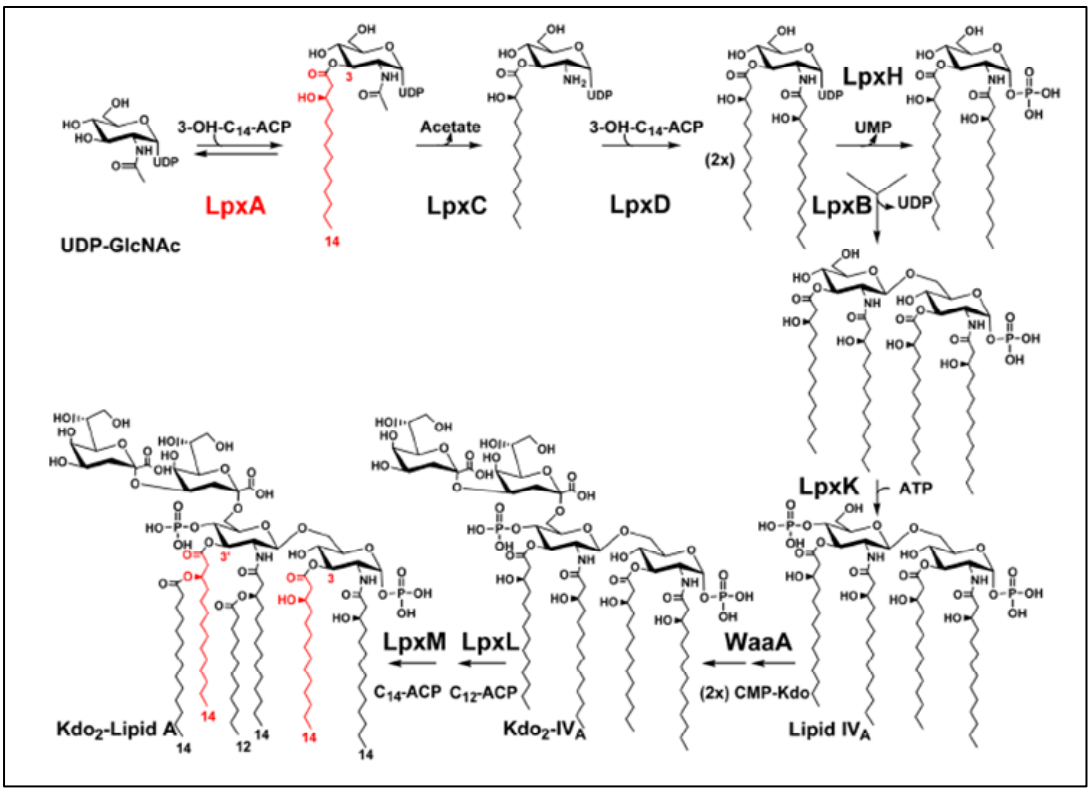

Figure 4. Biosynthetic pathway of Kdo2-lipidA in *E. coli* K12 .

Even though lipid A structure is highly conserved, depending on growth conditions or on environmental changes it has been found that lipid A from *E. coli* can undergo structural changes as the addition of palmitate, phosphoethanolamine or L-Ara4N residues. The addition of palmitate is under control of PhoP/PhoL system that is regulated by the presence of antimicrobial peptides and activated by low concentration of Mg^{2+}. *Pseudomonas aeruginosa*, an opportunistic pathogen highly problematic in Cystic Fibrosis (CF) (section II, chapter 7), produces a lipid A moiety that is modified with palmitate.[5]

Besides *Pseudomonas*, among the other CF opportunistic pathogens *Burkholderia* (chapter 3-6) was found to constitutively synthesize a lipid A bearing L-Ara4N substitutions. These groups are positively charged in physiological conditions, thus they reduce the net charge surface of the outer membrane inferred by LPS molecules increasing bacterial resistance against cationic antimicrobial compounds as polymyxin or CAMP (cationic antimicrobial peptides).

It has been found that in other species additional enzymes, not present in *E. coli*, are responsible for further structural modifications. For instance, the presence of late functioning phosphatases in *Rhizobium etli, Rhizobium leguminosarum* and in *Francisella tularensis* induces the synthesis of lipid A species partially or completely dephosphorylated.[3] Further, in *Rhizobiaciae* species, dephosphorylated GlcN I can be oxidized to aminogluconate. Moreover, a very frequent substitution is that of galacturonic acid residues that can be attached either on the Kdo moiety or on the lipid A backbone. Additional structural modifications can be a high heterogeneity in fatty acid length, the presence of unusual long chain secondary fatty acid (as in *Rhizobiaceae*) and/or deacylation at position 3/3'. Lipid A backbone from *Aquifex pyrophilus* lacks phosphate groups,in turn substituted by galacturonic acid residues and, in addition, as for others Gram negative bacteria, is constituted by a backbone of 2,3-diamino-2,3-dideoxy-D-glucose (DAG) residues.

The bioactivity of lipid A is strictly dependent on its primary structure: variations in number, distribution of fatty acids or the presence of polar groups strongly influence the three-dimensional arrangements and the biological properties of these endotoxins. Lipid A may act as agonist or antagonist. In the first case, in moderate concentration, its presence potentiates the immune resistance of the host. If agonist lipid A is present in high concentration, it stimulates a strong inflammatory response that can induce septic shock and cellular death. Studies on lipid A structure and bioactivity isolated from different bacteria have shown that the hexa-acylated asymmetric and bis-phosphorylated lipid A from *E. coli* (figure 3) is the most stimulatory agonistic structure in mammals. As for antagonist lipid A species, they can modulate or inhibit the inflammatory response induced by agonist species in a competitive manner. Typically, an antagonist structure is the tetra acylated lipid A, named lipid IVa, that is the biosynthetic precursor of *E. coli* agonistic lipid A (figure 4). The toxicity of these molecules is certainly dependent on their capacity of interacting with immune receptors. This interactions are correlated to two interconnected structural parameters: the molecular shape of the endotoxin and the tilt

angle between the disaccharidic backbone and acyl chains. The former accounts for the three-dimensional structure assumed by molecular species embedded in the lipid bilayer and exposed toward the external environment; the latter reveals the inclination of lipid A hydrophilic moiety respect to the hydrophobic portion. Lipid A molecular shape, responsible for the supramolecular arrangements of endotoxins, influences their ability to be recognised by host receptors. It has been found that in aqueous solution, at 37°C, in physiological conditions the most active form of lipid A has a truncated cone that drives to a hexagonal supra-structure while antagonist lipid A assume a cylindrical shape that leads to a lamellar structure (figure 5a).[6]

As for tilt angle, the most active conical structure has a tilt angle >50°, while the antagonist structures are characterized by smaller values of tilt angles (figure 5b).[7] This physical parameter reveals the exposure of hydrophobic task to receptors, thus the endotoxin affinity for the hydrophobic binding site of the innate immune multimeric receptors.

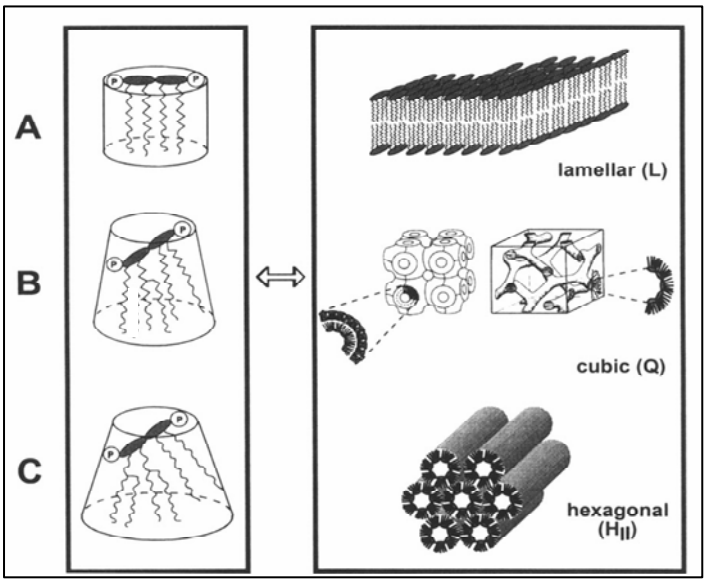

Figure 5a The molecular conformation of lipid a influences supramolecular structure of LPS aggregates

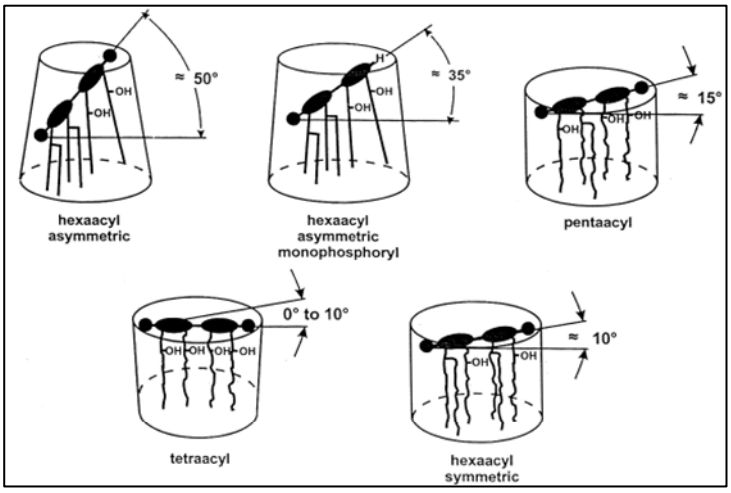

Figure 5b The inclination of sugar backbone respect to the membrane surface (tilt angle) depends on the number and the distribution of acyl chains.

1.2.2 Structure and biological activity of core oligosaccharide

Core oligosaccharide is typically composed up to fifteen residues and can be distinguished in inner core and outer core regions (figure 2).[4] The inner core portion is proximal to lipid A, is well conserved and consists of characteristic monosaccharides. The first residue that is covalently linked to lipid A is a 3-deoxy-D-*manno*-octulosonic acid, Kdo, a hallmark for Gram negative microorganisms. Besides Kdo residue, core structures of *Pseudomonadaceae* and *Enterobacteriaceae* and many other species, are constituted by L-*glycero*-D-*manno* heptose (L,D-Hep) and are often decorated with charged substituents like phosphate, pyrophosphate, Ara4N or uronic acids. As Ara4N residues increases cellular resistance against cationic antimicrobial compounds (see paragraph 1.2.1), anionic groups contribute to the definition of the negative charge of LPS molecules whose localization is stabilized by ionic interactions with divalent cations that favour the interconnection among LPS molecules. Frequently, there have been reported inner core structures containing other peculiar residues as D-*glycero*-D-*talo*-octulosonic acid (Ko), found in *Acinetobacter* or *Burkholderia* species, where the presence of the less prevalent D-*glycero*-D-*manno* heptose residue (D,D-Hep) has been also described.[8] The outer core region is the most exposed portion, often branched, and is characterized by a higher structural variability than the inner core. It is commonly composed by hexoses and it may also contain residues as 6-deoxy-L-mannose (L-Rha) and N-acetyl-2,6-dideoxy-D-glucosamine (D-QuiNAc).

In bacteria producing lipooligosaccharide (LOS, LPS lacking the O-chain), as many *Burkholderia*, *Nesseria meningitis*, *Nesseria gonorrhoeae, Haemophylus influenzae*, the core portion accounts for serological specificity and is recognised by the host adaptive immune system. Since in rough type bacteria the core oligosaccharide is the most exposed portion, bacterial viability and resistance against antimicrobial compounds are strictly dependent on its chemical structure.

The causative agent of bacterial meningitis, *N. meningitidis*, is a rough bacterium[9] and its LPS core oligosaccharide is the antigenic determinant recognised by the antibody-dependent immune response. It contains residues as N-acetylneuraminic acid (NeuAc) or L-fucose (L-Fuc) that is a reminder of human glycosphingolipids. This mimicry of host cellular surface components increases pathogen resistance against phagocytosis and host bactericidal activity.

1.2.3 Structure and biological activity of the O-chain

The O-chain is the polymeric portion of LPS.[4] Its molecular weight can reach up to 60 KDa. It can be a homopolymer or a heteropolymer, linear or branched, characterized by a repeating unit that may contain from one to ten residues. It is high variable and heterogeneous even among the same bacterial species, contains different kinds of monosaccharides and can be decorated with non-carbohydratic substituents, often present in a non-stoichiometric amount, thus increasing their structural heterogeneity. The O-chain is the antigenic moiety of smooth colonies and, in most cases, is necessary for bacterial pathogenesis and survival. During the early stage of host invasion, bacteria undergo the "phase variation", a mechanism of adaptation that involves antigenic determinants, often polysaccharides.[10] Very frequent changes regard the length or the primary sequence of the O-chain. *Helicobacter pylori* resides in the acidic environment of human stomach and it has been found that many LPS biosynthetic genes are involved in phase variation while a rough LPS mutant of *H. pylori* has a deep reduced colonising ability. Phase variation in *Francisella* species also involves O-chain structure: regulation of O-chain length seems to be essential for serum resistance and cellular growth. Besides its importance in bacterial interaction with the immune system, the O-chain has also a protective role, preventing phagocytosis uptaking and recognition by serum complement, since it masks bacterial virulence factors from host recognition. Moreover, it constitutes a physical barrier necessary for bacterial viability that prevent cellular dehydration and promotes colonies adhesion.

1.3 LPS involvement in immune response

Highly developed organisms defend themselves from microbial infections through the immune response. This is divided into two complex and diverse mechanisms, the innate and the adaptative immune response: they act in different time periods of the infection but are strictly interconnected.

The first line of defence is the *innate immune response* that act through ancient and highly conserved mechanisms. It guarantees an aspecific and immediate defence against pathogens since it is able to recognise peculiar bacterial molecules as "non-self" but is unable to provide an immunological memory.[2] Innate immunity operates through a recognition of bacterial conservative molecular targets that remain invariant among different species and are essential for their survival. This process is activated by the

interaction of PAMP (Pathogen Associated Molecular Pattern) with the PRR (Pattern Recognition Receptors) of the host. This event causes the recruitment of phagocytes, leukocytic cells, that exert their bactericidal action processing the microbe through phagocytosis (figure 6).

Once the innate immune response is activated, it starts and control the *adaptative immunity*. This consists in the ability to recognise and to destroy pathogens with high specificity, is activated about 90 hours after the infection and creates an immunological memory. Adaptative immunity acts through the recruitment of leukocytic cells, the lymphocytes (T and B cells) and antibodies (figure 6). Leukocytes activated with the immune response, after the phagocytosis, expose bacterial antigenic targets on their cellular surface. These are recognised and destroyed by T helper cells that produce cytokines recalling other T cells. On the other side, B cells expose on their cellular surface antigens that are recognised by T helper cells that stimulated the proliferation of B cells able to produce specific antibodies.

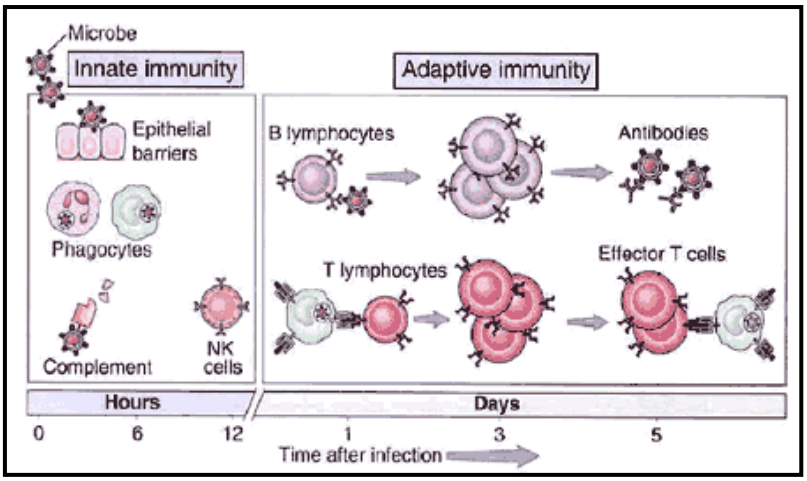

Figure 6 Innate and adaptative immunity scheme

LPS are immunogenic molecules also identified as PAMP since they are among the main virulence factors for Gram negative bacteria. The real endotoxic principle of these molecule is the lipid A since its recognition immediately activates the innate immune system of the host. Small amounts of LPS are recognised and alert the host immune response for fighting the infection. If the inflammatory response is amplified and uncontrolled, due to the high toxicity of the LPS from the infecting pathogen, there may occur a fulminating septic shock syndrome. The core oligosaccharide or, in smooth

bacterial colonies, the O-chain, are the antigenic moieties recognised by the adaptative immunity.

The first host protein involved in LPS recognition is a blood-stream protein, the LBP (lipopolysaccharide binding protein) that forms a high affinity complex with lipid A moiety of LPS released from bacterial lysis or replication, or still bound to the outer membrane of the intact pathogen cell.[11] The N-terminal domain of LBP is responsible for the LPS/lipid A binding while the C-terminal domain is specific for the further recognition by CD14. This latter receptor does not participate directly to the inflammatory cascade since it is lacking a trans-membrane domain. The CD14 can be found in two forms, soluble and membrane bound, and has a crucial role in the enhancement of host response to endotoxins since it facilitates the recognition of LPS by the final receptor complex MD2-TLR4 (figure 7). TLR4 belongs to the Toll like receptors family that encloses different receptors recognizing a wide range of antimicrobial compounds. To date, eleven TLRs have been described in mice and ten in humans. These receptors have a common extracellular leucine-rich repeats domain with a horseshoe-like shape, a single transmembrane region and a TIR intracellular domain that shares sequence similarity with *Drosophila* Toll.[11] TLR4 is specific for LPS recognition; with the myeloid differentiation factor 2 (MD2), it constitutes an heterodimer that recognizes a common structural motif in different LPS molecules. The binding with an agonist lipid A structure causes the dimerization of TLR4 extracellular domains, consequently, the receptor multimer is formed by two copies of LPS-TLR4-MD2 complex. This triggers the recruitment of specific proteins to the intracellular TIR domain and activates the signalling cascade.[12] It has been shown that LPS binding and complex dimerization does not affect TLR4 and MD2 folding. MD2 is folded into a single domain consisting of two β-sheets: one containing three antiparallel β-strands, the other six. Between these sheets there is a large and deep hydrophobic cavity for ligand binding. LPS binds to this pocket and immediately mediates the dimerization of the two TLR4-MD2 complexes. Cristal structures of complexes with the hexa-acylated lipid A component of *E. coli* LPS showed that all the acyl chains of lipid A interact with hydrophobic pocket of MD-2 whereas the amide-linked fatty acid on the GlcNI is partially exposed to the MD-2 surface creating an hydrophobic interface essential for the interaction for the second TLR4 receptor. The phosphate groups of the lipid A interact with a cluster of positively charged residues present on TLR4, MD2 and the second TLR4 receptor of the multimeric complex. Both hydrophobic and hydrophilic interactions contribute to the main dimerization interactions. Studies on the

complex with antagonist structures, as lipid IVa (figure 4), have shown that the four fatty acids completely fill the hydrophobic cavity of MD2. Since no structural changes occur in MD-2 binding pocket when it is linked to the agonistic hexa-acylated lipid A, it has been proposed that the additional space for the two further acyl chains is created displacing glucosamine backbone that exposes phosphate groups for ionic interaction that favoured complex aggregation. In antagonist structures the lack of phosphate groups and/or fatty acid exposure on MD-2 surface cause the complete absence of toxic activity.

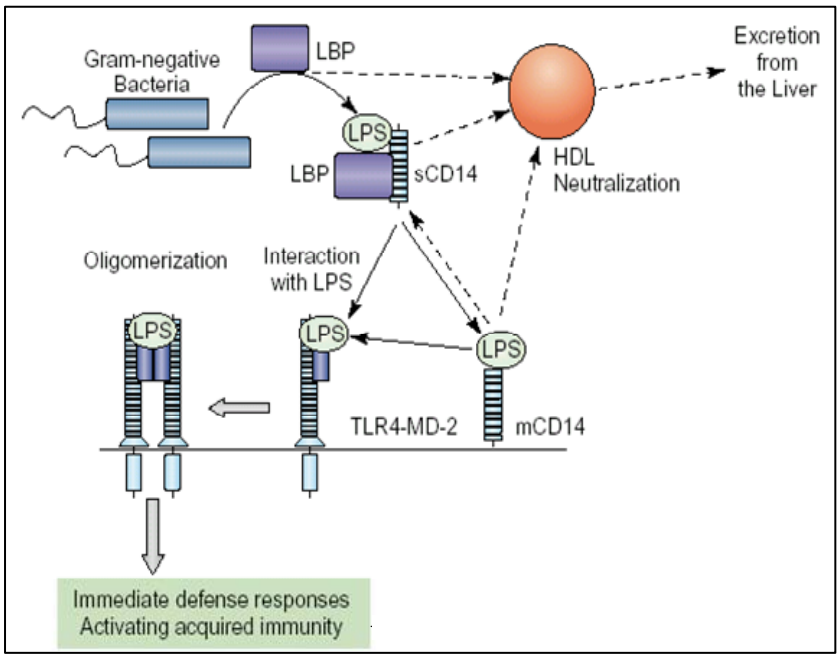

Figure7. Gram negative infection: LPS recognition.

1.4 Gram negative infections in Cystic Fibrosis disease

Cystic fibrosis (CF) is a genetic disease diffused in Caucasian population, affecting about one individual on 2500 live birth. It is induced by a point mutation in gene cluster encoding the cystic fibrosis transmembrane conductance regulator (CFTR), a protein of 1480 residues. The most common disorder is the ΔF508; this leads to a single amino acid mutation that generates a failure in CFTR folding and maturation. CFTR is a member of ATP-binding cassette superfamily (ABC) present on the apical membrane of the epithelial cells. It maintains the ion and fluid homeostasis since it is the unique ABC protein that functions as ion channel. It is constituted by two transmembrane domains (TMD1 and TMD2), by two nucleotide-binding domains (NBD1 and NBD2) and a regulatory site that are cytosolic.[13]

The role of CFTR results essential since its dysfunction causes a CF phenotype characterized by a multiorgan collapse, bronchiectasis, pancreatic enzyme insufficiency

and death. Moreover, inactive CFTR causes a failure in innate defence against pathogens thus producing chronic bacterial infections. Innate immunity guarantees a rapid and aspecific response to pathogens sensing their virulence factors (see paragraph 1.3). Among the wide range of innate immune mechanisms, those affected by CFTR dysfunction regard the mucociliary clearance system (MCC) that protects the human respiratory tract, the recruitment of phagocytic cell, of PRRs (see paragraph 1.3) and of a large ensemble of antimicrobial compounds, and the immediate production of reactive oxygen species (ROS). Below is sketched a section of the airway surface liquid (ASL) in lung epithelial surface (figure 8).[14]

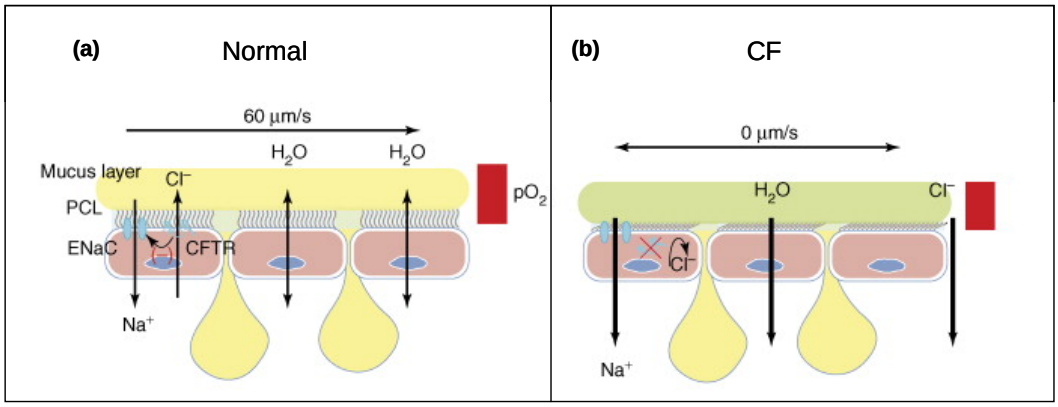

Figure 8 Normal mucus clearance mechanisms (a) and failure of CF mucus clearance (b)

In a normal epithelium surface there is the mucus layer, prevalently constituted by mucins, that is positioned on a periciliary liquid layer (PCL). In a healthy tissue the mucus allows an efficient ciliar beat and provides for a lubricant activity (figure 8a). The hydration is guaranteed by the capacity of normal epithelia to absorb and secrete salts with water moving osmotically in response to salts gradient. While CFTR is the Cl^- channel, the epithelia Na^+ channel (ENaC) and the Na^+/K^+-ATPase regulate Na^+ transport in and out the membrane. In healthy conditions, an ASL reduction inhibits ENaC, Cl^- is secreted through the CFTR channel and the consequent water osmotic passage across the membrane reconstitutes the ASL hydration. Mucus clearance is guaranteed by CFTR that acts either as Cl^- channel or as an inhibitor of the ENaC. In a CF tissue impaired CFTR provokes an unregulated Na^+ adsorption and a low secretion of Cl^-. The consequent dehydration causes a collapse of mucus layer on PCL. Mucus adhesion on airway surface generates airflow obstruction and creates an ideal habitat for a wide range of microorganisms causing inflammation and chronic infection.

Viscous mucus generates a barrier in submucosal glands ducts blocking the secretion of cathelicidine antimicrobial peptides (CAMP), as β-defensins, that kill bacteria. Further, beyond physical obstruction, it has been hypothesized that CF tissue is characterized by a hypertonic milieu that inhibits antimicrobial peptides action.[15] In addition, high viscosity affects neutrophils migration avoiding their encountering with microbes. This causes pathogens proliferation and deep changing in bacterial phenotype; in many cases, bacteria start producing biofilm that aids cells adhesion, bacterial persistence and chronic infections. Recently, it has been demonstrated that lysosomal CFTR is also involved in phagosomal pH control. Lysosomes are cellular organelles containing digestive enzymes that act in acid conditions (pH= 4.5). During their maturation process, lysosomes fuse with phagosomes, vacuoles able to engulf particles through phagocytosis; this generates phagolysosomes in which all the particles phagocytised are degraded by lysosomal enzymes. CFTR ensures lysosomal acidification and a bactericidal activity, promoting H^+ accumulation by the lysosomal V-type H^+-ATPase, since it is the channel of H^+ counter ion (Cl^-). Thus, in CF phenotype there is an alkalinization of phagolysosomes lumen that impairs their antimicrobial activity.[16]

Defective acidification in lysosomes also promotes ceramide accumulation. Biological membranes are mainly constituted by cholesterol, sphingomyelin and phospholipids. In lysosomes sphingomyelin is converted to ceramide through the acid sphingomyelinase (Asm). Then ceramide is degraded in sphingosine by acid ceramidase (Ac). Lysosomes alkalinization in respiratory cells induces an imbalance of both Asm and Ac activities that leads to a net accumulation of ceramide. As a consequence, the rate of cell death increases, there is an accumulation of DNA that facilitated pathogens infections. Moreover, ceramide accumulation also induces a pro-inflammatory status since there is an increase synthesis and release of cytokines.[16]

Further, the presence of viscous mucus in CF individuals also impairs neutrophils in bacterial killing. Neutrophils posses two type of killing mechanisms: the non-oxidative type and the oxidative one. The former is based on the action of lysosomal enzymes, lysozime, cationic proteins, defensis and lactoferrin. The latter requires the presence of O_2 since it generates ROS as H_2O_2 and O_2^-, that are toxic oxygen metabolites. NADPH oxidase reduces O_2 to the instable species O_2^- that dismutes in H_2O_2 thus favouring the action of an enzyme, the myeloperoxidase (MPO), that uses the H_2O_2 product with the ion chloride to generate hypochlorus acid, a potent antimicrobial oxidant able to induce peptide-bond scission. Viscous mucus creates a microaerobic environment in which the

oxygen is consumed by pathogens colonies. This causes the lacking of ROS products and impairs the neutrophils oxidative killing. Moreover, pathogens intrinsically resistant to non oxidative killing or able to change their phenotype in order to resist to it, persist in CF respiratory tracts. Thus, while *Burkholderia cepacia* complex species, constitutively resistant to non-oxidative killing, cause feared disease in CF, *Pseudomonas aeruginosa* and *Staphylococcus aureus*, both sensitive to non-oxidative and oxidative killing, switch to a mucoid phenotype able to resist to neutrophils killing.[16]

In addition, besides the role of chloride channel, whose deficiency cause all the consequences mentioned above, CFTR is also considered part of the innate immune system since epithelial cells use CFTR as a receptor for *P. aeruginosa* and internalize the bacterium removing it from the airway. Recognition occurs through the interaction between the outer core moiety of *P. aeruginosa* LPS and a region of amino acid 108-117 located in the first extra-cellular domain of CFTR. Thus, in a CFTR defective individual, impaired phagocytosis causes a massive presence of bacterial cells that triggers *P. aeruginosa* infection.[17]

Among CF pathogens, the dominant ones are *Pseudomonas aeruginosa* and a group of closely related species known as *Burkholderia cepacia* complex (Bcc). These are opportunistic pathogens ubiquitously found in Nature. Further, other pathogens as *Haemophilus influenza*, *Staphylococcus aureus*, *Achromobacter xylosoxidans*, *Ralstonia* and *Pandoreae* species are growing in importance.

About 70%-80% of CF patients became chronically infected with *Pseudomonas aeruginosa*.[18] Epidemiology of *P. aeruginosa* is characterized by an early stage of infection, that lasts about three months, followed by a chronic establishment of the inflammation. During the first period there is co-infection of different *P. aeruginosa* strains but then, with evolving of the inflammation, a single clone remains established. Typically, in chronic infections emerges a mucoid strain able to biosynthesize alginate and biofilm thus increasing pulmonary exacerbation. Antibiotic therapies stress bacteria that are "hypermutable" that means that they are characterized by an enhanced mutation frequency that allow their adaptation to the external environment. As for the second most dominant pathogen, *Burkholderia* is less prevalent than *Pseudomonas* but s responsible for the most feared infections. *Burkholderia* epidemiology is characterized by an elevated patient to patient transmissibility, an high resistance to the normal antibiotic therapies and, depending on the infecting strain, by a deadly and fulminating exacerbation of lung function known as "cepacia syndrome".[8] *Burkholderia* CF pathogens are grouped into

Burkholderia cepacia complex, a class of pathogens that encloses more then ten species, phenotipically similar, identifiable only for the genotype, known as *genomovars*. Infections from *Burkholderia* have a profound effect on CF patients life. The high transmissibility of Bcc strains induces many hospitals and CF centres to adopt segregation policy and rigorous restrictions in order to limit contacts among patients. The enormous sacrifices of CF patients are rewarded by the decrease of Bcc infections. Unfortunately, it is possible to acquire these Bcc pathogens from natural reservoirs. *Burkholderia* species, in fact, are ubiquitous in nature and, in past years, they were used for biotechnological applications until it was discovered that they are opportunistic pathogens.

Besides LPS, as they are Gram negative bacteria, a number of potential virulence factors have been described for Bcc isolates; among these there are cable pili, flagella, surface exopolisaccharide, type III secretion system (TTSS), superoxide dismutase, proteases and quorum sensing system. Despite this, Bcc species does not have the same toxicity since their virulence is highly complex. More specifically, among all the genomovars, *B. cenocepacia* clonal lineage ET-12 (genomovar III) accounts for the most dangerous infections associated with cepacia syndrome and can replace other less virulent strains in infected individuals. It has been found that strains from *B. cenocepacia* have both the *cbl* gene coding for cable pili, that enhances cells adhesion to CF epithelium, and the DNA fragment, the *Burkholderia cepacia* epidemic strain marker (BCESM). These genetic features are characteristic of epidemic strains. As for the other genomovars, also high spread and mortal rates are connected to *B. multivorans* (genomovar II) infections and, in some centres, *B. multivorans* recovery exceeds that of *B. cenocepacia*. Despite this, clinical outcome cannot be predicted since the same strain may be responsible of different inflammation evolvements also depending on the host response. Thus, pathogenesis depends on a wide range of factors that go from the virulence factors to the host-bacteria interactions and possible interaction among all the colonizing pathogens.[19] Up to now, lung transplantation is the only treatment for end-stage CF patients and, whilst invasive and aggressive, it improves both quantity and quality of CF patient life. Infecting strains have a significant clinical relevance in lung transplantation, since it has been demonstrated that the pre-transplantation strain is responsible for post-operative period and transplant outcome. Due to their high pathogenicity, currently, many centres refuse transplant to Bcc infected individuals. Commonly, pre-operative infections by *B. cenocepacia* are associated to poor outcomes in lung transplantation. In a retrospective study performed by de Soyza and colleagues at the Freeman Hospital (UK), were studied eleven CF patients with pre-

operative Bcc infections. Depending on the genomovars, there were different lung transplantation outcome. All transplanted recipients infected by *B. cenocepacia* died after an early post-operative stage of cepacia syndrome illness, while all the others survived. Interestingly, most of survived patients continued to have Bcc positive cultures in their expectorate without the evidence of a pulmonary disease.

Nowadays, even though many studies are focused on gene therapies, a wide branch of research is focused on the epidemiology, the pathogenicity and the treatment of CF pathogens infections that are deadly consequences of a genetic disorder. Thus, studies on CF pathogens virulence factors are aimed to elucidate their chemical structure and biological activity, aid to identify new targets for therapies.

References

1. Madigan M, Artinko MA, Parker J. *Biology of microoganism* (Ed.: T. Brock) Pearson education international, New York, 2003.
2. Alexander C, Rietschel ET. Bacterial lipopolysaccharides and innate immunity. *J. Endotoxin Res.* (2001). 7: 167-202.
3. Raetz CR, Reynolds CM, Trent MS, Bishop RE. Lipid A modification systems in gram-negative bacteria. *Annu Rev Biochem.*(2007) 76:295-329.
4. Raetz CRH, Whitfield C. Lipopolysachharide endotoxins. *Annu. Rev. Biochem.*(2002) 71: 635-700.
5. Ernst RK, Yi EC, Guo L, Lim KB, Burns JL, Hackett M, Miller SI. Specific lipopolysaccharide found in cystic fibrosis airway *Pseudomonas aeruginosa*. *Science* (1999) 286: 1561-1565.
6. Netea MG, van Deuren M, Kullberg BJ, Cavaillon JM, van der Meer JW. Does the shape of lipidA determine the interaction of LPS with Toll-like receptors? *Trends Immunol* (2002) 23: 135–139.
7. Seydel U, Oikawa M, Fukase K, Kusumoto S, Brandeburg K. Intrinsic conformation of lipid a is responsible for agonistic and antagonistic activity. *Eur. J. Biochem.* (2000) 267: 3032-3039.
8. De Soyza A, Silipo A, Lanzetta R, Govan JR, Molinaro A. Chemical and biological features of *Burkholderia cepacia* complex lipopolysaccharides. *Innate Immun*. (2008) 14: 127-144.
9. Tsai CM, Jankowska-Spephens E, Mizamur RM, Cipollo JF. The fine structure of *Neisseria meningiditis* lipooligosaccharide from the M986 strain and three of its variants. *J. Biol. Chem.* (2009) 284: 4616-4625.
10. Lukacova M, Barak I, Kazar J. Role of structural variations of polysaccharide antigens in the pathogenicity of Gram-negative bacteria. *European society of clinical microbiology and infectious disease* (2007) 14: 200-206.
11. Pålsson-McDermott EM, O'Neill LA. Signal transduction by the lipopolysaccharide receptor, Toll-like receptor-4. *Immunology* (2004) 113:153-162.

12. Park BS, Song DH, Kim HM, Choi BS, Lee H, Lee JO. The structural basis of lipopolysaccharide recognition by the TLR4-MD-2 complex. *Nature* (2009) 458: 1191-5.
13. Riordan JR. CFTR function and prospects for therapy. *Annu. Rev. Biochem* (2009) 77: 701-726.
14. Boucher RC. Cystic fibrosis: a disease of vulnerability to airway surface dehydration. Trends in Molecular Medicine (2007) 16: 231-240.
15. Smith JJ, Travis SM, Greenberg EP, Welsh MJ. Cystic fibrosis airway epithelia fail to kill bacteria because of abnormal airway surface fluid. *Cell* (1996) 85:229-236.
16. Doring G, Gulbins E. Cystic fibrosis and innate immunity: how chloride channel mutations provoke lung disease. Cellular Microbiology (2009) 11: 208-216.
17. Pier GB. *Pseudomonas aeruginosa* lipopolysaccharide: a major virulence factor, initiator of inflammation and target for effective immunity *Int J Med Microbiol.* (2007) 297: 277-95.
18. Govan JRW, Brown AR, Jones AM. Evolving epidemiology of *Pseudomonas aeruginosa* and the *Burkholderia cepacia* complex in cystic fibrosis lung infection. *Future microbiol.* (2007) 2: 153-164.
19. De Soyza A, Corris PA. Lung transplantation and the Burkholderia cepacia complex. *The Journal of Heart and Lung Transplantation* (2003) 22: 954-958

Chapter 2

STRUCTURAL ANALYSIS OF LIPOPOLYSACCHARIDES AND LIPOOLIGOSACCHARIDES

2.1 Isolation of LOS and LPS

The procedures used for the isolation of S- and R-form of lipopolysaccharides are usually different. Gram-negative cells are sequentially extracted with two complementary procedures. Typically, rough-type LPS (LOS) are extracted with a phenol-chloroform-petroleum ether procedure (PCP) while smooth-type LPS are extracted with the hot phenol-water procedure. [1,2]

Due to its lipophilic nature, LOS is extracted from lyophilised cells with PCP mixture and then precipitated from pure phenol adding drops of water. After this extraction, cells undergo a second treatment with 90% phenol/water 1:1 at 68°. The two phases are then dialysed and digested with nucleases (DNase and RNase) and proteases in order to remove all the cellular contaminants. Typically, the presence of the long O-chain moiety increases the hydrophilic nature of endotoxins and generally LPS molecules are extracted in the water phase even though several factors, as the presence of hydrophobic residues, charged groups or the length of the polysaccharidic chains, may modulate LPS solubility in water.

LPS or LOS molecules are then detected through polyacrylamide SDS electrophoresis gel (PAGE) and stained with silver nitrate. LOS molecules, given their low molecular weight, are revealed by the presence of a dark band that migrates at the bottom of the gel. As for LPS, it is represented by a “ladder-like” migration patterns due to the presence of polysaccharidic moieties differing for the number of repeating units.

2.2 Structural characterization of glycolipids

The amphiphilic nature of the LPS molecules makes difficult the study of such molecules due to the tendency to form micelles with low solubility in both aqueous and organic systems. This problem can be overcome by separating the lipophilic portion of the lipid A from the rest of the macromolecule. Thus, the lipid A can be obtained treating the LPS with a mild acid hydrolysis usually with 1% acetic acid at 100°, which selectively cleaves the acid-labile ketosidic linkage of Kdo, particularly sensitive to these acid conditions. The

primary structure of the O-chain is studied performing the acidic treatment on LPS molecule: the water soluble phase recovered after this treatment contains the O-specific chain with the core oligosaccharide attached, whose contribution is negligible due to the presence of overwhelming repeating oligosaccharide units composing the O-chain portion.
Even though the core oligosaccharide can be studied by mild acid hydrolysis performed on LOS molecules, Kdo reducing unit produces a microheterogeneity that can render the study of the oligosaccharide difficult. Thus, typically, the common procedure to determine the primary structure of the core portion is a fully de-acylation performed through mild hydrazinolysis followed by a strong basic hydrolysis (KOH 4M, 120° C, 16h) to obtain the cleavage of N- and O-linked acyl chains.
Once saccharidic and polysaccharidic moieties are isolated, they are subjected to further investigations in order to determine their the primary structure.
Since the combination in which the sugar molecules can be linked are unlimited, the strategy requires combined approaches involving analytical, spectroscopic and spectrometric procedures that allow the determination of:

- the qualitative and quantitative composition of monosaccharide residues
- the absolute configuration of each monosaccharide
- the ring size
- the attachment points of the monosaccharides
- the anomeric configuration of the linkages
- the sequence of monomers
- the location of non-carbohydrates substituents

Additional information on the nature and the sequence of monomers can be obtained from selective cleavages of the polysaccharide (partial acid hydrolysis, acetolysis, Smith degradation, β-elimination, solvolysis).

2.2.1 Chemical methods for the sugar analysis

The identification of the nature of the sugar residues is possible through a GC or GC-MS analysis of monosaccharides previously derivatized. The procedure starts with a methanolysis of the saccharide sample with MeOH/HCl 0.5-2M, 85°C, followed by acetylation of the released monosaccharides. The acetylated *O*-methyl glycosides are then

injected to GC and identified via comparison with standard or to GC-MS and identified through the fragmentation pattern and the retention time.

Another chemical degradation used for the sugar analysis leads to the formation of alditol acetylated derivatives. They are obtained from an acid hydrolysis followed by reduction of reducing monosaccharides and acetylation. The alditols acetylated are then injected and analysed via gas-chromatographic techniques.

When the solvolysis is performed with an enantiomerically pure alcohol as 2-(+)-octanol, the absolute configuration of the monosaccharide residues can be determined.[3] The retention time of the acetyl 2-(+)-octyl glycosides is compared with the one of a standard mixture of *O*-2-(±)-octyl-glycosides of standard monoses in D or L configuration. From the comparison of the retention time of the octyl-glycosides of the sample with those of the standard, the D- or L- configuration of the monosaccharides can be assigned.

The determination of the ring size and of the attachment point of the monosaccharides via mass spectroscopic methods is performed via the methylation analysis.[4,5] The sample is methylated at its free hydroxyl groups, hydrolysed, reduced whit $NaBD_4$ and acetylated. These partially methylated alditols acetylated are then subjected to GC-MS analysis. The position of the acetyl groups in the fragments accounts for the attachment point or for the position of ciclyzation of the pyranose or furanose cycle. The methyl groups correspond to free positions, not involved in linkages. The reduction of the carbonilic function with sodium borodeuteride discriminates the fragments originated from the reduced position (even masses) form those originated from the last position (odd masses)

2.2.2 Mass Spectrometry

Mass spectrometry has become a powerful complementary method for structural analysis of lipopolysaccharides and lipooligosaccharides especially with the development of soft ionization techniques like MALDI (Matrix Assisted Laser Desorption Ionisation), ESI (ElectroSpray Ionisation), and the fragment analysis in MS/MS experiments. Usually, for carbohydrates, MALDI and ESI MS spectra are performed in negative ion mode, due to the presence of the hydroxyl groups that can easily lose a proton and acquire a negative charge, nevertheless spectra in positive ion mode are also performed.

The MALDI and ESI techniques show high sensitivity also at relatively high molecular mass and provides good spectra of intact molecular ions of lipopolysaccharides.

In case of LOS, the use of high laser power settings in MALDI spectra allows to obtain fragments due to the cleavage of the labile ketosidic linkage of the Kdo. In the deriving spectra there are three regions of signals originated by the lipid A, the core oligosaccharide and the intact LOS.
In LPS, due to the dispersion of molecular weight of the O-polysaccharide, information on the size of the repeating unit can be deduced.

2.2.3 NMR Spectroscopic methods

NMR spectroscopy yields the most complete picture of an oligo- and a poly-saccharide structure and behaviour in solution. A combination of homo- and hetero-nuclear 2D-NMR experiment (DQF-COSY, TOCSY, NOESY, ^{13}P-^{1}H HSQC, ^{13}C-^{1}H HSQC, HMBC) are performed in order to assign all the spin systems, to determine the location and the nature of non-glycoside substituents and to characterize the sugar sequence. The evaluation of NMR chemical shifts and coupling constants are sufficient for the identification of the monosaccharide composition. The proton resonances obtained by COSY and TOCSY spectra are used to assign the spin system and to attribute the carbon resonances in the HSQC spectrum. The majority of the protons derived from the sugar bulk of non-anomeric and non-acylated protons are localised in a region comprises between 2.8-4.4 ppm. Anomeric signals appear in a spectral width of 4.4-5.8 ppm. $^{1}J_{C1,H1}$ and $^{3}J_{H1,H2}$ are diagnostic of the anomeric configuration. In sugar with the H-2 axial (glucose, galactose), a $^{3}J_{H1,H2}$ around 8 Hz is indicative of a β-orientation, whereas below 3 Hz of an α-configuration. Sugars with the H-2 equatorial (mannose) show both $^{3}J_{H1,H2}$ below 3 Hz. The $^{1}J_{C1,H1}$ values are also indicative of the anomeric configuration. A $^{1}J_{C1,H2}$ below 165 indicates a β-anomer, above 170 Hz a α-anomer.
NOESY and ROESY spectra are very useful in confirming the *intra*-residue assignment and the anomeric configuration. In fact, in β-configured sugars H-1 gives intra-residue NOE effect with H-3 and H-5, in α-configured only with H-2.
The downfield shift of ring proton signals (acylation shift) is useful to determine *O*- and *N*-acylation sites. *O*-phosphorylated protons undergo a similar down-field shift.
NOE contacts and long range correlations present in the HMBC spectra are useful in the location of non-carbohydrates substituents.

In the HSQC spectrum, the down-field shift of carbon resonances (glycosylation shift) allows to locate the positions of glycosidation. NOESY, ROESY and HMBC spectra are of great importance in attributing the inter-residue correlations allowing the determination of the sugar sequence in the polysaccharide chain.
^{31}P NMR and ^{1}H-^{31}P HSQC allow the localization of the phoshorylation sites.

2.3 Structural characterization of the lipid A

Lipid A may be obtained by LPS or LOS preparation to mild acid hydrolysis, by which the ketosidic linkage between Kdo and the distal D-glucosamine residue of the lipid A backbone is cleaved.
The lipid A characterization requires the determination of:

- the sugar backbone
- the amide and the ester linked fatty acids
- the distribution of the acyl chains on the sugar backbone
- the phosphorylation sites
- if present, phosphate substituents and their location
- sites of heterogeneity localised in the number, the type an the distribution of the acyl chain or induced by the non-stoichiometric presence of phosphate substituents.

In order to achieve the lipid A primary structure, partial degradation can be performed and the product analysed via MS and NMR methodologies.
The determination of the nature, the ring size, the attachment point and the absolute configuration of the sugar components of the lipid A has been already described (see paragraph 2.2.1).

2.3.1 Chemical methods for fatty acids analysis

As a characteristic feature, lipid A contains saturated and unsaturated fatty acids, in ester and in amide linkages. Total fatty acid content is obtained by acid hydrolysis. Lipid A is first treated with HCl 4M (4h, 100°C) and then neutralized with NaOH 5M (30 min, 100°C). Fatty acids are then extracted in $CHCl_3$, methylated with diazomethane and analyzed by GC-MS. In order to obtain the ester bound fatty acids, complete *O*-deacylation of the product can be performed in basic conditions with stronger alkali (NaOH 0.5M, 85°, 2h). Fatty acids are then methylated with diazomethane and analyzed by GC-MS as

methyl-ester. The amide-linked fatty acids can be recognized by difference between total and ester-linked fatty acid.[6]

2.3.2 Spectrometric methods

Mass spectrometry is the most useful approach for lipid A structural determination. MALDI and ESI analyses allow the precise description of the acylation pattern of the molecule. The MS spectra can be performed in both negative and positive ion mode and furnish complementary information. The acidity of the phosphate groups at position 1 and 4' make possible their easy deprotonation and the formation of negative ions. The negative ion spectra furnish a representation of the lipid A family and of its structural peculiarity.
MS analysis of intact lipid A describes the overall molecular weight of the molecule. Further approaches, as selective chemical degradations of the molecule, are aimed to the definition of lipid A acyl pattern. The amide linked fatty acids are identified by MS analysis of completely de-*O*-acylated lipid A with hydrazine. Additionally, a very useful approach is the treatment with NH_4OH that combines ammonium hydroxide hydrolysis and MS analysis.[7] The procedure exploits the lower stability, under mild alkaline conditions, of acyl and acyloxyacyl esters with respect to that of acyloxyacyl amides. The ammonium hydroxide hydrolysis selectively splits acyl and acyloxyacyl esters, leaving the acyl and acyloxyacyl amides unaffected, thus in MS spectra all the amide-linked groups are revealed. If the distribution of acyl chains is asymmetric, positive ion MS spectra are useful in the identification of the fatty acids present on the non-reducing GlcN. Positive ion spectra can be performed on both intact and totally de-phosphorylated lipid A. Such spectra show prominent sodium and potassium adduct ions and comprise laser induced in-source fragment ions resulting from the cleavage of the glycosidic linkage of the disaccharide backbone. The formation of oxonium ions is mainly observed from non-reducing distal GlcN. The identification of the oxonium ions can be very useful to obtain information on the GlcN II substituents concerning the nature, the number and, when possible, the distribution of primary and secondary fatty acids on the distal glucosamine.
The analysis of negative and positive mass spectra furnishes indication of the presence of non-stoichiometric phoshorylation sites. The intact or the fully *O*-deacylated lipid A are used to study the location of the phoshorylation sites.

2.3.3 Spectroscopic methods

The nuclei of interest in the NMR studies are ^{1}H, ^{13}C and ^{31}P. The measurement of NMR spectra furnishes information on the nature of the sugar and the phosphate residues present, the anomeric configuration, the attachment point, the sequence of sugar residues, the acylation and the phoshorylation sites, the nature of carbohydrate and non-carbohydrate substituents on the polar heads and on the acyl chains.

The amphiphilic nature of the lipid A, due to the simultaneous presence of hydrophilic and lipophilic portions and its structural microheterogeneity makes the execution of good NMR experiments a very difficult task. The tendency to form aggregate and the low solubility shows poorly resolved spectra. The first step to run NMR experiments requires to find a good solvent system, since the dissolution of lipid A in useful solvents for NMR analysis is still a problem. Mixture of deuterated solvents can be used, like chloroform/methanol or chloroform/methanol/water, depending on the nature of the lipid A family. Several lipid A often reveal good solubility in DMSO-d_6 at relatively high temperature (around 40°) and the ^{1}H-NMR spectra of the product are of good quality. The selection of DMSO as a finer solvent for lipid A seems a good way out for the preparation of complicated mixtures of deuterated solvents and no degradation occurs in these conditions. Furthermore, the solvent and water signals fall neither in the anomeric nor in the sugar ring region of the ^{1}H-NMR spectrum, allowing easier assignation of all key resonances. In addition, the non exchanged amide protons in the deshielded region of the spectrum are a good alternative starting point to assign all signals of the intact lipid A species.

A combination of homo- and hetero-two-dimensional NMR experiments (COSY, TOCSY, ROESY, HSQC, HMBC) are performed to assign the sugar backbone of the lipid A mixture signals.

The ^{1}H NMR spectra can be divided in five regions:

- the amide resonances near 6.5-7.5 ppm
- anomeric and acyloxy protons (protons geminal to *O*-acylated carbon, present in both sugar and acyl moieties) between 5.5-4.5 ppm.
- ring protons and β-protons of β-hydroxy fatty acids between 4.5-3 ppm
- α-methylene protons of fatty acids at 3-2 ppm
- the β,γ,…ω protons of the methyl and distal methylene groups at 0.8-2.0 ppm

The carbon resonances present the sequent regions:

- the anomeric carbons resonate between 90-105 ppm

- the ring carbons between 52-78 ppm
- the carbons of the acyl chains at 27-32 and 13-14 ppm

The identification of the sugar moieties is possible by determining the number of different spin systems corresponding to each sugar residue. These spin systems could be easily assigned starting from the amide proton in the TOCSY spectrum that resonates in a deshielded region. The two nitrogen bearing carbon signals resonate at 50-54.0 ppm, giving evidence of 2-amino-2-deoxy residues. The $^{1}J_{C1,H1}$ and $^{3}J_{H1,H2}$ coupling constants, the NOE contacts and the chemical shift values allow to assign the α- and the β-configuration of the GlcNs. The intra-ring $^{3}J_{H,H}$ and the chemical shift values allow to assign the *gluco* configuration and the $^{4}C_{1}$ conformation for two GlcNs.

The acylation sites can be easily determined analyzing the proton chemical shift values. The *O*-acylation causes downfield chemical shift resonances. Both the H-3 and H-3' of GlcNs and the β-protons of acyloxyacyl moieties undergo this acylation shift and resonate in the anomeric region. Analogously, the downfield chemical shift value of H-2 and H-2' at 3.8 and 3.7 ppm is due to *N*-acylation.

The sequence of the carbohydrate residues can be gained by the ROESY and HSQC spectra. The β-(1→6) linkage between the GlcN residues is proven by the glycosidation shift that causes significant downfield displacement of C-6 of GlcNII (resonating around 69-70 ppm) and the strong intraresidual NOE contact of the anomeric proton of the β-GlcN with the proton H-1 with H-6_a of the α-GlcN. The complete assignment of NMR data allow the identification of eventual other substituents as Ara-4N, GalA, β-hydroxy butirric acid, ethanolamine.

The *O*-phoshorylation causes downfield shift, particularly marked in the H-1 of the α-GlcNI, resonating at 5.5-5.6 ppm. The nature of the phosphate substituents and their location can be achieved by the execution of ^{31}P NMR and ^{31}P-^{1}H HSQC spectra.

A monophosphate monoester group resonates between 2 and –0.6 ppm, a monophosphate diester between –1 and –3 ppm, a pyrophosphate (di-phosphate diester) around –10 and –12 ppm, a phosphoramide up to 10 ppm.

The location of the phosphate group is achieved by the proton-phosphorous correlations in the ^{31}P-^{1}H HSQC.

References

1. Galanos C, Luderitz O, Westphal O. A new method for the extraction of R lipopolysaccharides. *Eur. J. Biochem.* (1969) 9: 245-249.

2. Westphal O, Jann K. Bacterial lipopolysaccharides: extraction with phenol-water and further applications of the procedure. *Methods Carbohydr. Chem.* (1965) 5**:** 83–91.

3. Leontein K, Lönngren J. Determination of the absolute configuration of sugars by Gas-Liquid Chromatography of their acetylated 2-octyl glycosides. *Methods Carbohydr. Chem.* (1978) 62: 359-362.

4. Hakomori S. A rapid permethylation of glycolipid, and polysaccharide catalyzed by methylsulfinyl carbanion in dimethyl sulfoxide. *J. Biochem.* (1964) 55: 205-208.

5. Molinaro A, De Castro C, Lanzetta R, Evidente A, Parrilli M, Holst O. Lipopolysaccharides possessing two L-glycero-D-manno-heptopyranosyl-alpha -(1-->5)-3-deoxy-D-manno-oct-2-ulopyranosonic acid moieties in the core region. The structure of the core region of the lipopolysaccharides from *Burkholderia caryophylli*. *J. Biol. Chem.* (2002) 277: 10058-10063.

6. Rietschel ET. Absolute configuration of 3-hydroxy fatty acids present in lipopolysaccharides from various bacterial groups. *Eur. J. Biochem.* (1976) 64: 423-428.

7. Silipo A, Lanzetta R, Amoresano A, Parrilli M, Molinaro A. Ammonium hydroxide hydrolysis: a valuable support in the MALDI-TOF mass spectrometry analysis of lipid A fatty acid distribution. *J. Lipid Res.* (2002) 43: 2188-2195.

SECTION II

ENDOTOXIN ANALYSIS FROM CYSTIC FIBROSIS PATHOGENS

Chapter 3

STRUCTURAL LPS DIFFERENCES BETWEEN *BURKHOLDERIA MULTIVORANS* CLONAL STRAINS COLONISING PRE- AND POST-TRANSPLANTATED LUNGS.

In this study it has been defined for the first time the primary structure and pro-inflammatory activity of the LPS extracts from *Burkholderia multivorans* (genomovar II), which is one of the most common Bcc (Burkholderia cepacia complex) species isolated in CF centers (chapter 1, par. 1.4).[1] Herein, the structures of the LPS from clinical isolates pre- and post- lung transplantation were investigated. Such data are essential to elucidate the molecular modifications involved in the inflammatory process that occur pre- and post-surgery. Lung transplantation offers interesting insights into assessing possible host-pathogen interactions given that, following transplantation, any bacterial interaction will be with a lung allograft that does not bear CF epithelium or CFTR defects. Understanding how bacteria modify and adapt their LPS in new physiological conditions may allow greater understanding of LPS associated signaling.

3.1 Strain selection and SDS electrophoresis analysis of *B. multivorans* LOSs.

The project was in collaboration with the group of professor De Soyza from the Freeman Hospital of Newcastle, UK. They identified three patients who had paired pre- and post-transplantation strains of Bcc that demonstrated differences in rough LPS (lipo-oligosaccharide, LOS) migration patterns upon silver staining of 16% tricine SDS-gels (shown in figure 9a). Of these three patients one patient had *B. multivorans* infection, one had *B. vietnamensis* infection (see chapter 4) and one had *B. cenocepacia* infection (see chapter 5). Data here reported will be limited to the patient with *B. multivorans* infection. The pre transplant strain was isolated immediately pre-transplant and the post transplant strain was isolated at one week after transplantation (figure 9b).

3.2 Isolation and compositional analysis of LOS, Fr1 and Fr2 from *B. multivorans* pre and post transplantation.

LPS fractions from both clinical isolates were extracted and analyzed by SDS-PAGE. Both fractions consisted of rough type LPS chemotype (lipo-oligosaccharide, LOS) as suggested by the run at the bottom of the gel (figure 9a).

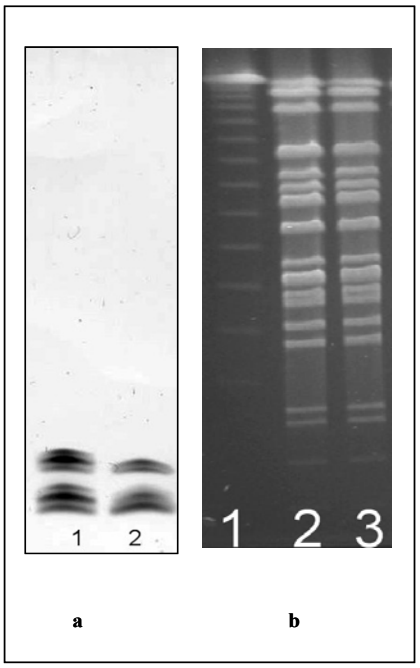

Figure 9. Evaluation LPS from B. *multivorans* pre- and post-transplantation. a) SDS gel of extracted LOS from clonal strains suggested migration differences when comparing pre transplant (Lane 1) to post transplant (lane 2). b) Pulsed Field Gel electophoretogram of paired pre and post transplant strain after *SpeI* enzyme digestion. The index case was known to have *B. multivorans* infection pre transplant. Lane 1 represents molecular weight markers. PFGE analysis demonstrated that the pre-transplant (lane 2) and post transplant strain (lane 3) were clonally identical

Monosaccharide and fatty acid analyses (see section III) of LOS isolated from *B. multivorans* pre- and post-transplantation showed the same content in sugar and fatty acids but only in post-transplantation strain the presence of an additional 8-substituted Ko residue was detected. The full compositional analysis of all fractions is reported in table 1.

3.3 Structural characterization of Fr1 product from *B. multivorans* pre-transplantation strain.

The usual mild acid treatment (see section III) on LPS from pre-transplantation strain yielded two fractions, **Fr1** and **Fr2**. The monosaccharide analysis of both fractions is shown in table 1.

A combination of homo- and heteronuclear 2D NMR experiment (DQF-COSY, TOCSY, ROESY, NOESY, ^{1}H-^{13}C HSQC, ^{1}H-^{13}C HSQC-TOCSY and ^{1}H-^{13}C HMBC, see section III and figures 10-11) was executed in order to assign all the spin systems of **Fr1** and to define the monosaccharide sequence.

Assignment	LOS *B.multivorans* pre-transplantation	Fr1	Fr2	LOS *B.multivorans* post-transplantation	Fr
3,4-substitued L,D-Hep	X	X	X	X	X
2,3,7-substitued L,D-Hep	X	X	X	X	X
terminal L,D-Hep	X	X	X	X	X
6-substitued D-Glc	X	X	X	X	X
terminal D-Glc	X	X	X	X	X
3-substitued L-Rha	X	X	X	X	X
terminal L-Rha	X	X	X	X	X
terminal L-Ara4N	X	-	-	X	-
6-substitued D-GlcN	X	-	-	X	-
terminal D-QuiN	X	X	X	X	X
3-substitued D-GalN	X	X	X	X	X
4,5-substitued Kdo	X	X	X	X	X
8-substitued Ko	-	-	-	X	-
terminal Ko	X	X	-	X	-

Table 1. Chemical composition analysis of the intact **LOS**, **Fr1** and **Fr2** fractions isolated from *B. multivorans* pre lung transplantation and of the intact **LOS** and **Fr** fraction isolated from the strain post transplantation.

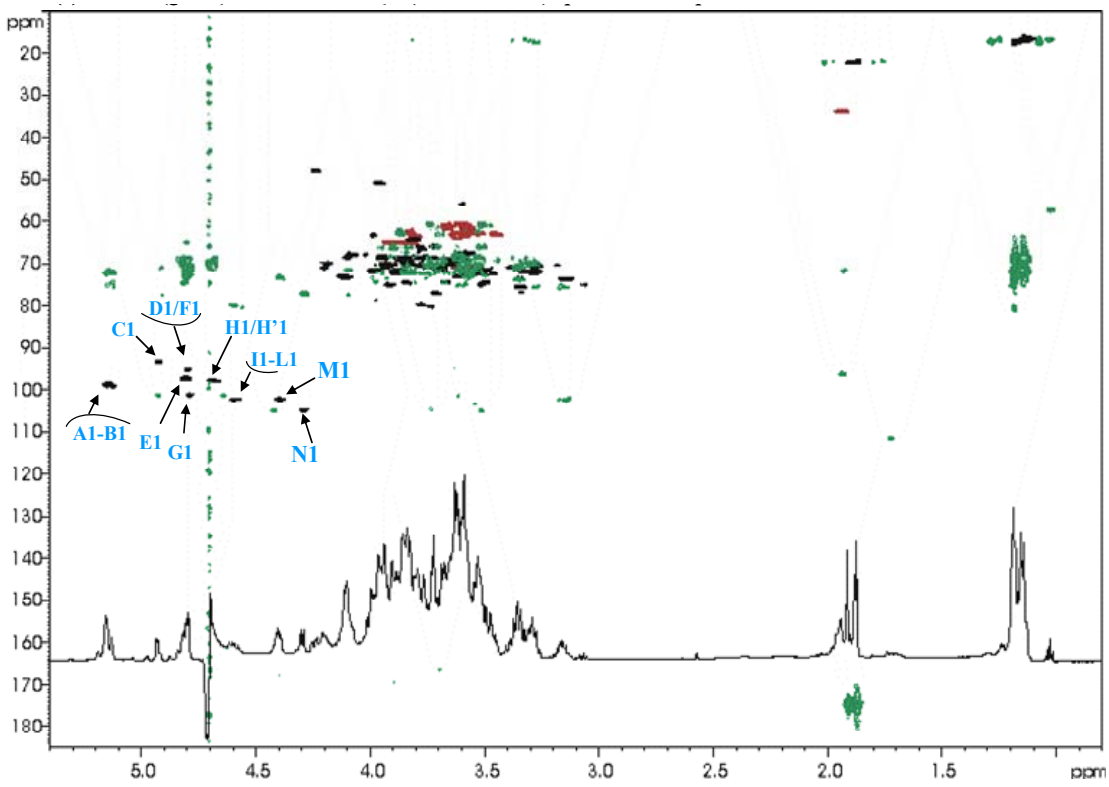

Figure 10. HMBC (green) and DEPT-HSQC (black and red) spectra of Fr1 product

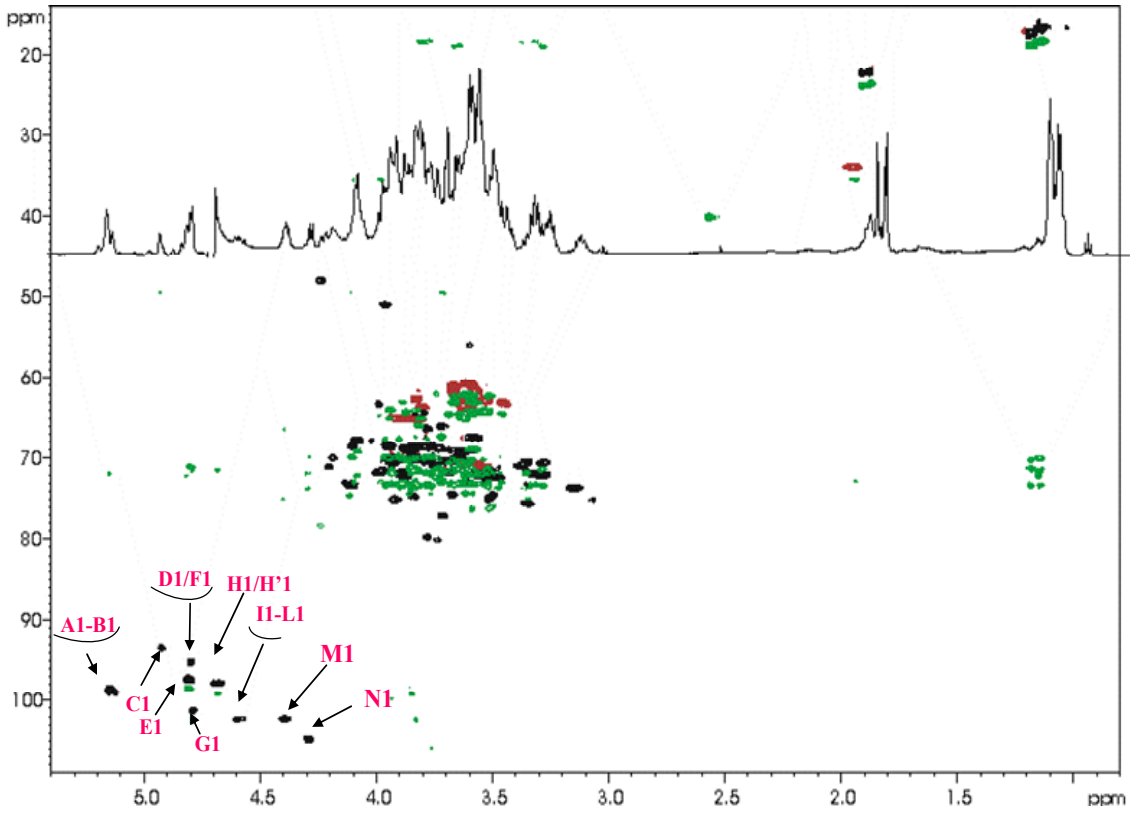

Figure 11. HSQC-TOCSY (green) and DEPT-HSQC (black and red) spectra of Fr1 product

In the anomeric region of the ^{1}H-NMR spectrum (figure 12a) twelve anomeric signals were identified (**A-N**, see table 2). Furthermore, the signals at 1.94/2.05 ppm were identified as the H-3 methylene protons of the Kdo residue (**K**) whereas residue **J** of α-Ko was assigned starting from its oxymethine H-3 signal. The relative intensities of anomeric signals suggested the existence of a mixture of oligosaccharides with different length of the carbohydrate chain.

In accordance with the chemical analysis, spin systems **A**, **B**, **E, G** were all identified as L-*glycero*-D-*manno*-heptose whereas spin systems **C** and **I** were identified as 2-deoxy-2-amino-galactose, both acetylated at C2 position. Spin systems **M** and **N** were identified as glucose residues while **D**, **H** and **H'** were recognized as α-rhamnose residues. Residue **L** (H-1 at 4.68 ppm) was recognized as a β-quinovosamine acetylated at C2 position.

The oligosaccharide sequence reported below (species **X**) was established identifying the inter-residual NOE contacts (figure 12b) and the long range correlations present in the HMBC spectrum:

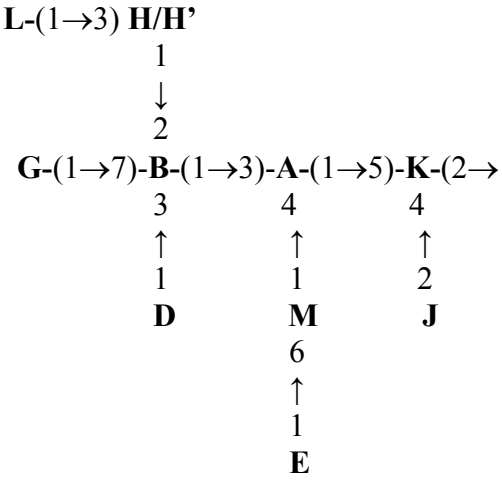

Species **X**

An alternative glycoform of the α-rhamnose **D** was found, namely residue **F**, identified as a 3-α-Rha residue. This was glycosilated by residue **I** of β-GalNAc that was in turn substituted at O-3 by the α-GalNAc **C**. Additionally, residue **C** was glycosylated at position 3 by the terminal β-Glc **N**. The linkage between these residues was attested by NOE contacts (figure 12b) and confirmed by scalar correlations in the HMBC spectrum. Thus, the oligosaccharide sequence (species **Y**) reported below differed from the previous one for the presence of the additional terminal trisaccharide:

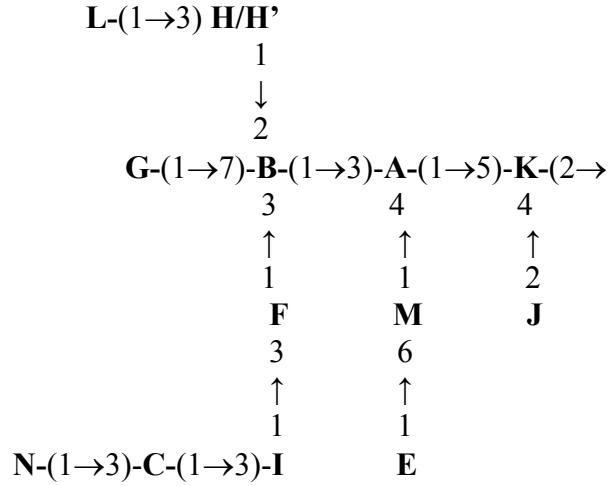

Species **Y**

	Chemical shift δ (^{1}H/^{13}C)							
Unit	**1**	**2**	**3**	**4**	**5**	**6**	**7**	**8**
A	5.15	3.93	3.91	3.94	3.62	3.85	3.66/3.57	
3,4-α-Hep	98.7	70.6	70.5	70.2	72.8	68.8	61.7	
B	5.12	4.19	3.83	3.85	3.79	3.79	3.62/3.56	
2,3,7-α-Hep	99.0	71.2	69.8	69.2	70.4	66.4	70.73	
C	4.92	4.23	3.71	4.11	3.97	3.63/3.45		
3-α-GalN	93.4	47.9	77.1	73.2	71.5	63.1		
D	4.81	3.75	3.68	3.32	3.80	1.13		
α-Rha	97.2	70.6	71.4	71.9	70.3	16.6		
F	4.81	3.75	3.77	3.38	3.82	1.13		
3-α-Rha	97.2	70.6	79.9	70.9	70.0	16.6		
E	4.80	3.84	3.94	3.89	3.56	3.86	3.52/3.58	
t-α-Hep	97.3	70.0	70.1	71.5	71.8	68.6	62.8	
G	4.78	3.82	3.71	3.71	3.51	3.83	3.52/3.59	
t-α-Hep	101.3	69.9	70.3	70.5	71.6	69.9	62.9	
H'/H	4.68	3.84	3.73	3.28	3.73	1.17		
3-α-Rha	97.8	69.9	80.3	70.5	70.8	17.2		
I	4.60	3.95	3.66	3.99	3.51	3.58/3.67		
3-β̃-GalN	102.4	50.9	74.38	71.9	75.01	60.8		
L	4.57	3.59	3.66	3.05	3.35	1.18		
t-β-QuiN	102.3	55.9	75.5	75.0	75.5	16.9		
M	4.39	3.15	3.34	3.28	3.56	3.82/3.89		
6-β-Glc	102. 3	73.5	75.6	70.5	72.0	65.3		
N	4.29	3.35	3.47	3.37	3.75	3.50/3.60		
t-β-Glc	104.9	70.4	72.31	70.8	68.4	60.8		
J	---	---	3.74	3.87	3.95	3.54	3.92	3.59/3.83
t- α -Ko	---	---	70.8	68.8	70.2	72.3	70.4	63.7
K	---	---	1.94/2.05	3.97	4.09	3.68	3.90	3.61/3.79
4,5 -α-Kdo	---	---	33.8	71.6	68.4	71.6	71.8	63.7

Table 2. ^{1}H and ^{13}C NMR chemical shifts (ppm) of sugar residues of the core-lipid A region of the oligosaccharide **Fr1**. The heptose residues possess a L-*glycero*-D-*manno* configuration, rhamnose residue a L-configuration, the other residues a D-configuration.

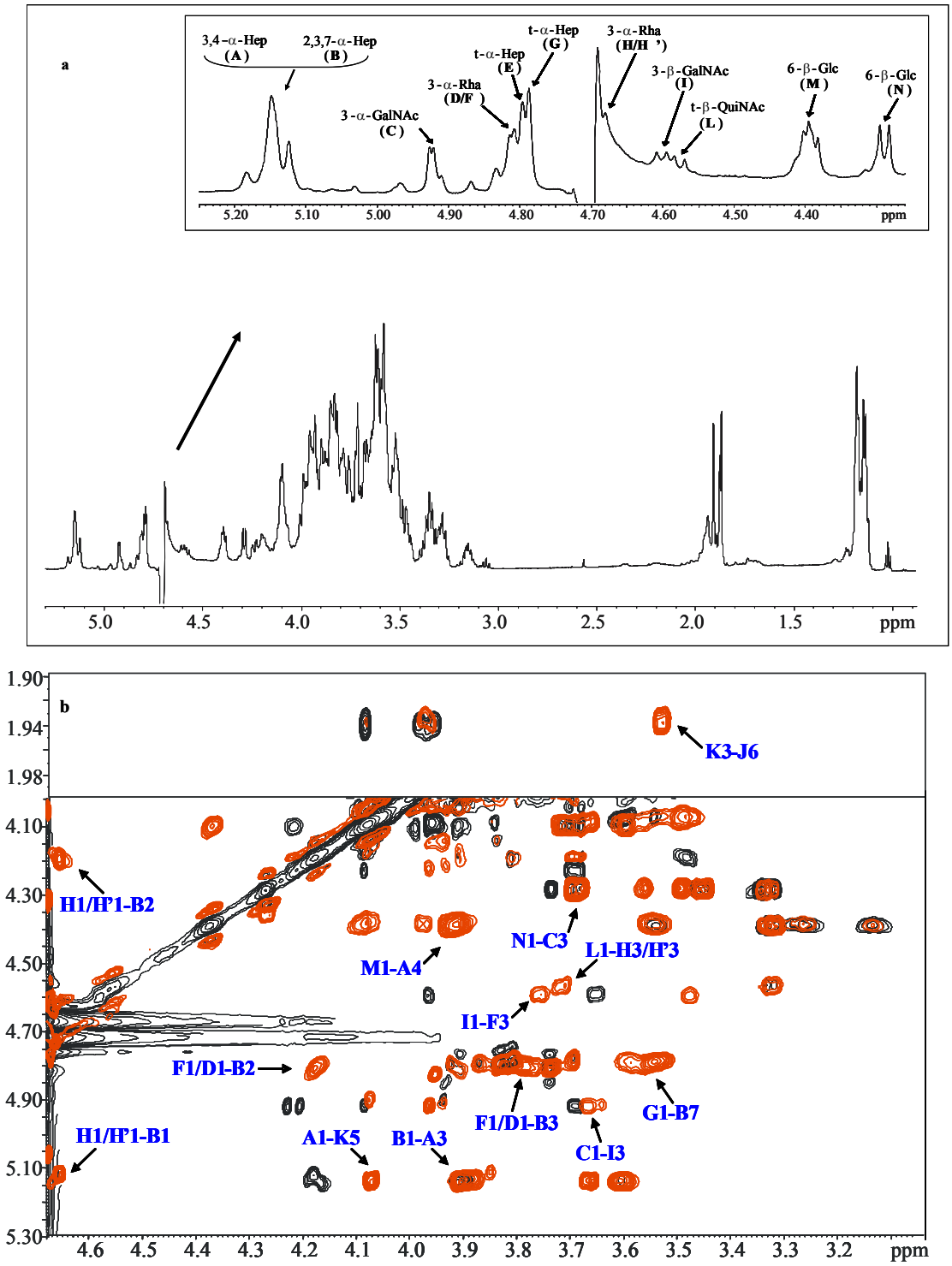

Figure 12. NMR structural investigation of Fr1 product. a)1H NMR spectrum of Fr1 product with a zoom of the anomeric region. b) Zoom of the ROESY (red) and TOCSY (black) spectra of oligosaccharide Fr1. Monosaccharide labels are indicated in table 2.

3.4 MALDI-MS characterization of Fr1 and Fr2 products from *B. multivorans* pre-transplantation.

The oligosaccharide structures above hypothesized were confirmed by MALDI mass spectrometry. The negative mass spectrum (figure 13a) showed two peaks, at *m/z* 1883.2 and at *m/z* 2264.1, matching with the oligosaccharide **X** and **Y** ($\Delta m/z \cong 568$ Th from 1696.3) assigned by NMR analysis and a further peak at *m/z* 1696.3 that differed from **X** by a β-QuiNAc residue. Likewise, **Fr2** fraction underwent mass spectrometric investigation. The negative ion MALDI mass spectrum of the oligosaccharide mixture **Fr2** (figure 13b) showed ion peaks related to **Fr1** oligosaccharides but lacking the Ko residue($\Delta m/z \cong 236$ Th)**.**

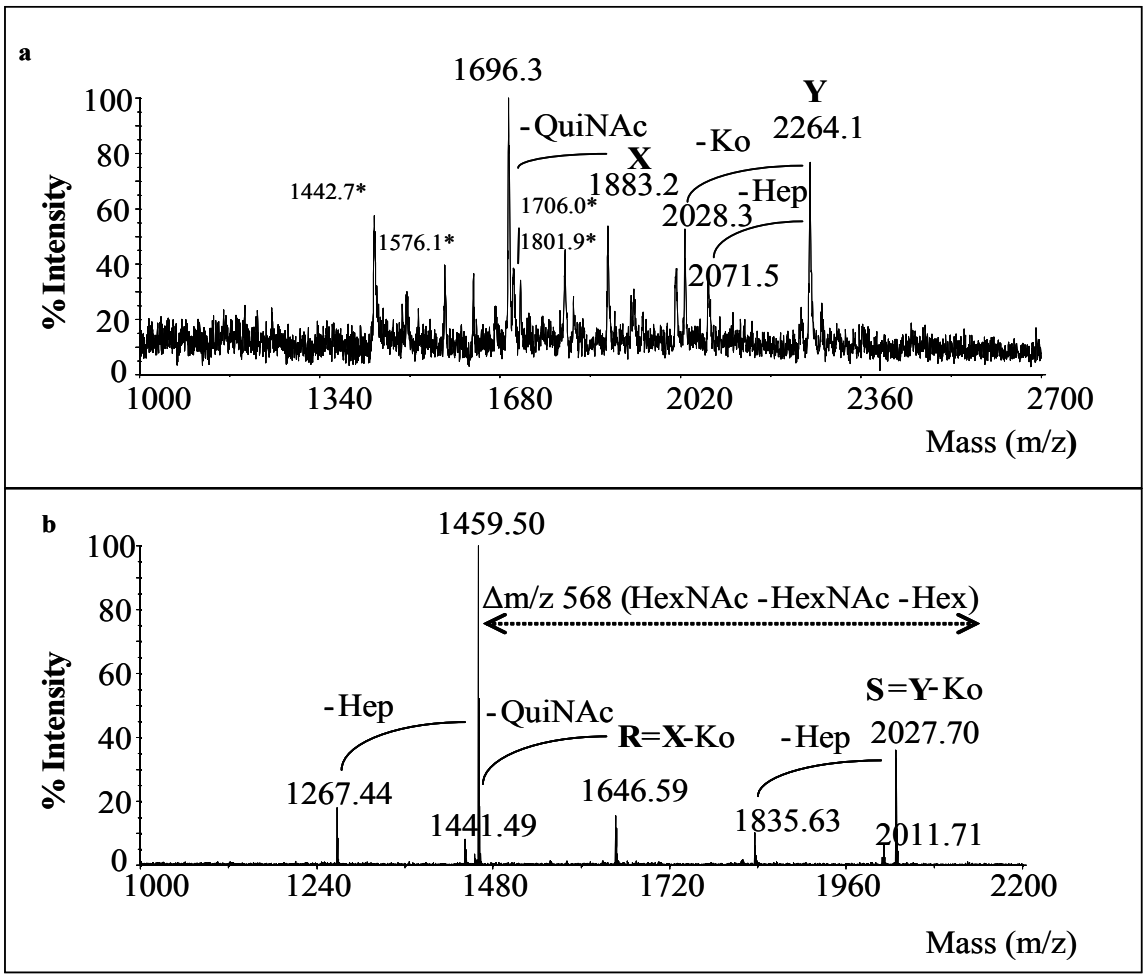

Figure 3. Negative ion MALDI mass spectrum of **Fr1** (a) and **Fr2** (b) oligosaccharides. a) Species **X**, **X**-QuiNac and **Y**, matching with NMR analysis, are the main peaks. Ions identified as Lipid A species (indicates with asterisks) are also visible. b) High resolution negative MALDI mass spectrum of **Fr2** oligosaccharide acquired in reflectron mode. Peaks **R** and **S** are related to oligosaccharides **X** and **Y** lacking the Ko moiety, respectively. Ions due to species missing QuiNAc and Hep residues are also present.

Taken together these information yielded the full oligosaccharide sequence deriving by from *B. multivorans* pre-transplantation LPS as the one depicted below:

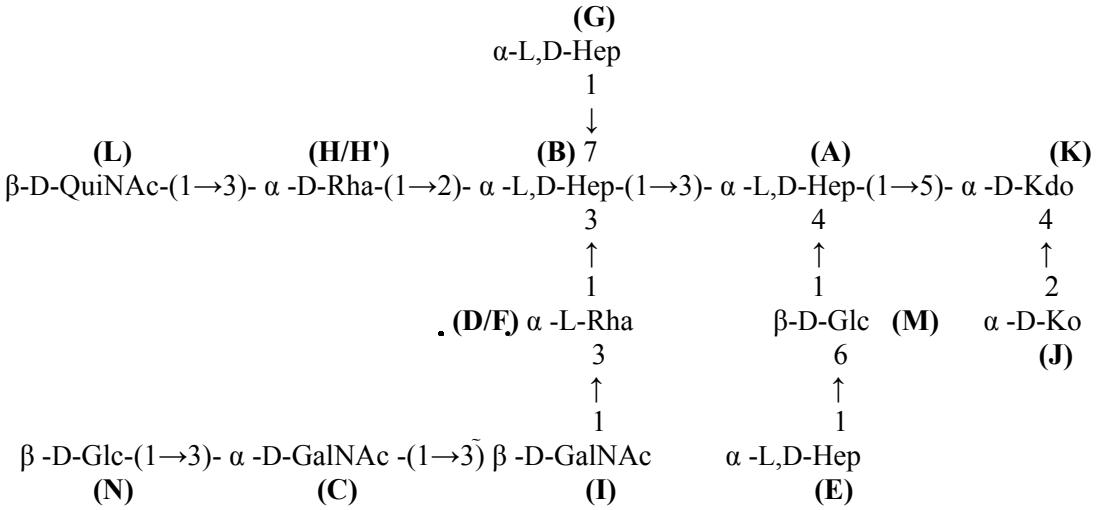

3.5 MALDI-MS characterization of oligosaccharide product from *B. multivorans* post-transplantation strain.

As for the pre-transplantation strain, the LOS extracted from *B. multivorans* post-transplantation strain underwent the same treatment and one oligosaccharide fraction, namely **Fr,** was isolated by gel-permeation chromatography. The compositional analysis of the fractions is reported in table 1. Both the NMR (not shown) and the MS data gave evidence of a saccharide sequence identical to the **Fr2** fraction found in the pre-transplantation strain (figure 14).

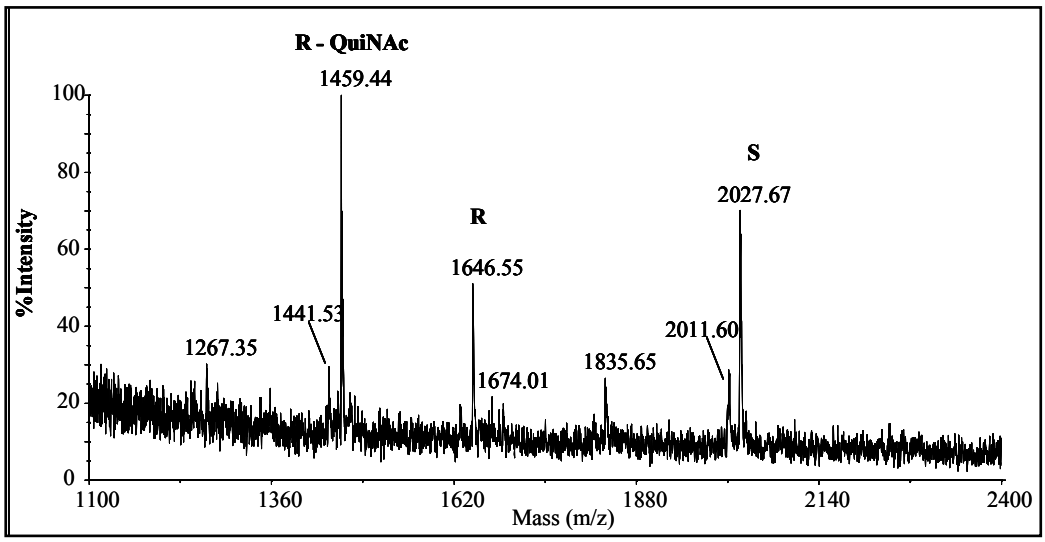

Figure 14. Negative ion MALDI mass spectrum of **Fr** product acquired in reflectron mode.

3.6 Structural characterization by MALDI mass spectrometry of the intact LOS from *B. multivorans* pre-transplantation.

In order to gain further information on both lipid A and core oligosaccharide structures, intact LOS were analyzed by MALDI MS by using our sample preparation procedure specifically set up for such amphiphilic molecules (see section III). The negative ion MALDI mass spectrum obtained before transplantation is shown in figure 15. At molecular masses from 1000 to 2500 *m/z* (figure 15a), two peaks related to the core oligosaccharide were found. Peak **OS1** at *m/z* 1677.6 matched with a nonasaccharide constituted of four Hep, one Hex, two dHex, one Kdo and one Ko residue whereas peak **OS2** at *m/z* 2245.3 corresponded to the dodecasaccharide carrying the adjunctive Hex-HexNAc-HexNAc trisaccharide ($\Delta m/z \cong 568$ Th from **OS1**), confirming above structural assignments. The same mass region also comprised ion peaks deriving from a mixture of tetra- and penta-acylated lipid A; species $\mathbf{L_1}$ at *m/z* 1444.0 matched with a tetra-acylated bis-phosphorylated disaccharide backbone carrying in ester linkage one 14:0 (3-OH) and in amide linkage two 16:0 (3-OH) acyl chains, one of which, on the GlcN II, was further substituted by a secondary 14:0 fatty acid (30). Species $\mathbf{L_2}$ and $\mathbf{L_3}$ were tetra-acylated Lipids A carrying one and two Ara4N (4-deoxy-4-amino- arabinose) residues (see table 1). Species $\mathbf{L_4}$ (*m/z* 1670.2), $\mathbf{L_5}$ (*m/z* 1801.3) and $\mathbf{L_6}$ (*m/z* 1932.5) were the penta-acylated Lipids A carrying two ester-linked 14:0 (3-OH) and zero, one and two Ara4N residues respectively.

The location of the secondary fatty acid 14:0 on the GlcN II was moreover identified by mass spectrometry analysis of the lipid A moiety after acetate buffer hydrolysis. The positive ion MALDI mass spectrum (not shown), presented an in-source fragmentation due to the rupture of the glycosydic linkage between the lipid A GlcN units, thus giving rise to a triacylated oxonium ion at m/z 933.10 carrying one 14:0 (3-OH), one 14:0, and one 16:0 (3-OH) residue at the non-reducing GlcN unit. In order to assign the secondary fatty acid position, the LOS was hydrolyzed with ammonium hydroxide[2] and the obtained product was again analyzed by MALDI MS (not shown).

Assignment of the main LOS molecular ions (figure 15b) emerged from the combination of the lipid A moieties and the core oligosaccharides. Species composed by tetra-acylated and penta-acylated lipid A and **OS1** were found. A minor peak was moreover identified at m/z 3439.3 and assigned to the species $\mathbf{L_2}$**+OS1** bearing in addition the QuiNAc unit at

core oligosaccharide. At higher masses, species resulting by the combination of **OS2** and tetra and penta-acylated lipid A were also present.

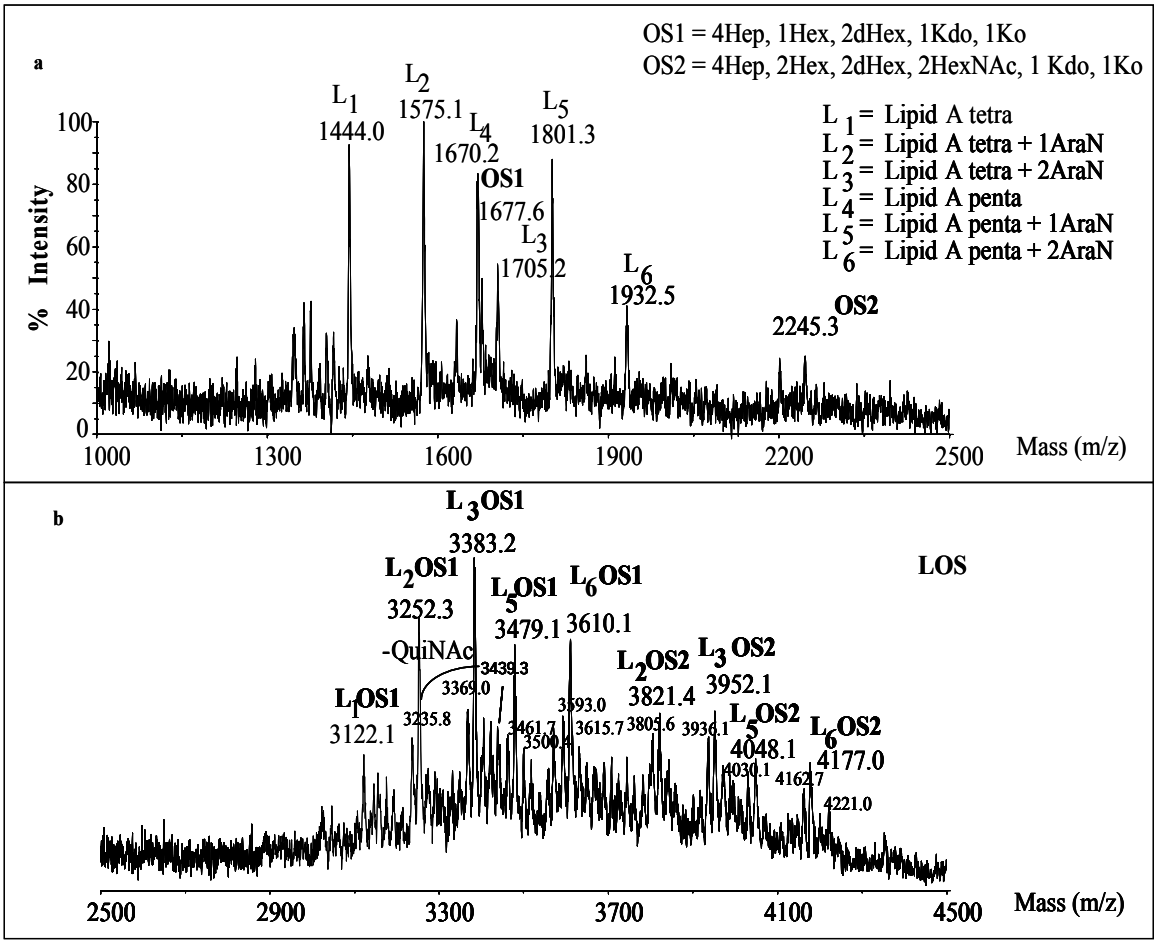

Figure 15. Negative ion MALDI mass spectrum of intact LOS from *B.multivorans* pre-transplantation. a) Low mass-range (1000-2500 Th): in this region, ion fragments due to *core* oligosaccharides OS1 and OS2 and to Lipid A species are present. b) High mass range (2500-4500 Th): in this region peaks due to intact LOS molecular ions are present.

3.7.Structural characterization by MALDI-MS of the intact LOS from *B. multivorans* post-transplantation.

MALDI MS analysis of LOS isolated from the bacterial strain after lung transplantation was performed as well, as shown in figure 16. Also in this case either peaks attributable to intact LOS or ions related to fragments *core* and lipid A were visible. In the mass-range between 1000 and 2500 Th (figure 16a), species **OS1** at *m/z* 1677.7 and **OS2** at *m/z* 2245.1 were identical to those observed in the LOS from *B. multivorans* pre-transplantation. In accordance to compositional analysis, a peak at *m/z* 1808.5 ($\Delta m/z \cong 131$) corresponding to **OS1** oligosaccharide carrying an Ara4N unit linked to Ko was identified. With regard to

Lipid A moieties, here were found predominantly the tetra-acylated $\mathbf{L_1}$ and $\mathbf{L_2}$ species differing by one Ara4N residue, being $\mathbf{L_3}$,$\mathbf{L_4}$ and $\mathbf{L_5}$ Lipid A present only in minor amount. Penta-acylated species $\mathbf{L_6}$ with two Ara4N residues was not detected. The MS profile related to LOS molecular ions (figure 16b) showed peaks reflecting quantitatively the relative amount of lipid A species. The main ion peaks were given by the combination of **OS1** with tetra-acylated lipid A ($\mathbf{L_1}$+**OS1** at *m/z* 3122.2, $\mathbf{L_2}$+**OS1** at *m/z* 3253.1 and $\mathbf{L_3}$+**OS1** at *m/z* 3384.1). The possibility to have an AraN residue linked non-stoichiometrically to the lipid A or to the core region led to multiple assignments, as indicated in figure 16b. Also in this spectrum, an ion peak at *m/z* 3439.9 was present owing to the non stoichiometric amount of terminal QuiNAc residue.

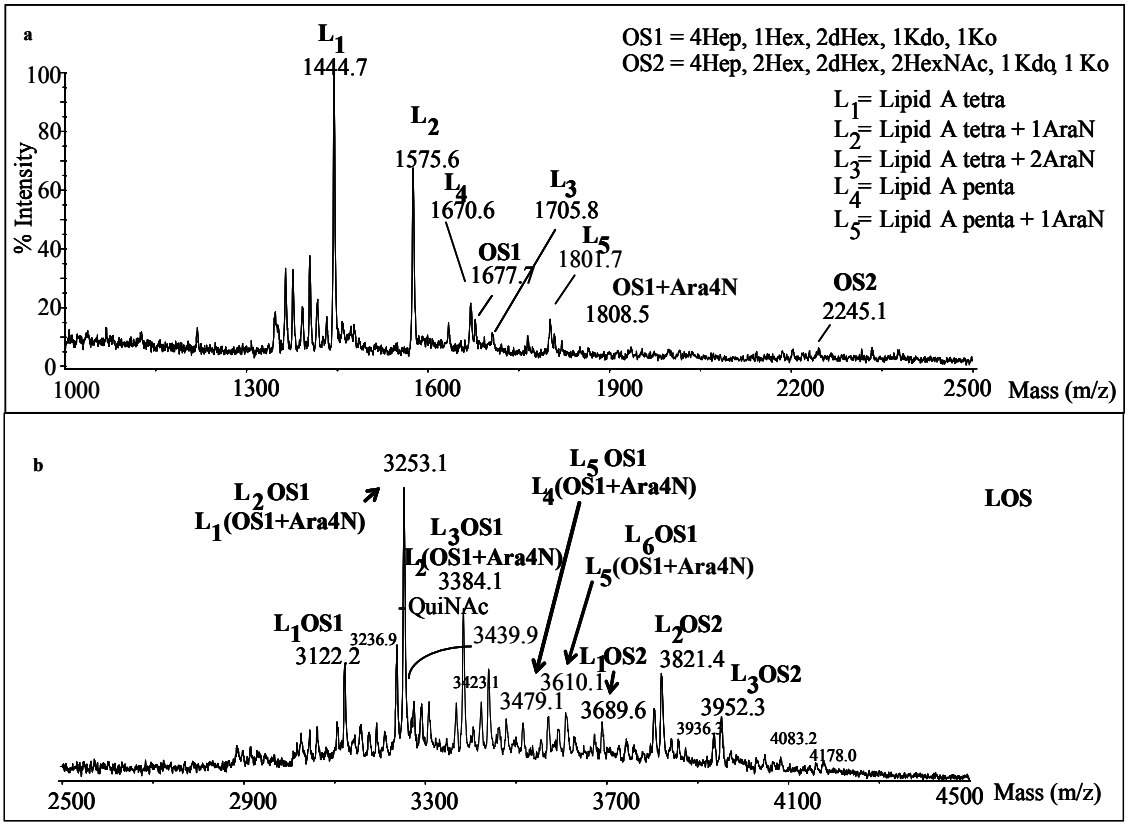

Figure 16. Negative ion MALDI mass spectrum of intact LOS from *B.multivorans* post-transplantation. a)In the low mass-range it is noteworthy the presence of oligosaccharide specie OS1 carrying an additional Ara4N residue. b) High mass region of the same spectrum: the majority of peaks originate from multiply assigments due to non-stoichiometric linkage of a Ara4N residue with the *core* portion or the lipid A species.

The above MS results on intact LOSs are consistent with the previous structural hypotheses allowing us to acquire further definite molecular details.

It is worth of note that such precise and punctual MS approach on LPS like molecules discloses new avenues on the analysis on such molecules since it is carried out on the intact endotoxin and thus excludes any structural alteration owing to samples manipulation.

3.8 Biological activity of *B. multivorans* pre and post transplantation LOSs and lipid A moieties.

The LOS molecules isolated pre- and post- lung transplantation were tested for their pro-inflammatory activity of eliciting TNF-alpha induction from human myelomonocytic U937 cells (figure 17a). Key Histograms represent TNF induction (ng) at 24 hours. U937 cells were stimulated with 100ng of purified LPS including E. coli O55 as positive control. US represents unstimulated cells (negative control). Purified LPS from strains LMG 14273 (*B. multivorans*) and LMG 12614 (*B. cenocepacia* ET-12) as previously reported[3] was also used as comparators. "Pre" represents the TNF induction elicited by the pre-transplant clonal *B. multivorans* strain. "Post" represents the biological activity of 100ng of extracted LOS from the post transplant strain and was significantly lower than the pre-transplant strain ($p<0.001$). Herein it has been confirmed a previous findings that LMG 12614 (*B. cenocepacia* ET-12 epidemic strain) and *E. coli 055* were more potent TNF-alpha inducers than any of the *B. multivorans* strains tested (LMG 14273 and the paired pre and post transplant strains).

In figures 17b and 17c was reported the NF-KB induction elicited by extracted lipid A and LPS/LOS in transfected TLR 4 / MD2 / CD 14 HEK cell lines. In figures pre- and post- represent a *B. multivorans* strain pre transplantation and post transplantation respectively at doses of 10ng/ml (vertical striped bar) or 100ng/ml (checkerboard bar). Negative Control (culture media only) is represented by C (open bar) and *E. coli* (closed bar) represents the biological activity of 10ng/ml of the positive control *E. coli 055* LPS. The reporter assay is measured in relative light units (RLU). There was, in general, a greater biological activity at induction of NF KB observed for the LOS as compared to the extracted lipid A, thus implying a biological role also for the core region. All stimulants were relatively potent attaining similar levels of NF-KB at ng concentrations. The biological activity of the *B. multivorans* strains were however less potent than that achieved by the *B. cenocepacia* ET-12 strain (not shown). Moreover, the lipid A isolated prior to transplantation from the *B. multivorans* strain induced greater activation in the NF-KB reporter assay than after transplantation, although these differences were not statistically significant. This confirms

the significant differences observed in the cytokine output in the U937 assay that were likely to reflect signaling through the TLR4/MD2 complex.

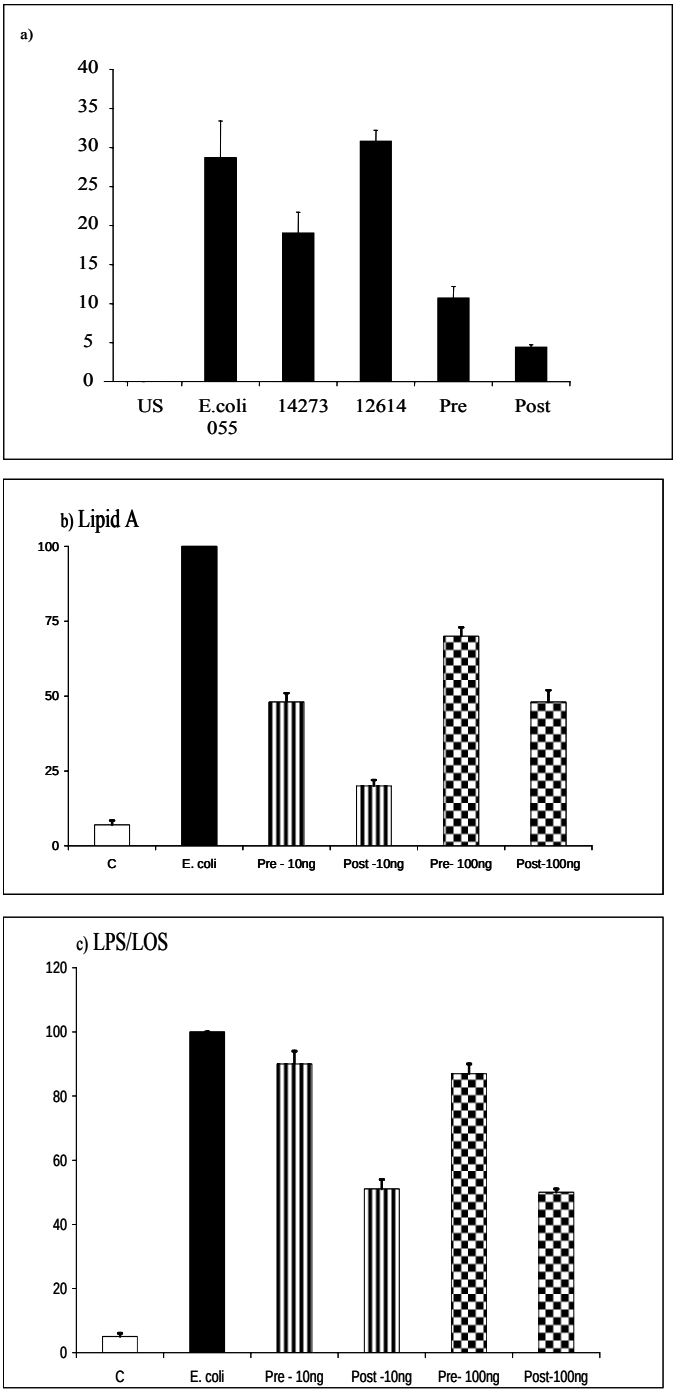

Figure 17. Biological assays of pre- and post- transplantation isolated LOS and Lipid A moieties a) TNF induction from U937 cells elicited by standard LPS and paired clonal strains. b, c) NF-KB induction elicited by extracted lipid A and LPS/LOS in transfected TLR 4 / MD2 / CD 14 HEK cell lines.

3. 9 Discussion

The analysis of core oligosaccharide from *Burkholderia multivorans* pre- and post- lung transplantation clinical isolates revealed a novel oligosaccharide core structure.

The *Burkholderia* genus has a highly conservative LPS inner core structure with several characteristics replicated in the current study. The main feature is the presence in the inner core of the [3,4-α-L,D-Hep-(1→5)-α-D-Kdo-(4→2)-α-D-Ko] trisaccharide.[4] Notably, within the genus, the Ko residue is frequently not terminal but further links an Ara4N residue that, in the case analyzed herein, is only present in the post-transplantation strain. The heptose residue bears in the main sugar chain another heptose linked at C-3 and glycosilated at C-4 by a β-D-Glc; this latter can be optionally glycosilated either by terminal α-Glc[5,6] or by a terminal α-Hep, as in this case, composing a Hep-(1→6)-Glc disaccharide. Moreover, in the outer core region, the presence of a non-stoichiometric [β-D-Glc-(1→3)-β-D-GalNAc-(1→3)-α-D-GalNAc] trisaccharide sitting on a rhamnose residue is noteworthy as it is likely pre-assembled and then attached.

The main structural changes between the clonal strains were found in the different distribution of the lipid A species. The lipid A moiety from both species possessed a carbohydrate backbone characterized by a [P→4-β-D-Glc*p*N-(1→6)-α-D-Glc*p*N-1→P→Ara4N] sequence, already found in other Bcc genomovars.[4] The lipid A from *B. multivorans* pre-transplantation comprised a mixture of penta- and tetra-acylated species in similar proportions carrying up to two Ara4N residues. The post-transplantation *B. multivorans* strains' LPS demonstrated marked changes in the distribution and composition of lipid A species with an overall lower level of acylation and substitution by Ara4N. In particular, there was a negligible amount of penta-acylated species with a predominance of tetra-acylated lipid A. Furthermore, each species carried no more than one Ara4N residue.

The core oligosaccharide sequence of *B. multivorans* species investigated was distinct from that of *B. cenocepacia*.[5] It has been postulated that *B. cenocepacia* biological activity and survival is in part dependent on the presence of a complete LOS as a *B. cenocepacia* mutant strain lacking a complete LPS core oligosaccharide is sensitive to the antimicrobial peptides and polymyxin B.[7] Moreover, in *B. multivorans*, a superior activity at induction of NF-KB was observed for the complete LOS as compared to lipid A (figure 17b,c), indicating a function for the core region as well. The differences in the core oligosaccharide between the two genomovars could contribute to clinical phenotypes (inflammatory syndromes). The core portion in *B. multivorans* contributed to the bacterial

resistance to antimicrobial compounds. The net charge surface on the external membrane of Gram negative bacteria is felt to play a key role in pathogenesis. LPS from the *Burkholderia* genus are frequently positively charged or in an isoelectric state. This is closely related to the abundance of aminoarabinose (Ara4N) residues present in the lipid A-inner core and confers resistance to antibiotic compounds and host cationic antimicrobial peptides. In physiological conditions Ara4N moieties are positively charged and reduce the net charge surface on the external membrane weakening the ionic attraction for respiratory tract antimicrobial defensins. The inherent resistance of these microorganisms to polymyxin B, a cyclic polycationic antibiotic peptide that has highly affinity for negatively charged bacterial LPS, is likely to be Ara4N dependent. These residues prevent the antimicrobial action of polymyxin B, namely increasing permeability in bacterial outer membrane.[8]

Peri-transplant processes that promote increased bacterial defensin resistance are suggested by the observation of a new Ara4N moiety on the inner core portion of lipid A from *B. multivorans* post-transplantation. There are many possible explanations for this observation including the effect of antibiotics administered during the transplant operation. It is interesting to speculate that, post transplantation, the replacement of CF epithelium with a normal airway epithelium would increase defensin activity by normalising high airway sodium content (a known inhibitor of defensin activity).

In addition, the correlation between increasing acylation of lipid A with a greater cytokine induction capacity has previously been reported in *Pseudomonas*[9] and *Burkholderia*.[3] The lipid A from *B. multivorans* pre-transplantation had a comparable amount of penta and tetra-acylated lipid A species and a notable abundance of Ara4N moieties. Interestingly, the lipid A from *B. multivorans* post-transplantation was less toxic in our U937 cell and HEK TLR4/MD2 bioreporter assays. These data confirm the lipid A changes are recognized at the human TLR-4 receptor. A reduction in cytokine induction may allow bacteria to survive in a more hostile environment.[10-12]

In the new environment post transplantation, *B. multivorans* decreases the immunostimulant activity of lipid A by decreasing its acylation pattern and reducing the consequent host immune response. A further adaptation that increases the antimicrobial resistance, is the addition of an Ara4N residue to the outer core Ko residue. This has been recognised as central in the bacterial ability to resist to cationic antimicrobial compounds and antibiotic as β-lactams.

Further elucidation of controllers of acylation status may offer the development of therapeutic strategies and new treatments for the management of Gram negative infections in Cystic Fibrosis.

References

1. Ieranò T, Silipo A, Sturiale L, Garozzo D, Brookes H, Khan CM, Bryant C, Gould FK, Corris PA, Lanzetta R, Parrilli M, De Soyza A, Molinaro A. The structure and pro-inflammatory activity of the lipopolysaccharide from *Burkholderia multivorans* and the differences between clonal strains colonizing pre- and post-transplanted lungs. *Glycobiology* (2008) 18: 871-81.
2. Silipo A, Lanzetta R, Amoresano A, Parrilli M, Molinaro A.. Ammonium hydroxide hydrolysis: a valuable support in the MALDI-TOF mass spectrometry analysis of lipid A fatty acid distribution. *J. Lipid Res.* (2002) 43: 2188-2195.
3. De Soyza A, Ellis CD, Khan CMA, Corris PA, Demarco de Hormaeche R. *Burkholderia cenocepacia* lipopolysaccharide, lipid A, and proinflammatory activity. *Am. J. Respir. Crit. Care Med* (2004). 170: 70-77.
4. De Soyza A, Silipo A, Lanzetta R, Govan JR, Molinaro A. Chemical and biological features of *Burkholderia cepacia* complex lipopolysaccharides. *Innate Immun*. (2008) 14: 127-144.
5. Silipo A, Molinaro A, Ieranò T, De Soyza A, Sturiale L, Garozzo D, Aldridge C, Corris PA, Khan, CMA, Lanzetta R, Parrilli M. The complete structure and pro-inflammatory activity of the lipooligosaccharide of the highly epidemic and virulent Gram-negative bacterium *Burkholderia cenocepacia* ET-12 (Strain J2315). *Chem. Eur. J.* (2007) 13: 3501– 3511.
6. Molinaro A, De Castro C, Lanzetta R, Evidente A, Parrilli M, Holst O. Lipopolysaccharides possessing two L-glycero-D-manno-heptopyranosyl-alpha-(1-->5)-3-deoxy-D-manno-oct-2-ulopyranosonic acid moieties in the core region. The structure of the core region of the lipopolysaccharides from *Burkholderia caryophylli*. *J. Biol. Chem.* (2002) 277: 10058-10063.
7. Loutet SA, Flannagan RS, Kooi C, Sokol PA, Valvano MA. A complete lipopolysaccharide inner core oligosaccharide is required for resistance of *Burkholderia cenocepacia* to antimicrobial peptides and bacterial survival in vivo. *J. Bacteriol.* (2006) 188: 2073-2080.
8. Shimomura H, Matsuura M, Saito S, Hirai Y, Isshiki Y, Kawahara K. Unusual interaction of a lipopolysaccharide isolated from *Burkholderia cepacia* with polymyxin B. *Inf. & Immun* (2003).71: 5225-5230.
9. Ernst RK, Yi EC, Guo L, Lim KB, Burns JL, Hackett M, Miller SI. Specific lipopolysaccharide found in cystic fibrosis airway *Pseudomonas aeruginosa*. *Science* (1999) 286: 1561-1565.
10. Reife RA, Coats SR, Al-Qutub M, Dixon DR, Braham PA, Billharz RJ, Howald WN, Darveau RP. Porphyromonas gingivalis lipopolysaccharide lipid A heterogeneity: differential activities of tetra- and penta-acylated lipid A structures on E-selectin expression and TLR4 recognition. *Cell. Microbiol*. (2006) 8: 857-868.

11. Munford RS, Varley AW. Shield as signal: lipopolysaccharides and the evolution of immunity to gram-negative bacteria. *Plos Pathogens* (2006) 2 : e67.
12. Raetz CR, Reynolds CM, Trent MS, Bishop RE. Lipid A modification systems in Gram-negative bacteria. *Annu Rev Biochem.*(2007) 76:295-329.

Chapter 4

STRUCTURAL CHARACTERIZATION OF *BURKHOLDERIA VIETNAMIENSIS* LIPOOLIGOSACCHARIDE FROM CYSTIC FIBROSIS ASSOCIATED LUNG TRANSPLANTATION STRAINS

Burkholderia vietnamiensis is a Gram-negative bacterium initially characterized from a group of nitrogen-fixing bacteria colonizing the rhizosphere of rice cultivated in Vietnam.[1] Later, this strain was found to correspond to the *genomovar* V species belonging to the *Burkholderia cepacia* complex isolated from CF patients.[2] Herein it has been described the complete structure and pro inflammatory activity of the endotoxin from *B. vietnamiensis*.[3] The work is focused on the analysis of two LOS extracted from clonal strains of *B. vietnamiensis* (see chapter 3): one isolated from a CF patient prior to transplantation (interacting with CF epithelium) and its clonal strain isolated post lung transplantation (interacting with normal donor lung epithelium). Since the endotoxin analysed belongs to clonal strains isolated in CF airways pre and post lung transplantation we can pursue the hypothesis that endotoxin structural changes through chemical modulation of LPS alters bacterial mechanisms of adaptation to different biological niches such as the end stage CF lung as compared to the normal lung allograft.

4.1 Isolation, SDS electrophoresis analysis of *B. vietnamiensis* LOSs.

B. vietnamiensis paired strains known to be of clonal origin, based on pulsed field gel electrophoresis experiments, were then prepared for LPS extraction. LPS was isolated according to usual hot phenol-water protocol (see section III). SDS-PAGE of *B. vietnamiensis* LPS fraction revealed that the extracted *B. vietnamiensis* lipopolysaccharide was a rough type LPS, i.e., a lipooligosaccharide (LOS). Further, as for clonal strains of *B. multivorans* and *B. cenocepacia* (paragraph 3.1), the analysis revealed an alteration in migration patterns between the LOS isolated from the pre and post transplantation strain.

4.2. Isolation and structural characterization of oligosaccharide fractions from *B. vietnamiensis* pre and post- transplantation LOS.

Monosaccharide analysis yielded same results either for LOS isolated pre- or post-transplantation, all sugar residues were in pyranose rings (see section III). All the results obtained on the products analysed are reported in table 3. Fatty acids analysis revealed in both cases the presence of (*R*)-3-hydroxyhexadecanoic (16:0 (3-OH)) in amide linkage and (*R*)-3-hydroxytetradecanoic (14:0 (3-OH)) acid and tetradecanoic acid (14:0) in ester linkage. The overall chemical composition of lipid A matched with the archetypal structure of *Burkholderia* lipid A.

Assignment	LOS *B.vietnamiensis* pre-transplantation	Oligosaccharide fraction isolated pre-transplantation	LOS *B.vietnamiensis* post-transplantation	Oligosaccharide fraction isolated post-transplantation
3,4-substitued L,D-Hep	X	X	X	X
2,3,7-substitued L,D-Hep	X	X	X	X
terminal L,D-Hep	X	X	X	X
7-substitued L,D-Hep	X	X	X	X
terminal D-Glc	X	X	X	X
terminal D-Gal	X	X	X	X
terminal L-Rha	X	X	X	X
terminal L-Ara4N	X	-	X	-
6-substitued D-GlcN	X	-	X	-
3-substitued D-GalN	X	X	X	X
4,5-substitued Kdo	X	X	X	X
terminal Ko	X	X	X	X

Table 3 Monosaccharide composition of pre and post transplantation LOS.

A mild acid hydrolysis promoted by acetate buffer, carried out on pre and post-transplantation LOSs molecules, yielded in both cases an oligosaccharide fraction that was purified by gel permeation chromatography (section III). Monosaccharide analysis of both fractions (reported in table 3) and 1D NMR analysis gave the evidence of two identical oligosaccharides portions isolated from the two LOSs analysed.

A combination of homo- and heteronuclear 2D NMR experiments (DQF-COSY, TOCSY, ROESY, ^{1}H-^{13}C HSQC, ^{1}H-^{13}C HSQC-TOCSY and ^{1}H-^{13}C HMBC, see section III) was executed on the most abundant product, i.e. the oligosaccharide fraction isolated post lung transplantation, in order to assign all the spin systems and to define the monosaccharide

sequence. In the anomeric region of the ^{1}H-NMR spectrum (figure 18a) ten anomeric signals were identified (**A-L**, table 4); the signals at 1.97/2.01 ppm were endorsed as the H-3 methylene protons of the Kdo residue. The relative intensities and the shifts of anomeric signals suggested a marked heterogeneity typical of a mixture of oligosaccharides, likely due to the presence of non-stoichiometric carbohydrate substitutions and to the presence of a reducing end.

Spin systems **A, B, D, E, F** (table 4), were all identified as α-heptose residues, as indicated by their $^{3}J_{H1,H2}$ and $^{3}J_{H2,H3}$ coupling constants (below 3 Hz) and by the *intra*-residual NOE of H-1 with H-2. The ^{13}C chemical shift values of C-6 of these heptose residues (all below 71 ppm) confirmed these as L-*glycero*-D-*manno*-heptose, in accordance with the chemical analysis.

Spin systems **C** and **G** (H-1 at 4.97 and 4.70 ppm, respectively) were identified as 2-deoxy-2-acetamido-D-galactose, as indicated by their $^{3}J_{H3,H4}$ and $^{3}J_{H4,H5}$ values (3 Hz and 1 Hz, respectively) diagnostic of a *galacto*-configuration. The ^{1}H-^{13}C HSQC spectrum showed the correlation of both H-2 **C** (4.29 ppm) and H-2 **G** (4.00 ppm) with nitrogen bearing carbon signals at 47.9 ppm and at 51.38 ppm, respectively. The down-field shift of proton resonances of both H-2 were diagnostic of *N*-acetylation at these positions. The chemical shifts of H-1 and C-1 of residue C (4.97 and 92.63 ppm), the $^{3}J_{H1,H2}$ coupling constant (3.2 Hz) and the *intra*-residual NOE contact of H-1 with H-2 were all in agreement with α-anomeric configuration of residue **C**; the chemical shifts of H-1 and C-1 of residue **G** (4.70 and 100.6 ppm respectively), the $^{3}J_{H1,H2}$ value (8.2 Hz) and the *intra*-residual NOE contact of H-1 with H-3 and H-5 evidenced a β-anomeric configuration for this residue.

Spin system **I** (table 4) was identified as glucose, as indicated by the large $^{3}J_{H,H}$ values of ring protons (above 10 Hz). The strong *intra*-residue NOE contacts of H-1 with H-3 and H-5 together and the $^{3}J_{H1,H2}$ coupling constant (7.8 Hz) were diagnostic of β-anomeric configuration.

Residue **L** was identified as a β-galactose as attested by $^{3}J_{H3,H4}$ and $^{3}J_{H4,H5}$ low values, and by the presence of the *intra*-residual NOE contact of H-1 with H-3 and H-5.

Residues **H** (H-1 at 4.69 ppm) was recognized as a α-rhamnose residue since, in TOCSY spectrum, scalar correlations of the ring protons with methyl signals in the shielded region at 1.16 ppm were visible. The *manno* configuration of these spin system was established by $^{3}J_{H1,H2}$ and $^{3}J_{H2,H3}$ values (below 3 Hz) whereas the α-configuration was assigned by the *intra*-residual NOE contact of H-1with H-2 and chemical shift of its H-5 and C-5.

The spin system of Kdo **K** has been assigned starting from the diastereotopic H-3 methylene proton signals, resonating at 1.97 and 2.01 ppm ($H\text{-}3_{ax}$ and $H\text{-}3_{eq}$, respectively). Because of its free reducing end, the Kdo residue was present in multiple forms, nevertheless, the signals belonging to the α-reducing unit were clearly assignable. Residue **J**, D-*glycero*-D-*talo*-oct-2-ulosonic acid (Ko) was detected by the presence of the characteristic *inter*-residue NOE contact, in 2D ROESY spectra, between H_{3eq} of Kdo moiety **K** and H-6 of Ko (**J**) that is also diagnostic for the α-D-Ko-(2→4)-α-D-Kdo linkage.[4,5] As consequence of Kdo heterogeneity also the close Ko residue was present as multiple spin systems and only the major one has been fully assigned.

The oligosaccharide sequence was established on the basis of the interesidual NOE contacts identified in the ROESY spectrum (figure 18b) and the long range scalar correlations present in the HMBC spectrum (not shown).

The linkage of the heptose **B** to O-5 of Kdo **K** was proven by the NOE connectivity between H-1 of the heptose **B** (5.18 ppm) and H-5 of Kdo (4.13 ppm). Given the L,D relative configuration of heptose **B**, the presence of further NOE contacts between H-1 of the heptose **B** and H-6 and H-7 of **K** ultimately proved D-configuration for Kdo residue (Bock et al., 1994).

Residue **B** was in turn substituted at O-3 and O-4. The NOE contacts (figure 18b) of H-4 and H-3 B, with H-1 of residue **I** (4.45 ppm) evidenced that the O-4 of α-heptose B was glycosylated by residue **I** of β-glucose. Residue **B** was also substituted at O-3 by residue **A** of α-heptose, according to the NOEs (Figure 18b) of H-3 and H-2 **B** with H-1 **A** (5.29 ppm).

Unit **A** was glycosylated at O-2 by the rhamnose residue **H**, as demonstrated by the NOE contacts of H-1 **H** (4.69 ppm) with H-1 and H-2 **A** (5.29 and 4.13 ppm). Residue **A** was also substituted at O-3 by the β-GalNAc **G** as confirmed by the strong NOE contacts between H-1 **G** and H-3 **A**. Eventually, residue **A** was also glycosylated at O-7 by the terminal α-heptose **F**, as attested by the NOE contact between H-1 **F** and H-7 **A**. An alternative spin system was identifiable for residue **F**, namely residue **E**, recognized as a 7-α-substituted heptose that was, in turn, non stoichiometrically glycosylated at position 7 by the α-heptose **D**, as shown by the NOE contact of H-7 **E** (3.61 ppm) with H-1 **D** (4.81 ppm).

β-GalNAc residue **G** was glycosylated at O-3 by residue **C** as attested by the NOE contact of H-3 **G** with H-1 of residue **C**. Additionally, residue **C** was glycosylated at position 3 by

the terminal β-Gal **L** as proven by the NOE contact between H-1 of residue **L** and H-3 of residue **C**.

Thus in summary, methylation analysis, MS (see below) and 2D NMR data allowed to establish the overall oligosaccharide sequence for the post transplantation LPS and is reported below.

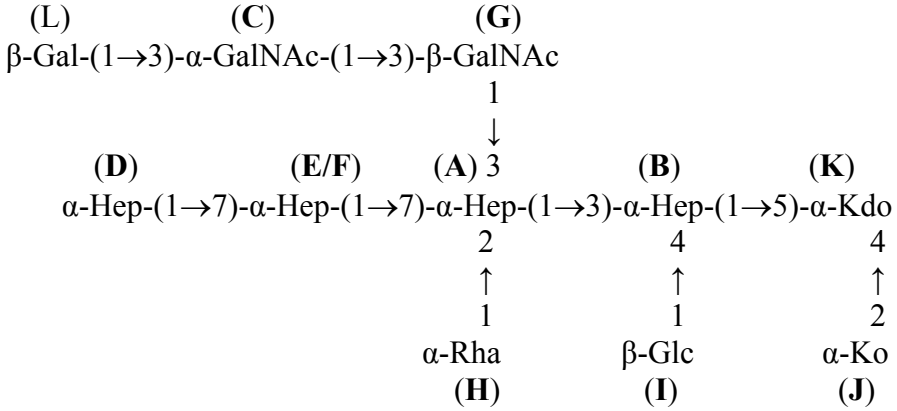

Chemical shift δ ($^{1}H/^{13}C$)								
Unit	**1**	**2**	**3**	**4**	**5**	**6**	**7**	**8**
A	5.29	4.13	3.97	3.88	3.64	3.96	3.60	
2,3,7-α-Hep	98.08	77.69	79.48	68.80	72.90	70.40	70.50	
B	5.18	3.95	4.03	4.20	4.11	3.96	3.90/3.67	
3,4-α-Hep	98.54	71.70	71.80	72.70	72.20	68.70	63.70	
C	4.97	4.29	3.67	4.16	3.70	3.84/3.72		
3-α-GalN	92.63	47.90	77.58	68.53	71.20	61.50		
D	4.81	3.85	3.76	3.76	3.56	4.02	3.57/3.87	
t-α-Hep	101.78	70.00	70.40	70.40	71.89	68.40	62.70	
E	4.80	3.87	3.72	3.72	3.53	3.95	3.61	
7-α-Hep	100.88	68.80	71.60	71.60	72.05	70.40	70.45	
F	4.79	3.87	3.72	3.72	3.51	4.02	3.66/3.89	
t-α-Hep	100.09	68.8	71.6	71.6	71.9	68.40	63.05	
G	4.70	4.00	3.69	3.84	3.58	3.72/3.65		
3-β̃-GalN	100.60	51.38	74.90	70.03	74.30	60.80		
H	4.69	3.86	3.76	3.26	3.87	1.16		
t-α-Rha	97.45	68.80	70.20	72.26	69.70	17.45		
I	4.45	3.17	3.38	3.26	3.36	3.85/3.69		
t-β-Glc	102.10	73.57	75.58	70.16	77.16	61.40		
L	4.32	3.40	3.53	3.81	3.62	3.63/3.70		
t-β-Gal	105.27	70.50	72.26	68.50	75.01	60.80		
J	---	---	3.74.	3.91	4.00	3.56	3.97	3.88/3.68
t-α-Ko	n.d.	n.d.	70.80	71.80	71.70	71.90	71.80	63.80
K	---	---	1.97/2.01	4.00	4.13	3.71	3.92	3.89/3.67
4,5-α -Kdo	n.d.	n.d.	34.80	71.60	68.40	71.50	71.80	63.70

Table 4. ^{1}H and ^{13}C NMR chemical shifts (ppm) of sugar residues of the core region of the LOS extracted from *B. vietnamiensis* strain isolated post lung transplantation (n.d.= not detected)

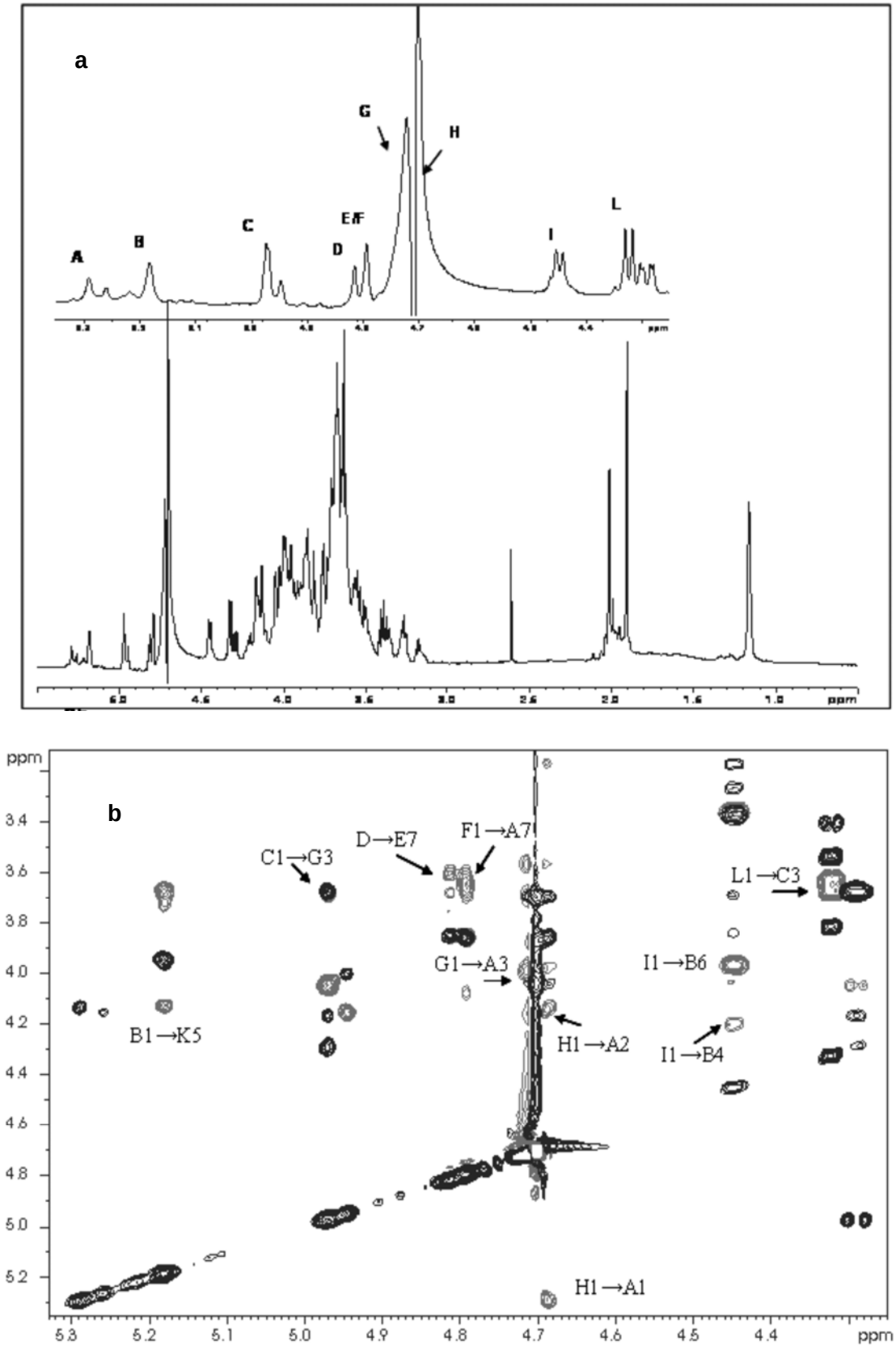

Figure 18. NMR spectra of oligosaccharidic fraction isolated post lung transplantation. a)^{1}H NMR spectrum with zoom of anomeric region. b) zoomed region of overlapped ROESY (grey) and TOCSY (black) 2D NMR spectra in which *intra*-residue NOE contacts are reported

4.3. Structural characterization by MALDI mass spectrometry of the intact LOS from *B. vietnamiensis* pre-transplantation

Intact endotoxins were analysed by MALDI-MS in order to gain further information on both lipid A and core regions. This approach is very useful since allows the study of integral LOS molecules, without any chemical manipulation, preventing the loss (either by alkaline or acid treatment) of labile groups typically present on LPSs such as phosphate, acetyl and others. LOS were analysed by using a sample preparation procedure specifically set up for such amphiphilic molecules (section III). The negative ion MALDI mass spectrum of intact pre- transplantation LOS is shown in figure 19. The spectrum presented, besides the molecular ions in the mass range 3300-4300 *m/z*, (figure 19b), fragments between 1400 and 2300 *m/z*, originating from the cleavage of the labile glycoside bond between Kdo and the lipid A moiety (figure 19a) and that yields either OS oligosaccharide ions or lipid A ions, thus it is very informative.[6] Particularly, the OS peak at *m/z* 1907.0 matched with a decasaccharide constituted of three Hep, two Hex, two HexNAc, one dHex, one Kdo, and one Ko residue, i.e., the mimimum core oligosaccharide structure described above by NMR spectroscopy. Other oligosaccharides, at *m/z* 2099.7 (OS + Hep), and at *m/z* 2291.7 (OS + 2 Hep), were also present, even though the latter was not detected in NMR analysis. The same mass region also encompassed ion peaks deriving by the presence of a mixture of tetra and penta-acylated lipid A (see figure 19a). Species $\mathbf{L_1}$ at *m/z* 1444.4 matched with a tetra-acylated bis-phosphorylated disaccharide backbone carrying in ester linkage one 14:0 (3-OH) and in amide linkage two 16:0 (3-OH) acyl chains, one of which, on the GlcN II, was further substituted by a secondary 14:0 fatty acid (see below). Species $\mathbf{L_2}$ at *m/z* 1574.5 ($\Delta m/z \cong 131$ from $\mathbf{L_1}$) and $\mathbf{L_3}$ at *m/z* 1706.4 ($\Delta m/z \cong 131$ from $\mathbf{L_2}$) were tetra-acylated lipid A carrying one and two Ara4N residues. Species $\mathbf{L_4}$ (*m/z* 1670.5), $\mathbf{L_5}$ (*m/z* 1801.4) and $\mathbf{L_6}$ (*m/z* 1931.5) were consistent with the penta-acylated lipid A carrying two ester-linked 14:0 (3-OH) with no, one and or two Ara4N residues, respectively.

In analogy with other lipid A from *Burkholderia*, the position of the secondary fatty acid 14:0 on the GlcN II was identified on the GlcN II by mass spectrometry analysis of the lipid A moiety after acetate buffer hydrolysis. Briefly, the positive ion MALDI mass spectrum (not shown), presented an in-source fragmentation due to the split of the glycosidic linkage between the two GlcN units, thus giving rise to a triacylated oxonium ion at *m/z* 933.1 carrying one 14:0 (3-OH), one 14:0, and one 16:0 (3-OH) residue at the

non-reducing GlcN unit. The information were then completed by analyses of the compound obtained by with ammonium hydroxide hydrolysis.[7]

The assignment of the main LOS molecular ions (figure 19b), resulted from the combination of the lipid A moieties and the core oligosaccharide species. Species LOS composed by tetra-acylated lipid A and OS were found at *m/z* 3353.4 (**L_1**+OS), *m/z* 3484.5 (**L_2**+OS), *m/z* 3615.8 (**L_3**+OS), *m/z* 3677.3 (**L_2**+OS+Hep), and *m/z* 3808.0 (**L_3**+OS+Hep). Species constituted by penta-acylated lipid A and OS were also present at *m/z* 3711.5 (**L_5**+OS), 3842.7 (**L_6**+OS), 3903.6 (**L_5**+OS+ Hep), 4034.6 (**L_6**+OS+ Hep), and 4226.5 (matching with **L_6**+OS +2Hep).

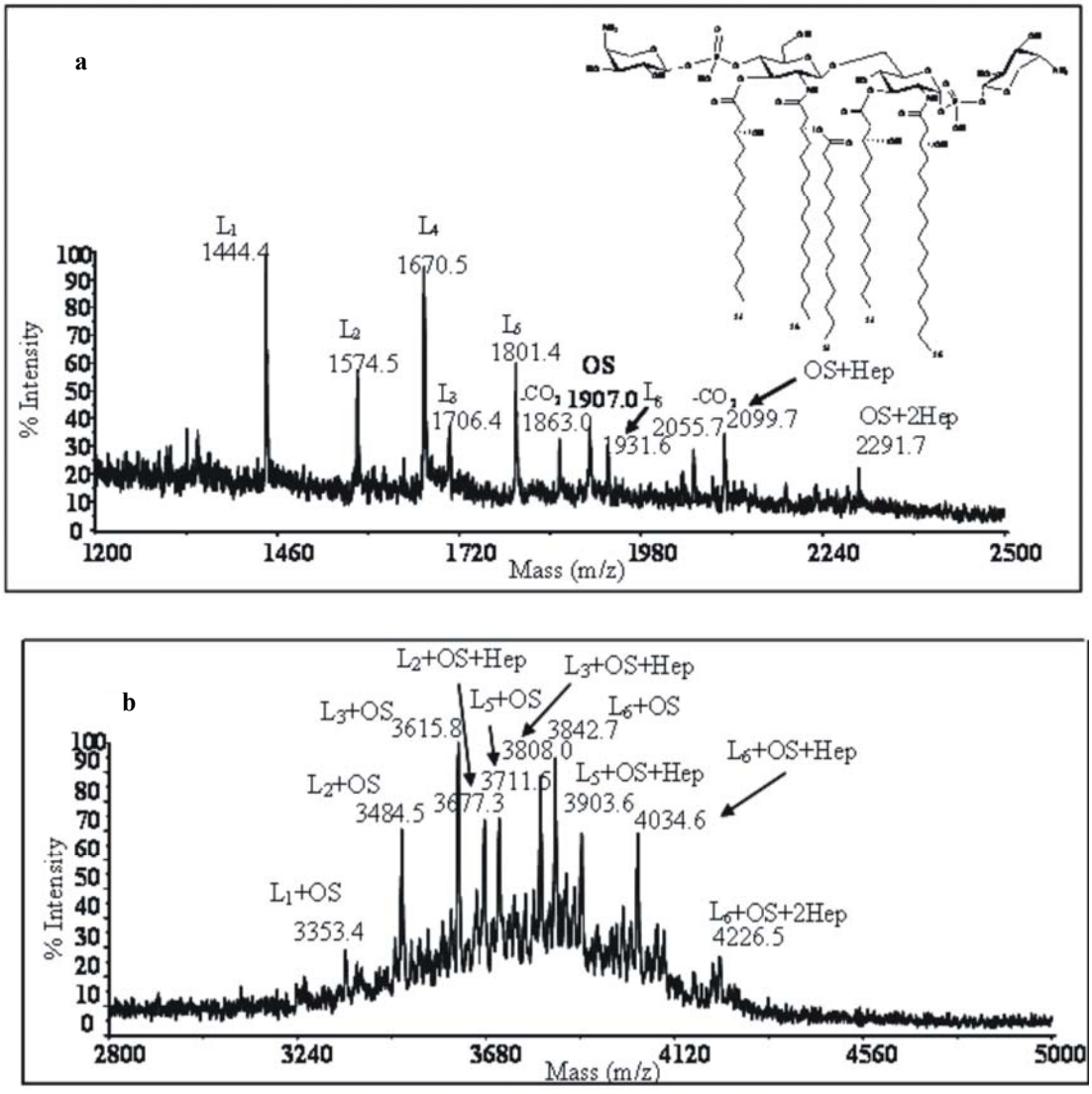

Figure19. Negative-ion MALDI mass spectrum of intact LOS isolated pre- lung transplantation. a) Low mass range (1200-2500 *m/z*). b) high mass range (2800-5000 *m/z*).

4.4. Structural characterization by MALDI-MS of the intact LOS from *B. vietnamiensis* post-transplantation

The same MALDI-MS analysis was carried out on intact LOS isolated after lung transplantation (figure 20). Even in this case ions related to fragments core and lipid A were visible in the mass-range between 1400 and 2300 *m/z* (figure 20a). As for pre-transplantation LOS the same oligosaccharide species were found, with the reference OS (at *m/z* 1907) and other ion peaks differing by one or two additional Hep residues. Conversely, post-transplantation LOS lipid A was constituted by tetra and penta-acylated species in a very different relative amount if compared to pre-transplantation lipid A. Predominantly, penta-acylated were present, and in particular $\mathbf{L_4}$ (*m/z* 1670.5), $\mathbf{L_5}$ (*m/z* 1801.5) and $\mathbf{L_6}$ (*m/z* 1932.6) bearing no, one or two Ara4N residues. $\mathbf{L_1}$ and $\mathbf{L_2}$ tetra-acylated lipid A were present only in few low amount whereas $\mathbf{L_3}$ species, with two Ara4N residues, was even not detectable.

Consequently, the MALDI-MS profile of post-transplantation LOS molecular ions (figure 20b) showed a peak distribution largely different from that found in the pre-transplantation strains since it mainly resulted by the combination of OS with penta-acylated lipid A ($\mathbf{L_4}$+OS) at *m/z* 3580.0, $\mathbf{L_5}$+OS at *m/z* 3711.0, and $\mathbf{L_6}$+OS at *m/z* 3842.4, $\mathbf{L_5}$+OS +Hep at *m/z* 3903.2, $\mathbf{L_6}$+OS +Hep at *m/z* 4034.5, $\mathbf{L_5}$+OS+ 2Hep at *m/z* 4095.8, and $\mathbf{L_6}$+OS+ 2Hep at *m/z* 4226.5. The ion species due to the combination of tetra-acylated lipid A $\mathbf{L_2}$ and OS were only present in little amount.

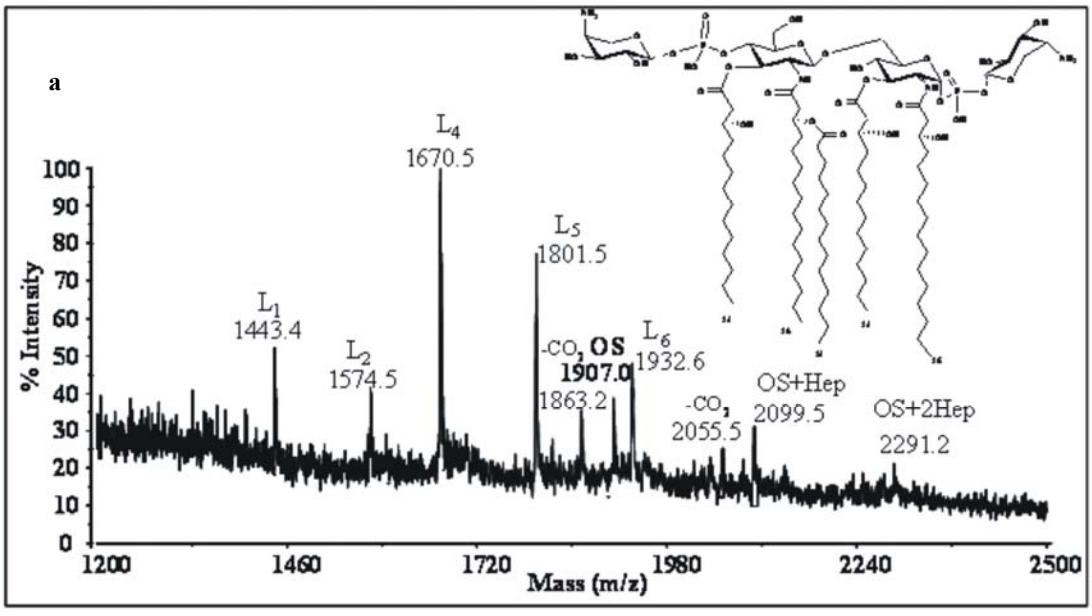

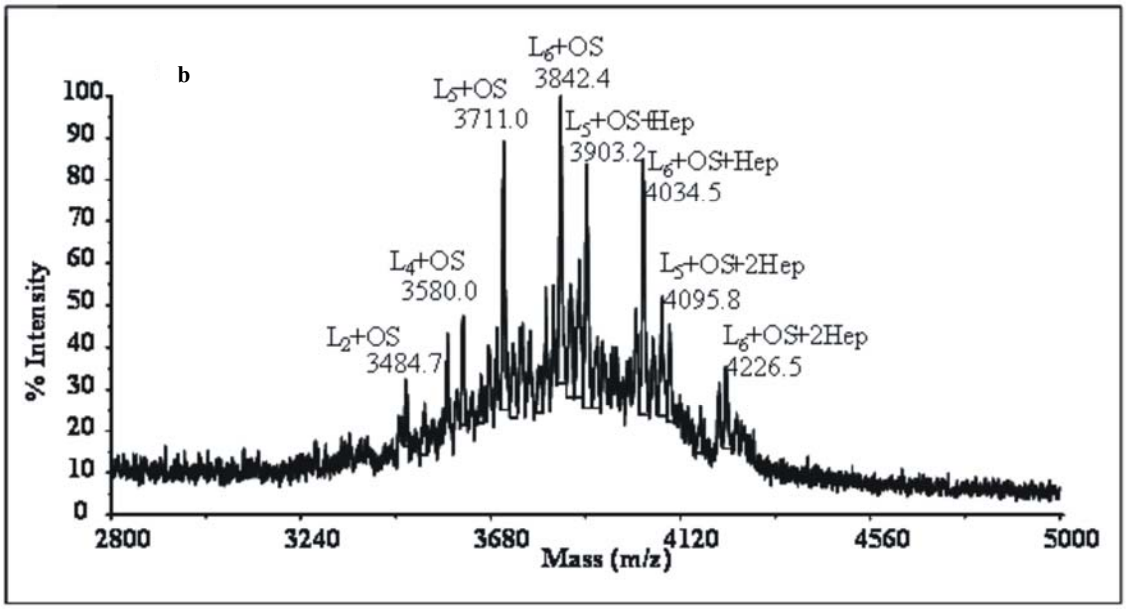

Figure20. Negative-ion MALDI mass spectrum of intact LOS isolated post- lung transplantation. a) Low mass range (1200-2500 *m/z*). b) high mass range (2800-5000 *m/z*).

4.5 Biological activity of *B. vietnamiensis* LOSs and lipid A moieties.

B. vietnamiensis LOS was tested for its pro-inflammatory activity in eliciting TNF-α induction from human myelomonocytic U937 cells (figure 21a). U937 cells were stimulated with 100ng of purified LPS including *E. coli* O55 as positive control. B.v1 pre and B.v1 post represent the TNF-α induction respectively elicited by the pre-transplant and post-transplant clonal *B. vietnamiensis* strain. These data demonstrated that statistically significantly higher TNF-α was induced by LOS extracted from the post transplantation *B. vietnamiensis* strain.

HEK 293 cell lines do not express Toll-Like receptors but can be specifically transfected with TLRs of interest and thus used to dissect pro-inflammatory signalling. The HEK cells after transfection with TLR4 and the co-signalling molecule MD2, were stimulated in quadruplicate, using doses of 10ng and 100ng of either LOS or lipid A. The effect of stimulation was assessed using a NF-kB reporter assay measured in relative light units (RLU). Stimulation with intact LOS elicited a greater response than with extracted lipid A suggesting a pro-inflammatory role for LPS core (figure 21b and 21c). Importantly the intact LOS was as strongly pro-inflammatory as the control *E. coli* in the HEK293 assay. The pattern of increased RLU induction (pro-inflammatory) activity induced by post

transplantation LOS (figure 21b) was not clearly demonstrated for the extracted post transplantation *B. vietnamiensis* lipid A (figure 21c).

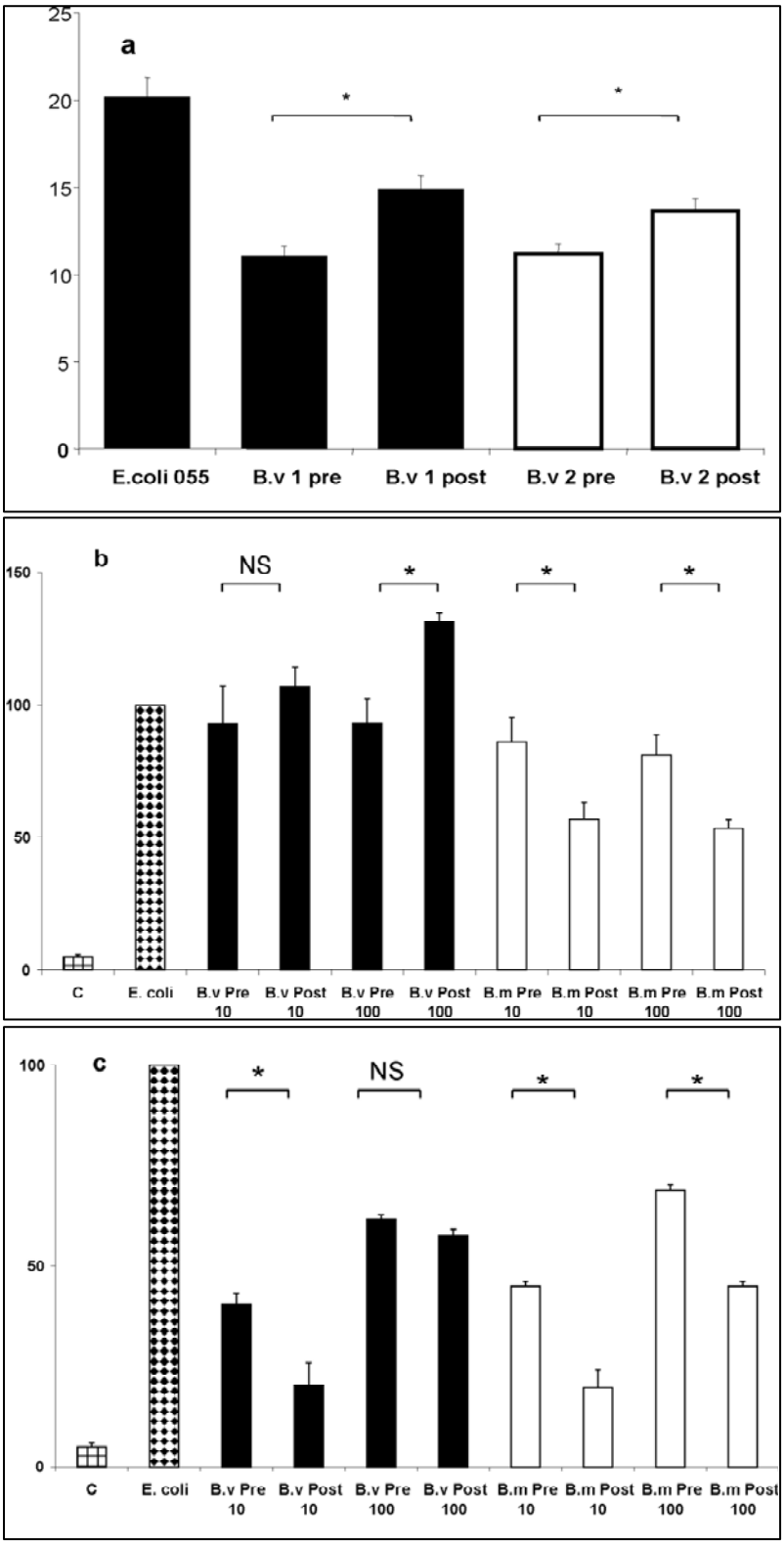

Figure 21. a) Key Histograms represent TNF-α induction (ng) at 24 hours. **b)** Comparison of LOS signalling through human Toll-like receptor-4 and MD2 complex in transfected HEK 293 cells. **c)** Comparison of extracted lipid A signalling through human Toll-like receptor-4 and MD2 complex in transfected HEK 293 cells.

4.6. Discussion

The two clonal *B. vietnamiensis* LOSs possess the same core oligosaccharide structure. This oligosaccharidic sequence has characteristic and highly conserved motifs already found in other *Burkholderia* LOS [8] that clearly suggest a common biosynthetic pathway shared between these related but genetically distinct bacteria. The inner core is constituted by the common motif: Hep-(1→3)-[β-Glc-(1→4)]-α-Hep-(1→5)-[α-Ko-(2→4)]-α-Kdo. In this *B. vietnamiensis* strain, the latter heptose residue is glycosylated at C-2, C-3 and C-7, as previously noted for *B. multivorans*;[9] however, the heptose carries at C-7 an additional heptose disaccharide, as found in *B. cenocepacia* ET-12 LOS.[10]

It is very likely that, as in *B. multivorans* LOS, the trisaccharide [β-D-Gal-(1→3)-α-D-GalNAc-(1→3)-β-D-GalNAc] is a reminder of the O-polysaccharide that is directly linked to the C-2 of the heptose.[9] In fact, a 2-deoxy-2-acetamido sugar functions as primer at the non reducing end of the core oligosaccharide region and its transfer to a lipid carrier initiates the O-antigen synthesis in O-polysaccharides that are synthesized by the Wzy-dependent pathway.[11]

The composition of the *B. vietnamiensis* lipid A moiety is consistent with other *Burkholderia* lipid A species, which also display tetra and pentaacylated lipid A bearing Ara4N residues.[8] The substitution of Ara4N in LPS molecules is essential for bacterial survival[12] since it prevents the interactions with antibiotic compounds and host antimicrobial peptides. These residues are positively charged in physiological conditions and so they reduce the net charge surface on bacterial membrane. Preventing the ionic attraction, the presence of these residues avoids membrane permeability induced by positively charged antimicrobial peptides.

Interestingly, if we compare lipid A moiety of the pre transplantation strain with the lipid A moiety of post transplantation strain, we find that the most abundant species in each LOS analysed have a different acylation pattern. The pre transplantation strains' LOS consists of a blend of tetra and pentaacylated lipid A with the same relative abundance, that can carry one or two Ara4N residues. Conversely, the post transplantation strain mainly comprises pentaacylated lipid A, bearing one or two Ara4N, with tetraacylated species present in minimal amounts. Biological tests performed on U937 myelomonocytic cells stimulated by the pure endotoxins analysed reveal a modest but not significant difference between the pro-inflammatory activity of the two LOSs. LOS post transplantation induces similar or greater levels of TNF-α secretion. This appears to contrast with results obtained

from clonal *B. multivorans* following transplantation (see chapter 3) where the post transplantation strain was associated with a shift toward less acylated lipid A and a significant reduction in TNF-α induction capacity.[9] The current study correlates well with the chemical differences noted in lipid A since, as it is generally found, a higher degree of lipid A acylation is related to more potent proinflammatory activity. Thus, the pentaacylated lipid A species (the most acylated species) produced by *B. vietnamiensis* is generally more strongly pro-inflammatory whereas the (pre-transplant) tetra-acylated species has statistically less biological activity in terms of TNF-α induction in the U937 assays. In the HEK 293 cell NF-KB bio-reporter assays an increase in biological activity was seen for post transplantation strain as compared to the pre transplantation strain when intact LOS was used as a stimulant but not when with the extracted lipid A stimulant. The reasons for this are unclear and require further studies.

The differences between the two *B. vietnamiensis* clonal strains analysed was limited to alterations in lipid A moieties, in contrast to the changes in both lipid A and core oligosaccharide found when comparing *B. multivorans* LOS isolated from clonal strains pre and post transplantation (chapter 3).[9]

References

1. Gillis M, Trân Van V, Bardin R, Goor M, Hebbar P, Willems A, Segers P, Kersters K, Heulin T, Fernandez MP. 1995. Polyphasic taxonomy in the genus *Burkholderia* leading to an emended description of the genus and proposition of *Burkholderia vietnamiensis* sp. nov. for $-N_2$ fixing isolates from rice in Vietnam. *Int. J. Syst. Bacteriol.* 45**:** 274-289.

2. Vandamme P, Holmes B, Vancanneyt M, Coenye T, Hoste B, Coopman R, Revets H, Lauwers S, Gillis M, Kersters K, Govan JRW. 1997. Occurrence of multiple genomovars of *Burkholderia cepacia* in cystic fibrosis patients and proposal of *Burkholderia multivorans* sp. nov. *Int. J. Syst. Bacteriol.* 47**:** 1188-1200.

3. Ieranò T, Silipo A, Sturiale L, Garozzo D, Bryant C, Lanzetta R, Parrilli M, Aldrige C, Gould FK, Corris PA, Khan CM, De Soyza A, Molinaro A. First structural characterization of *Burkholderia vietnamiensis* lipooligosaccharide from Cystic Fibrosis associated lung transplantation strains. *Glycobiology* (2009) 19: 1214-1223.

4. Birnbaum GI, Roy R, Brisson JR, Jennings HJ. 1987. Conformations of Ammonium 3-Deoxy-D-*manno*-2-octulosonate (KDO) and Methyl α- and β-Ketopyranosides of Kdo: X-Ray Structure and ^{1}H NMR Analyses. *J. Carbohydr. Chem.* 6: 17–39.

5. Isshiki Y, Kawahara K, Zähringer U. 1998. Isolation and characterization of disodium (4-amino-4-deoxy-β-L-arabinopyranosyl)-(1→8)-(D-*glycero*-α-D-*talo*-oct-2-ulopyranosylonate)-(2→4)-(methyl 3-deoxy-D-*manno*-oct-2-ulopyranosid)onate from the lipopolysaccharide of *Burkholderia cepacia* *Carbohydr. Res.* 313: 21-27

6. Sturiale L, Garozzo D, Silipo A, Lanzetta R, Parrilli M, Molinaro A. 2005. New conditions for matrix-assisted laser desorption/ionization mass spectrometry of native bacterial R-type lipopolysaccharides. *Rapid. Commun. Mass Spectrom.* 19: 1829-1834.

7. Silipo A, Lanzetta R, Amoresano A, Parrilli M, Molinaro A. 2002. Ammonium hydroxide hydrolysis: a valuable support in the MALDI-TOF mass spectrometry analysis of Lipid A fatty acid distribution. *J. Lipid Res.* 43: 2188-2195.

8. De Soyza A, Silipo A, Lanzetta R, Govan JR, Molinaro A. 2008. Chemical and biological features of *Burkholderia cepacia* complex lipopolysaccharides. *Innate Immun*. 14: 127-144.

9. Ieranò T, Silipo A, Sturiale L, Garozzo D, Brookes H, Khan CM, Bryant C, Gould FK, Corris PA, Lanzetta R, Parrilli M, De Soyza A, Molinaro A. 2008. The structure and proinflammatory activity of the lipopolysaccharide from *Burkholderia multivorans* and the differences between clonal strains colonizing pre and posttransplanted lungs. *Glycobiology*. 18: 871-81.

10. Silipo A, Molinaro A, Ieranò T, De Soyza A, Sturiale L, Garozzo D, Aldridge C, Corris PA, Khan CMA, Lanzetta R, Parrilli M. 2007. The complete structure and pro-inflammatory activity of the lipooligosaccharide of the highly epidemic and virulent gram-negative bacterium *Burkholderia cenocepacia* ET-12 (strain J2315). *Chemistry.* 13: 3501– 3511.

11. Perez JM, McGarry MA, Marolda CL, Valvano MA. 2008. Functional analysis of the large periplasmic loop of the *Escherichia coli* K-12 WaaL O-antigen ligase. *Mol. Microbiol.* 70: 1424-1440

12. Ortega XP, Cardona ST, Brown AR, Loutet SA, Flannagan RS, Campopiano DJ, Govan JRW, Valvano MA. 2007. A Putative Gene Cluster for Aminoarabinose Biosynthesis Is Essential for *Burkholderia cenocepacia* Viability**.** *J Bacteriol.* 189: 3639-44.

Chapter 5

STRUCTURAL ELUCIDATION OF A NOVEL *B. CENOCEPACIA* ET-12 LIPOOLIGOSACCHARIDE ISOLATED FROM A CYSTIC FIBROSIS PATIENT AFTER LUNG TRANSPLANTATION.

B. cenocepacia (genomovar III) is the most virulent species and is the most frequent isolated Bcc genomovar recovered from CF patients sputum. Genotyping studies showed that *B. cenocepacia* ET-12 clonal lineages are associated with the highest rates of morbidity and mortality in CF and are the main cause of poor outcomes in lung transplantation since they are responsible of the deadly exacerbation of infection known as "cepacia syndrome".[1]

This is the third and last part of the project focused on the Bcc endotoxin characterization isolated from CF patients that underwent to lung transplantation. The Newcastle group (see chapter 3) provided us for *B. cenocepacia* ET-12 endotoxin after recovering its two paired clonal strains pre and post lung transplantation from a CF patient, as described for the previous works (chapter 3 and 4). This study is centred exclusively on the characterization of endotoxin isolated post lung transplantation since the sample recovered pre lung transplantation was extracted in a few amount.[2] It is noteworthy that, despite of *B. cenocepacia* pre-operative infection, patient survived after lung transplantation. Even though bacterial virulence is complex, since it does not depend on a single factor, it is interesting to compare this novel structure with the one already published belonging to the most virulent clonal lineage of *B. cenocepacia* ET-12, strain J2315.[3]

5.1 Extraction, SDS electrophoresis and compositional analyses of *B. cenocepacia* LOSs.

LPS was extracted from lyophilized cells as described (see section III). The SDS-PAGE of LPS fraction revealed that the extracted *B. cenocepacia* lipopolysaccharide was a rough type LPS, i.e., a lipooligosaccharide (LOS).

Monosaccharide analysis on isolated LOS molecule revealed the presence of: L-glycero-D-*manno*-heptose (L,D-Hep), D-galactose (D-Gal), D-glucose (D-Glc), 2-amino-2-deoxy-D-glucose (D-GlcN), 4-amino-4-deoxy-L-arabinose (L-Ara4N), 3-deoxy-D-*manno*-oct-2-ulosonic acid (Kdo), D-*glycero*-D-*talo*-oct-2-ulosonic acid (Ko). Methylation analysis showed the presence of 6-substituted GlcN, terminal Gal, terminal Glc, 6-substituted Glc,

6-substituted Gal, 3,4-substituted Hep, 3,7-substituted Hep, terminal Hep, 4,5-substituted Kdo, terminal Ko. All sugar residues were in pyranose rings. Fatty acids analysis revealed the presence of (*R*)-3-hydroxyhexadecanoic (16:0 (3-OH)) in amide linkage and (*R*)-3-hydroxytetradecanoic (14:0 (3-OH)) acid and tetradecanoic acid (14:0) in ester linkage according with the typical structure of *Burkholderia* lipid A.[4]

5.2 Isolation and structural characterization of oligosaccharide from *B. cenocepacia* LOS

A mild acid hydrolysis promoted by acetate buffer (see section III), was executed on intact and purified LOS. An oligosaccharide fraction was recovered after centrifugation and purified on gel permeation chromatography. Monosaccharide analysis of this product confirmed the presence of: L-glycero-D-*manno*-heptose (L,D-Hep), D-galactose (D-Gal) and D-glucose (D-Glc). Methylation analysis showed the presence of terminal Gal, terminal Glc, 6-substituted Glc, 6-substituted Gal, 3,4-substituted Hep, 3,7-substituted Hep, terminal Hep and 5-substituted Kdo.

This fraction was analysed through homo- and heteronuclear 2D NMR experiments (DQF-COSY, TOCSY, ROESY, ^{1}H-^{13}C HSQC, ^{1}H-^{13}C HSQC-TOCSY and ^{1}H-^{13}C HMBC, see section III) in order to assign all the spin systems and to define the monosaccharide sequence. The fraction analysed was constituted by a blend of oligosaccharidic species characterized by not-stoichiometric substitutions. Thus, all NMR spectra presented an high heterogeneity augmented by the presence of the Kdo moiety reducing end. Even though the anomeric region of the ^{1}H-NMR spectrum was characterized by broad signals, it was possible to identify seven major anomeric signals I (**A**-**G**, figure 22a and table 5); while the signals at 2.05/2.20 ppm were attributed to the H-3 methylene protons of the Kdo residue.

Spin system **A** (H-1 5.30 ppm, table 5) was identified as a glucose residue, as indicated by the large $^{3}J_{H,H}$ values of ring protons (above 10 Hz). Low value of $^{3}J_{H1,H2}$ coupling constant (about 3 Hz) and the *intra*-residual NOE contact of H-1 with H-2 attested an α-anomeric configuration.

Spin systems **B**, **C**, **F** (table 5), were all identified as α-heptose residues, as indicated by their $^{3}J_{H1,H2}$ and $^{3}J_{H2,H3}$ coupling constants (below 3 Hz) and by the *intra*-residual NOE of H-1 with H-2. The ^{13}C chemical shift values of C-6 of these heptose residues (all below 71 ppm) confirmed these as L-*glycero*-D-*manno*-heptose, in accordance with the chemical analysis.

Spin system **D** (H-1 at 5.07 ppm) was identified as α-galactose, as indicated by its $^3J_{H3,H4}$ and $^3J_{H4,H5}$ values (3 Hz and 1 Hz, respectively) diagnostic of a *galacto*-configuration. The $^3J_{H1,H2}$ coupling constant (3.2 Hz) and the *intra*-residual NOE contact of H-1 with H-2 were all in agreement with α-anomeric configuration.

Spin systems **E** and **G** (H-1 at 5.00 and 4.62 ppm, respectively) were identified as glucose residues, as indicated by the large $^3J_{H,H}$ values of rings protons (above 10 Hz). The chemical shifts of H-1 and C-1 of residue **E** (5.00 and 97.81 ppm), the $^3J_{H1,H2}$ coupling constant (3.2 Hz) and the *intra*-residual NOE contact of H-1 with H-2 were all in agreement with α-anomeric configuration; the chemical shifts of H-1 and C-1 of residue **G** (4.62 and 102.8 ppm respectively), the $^3J_{H1,H2}$ value (8.2 Hz) and the *intra*-residual NOE contact of H-1 with H-3 and H-5 evidenced a β-anomeric configuration for this residue.

Because of its free reducing end, the Kdo residue **K** was present in multiple forms, nevertheless the signals belonging to the α-reducing unit were clearly assignable starting from the diastereotopic H-3 methylene proton signals, resonating at 2.05 and 2.20 ppm (H-3_{ax} and H-3_{eq}, respectively).

The oligosaccharide sequence was carried out evaluating all the interesidual NOE contacts identified in the ROESY spectrum (figure 22b) and the long range scalar correlations present in the HMBC spectrum (not shown).

The linkage of the heptose **B** to O-5 of Kdo **K** was proven by the NOE connectivity between H-1 of the heptose **B** (5.30 ppm) and H-5 of Kdo (4.28 ppm). Residue **B** was in turn substituted at O-3 and O-4. The NOE contacts (figure 22b) of H-4 and H-3 B, with H-1 of residue **G** (4.62 ppm) evidenced that the O-4 of α-heptose **B** was glycosylated by residue **G** of β-glucose. Residue **B** was also substituted at O-3 by residue **C** of α-heptose, according to the NOE (Figure 22b) of H-3 **B** with H-1 **C** (5.14 ppm). Residue **C** was also glycosylated at O-7 by the terminal α-heptose **F**, as attested by the NOE contact between H-1 **F** and H-7 **C**. Additionally, residue **C** was glycosylated at position 3 by the α-Glc **A** as proven by the NOE contact between H1 of residue **A** and H-3 of residue **C**. Residue **A** was in turn substituted by the terminal α-glucose residue **E** as attested by the HMBC correlation between H1 E and C6 **A** (not shown) and by the NOE contact between H1 **E** (5.00 ppm) and H6 **A**.

Finally residue **G** of β-glucose was substituted by the terminal α-galactose residue as attested by the presence of NOE correlations between H1 **E** (5.00 ppm) and H6 **G** (3.89 and 3.99 ppm).

Thus NMR analysis and chemical data allowed to establish the oligosaccharide sequence reported below:

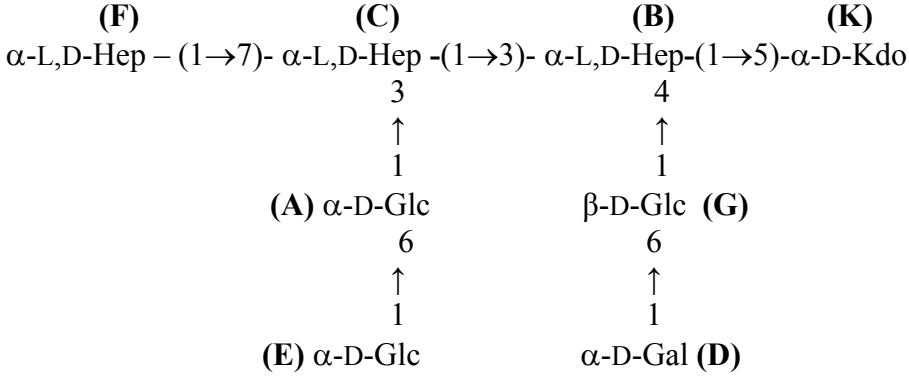

	Chemical shift δ (^{1}H/^{13}C)							
Unit	**1**	**2**	**3**	**4**	**5**	**6**	**7**	**8**
A	5.30	3.60	3.82	3.71	3.61	4.10/3.71		
6-α-Glc	100.15	71.7	73.10	71.60	71.80	65.23		
B	5.30	4.08	4.11	4.13	3.63	4.11	3.70/3.77	
3,4-α-Hep	99.21	70.40	71.99	72.10	71.80	69.80	63.60	
C	5.14	4.24	4.02	3.90	3.78	4.00	3.77/n.d.	
3,7-α-Hep	100.3	69.4	79.80	69.57	73.4	70.05	69.90	
D	5.07	3.84	3.90	4.03	4.00	3.77/3.87		
t-α-Gal	97.81	68.50	69.40	68.90	69.90	61.07		
E	5.00	3.59	3.78	3.45	3.87	3.86/3.79		
t-α-Glc	97.81	71.60	73.20	69.70	70.60	60.40		
F	4.94	4.01	3.88	3.66	3.89	4.04	3.71/3.76	
t-α-Hep	100.67	70.50	70.60	71.34	70.7	69.00	63.70	
G	4.62	3.35	3.53	3.47	3.68	3.89/3.99		
6-β-Glc	102.08	73.50	75.80	69.70	74.50	62.90		
K	---	---	2.05/2.20	4.16	4.28	4.13	4.00	3.88/ 3.77
5 -α-Kdo	n.d.	n.d.	34.00	71.25	69.27	70.90	71.06	62.70

Table 5. ^{1}H and ^{13}C NMR chemical shifts (ppm) of sugar residues of the core region extracted from *B. cenocepacia* LOS (n.d. = not detected).

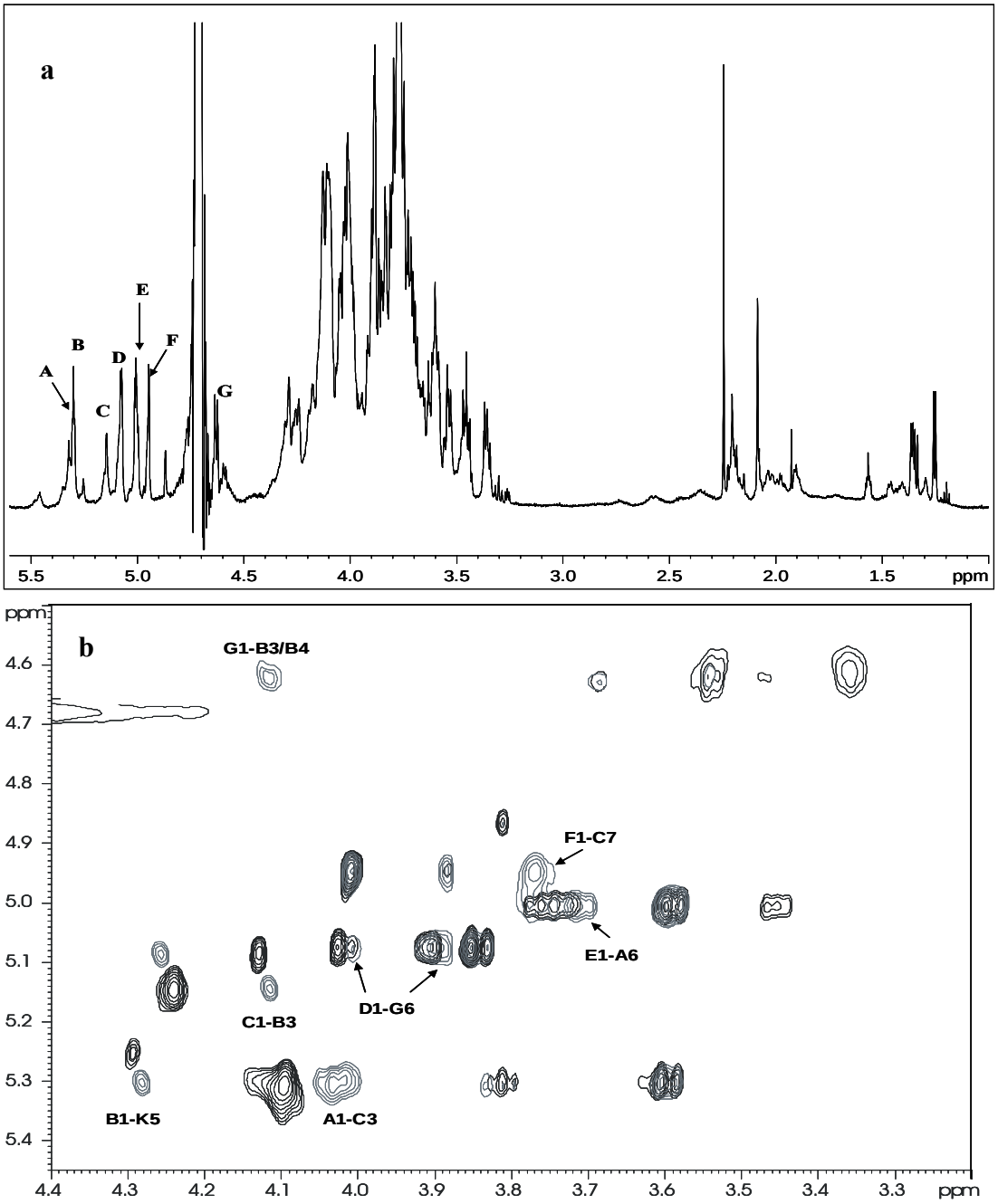

Figure 22. a)^{1}H spectrum of core oligosaccharide isolated from *B. cenocepacia* LOS. Anomeric signals of monosaccharides residues are indicated with alphabetical letters. b) Zoomed region of overlapped ROESY (grey) and TOCSY (black) 2D NMR spectra in which *intra*-residue NOE contacts are reported.

5.3 Structural characterization by MALDI mass spectrometry of the intact LOS

Intact LOS molecule was analysed by MALDI-MS using a sample preparation procedure specifically set up for such amphiphilic molecules (see section III). The negative ion MALDI mass spectrum of intact LOS is shown in figure 22. The spectrum presented

fragments between 1400 and 2000 *m/z*, originating from the β̃-elimination cleavage of the labile glycoside bond between Kdo and the lipid A moiety and that yields either OS oligosaccharide ions or lipid A ions, thus it is very informative. Particularly, the OS1 peak at *m/z* 1678.8 matched with a nonasaccharide constituted of three Hep, four Hex, one Kdo, and one Ko residue, i.e. the core oligosaccharide structure described above by NMR spectroscopy with the addition of Ko residue. Other oligosaccharide at *m/z* 1810.9 (OS2) matched with the same oligosaccharide, not detected in NMR analysis, that bears the additional Ara4N moiety as found for *Burkholderia* inner core, typically on Ko residue. The same mass region also presented ion peaks deriving by a mixture of tetra and penta-acylated lipid A. Species T_1 at *m/z* 1443.5 matched with a tetra-acylated bis-phosphorylated disaccharide backbone carrying in ester linkage one 14:0 (3-OH) and in amide linkage two 16:0 (3-OH) acyl chains, one of which, on the GlcN II, was further substituted by a secondary 14:0 fatty acid (see below). Species T_2 at *m/z* 1575.0 ($\Delta m/z \cong$ 131 from L_1) and T_3 at *m/z* 1705.6 ($\Delta m/z \cong$ 131 from L_2) were tetra-acylated lipid A carrying one and two Ara4N residues. Species P_1 (*m/z* 1670.3), P_2 (*m/z* 1800.8) and P_3 (*m/z* 1932.0) were consistent with the penta-acylated lipid A carrying two ester-linked 14:0 (3-OH) with no, one and or two Ara4N residues, respectively.

In analogy with other lipid A from *Burkholderia*,[4] the position of the secondary fatty acid14:0 on the GlcN II was identified on the GlcN II by mass spectrometry analysis of the lipid A moiety after acetate buffer hydrolysis. Briefly, the positive ion MALDI mass spectrum (not shown), presented an in-source fragmentation due to the split of the glycosidic linkage between the two GlcN units, thus giving rise to a triacylated oxonium ion at *m/z* 933.1 carrying one 14:0 (3-OH), one 14:0, and one 16:0 (3-OH) residue at the non-reducing GlcN unit. The information were then completed by analyses of the compound obtained by with ammonium hydroxide hydrolysis.[5]

Few signals in the region of the spectrum between 3000 and 3800 *m/z* attested a reduced heterogeneity of LOS molecules present. Considering the combination of the lipid A moieties and the core oligosaccharide species main LOS molecular ions were attributed. Peak at *m/z* 3385.7 represented a LOS species matched either with the tetra-acylated lipid A (T2) and OS2 (T2+OS2), or with the tetra-acylated lipid A T3 and OS1 (T3+OS1). Considering the major abundance of T2 species, this peak seems mostly due to the first combination. Similarly, peak at *m/z* 3254.6 matched either with T1+OS2 or with T2 +OS1 and, in this case, considering the abundances of the single species both the attribution were equally probable. Likewise for the two minor LOS peaks constituted by penta-acylated

lipid A. Even though peak at *m/z* 3612.2 could fit either with the combination (P2+OS2) or with (P3+OS1), the former is more probable. Finally the species at *m/z* 3481.4 should be equally interpreted either with the combination of (P1+OS2) or with (P2+OS1) that were equally probable.

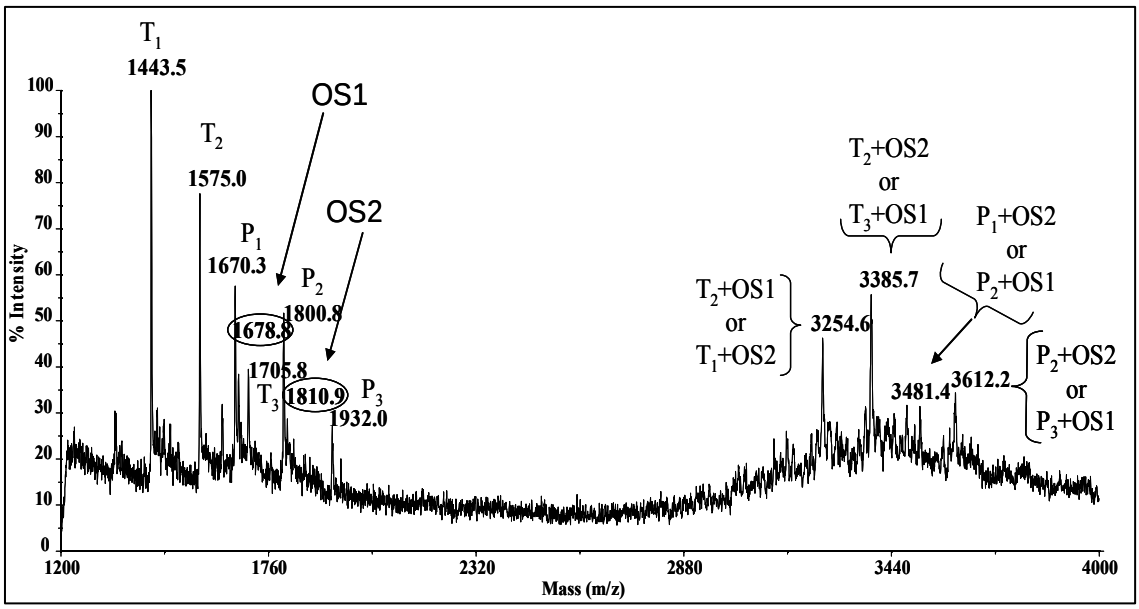

Figure 22. Negative-ion MALDI mass spectrum of intact LOS isolated from *B. cenocepacia* after lung transplantation. .In low mass range (1200-2000 *m/z*), lipid a and core oligosaccharides peaks are visible. LOS intact molecule peaks populates the high mass range region (2800-4000 *m/z*).

5.4 Biological activity of *B. cenocepacia* LOS

The LOS molecule isolated post- lung transplantation was tested for its pro-inflammatory activity of eliciting TNF-alpha induction from human myelomonocytic U937 cells (figure 23). Key Histograms represent TNF induction (ng) at 24 hours. U937 cells were stimulated with 10ng/mL of purified LPS or left unstimulated (US, negative control). Purified LPS from strains LMG 14273 (*B. multivorans*) and LMG 12614 (*B. cenocepacia* ET-12) were also used as comparators. Herein it has been showed that biological activity of *B. cenocepacia* LOS isolated after lung transplantation is a great THF-alpha inducer also if it is compared to the other *B. cenocepacia* ET-12 epidemic strain (LMG 12614).

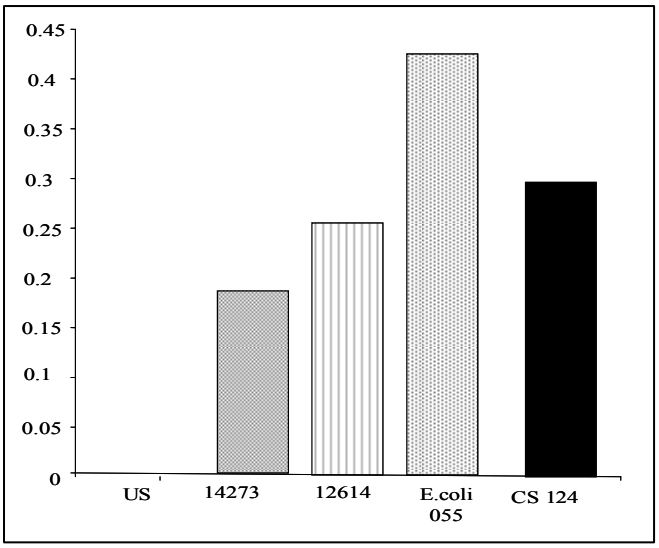

Figure 23. U937 macrophages were stimulated with 10ng /ml of extracted LPS or left unstimulated (US) for 24 hours. TNF secretion was assayed by ELISA. Strains of interest studied included LMG 14273 (*B. multivorans*), LMG 12614 (*B. cenocepacia* ET-12 clone) and CS 124 a post transplant *B. cenocepacia* ET-12 strain from a patient who survived following lung transplantation. Commercially available E. coli 055 LPS was sued as an internal control.

5.5 Discussion

Lung transplantation is the only therapy for CF patients at the end stage. Typically this treatment is contraindicated to CF patients that are affected by *B. cenocepacia* infections since they are the most aggressive and mortal.[6,7] The endotoxin analysed in this work was a clinical isolate extracted from a *B. cenocepacia* ET-12 clone infecting a CF patient who underwent a lung transplantation and survived. *B. cenocepacia* strain was recovered after transplant. The chemical structure of the endotoxin analysed presented peculiar and common features if compared to other *Burkholderia* LPS.[4] Lipid A moiety is constituted by a blend of tetra and penta acylated species of a GlcN disaccharide backbone bis-phosphorilated and, as for the already published LOS from *B. cenocepacia* ET-12 J2315 strain the tetra acylated species was the most abundant one.[3] Lipid A can also carry one or two Ara4N residues as for other *Burkholderia*.[4] It has been described that the biosynthesis and the transfer of Ara4N moiety is controlled by a gene cluster regulated by the operon *arn* found in *E. coli* and *S. thyphimurium* that is responsible for polymyxin resistance.[8] From NMR and MS analyses emerged that the core oligosaccharide is formed by a short

saccharidic chain in which we can distinguish the common *Burkholderia* inner core motif: Hep-(1→3)-[β-Glc-(1→4)]-α-Hep-(1→5)-α-Kdo. From MALDI spectra of the intact LOS molecule we can conclude that the additional Ko and Ara4N residues present in oligosaccharide moiety are linked to Kdo in order to form the known trisaccharide β-Ara4N-(1→8)-α-Ko-(2→4)-α-Kdo described for *Burkholderia*.[9] It is demonstrated that the presence of Ara4N residues on LPS is a structural modification that may occur after LPS transmigration on the cellular surface in response to peculiar to environmental conditions (as low concentration on Mg^{2+}) that require a reduction of the net negative surface charge. Typically, since LPS are constituted by Kdo, Ko and phosphate groups, they are responsible for the net negative charge of bacterial surface. Thus, normally cationic antimicrobial peptides, involved in the innate immune response against bacterial infections, and positively charged antibiotics, as polymixin B (PmB), exert their antimicrobial activity permeating bacterial membrane and killing cells. The presence on LPS of Ara4N residues, that are positively charged in physiological conditions, prevent bacterial killing since they reduce the total net negative charge of cellular surface.

Further, the core sequence contains the additional disaccharide Hex-(1→6)-Hex linked to the second Hep residue of the inner core as it was found for *B. cenocepacia* ET-12.[3] In addition, differently for the strain already characterised, the high conserved residue of β-Glc present in the inner core was in turn glycosilated at O6 by a terminal Gal residue as reported for *B. caryophylli* and for *B. multivorans*.[10,11]

In the case analysed herein, differently from the core oligosaccharide from *B. cenocepacia* ET-12,[3] bacteria biosynthesize a shortest core oligosaccharide portion. Starting from 3,7 branched heptose residue, in the known *B. cenocepacia* core, there is a α-galactose residue that is substituted by the trisaccharide α-L-Rha(1→3)-β-D-QuiNAc(1→7)-α-L,D-Hep(1→) at its C2. In the core structure here reported, an α-glucose residue replaces the α-galactose present in J2315 strain, as is also reported for XOA3 mutant of *B.cenocepacia* K56-2.[12] *B. cenocepacia* post transplantation core is truncated at α-glucose residue, thus it lacks the disaccharide Rha-QuiNac that is the remnant of the O-chain. Recent studies showed that O-chain biosynthesis in *B. cenocepacia* requires an adaptor sugar to which the reminder of the O-antigen repeating units become attached.[12] QuiNac is found to be the adaptor sugar whereas the terminal Rha residue is the first sugar of the repeating O-chain unit (Rha-GalNAc-GalNAc). The ligase responsible for β-D-QuiNAc(1→7)-α-L,D-Hep linkage, is coded by *waaL*, and its inactivation produces rough LPS mutants. In addition, the

identification of gene loci responsible for the biosynthesis of core oligosaccharide moiety in *B. cenocepacia* K56-2 allowed the creation of a set of gradual truncated mutants. These were utilised in the establishment of the core portion role in *B. cenocepacia* resistance to antimicrobial compounds, as PmB. It has been found that a progressive truncation of the core oligosaccharide leads to an increased sensitivity to PmB even though *B. cenocepacia* mutants are still more resistant to PmB than other pathogens with an intact core portion as *Salmonella* and *E. coli*. Thus, *B. cenocepacia* must possess additional mechanisms, independent from core length, that contribute to bacterial resistance to antimicrobial compounds. Moreover, a recent founding showed that *B. cenocepacia* truncated core mutants are not impaired to survive in macrophages, so bacterial viability is not compromised by a shortest saccharidic chain of LOS molecule.

References

1. De Soyza A, Ellis CD, Khan CMA, Corris PA, Demarco de Hormaeche R. *Burkholderia cenocepacia* lipopolysaccharide, lipid A, and proinflammatory activity. *Am. J. Respir. Crit. Care Med* (2004). 170: 70-77.

2. Ieranò T, Silipo A, Sturiale L, Garozzo D, Corris PA, Perry J, Lanzetta R, Parrilli M, De Soyza A, Molinaro A. Structural elucidation of a novel *B. cenocepacia* ET-12 lipooligosaccharide isolated from a cystic fibrosis patient after lung transplantation. *Eur. J. Org. Chem.* (2009) accepted for publication.

3. Silipo A, Molinaro A, Ieranò T, De Soyza A, Sturiale L, Garozzo D, Aldridge C, Corris PA, Khan, CMA, Lanzetta R, Parrilli M. The complete structure and pro-inflammatory activity of the lipooligosaccharide of the highly epidemic and virulent Gram-negative bacterium *Burkholderia cenocepacia* ET-12 (Strain J2315). *Chem. Eur. J.* (2007) 13: 3501– 3511.

4. De Soyza A, Silipo A, Lanzetta R, Govan JR, Molinaro A. Chemical and biological features of *Burkholderia cepacia* complex lipopolysaccharides. *Innate Immun*. (2008) 14: 127-144.

5. Silipo A, Lanzetta R, Amoresano A, Parrilli M, Molinaro A.. Ammonium hydroxide hydrolysis: a valuable support in the MALDI-TOF mass spectrometry analysis of lipid A fatty acid distribution. *J. Lipid Res.* (2002) 43: 2188-2195.

6. Jones AM, Dodd ME, Govan JRW, Barcus VA, Doherty C, Morris J, Webb AK. *Burkholderia cenocepacia* and *Burkholderia multivorans*: influence on survival in cystic fibrosis. *Thorax* (2004) 59: 948-951.

7. De Soyza A, McDowell A, Archer L, Dark JH, Elborn SJ, Mahenthiralingam E, Gould K, Corris PA. *Burkholderia cepacia* complex genomovars and pulmonary transplantation outcomes in patients with cystic fibrosis. *The Lancet* (2001) 358: 1780-1781.

8. Raetz CRH, Whitfield C. Lipopolysaccharide endotoxins. *Annu. Rev. Biochem.*(2002) 71: 635-700.

9. Gronow S, Noah C, Blumenthal A, Lindner B, Brade H. Construction of the deep rough mutant of *B. cepacia* ATCC 25416 and characterization of its chemical and biological properties. *J. Biol. Chem.* (2003) 278:1647–1655.

10. Molinaro A, De Castro C, Lanzetta R, Evidente A, Parrilli M, Holst O. 2002. Lipopolysaccharides possessing two L-glycero-D-manno-heptopyranosyl-alpha -(1-->5)-3-deoxy-D-manno-oct-2-ulopyranosonic acid moieties in the core region. The structure of the core region of the lipopolysaccharides from *Burkholderia caryophylli*. *J. Biol. Chem.* 277: 10058-10063.

11. Ieranò T, Silipo A, Sturiale L, Garozzo D, Brookes H, Khan CM, Bryant C, Gould FK, Corris PA, Lanzetta R, Parrilli M, De Soyza A, Molinaro A. 2008. The structure and proinflammatory activity of the lipopolysaccharide from *Burkholderia multivorans* and the differences between clonal strains colonizing pre and posttransplanted lungs. *Glycobiology*. 18: 871-81.

12. Ortega X, Silipo A, Saldìas MS, Bates CC, Molinaro A, Valvano MA. Biosynthesis and structure of the *Burkholderia cenocepacia* K56-2 lipopolysaccharide core oligosaccharide. Truncation of the core oligosaccharide leads to increased binding and sensitivity to polymyxin B. *J. Biol. Chem.* (2009) 284: 21738-21751.

Chapter 6

STRUCTURAL STUDY OF O-ANTIGENS AND LIPID A MOIETIES PRODUCED BY *B. MULTIVORANS* C-1576 SMOOTH TYPE LIPOPOLYSACCHARIDE.

In this study the structures of the O-antigen and of the lipid A extracted from the LPS produced by *B. multivorans* strain C1576 were carried out.[1,2] This clonal lineage is the most virulent species belonging to genomovar II. Although *B. cenocepacia* is the predominant species in most CF centres, in the last years, in the UK, the isolation of *B. multivorans* exceeded that of *B. cenocepacia*.[3] The isolate used in this study, *B. multivorans* C1576, is one of the Edinburgh collection representing the Glasgow outbreak[4] when few CF children survived to adulthood; this isolate was also included in the panel of reference strains from the *B. cepacia* complex.[5] Structural and conformational analysis are essential basis in the discovery of new therapies targeted towards bacterial endotoxins that play a key role in the inflammatory process. The elucidation of the primary structure of the O-chain and of the lipid A has been performed through chemical analysis, mass spectrometry and 2D NMR spectroscopy. Moreover, a conformational study was executed with the aim of evaluating the spatial arrangements of the O-chain polymers by a combined approach of NMR spectroscopy, molecular mechanics (MM) and molecular dynamic (MD) calculations. Further, the analyzed lipid A moiety was then tested for its pro-inflammatory activity in a cystic fibrosis airways model, using the intestinal epithelial cell line Caco 2 cells, the IB3-1 cells, carrying ΔF508/W1282X CFTR mutation and an *ex vivo* model of culture explants of nasal polyps.

Such data are an essential pre-requisite to elucidate the inflammatory process following infection since they allow a clarification of LPS associated signalling.

6.1 LPS extraction and chemical characterization

LPS was extracted by the hot phenol/water procedure (see section III) and revealed by sodium dodecyl sulfate poliacrylamide gel electrophoresis (SDS-PAGE 12%). The LPS was further purified from other cell contaminants by enzymatic hydrolysis with DNAse, RNAse and proteinase K followed by dialysis and gel permeation chromatography. Lipid A and O-chain moieties were separately obtained by a SDS promoted mild acid hydrolysis. Lipid A compositional analysis revealed 6-substituted-D-GlcN and terminal-D-GlcN,

terminal-4-amino-4-deoxy-L-arabinose, whereas fatty acids analysis detected (R)-3-hydroxyhexadecanoic acid [C16:0(3-OH)] in amide linkage and (R)-3-hydroxytetradecanoic acid [C14:0(3-OH)] and tetradecanoic acid (C14:0) in ester linkage. The water soluble polysaccharide yielded from acid treatment on LPS was purified by gel-permeation chromatography. Chemical and methylation analysis performed on this water-soluble fraction showed the presence of 2-substituted-D-Manp; 3- substituted-D-Manp; 2-substituted-D-Rhap; 3-substituted-D-Rhap; 2,3-substituted-D-Rhap.

6.2 NMR analysis of the O-chain

The ^{1}H-NMR spectrum of the O-chain moiety is shown in figure 24a. A combination of homo- and heteronuclear 2D NMR experiment (DQF-COSY, TOCSY, ROESY, NOESY, ^{1}H -^{13}C HSQC, ^{1}H -^{13}C HMBC, see section III) was executed in order to assign all the spin systems and to define the saccharidic sequence. Complete assignment of the spin systems was obtained attributing the proton resonances by DQF-COSY and TOCSY spectra, and subsequently correlating each proton to its related carbon atom through the HSQC spectrum. The anomeric configuration of each monosaccharide unit was assigned on the basis of the $^{3}J_{\text{H-1,H-2}}$ coupling constant values obtained by the DQF-COSY, whereas the values of the vicinal $^{3}J_{\text{H,H}}$ ring coupling constants allowed the identification of the relative configuration of each sugar residue. Residues **A, C', D'** (H-1 at 5.22, 5.17 and 4.95 ppm respectively, table 6) were recognized as α-rhamnose residues since, in TOCSY spectrum, scalar correlations of the ring protons with methyl signals in the shielded region at 1.21, 1.22 and 1.23 ppm were visible. The *manno* configuration was established by $^{3}J_{\text{H-1,H-2}}$ and $^{3}J_{\text{H-2,H-3}}$ values (below 3 Hz), the α-configuration was assigned either by the *intra*-residual NOE contact of H-1 with H-2 and by H-5/C-5 chemical shift values for each residue. Furthermore, residue **A** was recognized as belonging to 3-*O*-methyl-rhamnose (acofriose) as deduced by the downfield shift of C-3 **A** (79.3 ppm, table 6), by the presence of a methoxy group at 3.41 and 56.8 ppm, that gave NOE with H-2 and H-3 **A**, and by the long range correlation present in the HMBC spectrum of **A**-3 with the methoxy group. Spin systems **B**, **C**, **D** (table 6), were all identified as α-mannose residues, as indicated by their $^{3}J_{\text{H-1,H-2}}$ and $^{3}J_{\text{H-2,H-3}}$ coupling constants (below 3 Hz) and by the *intra*-residual NOE of H-1 with H-2.

The analysis of scalar and dipolar *inter*-residual correlations in the 2D NMR spectra (figure 24b) allowed the identification of two coexisting polysaccharides, characterized by different repeating units. The down-field shift of carbon resonances identified the

glycosylated positions: O-2 of residues **A**, **B**, **C**, **C'** and O-3 of **D', D,** in full agreement with the methylation analysis.

As far as the first polysaccharide is concerned, residue **A** was glycosylated at O-2 by α-mannose **C**, as suggested by the NOE contacts of H-2 **A** (4.27 ppm) with H-1 **C** (5.18 ppm) (Figure 24b). Spin system **C** was in turn glycosylated at its O-2 by residue **D'**, as attested by the NOE contact between H-1 **D'** and H-2 **C**. Finally, residue **D'** was substituted at its C-3 by residue **A** as attested by the NOE between H-1 **A** and H-3 **D'** (Figure 24b). The sequence of this repeating unit was confirmed by the long-range scalar correlations found in the HMBC spectrum. Thus, all data were in agreement with the structure reported below, the repeating unit of polysaccharide **X** (figure 24c):

C **A** **D'**

$$[\rightarrow 2)\text{-}\alpha\text{-D-Man-}(1\rightarrow 2)\text{-}\alpha\text{-D-Rha-}(1\rightarrow 3)\text{-}\alpha\text{-D-Rha-}(1\rightarrow]_n$$

3

↓

OCH_3

As for the second polysaccharide, unit **C'** was glycosylated at O-2 by α-mannose **B**, as inferred by the NOE contacts of H-2 **C'** (4.02 ppm) with H-1 **B** (5.21 ppm). Furthermore, spin system **B** was substituted at its O-2 by residue **D** as suggested by the NOE contact between H-1 **D'** (4.97 ppm) and H-2 **B** (4.04 ppm). Residue **D** was in turn glycosylated at its O-3 by **C'** as supported by the NOE correlation between H-1 **C'** (5.17 ppm) and H-3 **D** (3.80 ppm). The presence of long-range correlations found in the HMBC spectrum confirmed the structure of polysaccharide **Y** as reported below (figure 24c):

B **C'** **D**

$$[\rightarrow 2)\text{-}\alpha\text{-D-Man-}(1\rightarrow 2)\text{-}\alpha\text{-D-Rha-}(1\rightarrow 3)\text{-}\alpha\text{-D-Man-}(1\rightarrow]_n$$

The integration of proton signals in the ^1H NMR belonging to both repeating units suggested that polysaccharide **X** was less abundant than polysaccharide **Y** (approximately 1: 1.5). This operation was feasible considering that the two O-polysaccharide possessed a similar molecular weight as testified by several size exclusion chromatographies and DOSY-NMR experiment.

Unit	1	2	3	4	5	6
Repeating unit X						
[→2)-**C**-(1→2)-**A**-(1→3)-**D'**-(1→]$_n$						
A	5.22	4.27	3.59	3.44	3.78	1.21
2-α-Aco	100.6	74.3	79.3	71.2	69.2	16.5
C	5.19	3.99	3.86	3.66	3.59	3.77/369
2-α-Man	100.4	78.4	69.9	66.7	73.3	60.2
D'	4.95	4.07	3.80	3.48	3.80	1.23
3-α-Rha	102.0	69.3	78.4	71.4	69.2	16.6
Repeating unit Y						
[→2)-**B**-(1→2)-**C'**-(1→3)-**D**-(1→]$_n$						
B	5.22	4.04	3.87	3.68	3.59	3.76/3.69
2-α-Man	100.5	78.2	69.9	66.7	73.3	60.7
C'	5.17	4.02	3.87	3.41	3.77	1.22
2-α-Rha	100.5	78.6	69.9	72.1	69.1	16.5
D	4.97	4.08	3.80	3.70	3.72	3.65/3.71
3-α-Man	101.9	69.7	78.4	65.9	73.2	60.7

Table 6. ^{1}H and ^{13}C NMR chemical shifts (ppm) of repeating unit **X** [→2)-α-Man-(1→2)-α-Aco-(1→3)-α-Rha-(1→]$_n$ and **Y** [→2)-α-Man-(1→2)-α-Rha-(1→3)-α-Man-(1→]$_n$. All sugar residues are in D-configuration. ^{1}H and ^{13}C chemical shifts for the methoxy group are 3.41 and 56.8 ppm respectively

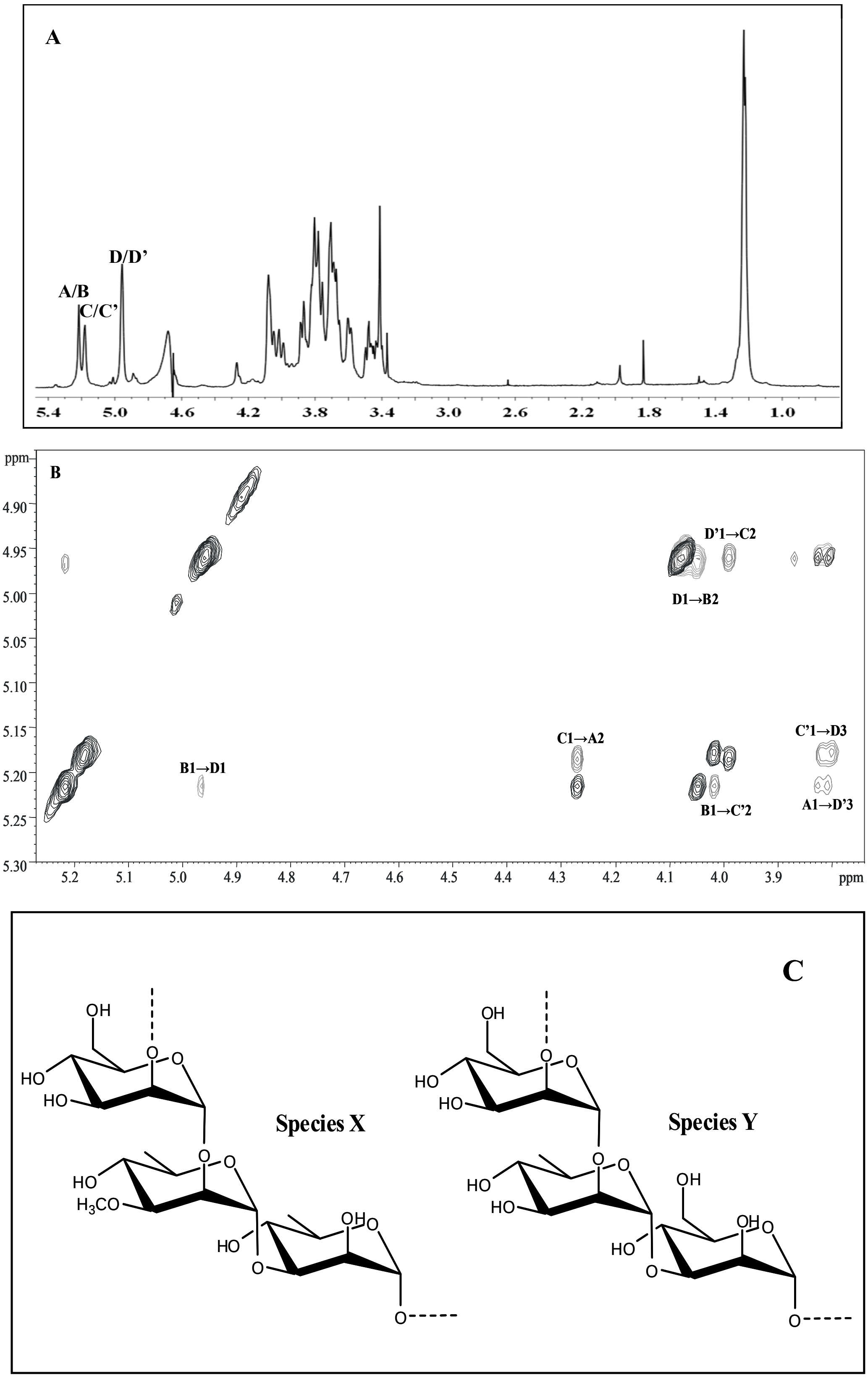

Figure 24. a) [1]H NMR spectrum (600 MHz) of the O-chain fraction isolated from *B. multivorans*. Key NMR signals are as indicated in table 6; b) Section of the ROESY (gray) and TOCSY (black) spectrum of O-chain fraction isolated from *B. multivorans*. Inter-residue NOE contacts are shown; c) Repeating units of polysaccharides X and Y

6.3 Conformational analysis: Molecular Mechanic and Dynamic calculations on the O-chain moiety

Since the conformation of a saccharidic chain is mainly defined by the relative orientation of the sugar moieties, i.e. by Φ and Ψ torsion angles, the first step in the conformational analysis was to build the potential energy surfaces for each disaccharide connected by a glycosidic linkage; Φ represents the torsion angle about H1-C1-O-CX' whereas Ψ about C1-O-CX'-HX'. For both **X** and **Y** repeating units three disaccharides (**C**-2**A** (Man→2Aco), **A**-3**D'** (Aco→3Rha), **D'**-2**C** (Rha→2Man) for **X** and **B**-2**C'** (Man→2Rha), **C'**-3**D** (Rha→3Man), **D**-2**B** (Man→2Man) for **Y**) were constructed and subjected to calculations using MM3* force field. Thus, molecular mechanics provided a first estimation of the conformational regions energetically accessible. The resulting adiabatic energy maps indicating global and local minima are reported in figure 25. Two typologies of glycoside linkages were individuated, both involving α-*manno* configured sugar moieties: the α-(1→2) linkage present in **D'**→2**C** and **C**→2**A** subunits of **X** and **D**→2**B** and **B**→2**C'** subunits of **Y**; the α-(1→3) linkage present in **A**→3**D'** subunit of **X** and **C**'→3**D** subunits of **Y**.

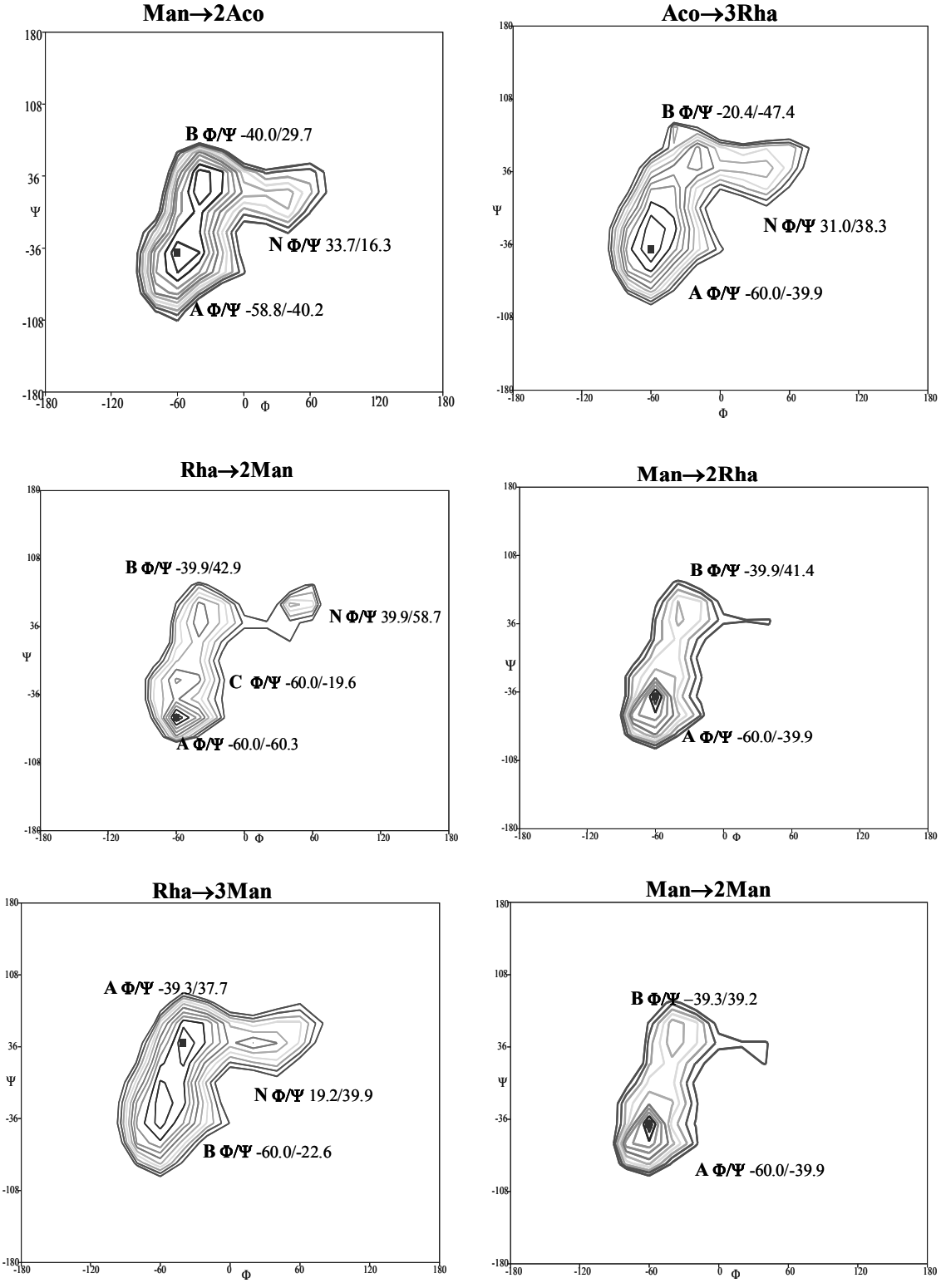

Figure 25. Relaxed energy maps for the disaccharide fragments which compose the two O-chain sequences **X**: [→ 2)-C-(1→2)-A-(1 →3)-D'-(1→]$_n$ and **Y**: [→2)-B-(1→2)-C'-(1→3)-D-(1→]$_n$. The position of the global and major local minima in the map are indicated; letter A indentifies the global minimum**.**

Each disaccharide unit spanned a considerable number of conformational states for both kinds of glycosidic torsions and adopted exo-anomeric conformations in the main energetic minima (figure 25); nevertheless, the MM calculation predicted the existence, in low amount, of conformational families populating the non-exo anomeric regions (figure 25, indicated with letter N). Additionally, all the maps showed a moderate flexibility around Φ torsion whereas they presented a higher flexibility around Ψ. angle covering a significant angular interval, in agreement with the α-anomeric orientation,[6] that generates low energy regions separated by few kJ/mol. This flexibility was particularly evident for the α-(1→2) glycosidic units.[7] It is worth noting that the presence of the acofriose unit did not induce considerable changes either in the orientation or in the potential energy surfaces of the α-(1→2) and α-(1→3) torsions. Actually, the adiabatic energy maps of Man→2Aco and Aco→3Rha in **X** and of the corresponding Man→2Rha and Rha→3Man disaccharides in **Y** were comparable (Figure 25), even though a variation in the location of the α-(1→3) minima was detectable because of a shift in the global minima: Φ/Ψ -60.0/-39.9 for Aco→3Rha with respect to -39.3/37.7 for the Rha→3Man unit.

For both polymers, a dodecasaccharide fragment composed of four repeating units was built from the global minima of the energy maps and the conformational behaviour was studied by using molecular dynamic simulation:

$C_1 \rightarrow 2A_1 \rightarrow 3D_1' \rightarrow 2C_2 \rightarrow 2A_2 \rightarrow 3D'_2 \rightarrow 2C_3 \rightarrow 2A_3 \rightarrow D'_3 \rightarrow 2C_4 \rightarrow 2A_4 \rightarrow D'_4$

Dodecasaccharide X

$B_1 \rightarrow 2C_1' \rightarrow 3D_1 \rightarrow 2B_2 \rightarrow 2C'_2 \rightarrow 3D_2 \rightarrow 2B_3 \rightarrow 2C'_3 \rightarrow D_3 \rightarrow B_4 \rightarrow 2C'_4 \rightarrow 3D_4$

Dodecasaccharide Y

The initial structures were extensively minimized and trajectory coordinates were sampled every ps; 10,000 simulations were performed in GB/SA water solvation model as implemented in MacroModel. Trajectories and Φ/Ψ scatter plots of the different glycosidic linkages, together with the population of each conformational family are shown in the following figure 26a,b and the averaged values of torsion angles and their standard deviation values are displayed in table 7.

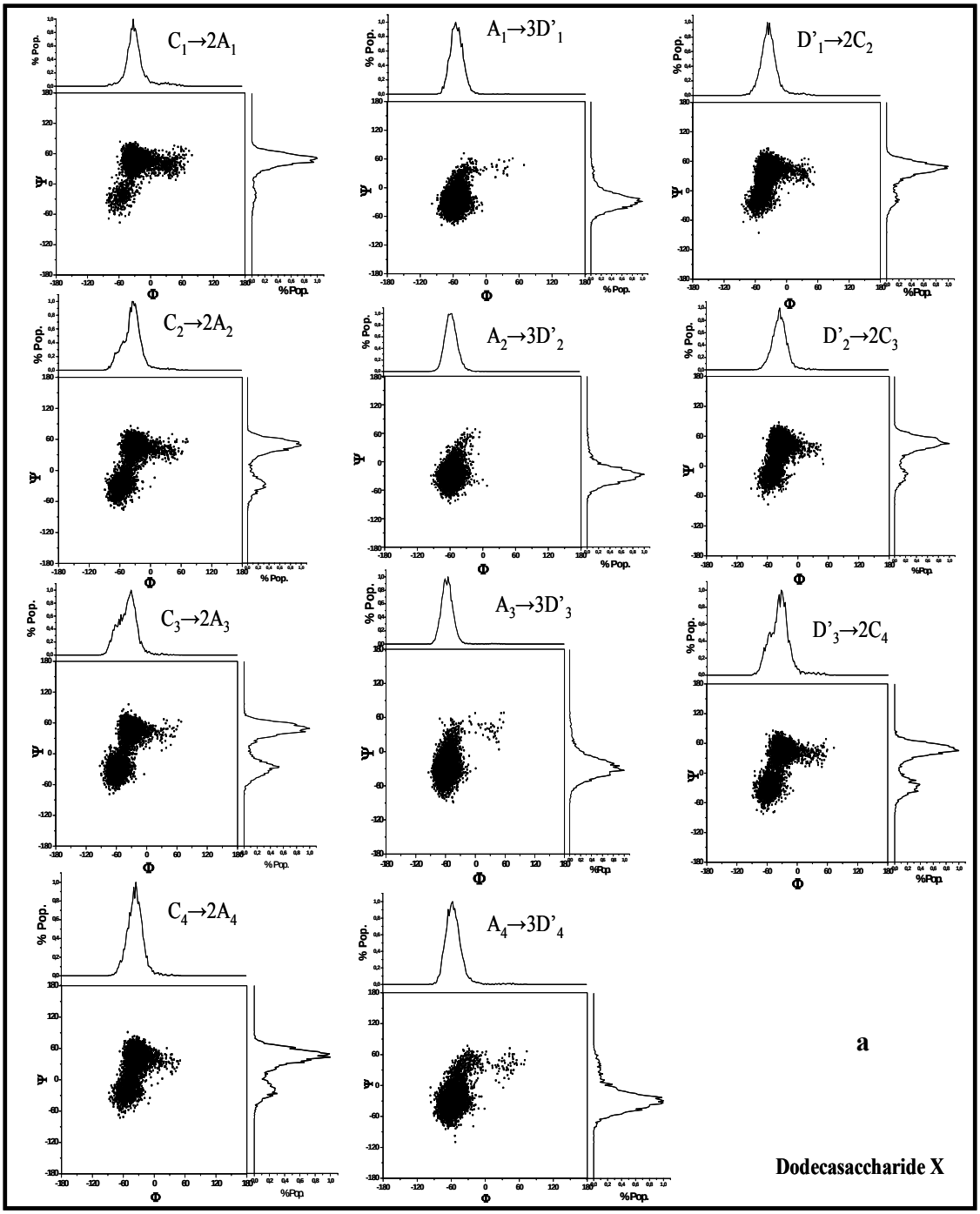
C1→2A1
A1→3D'1
D'1→2C2
C2→2A2
A2→3D'2
D'2→2C3
C3→2A3
A3→3D'3
D'3→2C4
C4→2A4
A4→3D'4
% Pop.
Ψ
Φ
%Pop.
a
Dodecasaccharide X

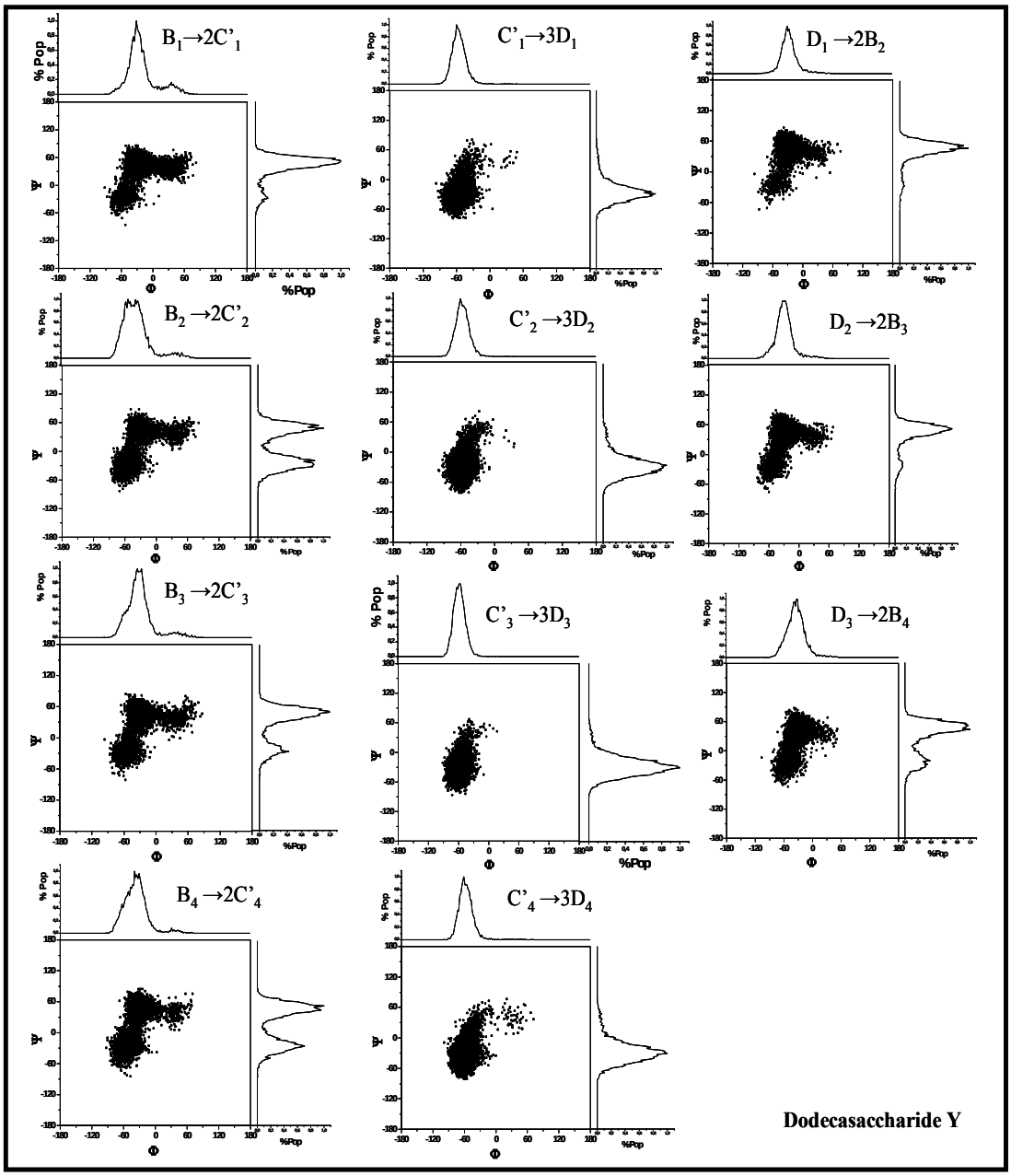
B1→2C'1
C'1→3D1
D1→2B2
B2→2C'2
C'2→3D2
D2→2B3
B3→2C'3
C'3→3D3
D3→2B4
B4→2C'4
C'4→3D4
% Pop
%Pop
Ψ
Φ
Dodecasaccharide Y

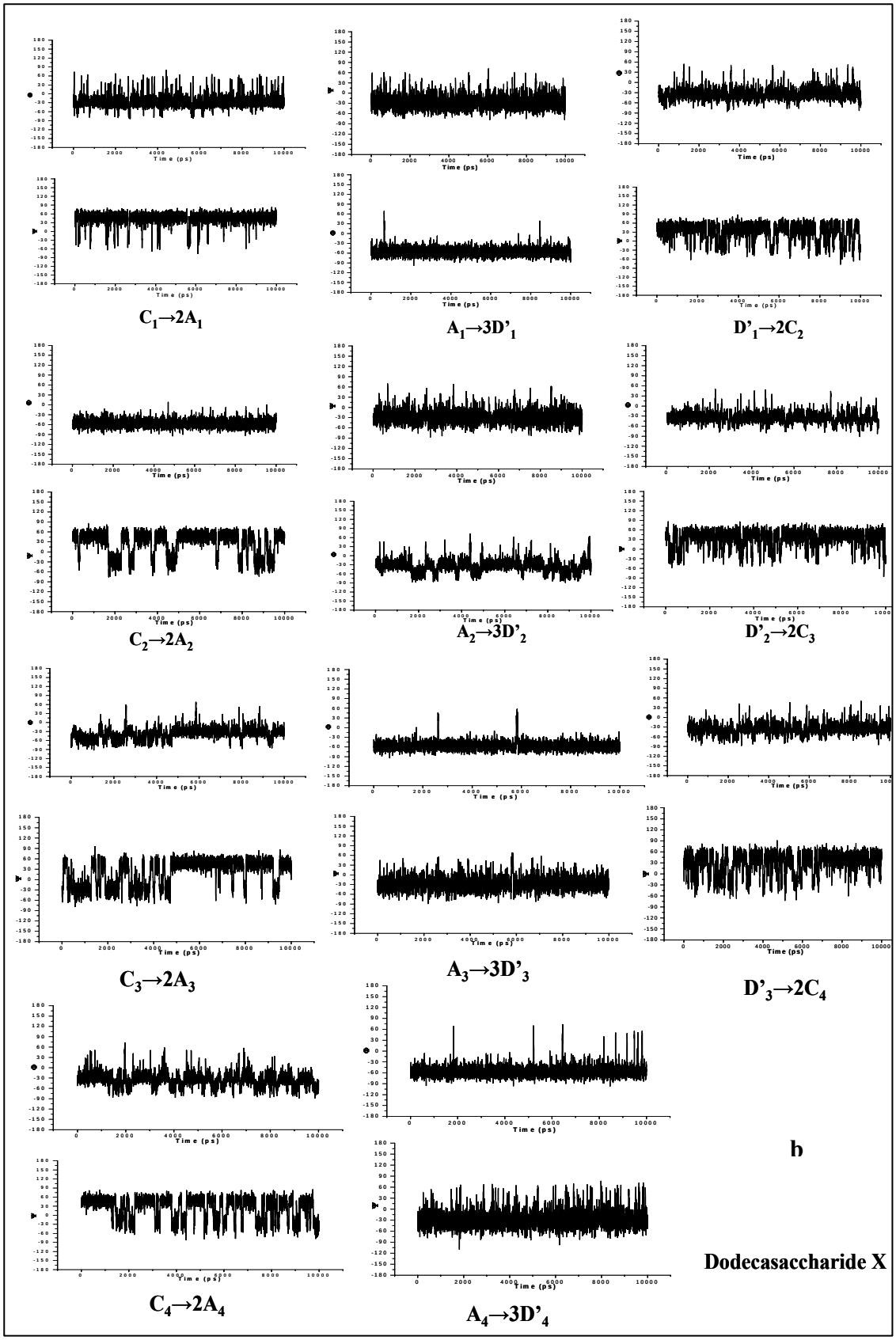
C1→2A1
A1→3D'1
D'1→2C2
C2→2A2
A2→3D'2
D'2→2C3
C3→2A3
A3→3D'3
D'3→2C4
C4→2A4
A4→3D'4
b
Dodecasaccharide X

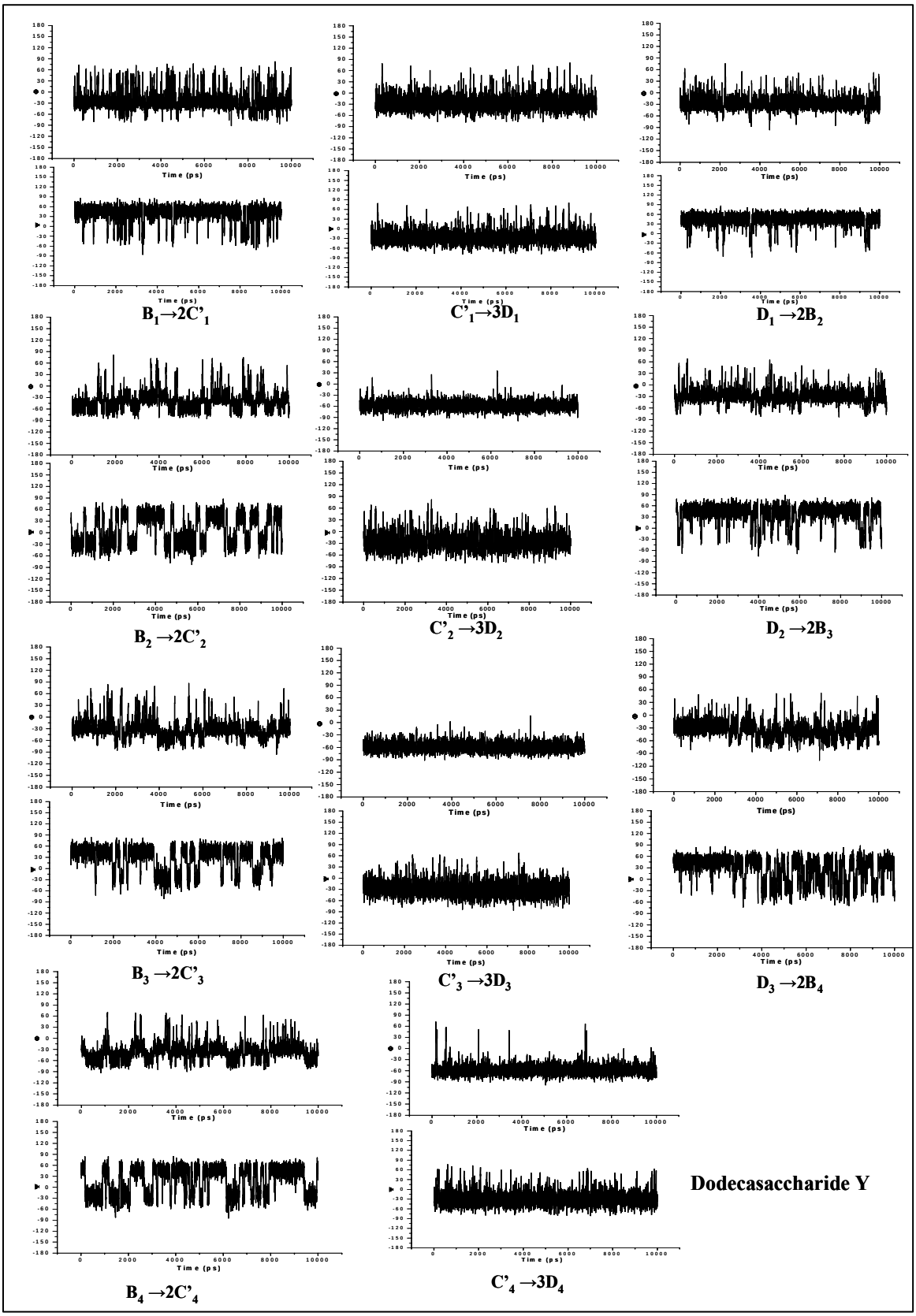

Figure 26. a)Scatter plot s of Φ *vs* Ψ values of both dodecasaccharide species **X** [→ 2)-C-(1→2)-A-(1→3)-D'-(1→]$_4$ and **Y** [→2)-B-(1→2)-C'-(1→3)-D-(1→]$_4$ with reported the populations of every conformational family ; b) Molecular dynamics trajectories of 10 ns MD simulations (Φ and Ψ *versus* time).

Dodecasaccharide X			*Dodecasaccharide Y*		
C_1-$2A_1$	Average Φ	-25.8±21.1	B_1-$2C'_1$	Average Φ	-21.7±27.4
	Average Ψ	42.4±22.6		Average Ψ	37.9±27.0
A_1-$3D_1$'	Average Φ	-55.0±12.7	C'_1-$3D_1$	Average Φ	-54.8±12.8
	Average Ψ	-25.5±20.1		Average Ψ	-24.8±21.4
D_1'-$2C_2$	Average Φ	-33.8±16.9	D_1-$2B_2$	Average Φ	-26.8±17.5
	Average Ψ	32.7±27.3		Average Ψ	42.5±21.4
C_2-$2A_2$	Average Φ	-35.3±20.0	B_2-$2C'_2$	Average Φ	-38.0±26.1
	Average Ψ	26.4±36.1		Average Ψ	7.8±38.6
A_2-$3D_2$'	Average Φ	-56.2±11.2	C'_2-$3D_2$	Average Φ	-56.0±12.4
	Average Ψ	-27.0±19.1		Average Ψ	-25.0±22.3
D_2'-$2C_3$	Average Φ	-35.2±15.4	D_2-$2B_3$	Average Φ	-28.5±19.1
	Average Ψ	31.4±29.1		Average Ψ	37.7±28.0
C_3-$2A_3$	Average Φ	-38.6±19.2	B_3-$2C'_3$	Average Φ	-30.8±25.1
	Average Ψ	19.4±38.7		Average Ψ	27.0±33.9
A_3-$3D'_3$	Average Φ	-56.1±13.7	C'_3-$3D_3$	Average Φ	-57.9±11.5
	Average Ψ	-25.7±20.5		Average Ψ	-27.4±20.2
D_3'-$2C_4$	Average Φ	-36.3±16.0	D_3-$2B_4$	Average Φ	-34.6±18.7
	Average Ψ	28.2±30.8		Average Ψ	26.2±33.7
C_4-$2A_4$	Average Φ	-36.1±20.3	B_4-$2C'_4$	Average Φ	-36.8±22.8
	Average Ψ	22.6±37.1		Average Ψ	16.7±38.0
A_4-$3D_4$'	Average Φ	-54.9±16.2	C'_4-$3D_4$	Average Φ	-56.5±15.6
	Average Ψ	-24.6±25.3		Average Ψ	-26.7±22.9

Table 7. Average Φ and Ψ values and Standard Deviation values from the MD simulation.
$C_1 \rightarrow 2A_1 \rightarrow 3D_1' \rightarrow 2C_2 \rightarrow 2A_2 \rightarrow 3D'_2 \rightarrow 2C_3 \rightarrow 2A_3 \rightarrow D'_3 \rightarrow 2C_4 \rightarrow 2A_4 \rightarrow D'_4$ **Dodecasaccharide X**
$B_1 \rightarrow 2C_1' \rightarrow 3D_1 \rightarrow 2B_2 \rightarrow 2C'_2 \rightarrow 3D_2 \rightarrow 2B_3 \rightarrow 2C'_3 \rightarrow D_3 \rightarrow B_4 \rightarrow 2C'_4 \rightarrow 3D_4$ **Dodecasaccharide Y**

A first analysis of MD results showed that trajectories remained in the broad low energy regions previously predicted by the MM calculation and that all glycosidic linkages for both **Y** and **X** species mainly adopted Φ values in accordance with the *exo*-syn anomeric

conformation, in agreement with the MM results and the experimental data, although some excursions in the non-*exo* regions principally for the reducing units were also observable. The simulation showed a slightly different behaviour and flexibility for the two topologies of glycosidic linkages, α-(1→3) and α-(1→2), present in both species and all involving α-*manno* configured sugar moieties. In fact, the combined examination of trajectories, population and statistical data showed the existence of a rather compact energy well for the α-(1→3) glycosidic linkages (α-Aco-(1→3)-α-Rha (**A**-3**D)** for species **X,** and α-Rha-(1→3)-α-Man (**C'**-3**D)** for species **Y** (figure 26a,b and table 7). Otherwise, a higher flexibility around the α-(1→2) linkages was evident by the analyses of simulation data (scatter plots, population of the conformational families and trajectories reported in figure 26a,b and table 7), showing that several transitions around the minima predicted by the MM calculation were visible. As confirmation, the standard deviation values for these α-(1→2) torsions reported in table 7 (linkages **C**-2**A** and **D'**-2**C** for species **X**, **B**-2**C'** and **D**-2**B** for species **Y**) confirmed the grade of flexibility around this junction, especially along Ψ torsion. Moreover, the statistical data in table 7 showed deviations of various average values of Φ and Ψ angles from those found with the MM calculations, confirming their spanning on a large interval of values during the simulation.

The computational models obtained from the MD were then compared to the experimental results. Ensemble average inter-proton distances for each molecule were extracted from dynamic simulations and translated into NOE contacts according to a full-matrix relaxation approach. The corresponding average distances obtained for the simulation from $\langle r^{-6} \rangle$ values were compared to those collected experimentally (table 8). A satisfactory agreement was observed between the calculated and the experimental values.

	Experimental	**Calculated**
C1-A2	2.36	2.33
A1-D'3	2.25	2.54
D'1-C2	2.29	2.29
B1-C'2	2.52	2.35
C'1-D3	2.13	2.54
D1-B2	2.21	2.30
B1-D1	2.68	2.67

Table 8. Experimental (from ROESY experiments) and calculated (from MD calculations) *inter*-proton distances for repeating unit **X** [→2)-**C**-(1→2)-**A**-(1→3)-**D'**-(1→]$_n$ and **Y** [→2)-**B**-(1→2)-**C'**-(1→3)-**D**-(1→]$_n$.

Given the extent of flexibility around the glycosidic linkages of both O-chain structures, as expected both polysaccharides adopted a variety of three dimensional shapes in rapid interchange. Snapshots of the most representative conformers of O-chain species **X** and **Y** are depicted in figure; both adopted a concave shape even tough with a different extension, more constricted in case of dodecasaccharide **X** and more extended in case of dodecasaccharide **Y**.

In order to definitely assess the conformational behaviour of oligomers composed of these two repeating units and possibly their influence on the macromolecular properties of O-chains, the same approach was applied to tetraeicosaccharides built with eight repeating units:

$[C\rightarrow 2A\rightarrow 3D']_8$ **tetraeicosaccharides X**

$[B\rightarrow 2C'\rightarrow 3D]_8$ **tetraeicosaccharides Y**

The simulation showed again a significant conformational freedom of both oligosaccharides, due to the flexibility of the glycosidic torsions, especially of the α-(1→2) linkage. Again, differences in the conformational behaviour could still be pointed out between the two molecules. In fact, tetraeicosaccharides **Y** [3)-α-D-Man(1→2)-α-D-Man-(1→2)-α-D-Rha(1→]$_8$ tends to behave as a cyclic shaped molecule by bringing in close proximity the sugars at the two terminal residues. Instead, tetraeicosaccharides **X** [3)-α-D-Rha(1→2)-α-D-Man-(1→2)-α-D-Aco(1→]$_8$ tends to adopt a more compact structure in which a minor sized elicoidal structure is formed by about seventeen residues of the whole chain (figures 27). In conclusion, chemical differences in the two repeating units **X** and **Y** imply different three dimensional shape of the two species giving rise to differently packed structures with a distinct extension and bulk.

Figure 27(a-d). View of representative structures and Connelly surfaces of the conformers for species **X** [→ 2)-C-(1→2)-A-(1 →3)-D'-(1→]$_n$ and **Y** [→2)-B-(1→2)-C'-(1→3)-D-(1→]$_n$ built with four and eight repeating units. For species **X** the inset shows the preferential disposition of the methyl groups of the acofriose units.

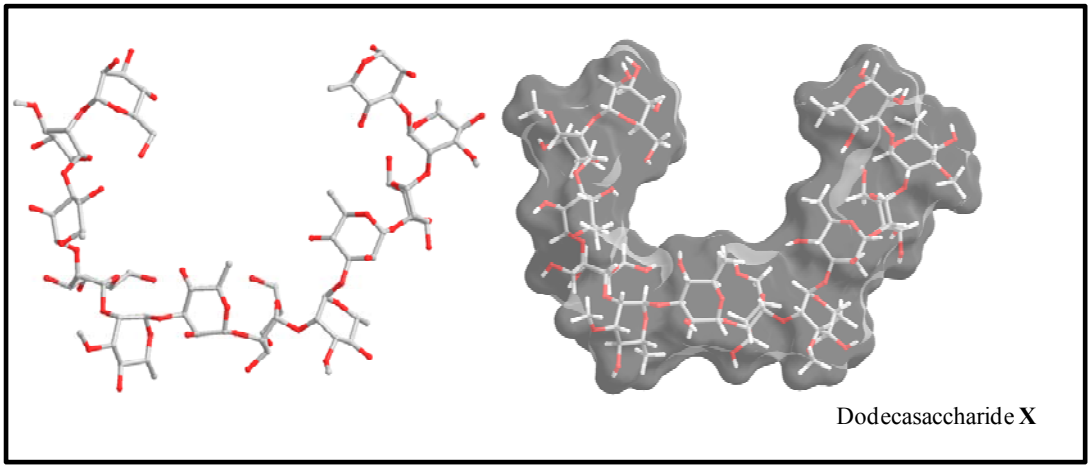

Dodecasaccharide **X**

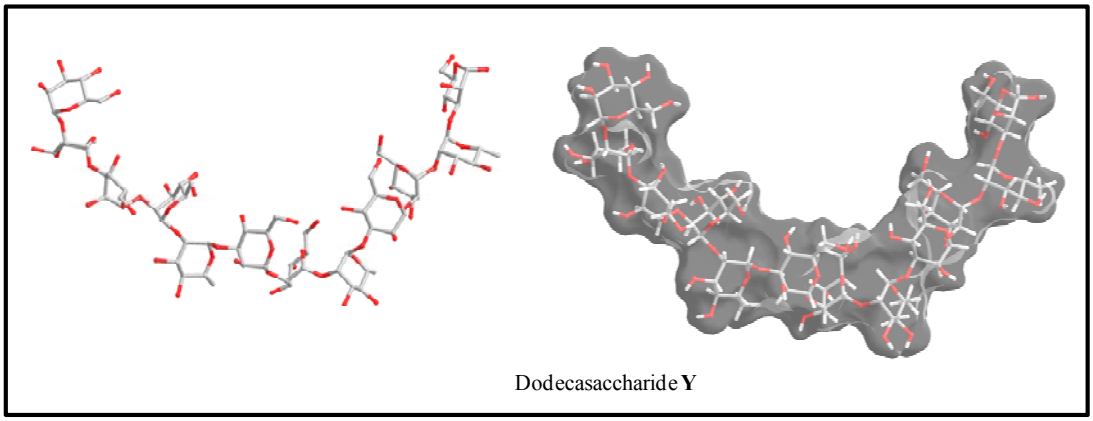

Dodecasaccharide **Y**

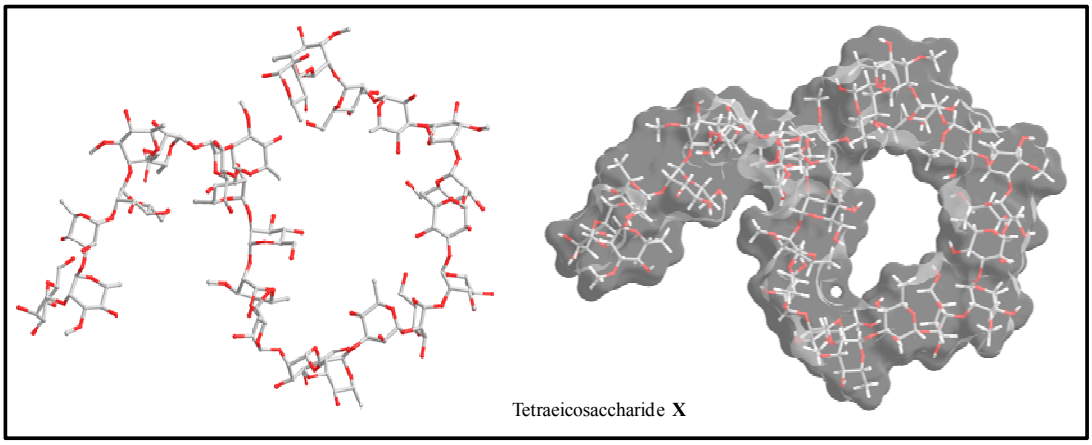

Tetraeicosaccharide **X**

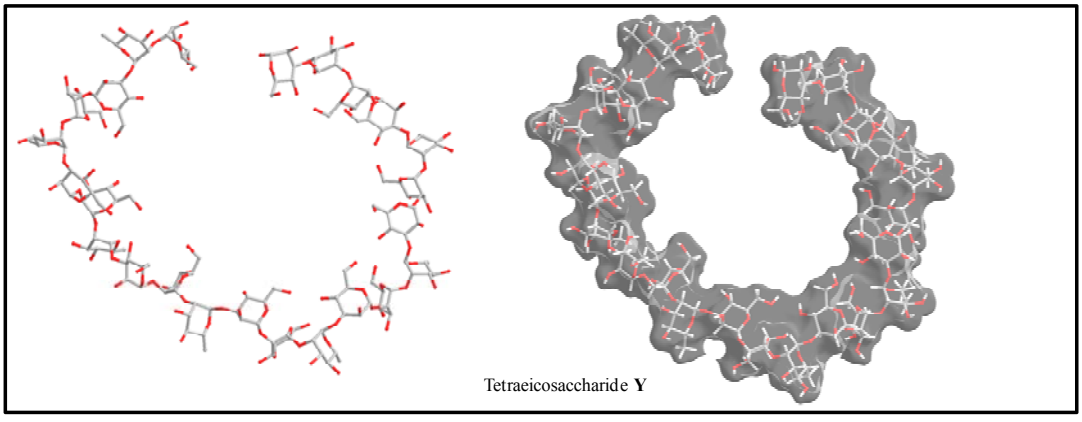

Tetraeicosaccharide **Y**

6.4. Structural characterization of *B. multivorans* C1576 lipid A.

The ESI mass spectrum of lipid A recorded in the negative ion mode showed a complex pattern of $[M-H]^-$ molecular ions (table 9 and figure 28), characterised by seven main (species **3, 4, 5, 6, 9, 12**, and **15** in table 9) and other minor peaks, representing an array of tri- to penta-acylated species.[8,9] The most intense pseudomolecular ion at 1495.2 m/z (species **4**) was assigned to a monophosphorylated glucosamine disaccharide backbone substituted by one 14:0 (3-OH), one 14:0, two 16:0 (3-OH) and one Ara4N residue, while the ion at 1364.1 m/z (species **3**) corresponded to the previous one lacking the Ara4N residue. Interestingly, a tetra-acylated lipid IVa analogue (species **5**) was also present at m/z 1511.2, that is to say, a lipid A ion carrying all primary fatty acids and additionally bearing a Ara4N group. The ion at m/z 1590.3 (species **6**) was attributed to a penta-acylated (two 16:0 (3-OH), two 14:0(3-OH) and one 14:0) monophosphorylated glucosamine disaccharide backbone, while species **9** at 1721.3 m/z carried an additional Ara4N residue. The ion at 1823.3 m/z (species **12**) was attributed to a bis-phosphorylated penta-acylated species with one Ara4N residue whereas species **15** contained an additional Ara4N residue.

The assignment of all the other ions, characterised by a much lower intensity, will not be discussed in details but it is reported in table 9. An expansion of the ESI mass spectrum showing some of these less intense ions is also reported in the inset of figure 28. They are characterised by variations in the number of acyl substituents, Ara4N residues, phosphate groups and Na^+ present as counterions of the phosphate groups.

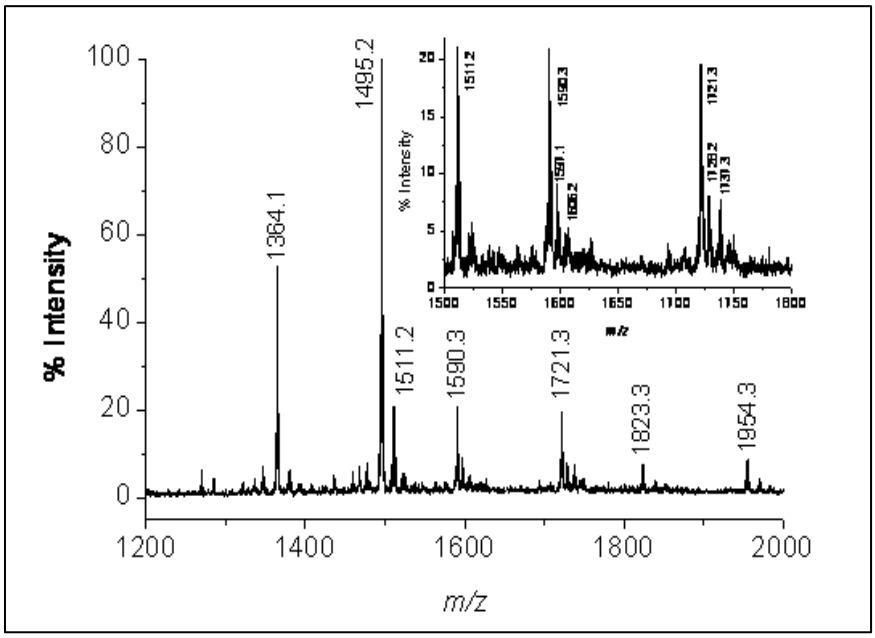

Figure 28. ESI mass spectrum recorded in the negative ion mode of a lipid A sample. In the inset an enlargement of the spectrum with less intense signals is shown.

Observed ion (m/z)	Species	Acyl substitutio	Proposed fatty acid, phosphate and carbohydrate composition
1269.0	**1**	Tri-acyl	2 x 16:0(3-OH), 1 x 14:0, 1 x Ara4N, 1P
1284.9	**2**	Tri-acyl	2 x 16:0(3-OH), 1 x 14:0(3-OH), 1 x Ara4N, 1P
*1364.1	**3**	Tetra-acyl	2 x 16:0(3-OH), 1 x 14:0(3-OH), 1 x 14:0, 1P
*1495.2	**4**	Tetra-acyl	2 x 16:0(3-OH), 1 x 14:0(3-OH), 1 x 14:0, 1 x Ara4N, 1P
*1511.2	**5**	Tetra-acyl	2 x 16:0(3-OH), 2 x 14:0(3-OH), 1 x Ara4N, 1P
*1590.3	**6**	Penta-acyl	2 x 16:0(3-OH), 2 x 14:0(3-OH), 1 x 14:0, 1P
1597.1	**7**	Tetra-acyl	2 x 16:0(3-OH), 1 x 14:0(3-OH), 1 x 14:0, 1 x Ara4N, 2P, $1Na^+$
1606.2	**8**	Penta-acyl	2 x 16:0(3-OH), 3 x 14:0(3-OH), 1P
*1721.3	**9**	Penta-acyl	2 x 16:0(3-OH), 2 x 14:0(3-OH), 1 x 14:0, 1 x Ara4N, 1P
1728.2	**10**	Tetra-acyl	2 x 16:0(3-OH), 1 x 14:0(3-OH), 1 x 14:0, 2 x Ara4N, 2P, $1Na^+$
1737.3	**11**	Penta-acyl	2 x 16:0(3-OH), 3 x 14:0(3-OH), 1 x Ara4N, 1P
*1823.3	**12**	Penta-acyl	2 x 16:0(3-OH), 2 x 14:0(3-OH), 1 x 14:0, 1 x Ara4N, 2P, $1Na^+$
1839.2	**13**	Penta-acyl	2 x 16:0(3-OH), 3 x 14:0(3-OH), 1 x Ara4N, 2P, $1Na^+$
1851.3	**14**	Penta-acyl	3 x 16:0(3-OH), 1 x 14:0(3-OH), 1 x 14:0, 1 x Ara4N, 2P, $1Na^+$
*1954.3	**15**	Penta-acyl	2 x 16:0(3-OH), 2 x 14:0(3-OH), 1 x 14:0, 2 x Ara4N, 2P, $1Na^+$
1970.4	**16**	Penta-acyl	2 x 16:0(3-OH), 3 x 14:0(3-OH), 2 x Ara4N, 2P, $1Na^+$
1982.3	**17**	Penta-acyl	3 x 16:0(3-OH), 1 x 14:0(3-OH), 1 x 14:0, 2 x Ara4N, 2P, $1Na^+$

Table 9. ESI MS negative pseudomolecular ions of lipid A from *B.multivorans*. Main peaks are marked with an asterisk and also shown in figure 28. Observed ions correspond to $[M-H]^-$ monoisotopic ions.

In order to fully assign the primary structure and location of the substituents of the lipid A polymorphic fraction, MS-MS experiments were carried out.

Isolation and fragmentation in the negative ion mode of the pseudomolecular ion at 1495.1 *m/z* gave rise to fragments formed by loss of 14:0 (3-OH) and Ara4N (figure 29), the former suggesting substitution at 3 and /or 3' position of the glucosamine residues with 14:0 (3-OH) fatty acid chains.

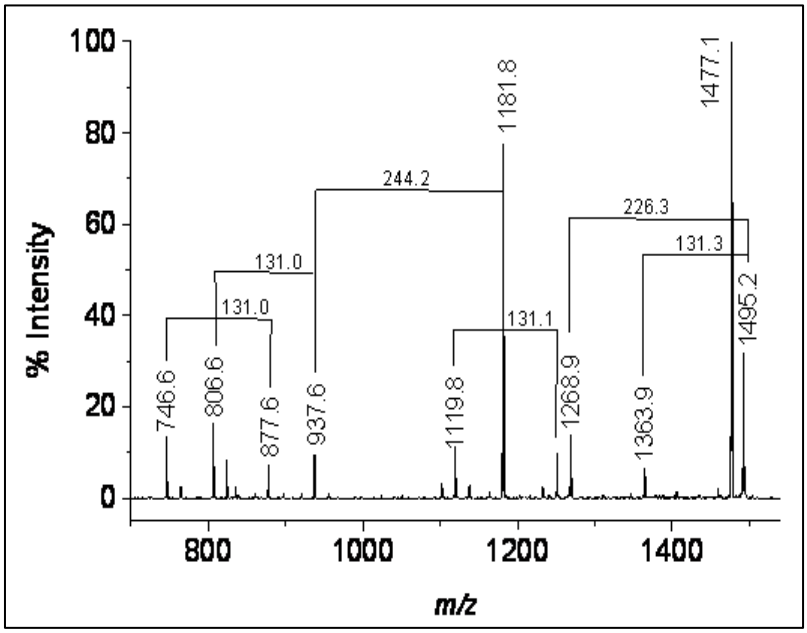

Figure 29. MS^2 of the ion at *m/z* 1495.1 in the negative ion mode

The positive ion-mode ESI mass spectrum showed just two main monophosphorylated sodium adducts at *m/z* 1162.0 and 1388.0: the first was ascribed to a tri-acylated species (two 16:0 (3-OH) and one 14:0 chains) while the second was attributed to a tetra-acylated species (two 16:0 (3-OH), one 14:0 (3-OH) and one 14:0 chains) (spectrum not shown). A signal with low intensity at 1541.0 *m/z* was attributed to the above described tetra-acylated species, substituted with a Ara4N residue and carrying a sodium counterion (data not shown). Isolation and fragmentation of the ion at 1388.0 *m/z* resulted in the identification of the oxonium ion at *m/z* 954.7 (Figure 30a) to which was assigned the following composition: one GlcN, one phosphate group with sodium as counterion, one 16:0 (3-OH), one 14:0 (3-OH) and one 14:0 chains. A high intensity signal at *m/z* 726.5 consistent with loss of the 14:0 fatty acid (228 Da) suggested that it was linked to the acyl amide moiety, as previously reported.[9] Thus, it was also possible to ascertain that in the monophosphorylated species the phosphate group is located on the O-4 of non reducing GlcN II. In the same spectrum, the ion at 1159.8 m/z was due to loss of a 14:0 fatty acid together with water. Its MS^3 mass spectrum (figure 30b) was very informative, since it showed ions deriving from the reducing as well as non-reducing ends. The oxonium ion at 726.4 m/z, present as anhydrous species, was consistent with the following composition: one GlcN, one phosphate group with sodium as counterion, one 16:0 (3-OH), and one 14:0 (3-OH). In the same spectrum the signal at 456.2 *m/z* was assigned to the sodium adduct of a GlcN residue acylated with 16:0 (3-OH), and its neutral characteristic suggested that it derived from the reducing end. Isolation and fragmentation of the ion at *m/z* 1541.0 to

establish the position of L-Ara4N was unsuccessful, because of the low intensity of this signal, and no oxonium ions were observed. However, the oxonium ions at 954.7 and 726.4 *m/z* clearly showed that the phosphate group is located on the GlcN at the non-reducing end, therefore signifying that the Ara4N substituent is also present on the same GlcN residue, given that it is always linked via phosphate.

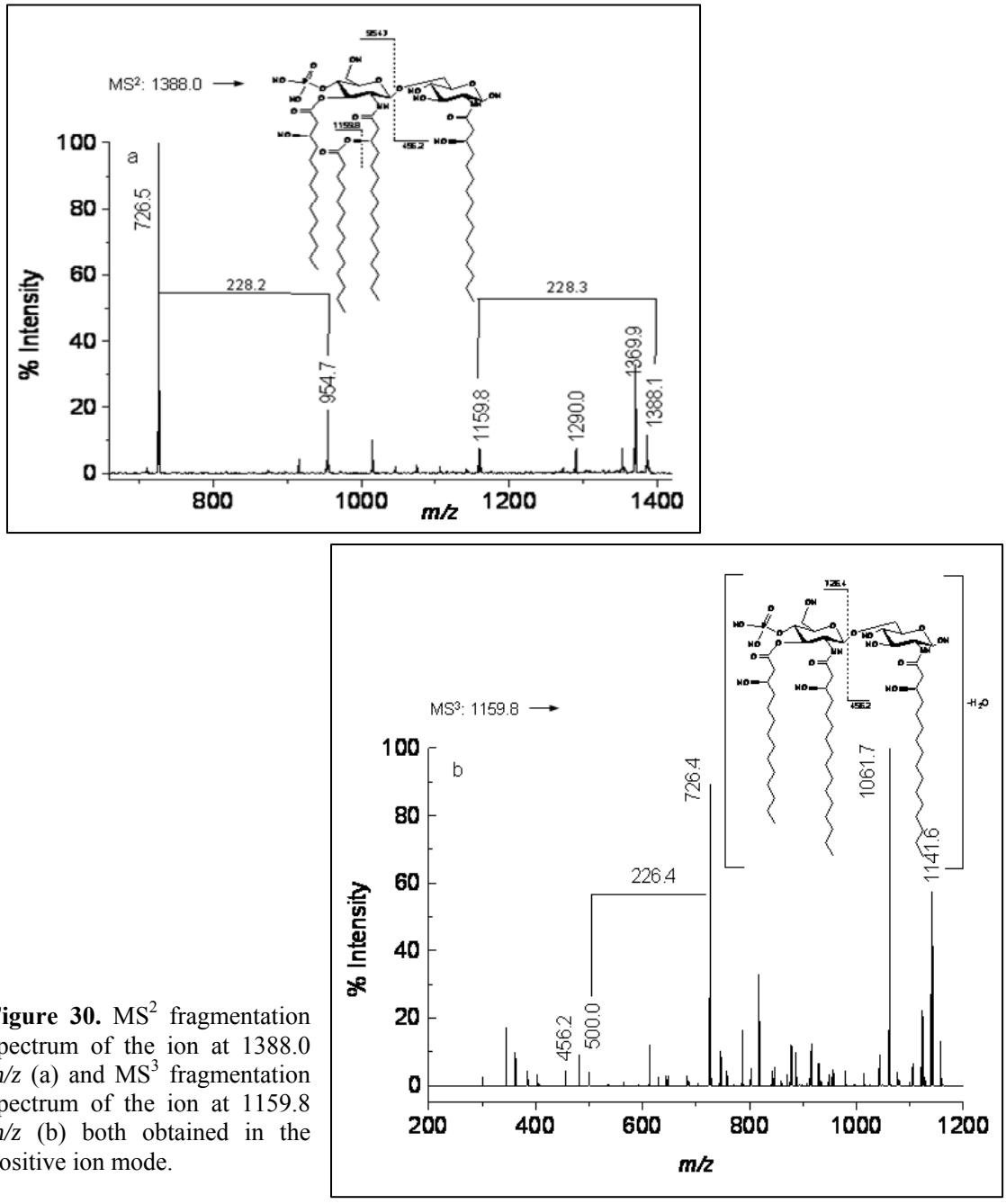

Figure 30. MS^2 fragmentation spectrum of the ion at 1388.0 *m/z* (a) and MS^3 fragmentation spectrum of the ion at 1159.8 *m/z* (b) both obtained in the positive ion mode.

An aliquot of lipid A was selectively *O*-deacylated by treatment with NH_4OH and then subjected to ESI MS analysis. In this way the amide-bound acyloxyacyl moieties were identified, since they were left unaltered by this selective ester hydrolysis reaction (see section III). The negative ion mode ESI mass spectrum obtained is reported in figure 3. As

for the native lipid A, the mass spectrum showed some intense signals (species **18**, **19**, **22**, **24**, **27**, and **31** in table 10) accompanied with other less intense ion peaks. The majority of the molecular forms obtained after NH_4OH treatment derived from loss of one 14:0 (3-OH) chain (Δ = 226.19 amu) from species present in the native sample. A smaller number of ions (species **18**, **20** and **21**) derived from loss of one 14:0 chain from molecular species present in the native sample. The pseudomolecular ion at 1058.8 *m/z* (species **18**) was attributed to a di-acylated monophosphorylated lipid A bearing a Ara4N residue and two 16:0 (3-OH) chains in amide linkage. The two main ions at *m/z* 1137.9, and 1268.9 (**19** and **22**) corresponded tri-acylated (two 16:0 (3-OH), one 14:0), monophosphorylated molecules differing for the presence of L-Ara4N ($\Delta m/z$ = 131.06). The third intense ion at *m/z* 1364.0 (species **24**) was assigned to a tetra-acylated form deriving from the loss of one 14:0 (3-OH) chain from species **6**. The ions at 1597.0 and 1728.0 *m/z* (species **31** and **32**) corresponded to a tetra-acylated, bis-phosphorylated forms differing for the content in Ara4N residues (table 10). The assignment of the less intense ions is not discussed in details but it is reported in table 10.

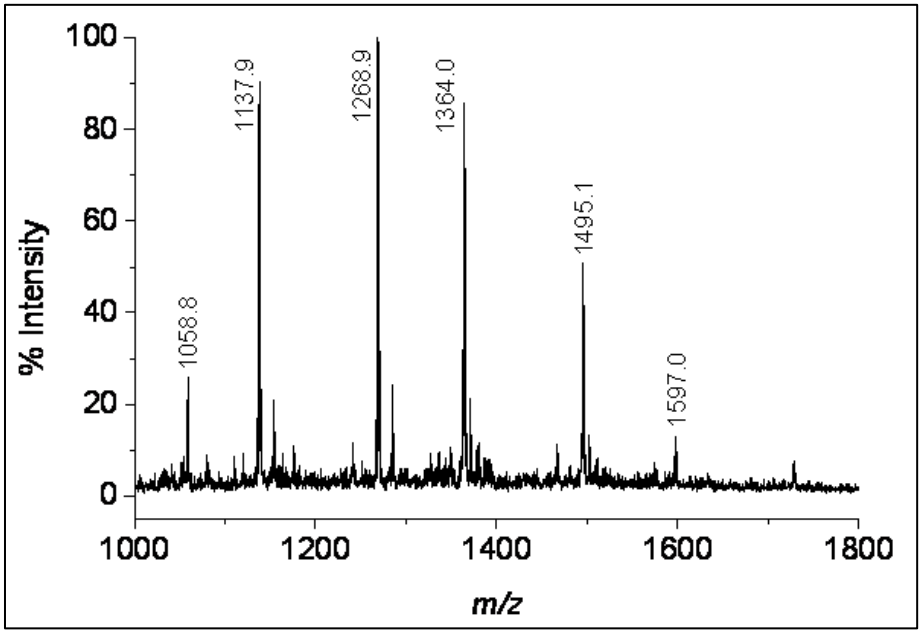

Figure 31. ESI mass spectrum recorded in the negative ion mode of a sample of lipid A after O-deacylation with NH_4OH.

Observed ion (m/z)	Species	Acyl substitution	Proposed fatty acid, phosphate and carbohydrate composition
*1058.8	**18**	Di-acyl	2 x 16:0(3-OH), 1 x Ara4N, 1P
*1137.9	**19**	Tri-acyl	2 x 16:0(3-OH), 1 x 14:0, 1P
1153.9	**20**	Tri-acyl	2 x 16:0(3-OH), 1 x 14:0(3-OH), 1P
1175.9	**21**	Tri-acyl	2 x 16:0(3-OH), 1 x 14:0(3-OH), 1P, $1Na^+$
*1268.9	**22**	Tri-acyl	2 x 16:0(3-OH), 1 x 14:0, 1 x Ara4N, 1P
1284.9	**23**	Tri-acyl	2 x 16:0(3-OH), 1 x 14:0(3-OH), 1 x Ara4N, 1P
*1364.0	**24**	Tetra-acyl	2 x 16:0(3-OH), 1 x 14:0(3-OH), 1 x 14:0, 1P
1370.9	**25**	Tri-acyl	2 x 16:0(3-OH), 1 x 14:0, 1 x Ara4N, 2P, $1Na^+$
1380.1	**26**	Tetra-acyl	2 x 16:0(3-OH), 2 x 14:0(3-OH), 1P
*1495.1	**27**	Tetra-acyl	2 x 16:0(3-OH), 1 x 14:0(3-OH), 1 x 14:0, 1 x Ara4N, 1P
1501.9	**28**	Tri-acyl	2 x 16:0(3-OH), 1 x 14:0, 2 x Ara4N, 2P, $1Na^+$
1511.1	**29**	Tetra-acyl	2 x 16:0(3-OH), 2 x 14:0(3-OH), 1 x Ara4N, 1P
1575.0	**30**	Penta-acyl	2 x 16:0(3-OH), 1 x 14:0(3-OH), 1 x 14:0, 1 x Ara4N, 2P
*1597.0	**31**	Penta-acyl	2 x 16:0(3-OH), 1 x 14:0(3-OH), 1 x 14:0, 1 x Ara4N, 2P, $1Na^+$
1728.0	**32**	Tetra-acyl	2 x 16:0(3-OH), 1 x 14:0(3-OH), 1 x 14:0, 2 x Ara4N, 2P, $1Na^+$

Table 10. ESI MS negative pseudomolecular ions of lipid A from *B. multivorans*, after NH_4OH treatment. Main peaks are marked with an asterisk and also shown in Figure 3. Observed ions correspond to $[M-H]^-$ monoisotopic ions.

In agreement with what already found in the intact sample, the positive ion mode ESI mass spectrum revealed two main sodium adducts at *m/z* 1161.8 and 1388.0. Isolation and fragmentation of the ion at 1161.8 *m/z* (data not shown) yielded an oxonium ion at 728.5 *m/z* composed by one GlcN, one sodium phosphate group, one 16:0 (3-OH) and one 14:0 chains. The loss of 228 Da (the 14:0 fatty acid) from the ion at 728.5 *m/z* resulted in a high intensity ion at 500.3 *m/z,* confirming the location of the 14:0 chain on the 16:0 (3-OH)

sitting on the non reducing GlcN residue, in agreement with the data found for the native lipid A.

All information gained from the experiments described above together with the data reported in figure 28 and table 9 lead to a complete picture of lipid A primary structure from *B. multivorans* C1576. The highest mass ion peak, **15** at *m/z* 1954.3 [M+Na^+] is consistent with a penta-acylated disaccharide backbone substituted by two phosphoryl-arabinosamine residues [β-L-Ara*p*4N-1-P→4-β-D-Glc*p*N-(1→6)-α-D-Glc*p*N-1→P-1-β-L-Ara*p*4N], carrying in ester linkage two 14:0(3-OH) chains and in amide linkage, two 16:0(3-OH) chains, one of which, on the GlcN II, is further substituted by a secondary fatty acid, a 14:0 residue. Species **12** (*m/z* 1823.3) lacks one Ara4N residue, while species **9** (*m/z* 1721.3) lacks also a phosphate group and bears one Ara4N on non reducing GlcN II. The ion **6** consists a monophosphorylated penta-acylated lipid A only bearing one phosphate with no other sugar units than the disaccharide backbone. The two major ion species (**3** and **4**) of the mass spectrum both consisted in tetra-acylated mono-phosphorylated species. The ion at *m/z* 1364.1 lacked the anomeric phosphate and a primary O-linked 14:0(3-OH) on one of the GlcNs whereas, as only difference, the ion peak at *m/z* 1495.2 possessed a further Ara4N residue linked to GlcN II *via* phosphodiester bond. On the same basis, species **5** could be defined as a unique tetra-acylated species bearing all primary fatty acids and phosphoryl-arabinosamine group at GlcN II whereas it possessed a free reducing end.

6.5 Effects of *Burkholderia multivorans* lipid A on intestinal CACO-2 cell lines and on CF airways

B. multivorans lipid A biological activity was investigated by inducing epithelial activation in different cell culture models. Firstly, the biological activity was analysed in a widely used intestinal epithelial cell line. Caco 2 cells were cultured for 24 hours in the presence of *Escherichia coli* LPS (EC-LPS) or lipid A from *B. multivorans* (BM-LipidA). LPS from *E. coli* was used as a well known inducer of epithelial activation.[11,12] The effects on tyrosine phosphorylation, a marker of epithelial activation[12] were assessed by confocal microscopy using the PY-99 antibody. Confocal images revealed that lipid A from *B. multivorans* was as effective as *E. coli* LPS in enhancing membrane tyrosine phosphorylation (figure 32a).

Additionally, to investigate whether *B. multivorans* lipid A was effective in triggering an inflammatory response in CF airways, epithelial cell line carrying a common

ΔF508/W1282X CFTR mutation were used. These CF airway epithelial cells show a constitutive inflammatory phenotype as a consequence of defective CFTR function,[11] and are hyper-responsive to LPS stimulation. In our experiments, lipid A stimulation in IB3 cells increased TNFα expression (Figure 32b), as compared to unstimulated cells. This indicates that it is as effective as *Pseudomonas aeruginosa* (PA) LPS stimulation.[13]

In order to assess whether lipid A was relevant in triggering airways inflammation *in vivo* in CF airways, an *ex vivo* model of culture explants of nasal polyps was used.[11] In such a model it was tested whether BMLA was as effective as PA LPS that was already reported to induce dramatic epithelial activation upon 4 h challenge of CF biopsies.[11] Even in this case, BMLA was highly effective in inducing tyrosine phosphorylation (figure 32c) and COX-2 expression with respect to the pattern observed in unstimulated nasal polyp mucosae (figure 32d). Moreover, the increase of IL-8 protein levels was detected in culture supernatants upon lipid A stimulation (figure 32d). These effects were similar to those obtained upon PA LPS stimulation.

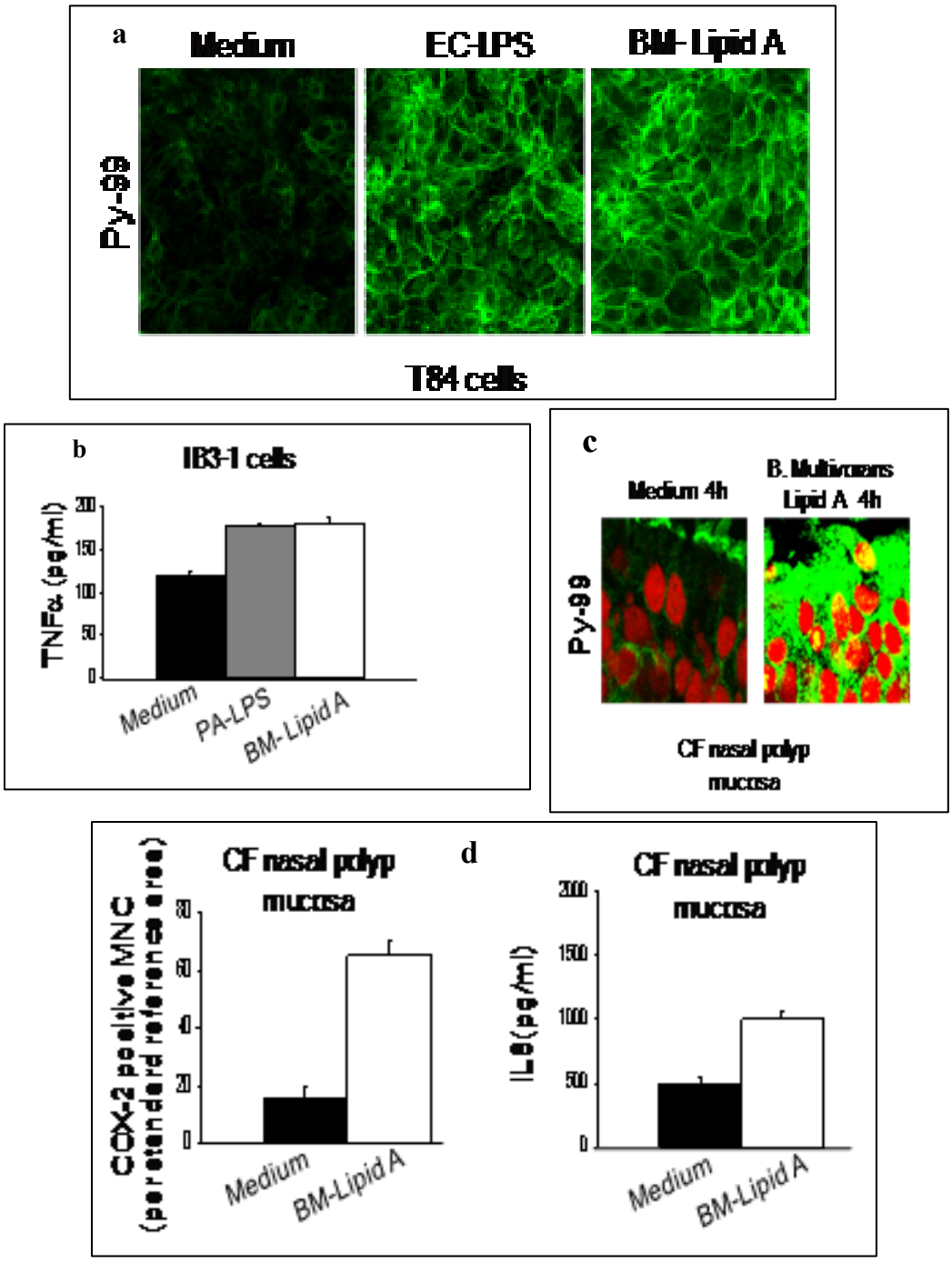

Figure 32. a) Confocal images of T84 cells incubated with medium alone, EC-LPS or BM-lipid A and immunostained with Py99 (green). BM-lipid A challenge for 24 hours induce an impressive increase of epithelial phosphotyrosine expression (Py99, green) in T84 cell lines. b) TNF-α secretion in IB3-1 cell line c) Confocal images of CF nasal mucosa incubated with medium alone or BM-lipid A and immunostained with Py99 (green). BM-lipid A challenge for 4 hours induce an impressive increase of epithelial phosphotyrosine expression (Py99, green) in CF nasal mucosa. CyTRAK orange (red) nuclear counterstaining. d) Induction of COX-2 protein expression by mucosal mononuclear cells (MNC) following BM-lipid A challenge (24 hours). IL-8 protein expression in culture supernatants after 4 hours of BM-lipid A challenge of nasal polyp explants from CF patients.

6.6 Discussion

The *Burkholderia multivorans* LPS object of this study derives by one of the major Cystic Fibrosis pathogens among the Bcc and possesses a mixture of two O-chain with different repeating units :

[→2-α-D-Man-(1→2)-α-D-Rha-(1→3)-α-D-Man-1→]$_n$ (species **Y**) (60 %)

and

[→2-α-D-Man-(1→2)-α-D-Aco-(1→3)-α-D-Rha1→]$_n$ (species **X**) (40 %).

There exists several O-antigen structures isolated and characterised from *Bcc* strains[14] although no data have been reported for *B. multivorans* so far. The biosynthesis of two different O-chain polysaccharides in Gram-negative bacteria is not so common, even though is usual for *Burkholderia* spp (*B, caryophylli*, *B. cepacia*, *B. vietnamensis*).[14] The O-antigens belonging to *Bcc* are rather simple structures with few sugars constituting the repeating unit, very often containing 6-deoxysugar (typically L-rhamnose), and, in case of trisaccharide repeating unit, with at least one sugar present twice. Actually, these features are also found in the O-antigens from *B. multivorans* strain C1576 since the two trisaccharide repeating units are both presenting α-*manno* configured 6-deoxy-sugars. Moreover, some other relevant peculiarities can be found in these structures; they both present D-configured rhamnose, that within *Bcc* LPS was only previously found in the O-polysaccharide of *B. cepacia*.[15] Furthermore, in species **X** the 2-substituted-α-Rha is stoichiometrically substituted by a methyl group at O-3 (acofriose). The presence of non carbohydrate appendages, such as a methyl group, is common to several antigens isolated from *Bcc* strains, often presenting *O*-acyl decorations, although the *O*-methyl substitution has been found for the first time decorating an O-polysaccharide from *Burkholderia* LPS. These chemical modifications contribute to define the physico-chemical properties of the extracellular surface. In fact, the presence of deoxy-sugars increases the hydrophobic character of both polysaccharides and in polysaccharide **X,** the degree of hydrophobicity is high and yields particular three- dimensional properties. Under the immunological point of view, the presence of rhamnose residues in the O-chain of several *Burkholderia* LPS has been be deemed to play a key role in the bacterial interaction with host recognition systems, i.e., in plant innate immunity.[16] Both oligosaccharides adopted a comparable shape even though with a different extension; in details, they did not assume an extended conformation, but both showed the tendency to approach a ring-like structure. The chain ends of the polymer containing the acofriose unit (species **X**) were closer than the ones possessing no

acofriose (species **Y**) giving rise to a more compact structure. This led to higher differences in the conformational arrangements when polymers were modelled with twenty-four monomers (eight repeating units). In fact, while the chain without acofriose moiety remained in an "open-ring" conformation, the other one seemed to wrap on itself creating a narrower loop in which about seventeen residues were required to form a cyclic substructure. Thus, again species **Y** adopted a more extended shape, as observable from the Connolly surface (figure 27), while the species **X** presented a more contracted structure. Another distinctive feature of the presence of the acofriose (3-*O*-methyl rhamnose) unit was the relative spatial disposition of all *O*-methyl groups, mainly extending towards the same direction to create a hydrophobic shield. In conclusion, the existence of two repeating units implied different three dimensional shapes giving rise to structures with a different packing and extension. This leads to supramolecular arrangements that allow the expression of specific serotype.

As for lipid A moiety, *B. multivorans* C1576 smooth-type LPS possesses a remarkably major mono-phosphorylated tetra-acylated lipid A species which may bear (or not) a further Ara4N residue. It is tempting to speculate that, within the same architectural framework, lipid A undergoes post-biosynthesis modifications and bioactivity modulation also depending by LPS size, i.e., the putative presence of the O-polysaccharide. This would explain, in case of *B. multivorans* LPS fraction, the existence of a *bis*-phosphorylated and penta-acylated lipid A as major species in the presence of a lipooligosaccharide (see chapter 3) while monophosphorylated and tetracylated species are present in case of a lipopolysaccharide. Within this frame, it was very interesting the detection, for the first time in *Burkholderia*, of a particularly underacylated form, the lipid IVa analogue species **5**, which obviously derives from the complete penta-acyl lipid A by a successive selective enzymatic hydrolysis of the secondary fatty acid and anomeric phosphate (and Ara4N).

Moreover, in this work it has also been demonstrated that lipid A is effective in triggering an inflammatory response in CF airways. By a multifaceted approach using either bronchial epithelial cell lines or human airways mucosal biopsies, it has been shown that the lipid A from *Burkholderia multivorans* is as effective as the LPS from *Pseudomonas aeruginosa* in inducing early features of innate immunity activation in CF biopsies. The used culture model represents a good and interesting approximation to *in vivo* studies since all the anatomical connections are retained and all cell types (epithelial, myeloid, lymphoid) still interact with neighboring cells within their natural environment. Moreover it has been demonstrated that nasal mucosa provides a suitable representation of CF chronic airways

inflammation.[11] This study revealed that lipid A is a potent trigger of inflammatory response and induces IL8 secretion, that recruits large numbers of neutrophils into the airways, and epithelial activation by triggering the p38-MAP-kinase pathway. The inhibition of p38-MAP kinase pathway is effective in controlling the features of inflammation induced upon BMLA stimulation.[2]

All together these results demonstrate that lipid A of *Burkholderia multivorans* is endowed with pro-inflammatory activity and also provide evidences that lipid A is at least one of the factors responsible for the pathogenicity of the *Burkholderia multivorans* in patients with Cystic Fibrosis.

References

1. Ieranò T, Silipo A, Cescutti P, Leone MR, Rizzo R, Lanzetta R, Parrilli M, Molinaro A. "Structural study and conformational behavior of the two different lipopolysaccharide O-antigens produced by the cystic fibrosis pathogen *Burkholderia multivorans*." *Chemistry-A European Journal* (2009), 15: 7156-66.

2. Ieranò T, Cescutti P, Leone MR, Luciani A, Rizzo R, Raia V, Lanzetta R, Parrilli M, Maiuri L, Silipo A, Molinaro A. "The lipid A of *Burkholderia multivorans* C1576 smooth-type lipopolysaccharide and its pro-inflammatory activity in a cystic fibrosis airways model." *Innate Immunity* (2009), accepted for publication.

3. Govan JR, Brown AR, Jones AM. Evolving epidemiology of *Pseudomonas aeruginosa* and the *Burkholderia cepacia* complex in cystic fibrosis lung infection. *Future Microbiol* (2007) 2: 153-164.

4. Whiteford ML, Wilkinson JD, McColl JH *et al.* Outcome of *Burkholderia* (*Pseudomonas*) *cepacia* colonisation in children with cystic fibrosis following a hospital outbreak. *Thorax* (1995) 50:1194-8.

5. Mahenthiralingam E, Coenye T, Chung JW *et al.* Diagnostically and experimentally useful panel of strains from the *Burkholderia cepacia* complex. *J Clin Microbiol* (2000) 38: 910-913.

6. Lemieux RU, Koto S, Voisin D. in *ACS Symposium Series* (Eds: A. Szarek, D. Horton), American Chemical Society, Washington, D. C., 1979, Vol. 87, 17.

7. Clément MJ, Imberty A, Phalipon A, Pérez S, Simenel C, Mulard LA, Delepierre M. Conformational study of the O-specific polysaccharide of *Shigella flexneri* 5a and of four related synthetic pentasaccharide fragments using NMR and molecular modeling. *J. Biol. Chem.* (2003). 278 : 47928–47936.

8. De Soyza A, Ellis CD, Khan ACM, Corris PA, Demarco de Hormaeche R. *Burkholderia cenocepacia* lipopolysaccharide, lipid A, and proinflammatory activity. *Am J Respir Crit Care Med* (2004). 170: 70-77

9. De Soyza A, Silipo A, Lanzetta R, Govan JR, Molinaro A. Chemical and biological features of *Burkholderia cepacia* complex lipopolysaccharides. *Innate Immun* (2008). 14: 127-144.

10. Sforza S, Silipo A, Molinaro A, Marchelli R, Parrilli M, Lanzetta R. Determination of fatty acid positions in native lipid A by positive and negative electrospray ionization mass spectrometry. *J Mass Spectrom* (2004) 39: 378-383.

11. Raia V, Maiuri L, Ciacci C, Ricciardelli I, Vacca L, Auricchio S, Cimmino M, Cavaliere M, Nardone M, Cesaro A, Malcolm J, Quaratino S, Londei M. Inhibition of p38 mitogen activated protein kinase controls airway inflammation in cystic fibrosis. *Thorax* (2005) 60: 773-80.

12. Maiuri L, Luciani A, Giardino I, Raia V, Villella VR, D'Apolito M, Pettoello-Mantovani M, Guido S, Ciacci C, Cimmino M, Cexus ON, Londei M, Quaratino S. Tissue transglutaminase activation modulates inflammation in cystic fibrosis via PPARgamma down-regulation. *J Immunol* (2008) 180: 7697-705.

13. Pier GB. *Pseudomonas aeruginosa* lipopolysaccharide: a major virulence factor, initiator of inflammation and target for effective immunity. *Int J Med Microbiol* (2007) 297: 277-295.

14. Vinion-Dubiel AD, Goldberg JB. Lipopolysaccharide of *Burkholderia cepacia* complex. *Journal of Endotoxin Research* (2003) 9: 201-213.

15. Cérantola S, Montrozier H. Structural elucidation of polysaccharides present in the lipopolysaccharide of a clinical isolate of B. cepacia. *Eur. J. Biochem.* (1997) 246: 360-366.

16. Mattos KA, Todeschini AR, Heise N, Jones C, Previato JO, Previato LM. Nitrogen-fixing bacterium *Burkholderia brasiliensis* produces a novel yersiniose A-containing O-polysaccharide. *Glycobiology* (2005) 15: 313-321.

CHAPTER 7

CONFORMATIONAL ANALYSIS OF CORE OLIGOSACCHARIDE ISOLATED FROM *B. CENOCEPACIA* ET-12 STRAIN.

Herein it has been performed a conformational analysis and a MD simulation (using AMBER software package) of the oligosaccharidic region of the LOS molecule extracted from a clinical isolate strain of *B. cenocepacia* ET-12 type strain LMG 16656 (also known as J2315). *B. cenocepacia* accounts for the majority of CF isolates and, within this grouping, there are a number of strains responsible for causing often fatal epidemics, in particular the ET-12 clone. The ET-12 strain predominates in several CF centers, has enhanced virulence and capacity of spread.[1] The higher mortality rates following lung transplantation appear restricted to ET-12 infected patients. For these reasons, it has been designed as the type strain and its genome was sequenced by Sanger centre. A structure to function relationship study on these endotoxins is required since LOS are the main virulence factors of Gram-negative bacteria and they have a strong biological activity responsible for bacterial pathogenicity.

The primary structure of the core-oligosaccharide portion isolated from *B. cenocepacia* ET-12 has been carried out through chemical analysis, 2D NMR and MALDI experiments:[2]

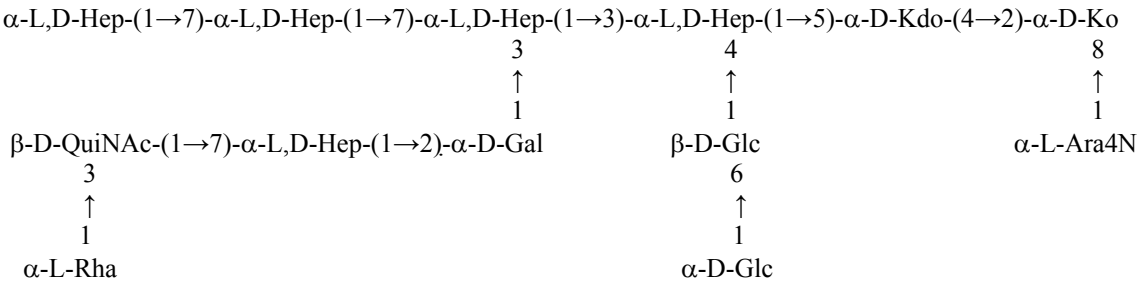

7.1 Conformational analysis of core oligosaccharide

Conformational analysis started with the definition of the relative orientation of sugar residues. Disaccharides were build considering all the possible conformers for each monomer unit, that is to say that were considered all the possible orientations of the hydroxymethyl group around the C5-C6 bond (*gauche-gauche* and *gauche-trans* for *gluco* and *manno* conformers; *trans-gauche* and *gauche-trans* for *galacto* conformers, and all the

orientation of hydroxyl ring groups (clockwise, c, and counter clockwise, r). The only exceptions were for C5-C6 bond of L-*glycero*-α-D-*manno*-heptose (α-L,D-Hep) residue, that was always considered in a *gg* conformation, and for C6-C7 bond of do and Ko that were instead considered in *tg* conformation as previously reported in literature.[3,4] Thus, considering all the possible values assumed by each couple of Φ (O_5-C_1-O-C_X) and Ψ (C_1-O-C_X-C_{X+1}), as descriptors of the torsion angle of a 1→X glycosidic linkage, adiabatic maps were built for each disaccharide. The conformational space of each disaccharidic fragment was explored stepping Φ and Ψ angles of 20° increments over the whole angular range. Energy maps (figure 33) were constructed and subjected to calculations using MM3 force field.[5]

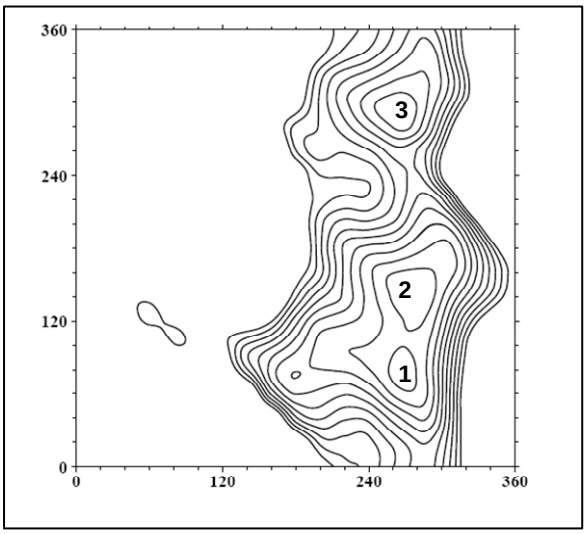

α-L-Rha-3-β-D-QuiNac

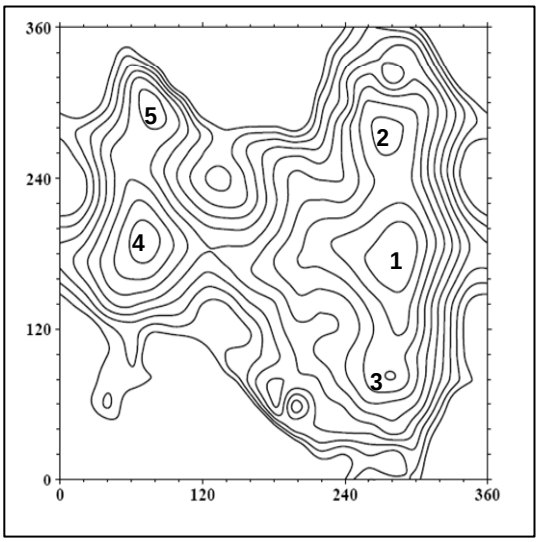

β-D-QuiNac-7-α-L,D-Hep

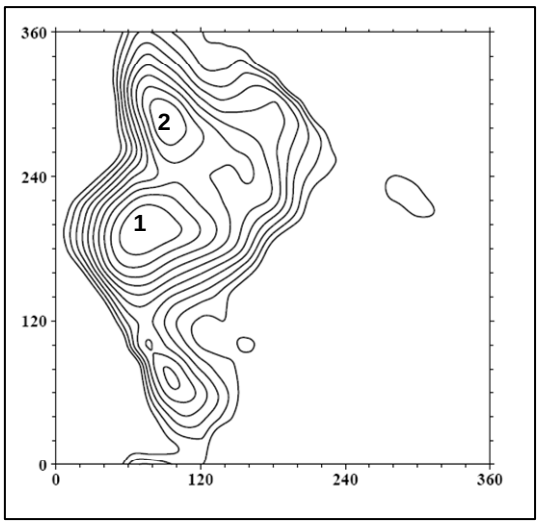

α-L,D-Hep-2-α- D-Gal

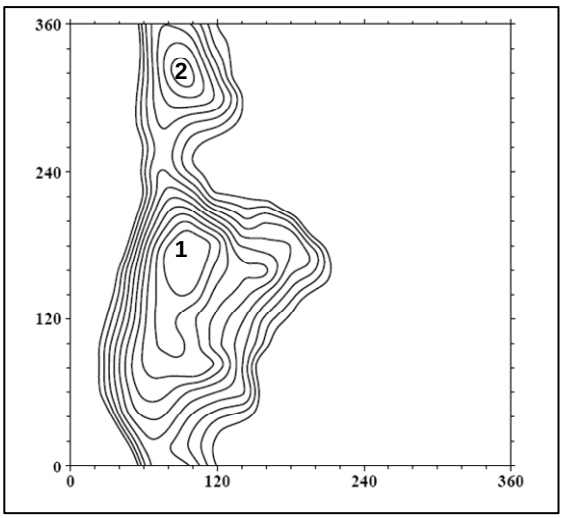

α-D-Gal-3-α-L,D-Hep

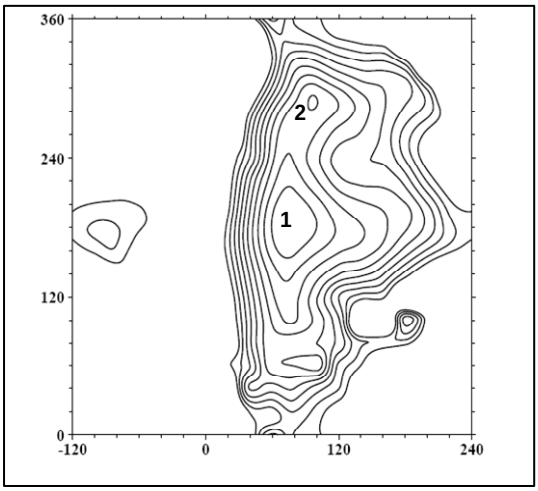

α-D-Glc-6-α-D-Gal_*tg*

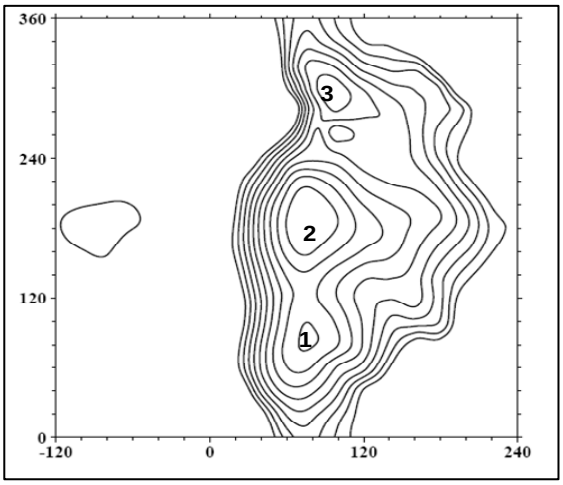

α-D-Glc-6-α-D-Gal_*gt*

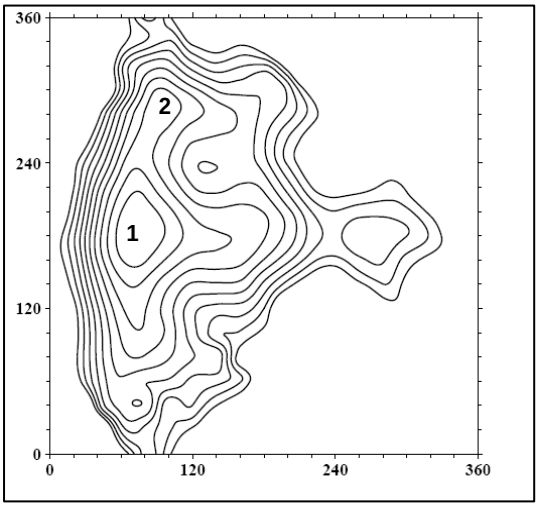

α-L,D-Hep-7-α- L,D-Hep

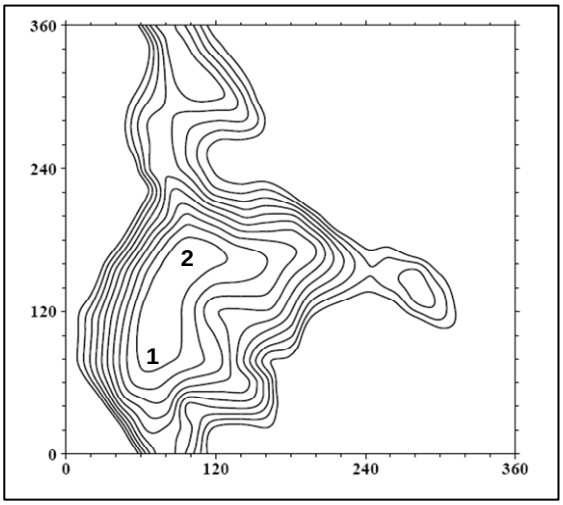

α-L,D-Hep-3-α- L,D-Hep

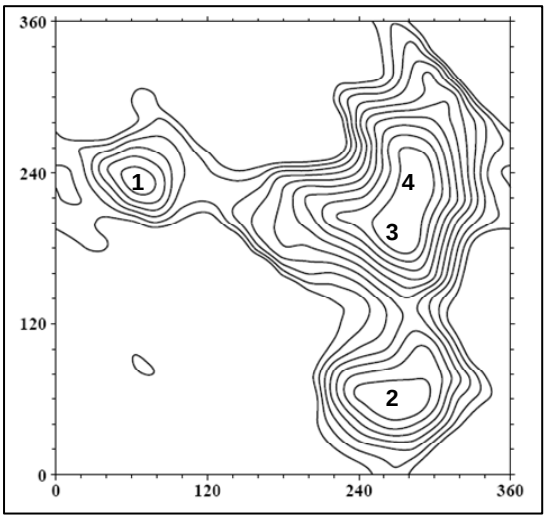

β-D-Glc-4- α-L,D-Hep

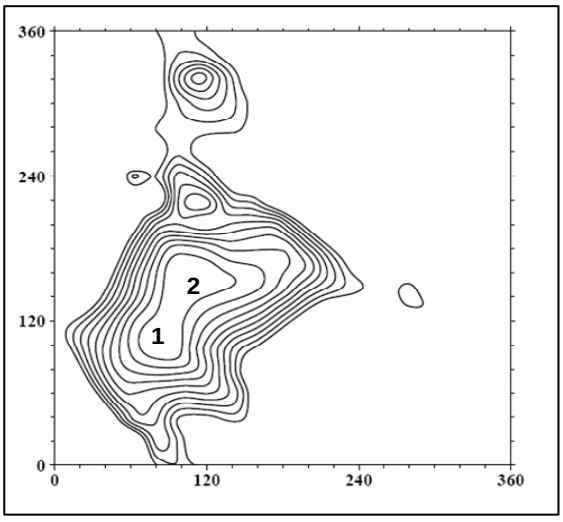

α-L,D-Hep-5-α-D-Kdo

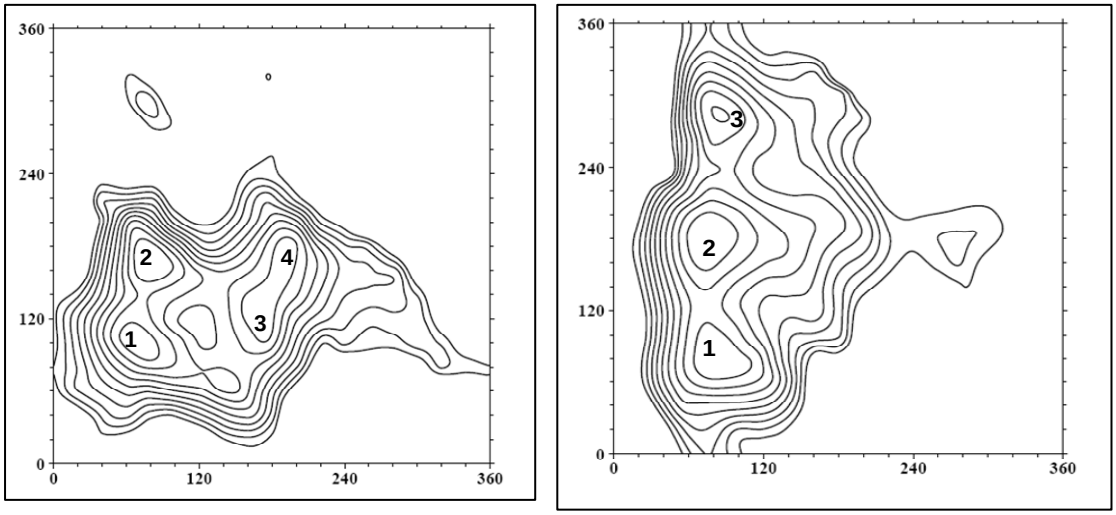

α-D-Ko-4-α-D-Kdo β-L-Ara4N-8-α-D-Ko

Figure 33. Adiabatic maps of each disaccharide constituting the core oligosaccharide from *B. cenocepacia* ET-12. For the α-D-Glc-6-α-D-Gal linkage, the orientation *gt* and *tg* of the hydroxymethyl group around the C5-C6 bond are both considered since they are equiprobable.The position of the global and major local minima in the map are indicated with numbers.

7.2 Molecular dynamics simulation

Considering the global minima of the energy maps, the tridecasaccharide was built and its conformational behaviour was studied by a molecular dynamic simulation in explicit solvent, using AMBER 8 package (University of California). Since in the oligosaccharidic sequence a disaccharide α-D-Glc-(1→6)-α-D-Gal is present, two oligosaccharide were build differing for the *gt* and the *tg* conformation at C5-C6 bond of galactose residue. Thus, a parallel analysis of the two possible situations (named oligo_*gt* and oligo_*tg*) was started in the same conditions. The Xleap program was run in order to obtain topology and coordinates files for both oligosaccharides considered. Monomers present in the oligosaccharidic sequence not included in Glycam database (D-QuiNAc, L-Ara4N, L,D-Hep, Kdo, Ko) were obtained through *antechamber* program. Glycam_06 force field was used[6] and the whole system was neutralized with the addition of a Na^+ ion; further, an octahedral box of water TIP3PBOX was added using a cut-off of 12 angstroms.

The initial structures were extensively minimized. Primarily, the system was minimised holding the solute fixed, and then the whole system was minimised. Further, in both cases

(for oligo_*gt* and *tg)*, the whole system was heated from 0 K to 300 K using a weak restrain on the solute. The system was then equilibrated at 300 K using constant pressure, removing the restrains on the solute and a MD simulation of 20,000 ps was started.

MD analysis results are reported below. Trajectories and Φ/Ψ scatter plots of the different glycosidic linkages and the population of each conformational family are shown in the following figure 34.

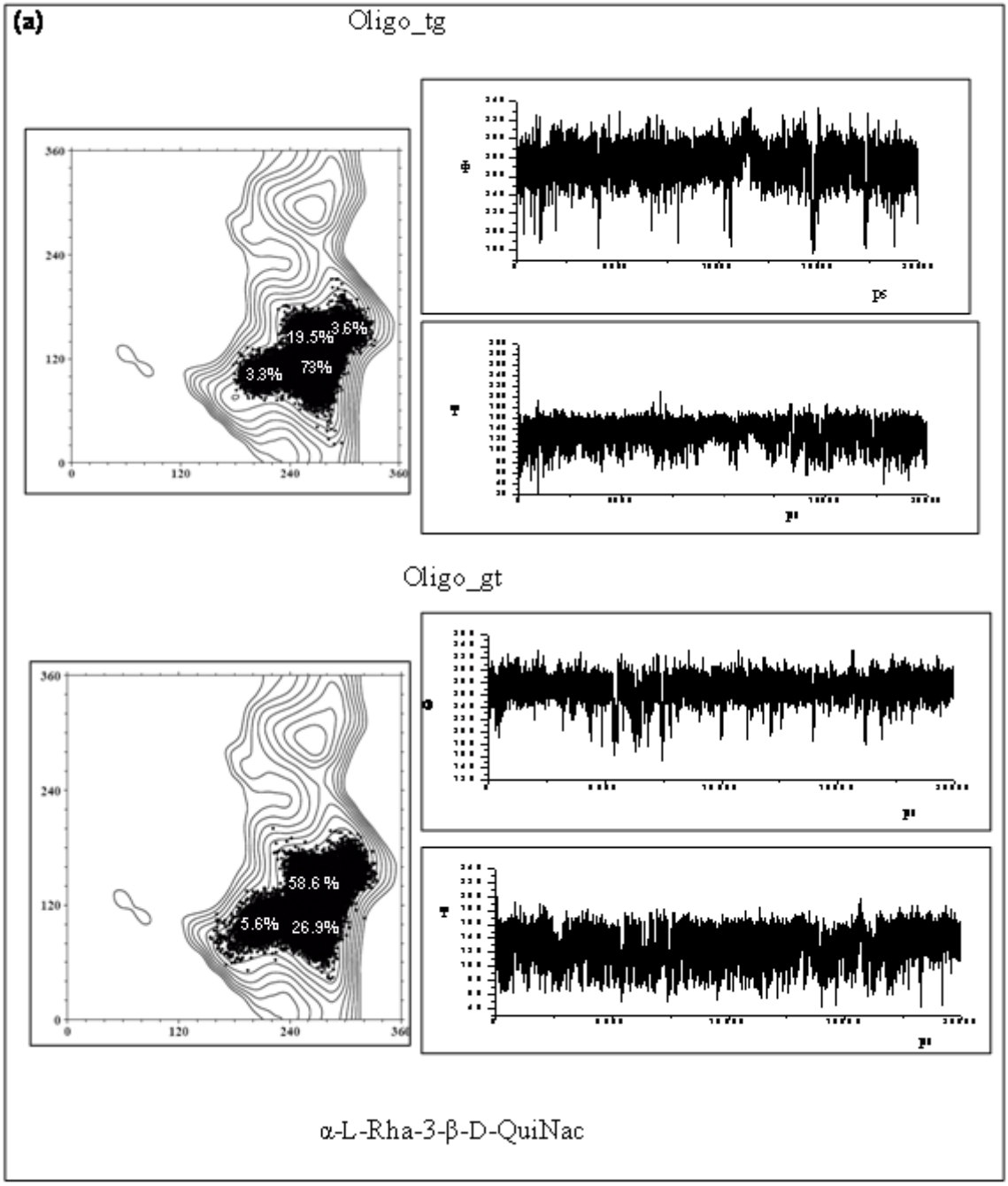

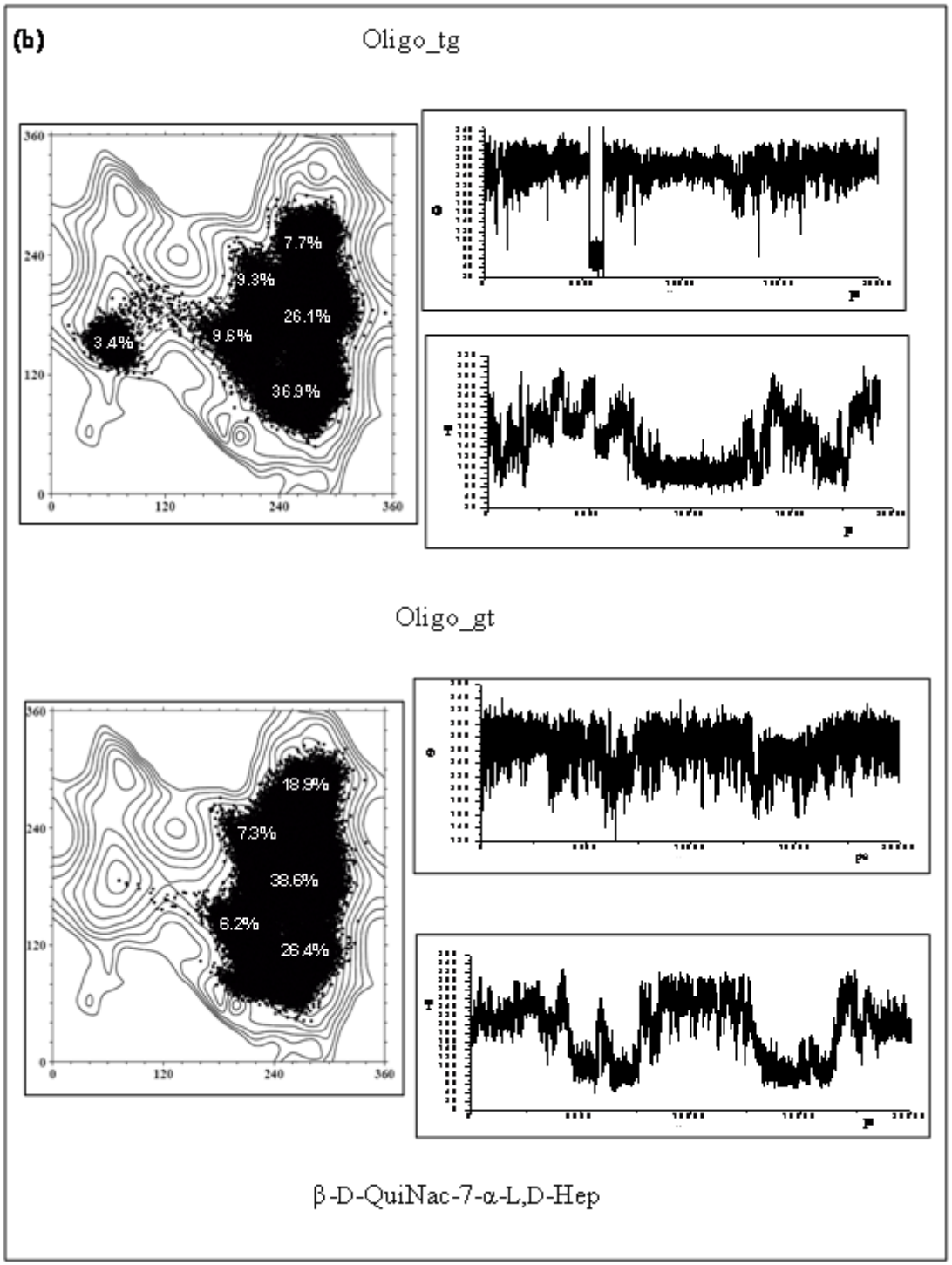
(b)
Oligo_tg
7.7%
9.3%
26.1%
9.6%
3.4%
36.9%
Oligo_gt
18.9%
7.3%
38.6%
6.2%
26.4%
β-D-QuiNac-7-α-L,D-Hep

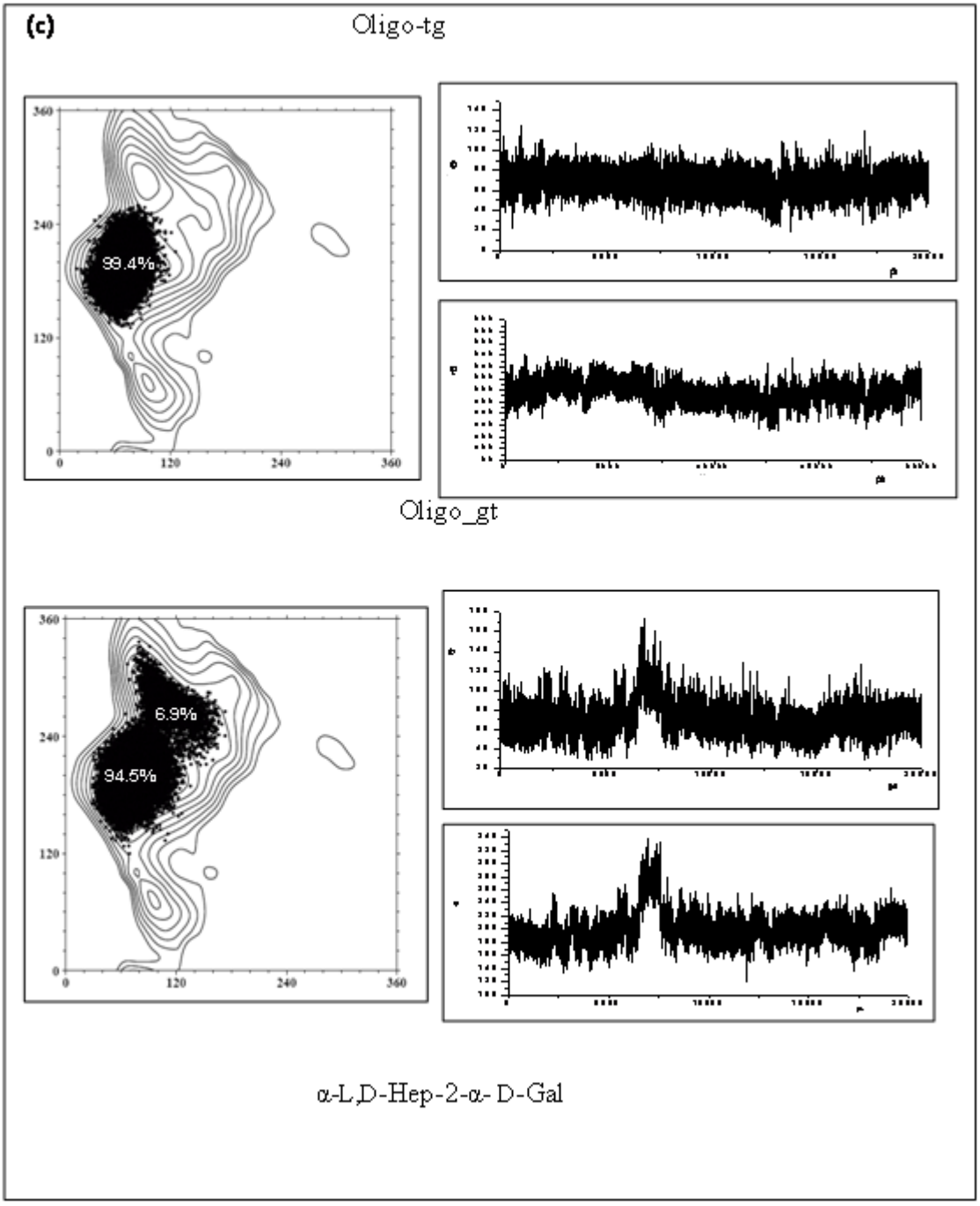
(c)
Oligo-tg
99.4%
Oligo_gt
6.9%
94.5%
α-L,D-Hep-2-α- D-Gal

(d)

Oligo _tg

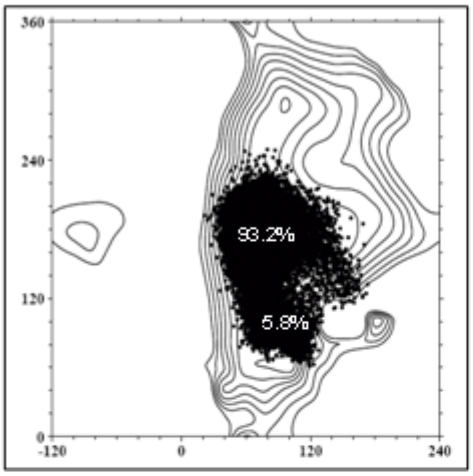

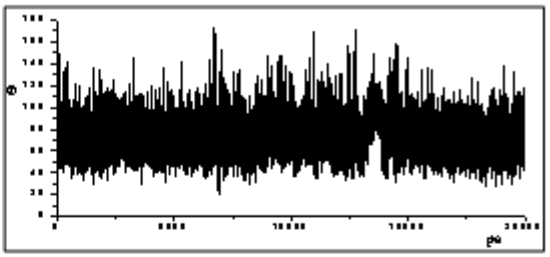

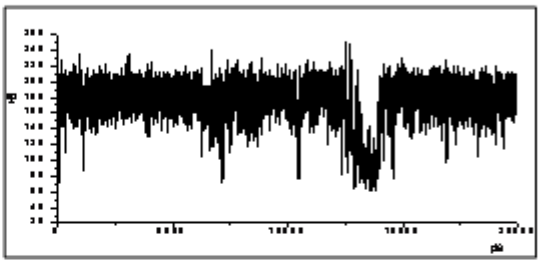

Oligo_gt

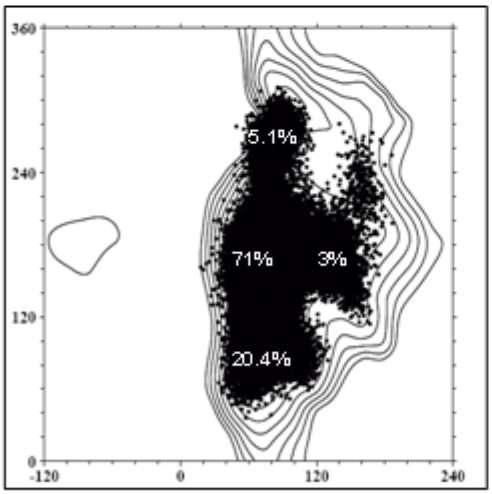

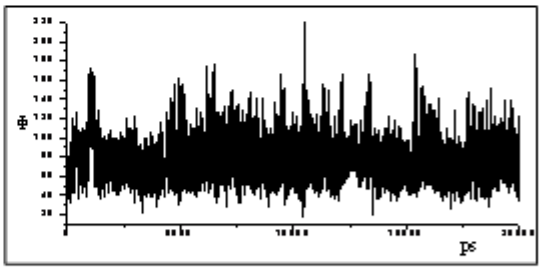

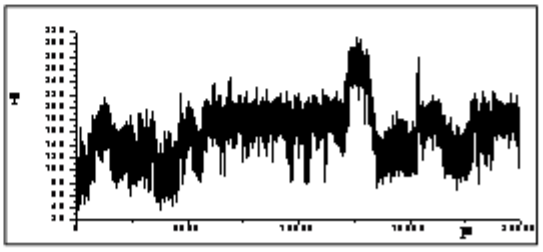

α-D-Glc-6-α-D-Gal

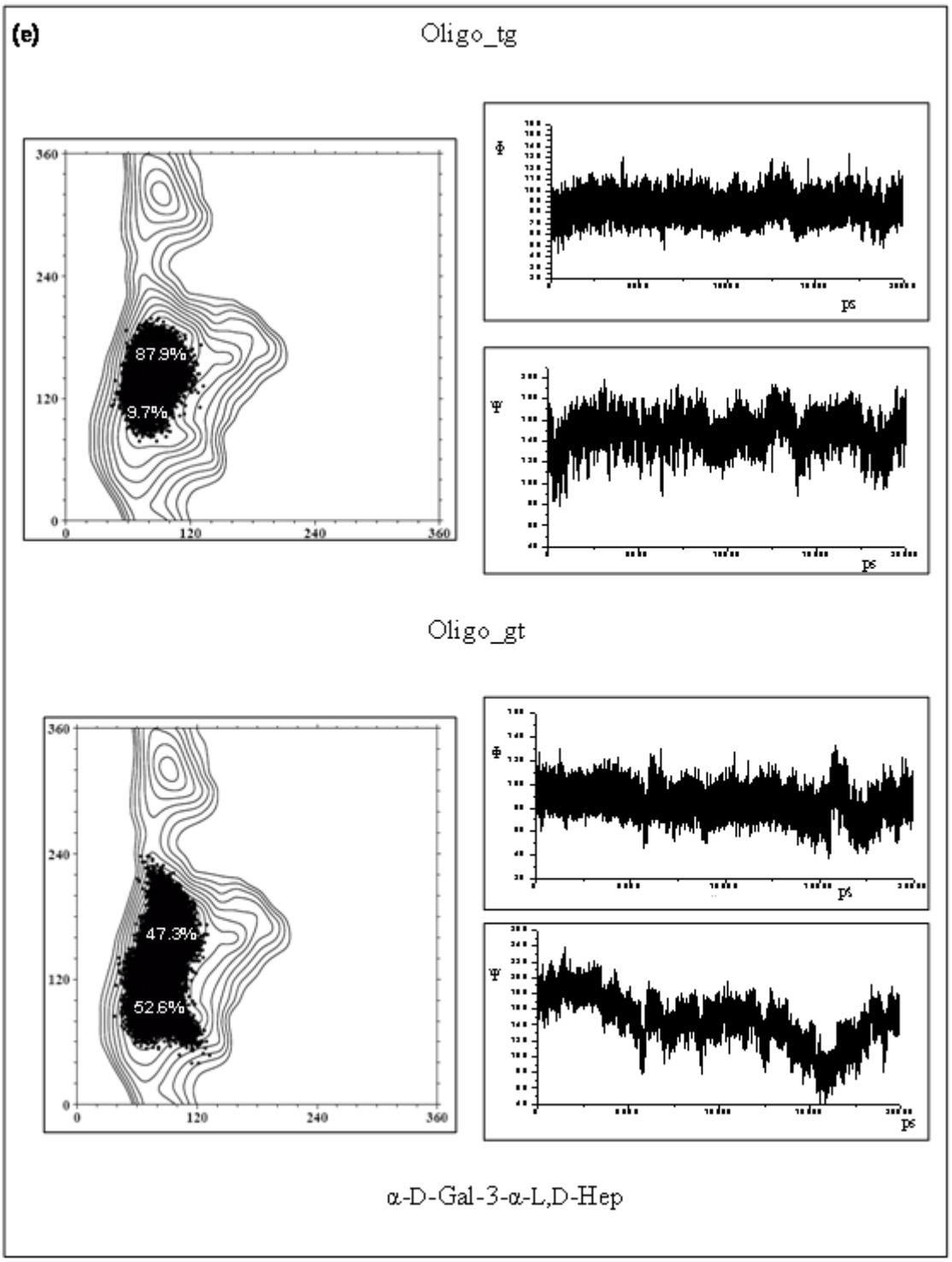
(e)
Oligo_tg
360
240
120
0
0
120
240
360
87.9%
9.7%
Φ
Ψ
ps
Oligo_gt
47.3%
52.6%
α-D-Gal-3-α-L,D-Hep

(f)

Oligo_tg

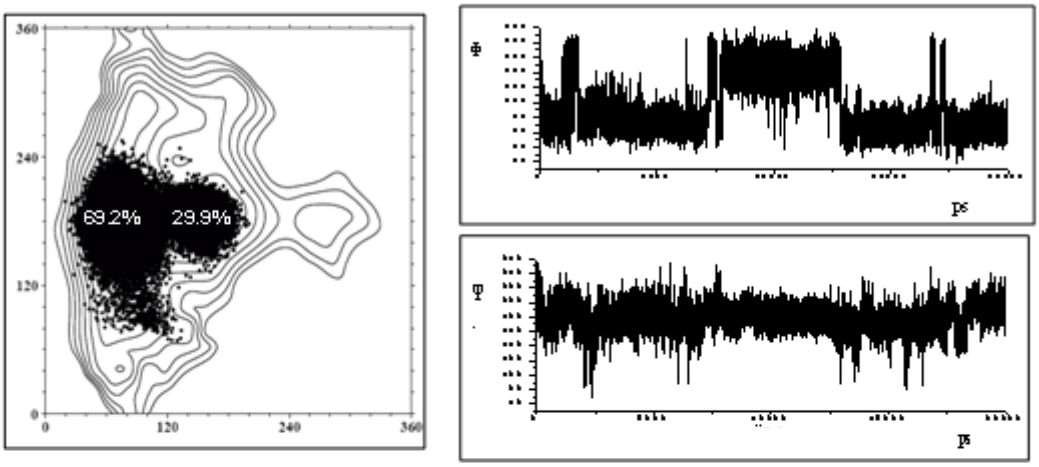

Oligo_gt

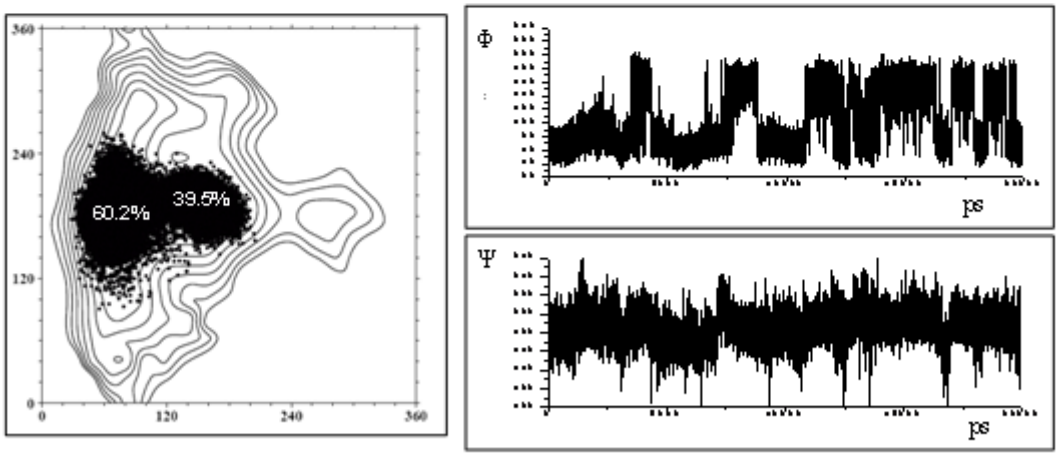

7α-L,D-Hep-7-α-L,D-Hep

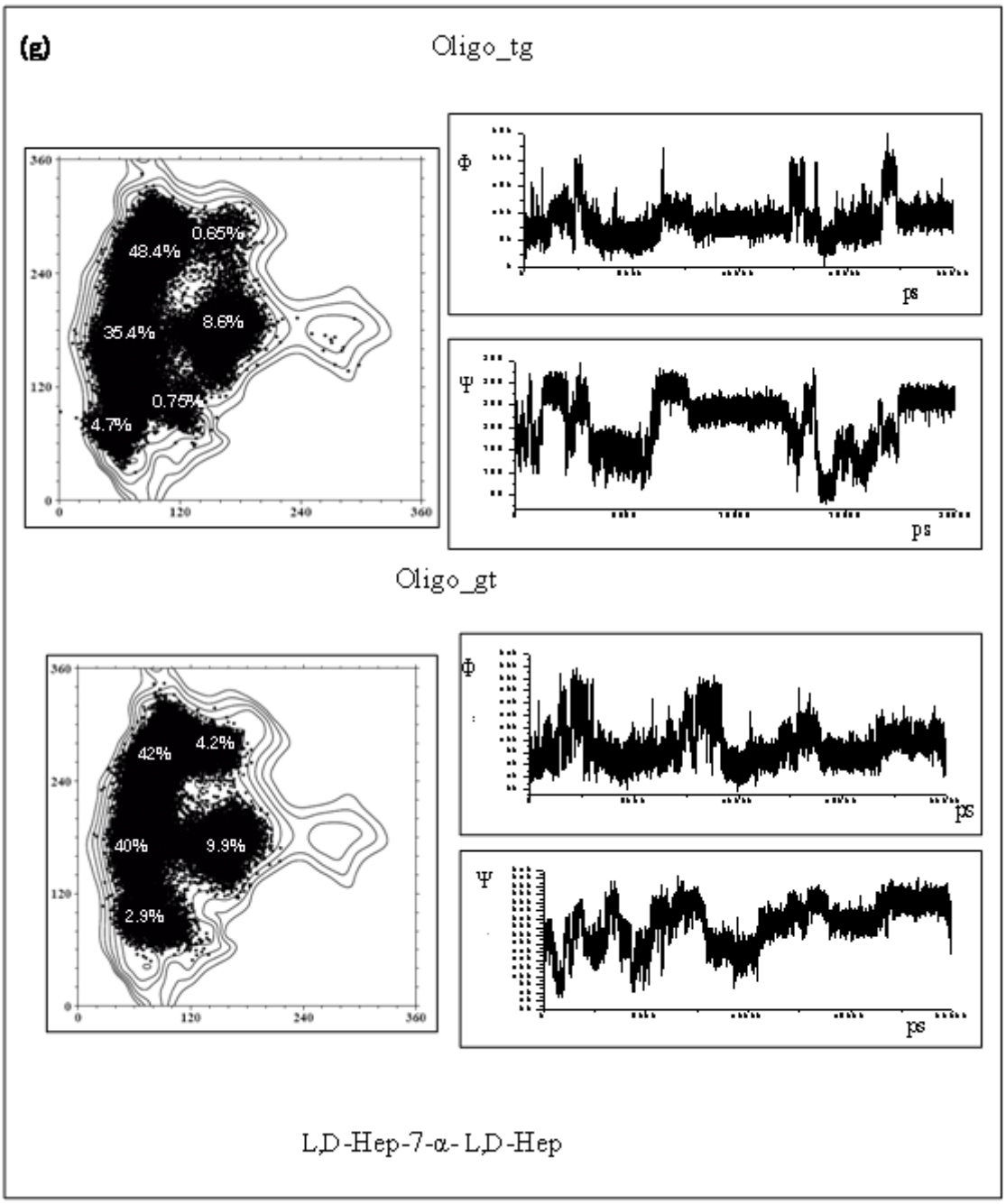
(g)
Oligo_tg
48.4%
0.65%
35.4%
8.6%
0.75%
4.7%
Φ
ps
Ψ
ps
Oligo_gt
42%
4.2%
40%
9.9%
2.9%
Φ
ps
Ψ
ps
L,D-Hep-7-α-L,D-Hep

(h)

Oligo_tg

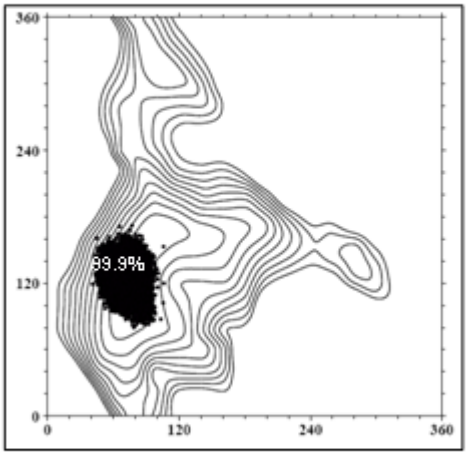

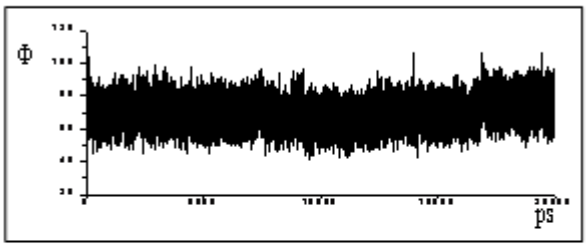

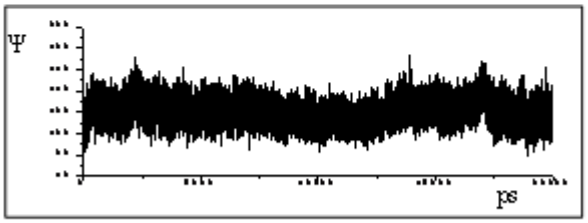

Oligo_gt

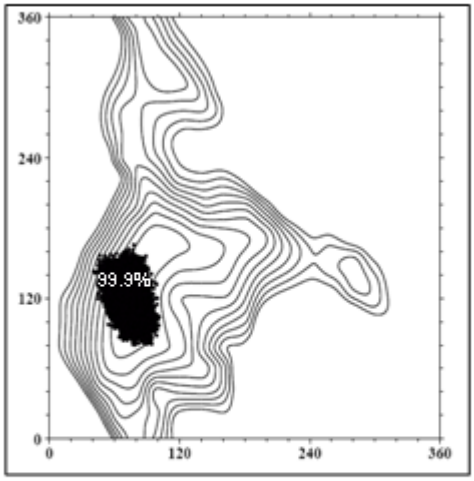

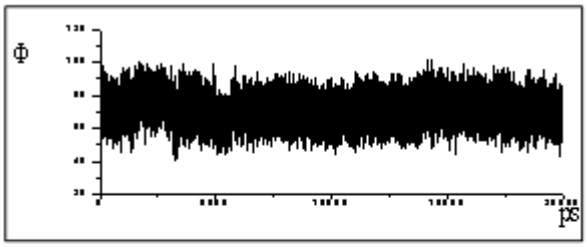

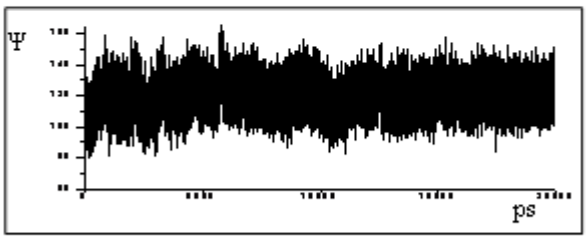

L,D-Hep-3-α-L,D-Hep

(i)

Oligo_tg

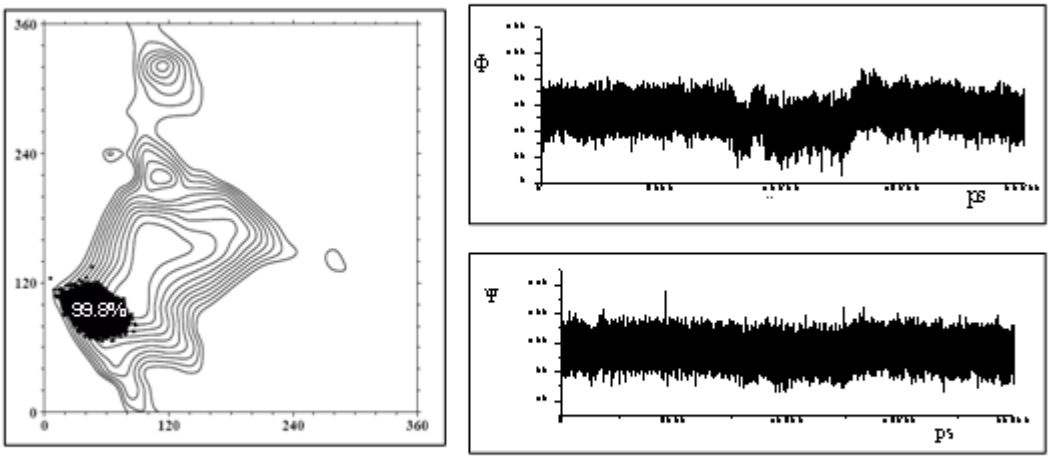

Oligo_gt

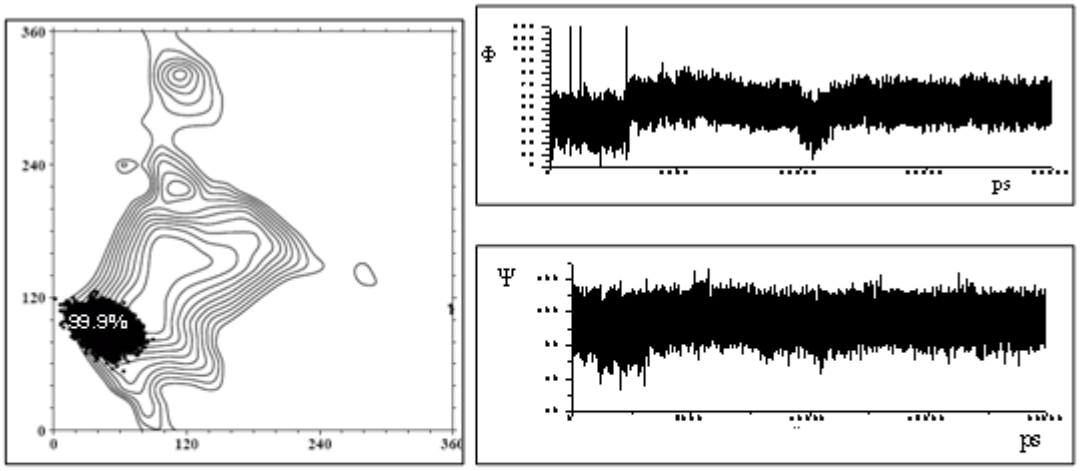

L,D-Hep-5-α-D-Kdo

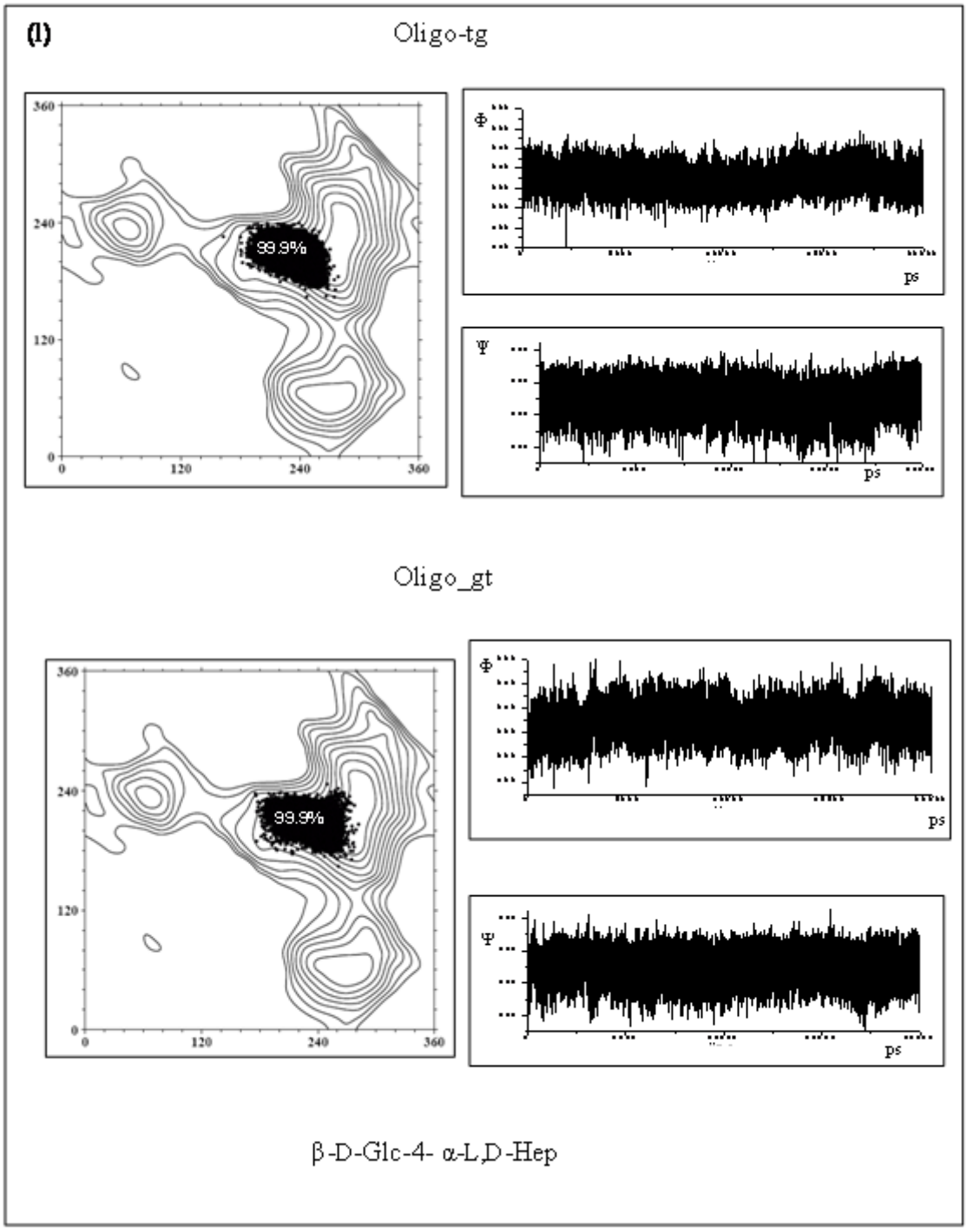
(I)
Oligo-tg
360
240
120
0
0
120
240
360
99.9%
Φ
ps
Ψ
ps
Oligo_gt
360
240
120
0
0
120
240
360
99.9%
Φ
ps
Ψ
ps
β-D-Glc-4- α-L,D-Hep

(m)

Oligo_tg

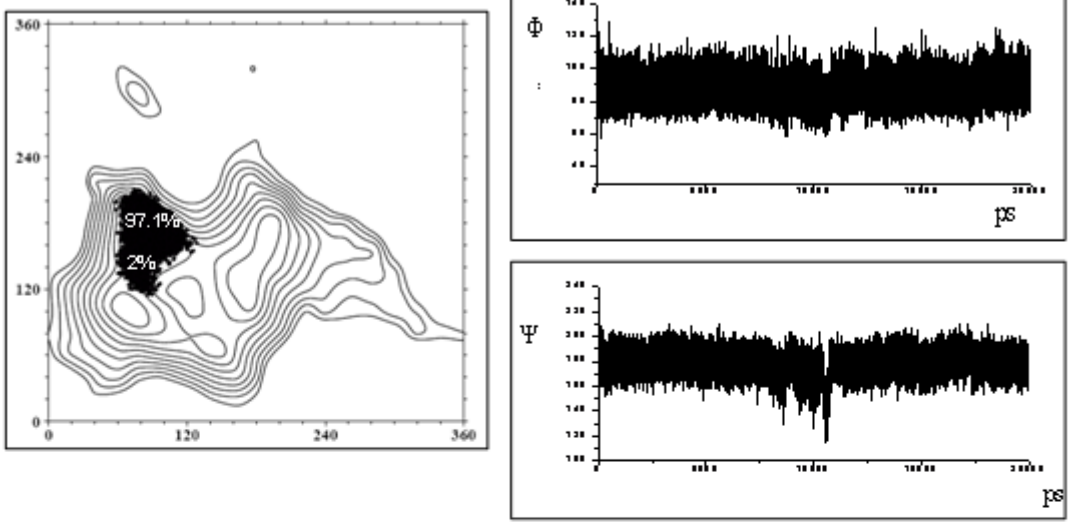

Oligo_gt

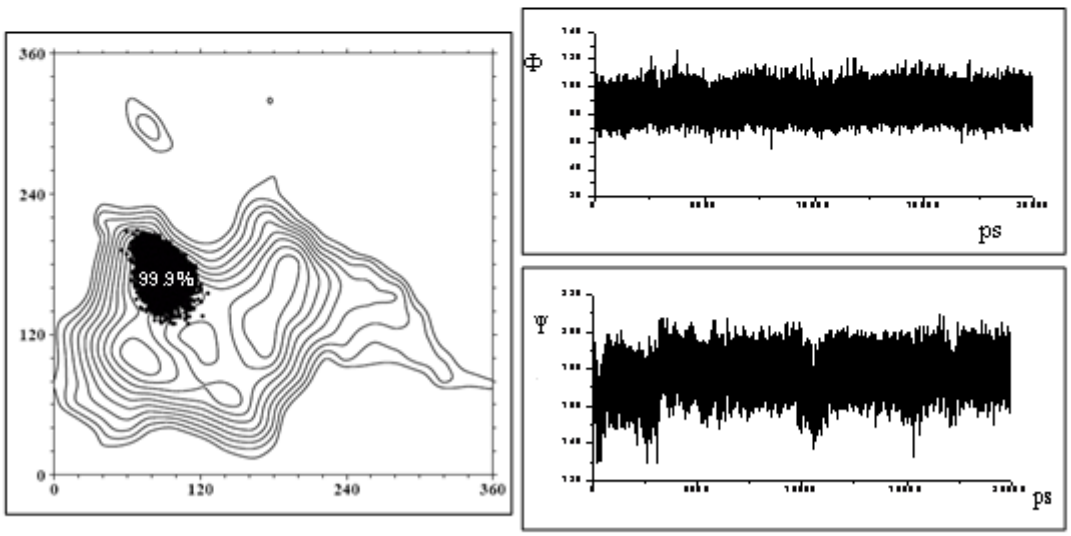

α-D-Ko-4-α-D-Kdo

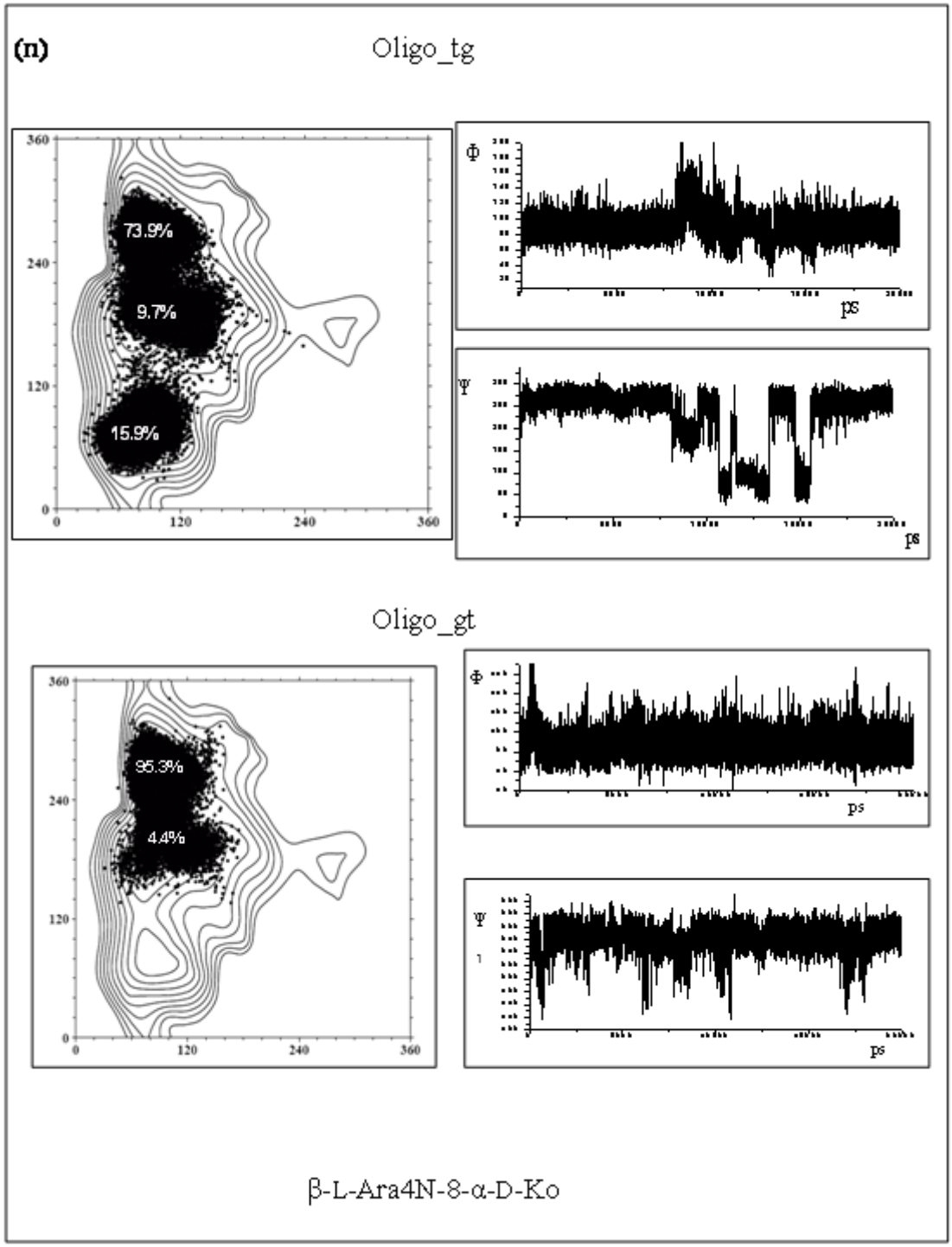

Figure 34 (a-n). Analysis of Φ/Ψ dihedrals for each disaccharidic moiety during 20 ns of MD simulation. In all the figures are reported, on the left, the population of values (in percentage) assumed by Φ and Ψ; on the right, it's showed Φ and Ψ behaviour in the whole simulation.

From a first analysis emerged that, during MD simulation, all the Φ/Ψ torsion angle values coincided with energetic minima predicted by the conformational analysis. As for α-L-Rha-3-β-D-QuiNAc linkage, there were no differences in Φ/Ψ values between the two oligosaccharide considered except for a different population of the conformational families (figure 34a). Glycosidic linkage of β-D-QuiNAc-7-α-L,D-Hep disaccharides was characterized, either in oligo*_gt* or in oligo*_tg*, by a high flexibility of Ψ angle whereas, exclusively in oligo*_tg*, it is noticeable the presence of a slightly populated family of conformers with a net change of Φ values (figure 34b). Low flexibility was found for glycosidic linkages of α-L,D-Hep-2-α-D-Gal and α-D-Gal-3-α-L,D-Hep disaccharides, since the majority of conformers for these segments is described by a couple of Φ and Ψ values centred around a single energetic minimum. Moreover, independently from the starting oligosaccharide, it is noteworthy that a strong rigidity has been found for disaccharidic moieties belonging to the inner core (α-L,D-Hep-3-α-L,D-Hep, β-D-Glc-4-α-L,D-Hep, α-L,D-Hep-5-α-D-Kdo and α-D-Ko-4-α-D-Kdo, figure 34h-m). As for α-D-Glc-6-α-D-Gal (figure 34d), a slight rigidity was found if the analysis started from oligo*_tg* while the same torsion angles were more flexible starting from oligo*_gt*. In the terminal branch, α-L,D-Hep-7-α-L,D-Hep-7α-L,D-Hep (Figure 34f-g), the very last segment, α-L,D-Hep-7-α-L,D-Hep, was characterized by a glycosidic linkage with an high degree of rotational freedom while the central glycosidic linkage, between 7-α-L,D-Hep-7α-L,D-Hep, is slightly rigid since the only variations are generated by two possible preferential conformations assumed by Φ torsion angle. Finally, the last disaccharide, β-L-Ara4N-8-α-D-Ko, was characterized by a slight flexibility for Ψ torsion angle that increases for oligo*_gt*.

Inter-proton distances carried out from the MD simulation were then compared to the experimental results. NMR 2D spectra analysed for structural assignation of native core oligosaccharide from *B. cenocepacia* J2315 strain presented a high heterogeneity due to multiple oligosaccharidic species coexisting in solution. This impaired NOE integration, since the overlapping of species present generates false NOE contact intensities. Thus t-ROESY experiments run on a *B. cenocepacia* K56-2 mutant, named XOA3, were analysed.[7] The core oligosaccharide structure of XOA3 and J2315 strains are identical except for the absence, in the mutant, of α-D-Glc-6-α-D-Gal disaccharide that is replaced by an α-glucose residue linked to the 3,7-Hep. The core oligosaccharide structure of the mutant is reported below, terminal α-L,D-Hep and β-L-Ara4N residues are not labelled by alphabetical letters since, like for J2315,[2] they were present in non-stoichiometric amount, so they are not detectable in NMR investigation:

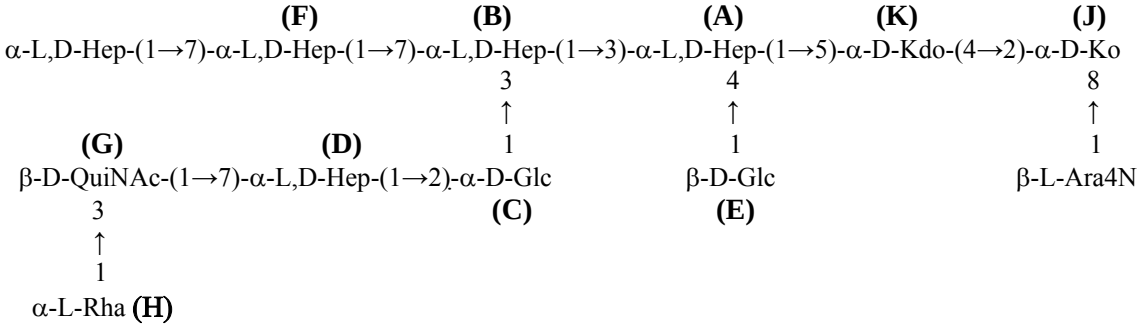

Thus, the structure considered was a good model that can be used in order to compare experimental NOE with the corresponding average distances obtained for the simulation from $<r^{-6}>$ values. Actually, a satisfactory agreement was observed between the calculated and the experimental distances values (table 11).

	Experimental *inter*-proton distances	**Calculated *inter*-proton distances (oligo_tg)**	**Calculated *inter*-proton distances (oligo_tg)**
H1-G3	2,83	2.31	2.28
G1-D7	3.60	2.84/2.61	2.61/2.64
D1-C1	2.49	2.31	2.39
D1-C2	2.77	2.78	2.73
C1-B3	2.35	2.16	2.26
F1-B7	2.34	2.48/2.72	2.61/2.64
B1-A3	2.59	2.30	2.29
E1-A4	2.47	2.31	2.31
A1-K5	2.62	2.89	2.91
K3-J6	2.88	2.96	2.93
K5-A5	2.59	2.75	2.71
B2-C5	2.93	3.28	3.35

Table 11. Experimental (from t-ROESY experiments) and calculated (from MD calculations) *inter*-proton distances for both oligo_gt and oligo_tg molecules.

As for 1→7 linkage involving heptose residues F and D, i.e. F1-B7 and G1-D7 in T-ROESY spectrum only NOE contacts from one of the two methylene protons were present and integrated although both distances were reported from MD analysis. Moreover, as shown in table 11, *inter*-proton distances, F1-B7 and G1-D7, are the mostly divergent from

simulation data. The under-estimation of NOE intensities is due to the proximity of these two anomeric signals (F and G) to the suppressed water signal.

Given the extent of flexibility around the glycosidic linkages, both oligosaccharides adopted a variety of three dimensional shapes in rapid interchange. Snapshots of the most representative conformers are depicted in figure 35.

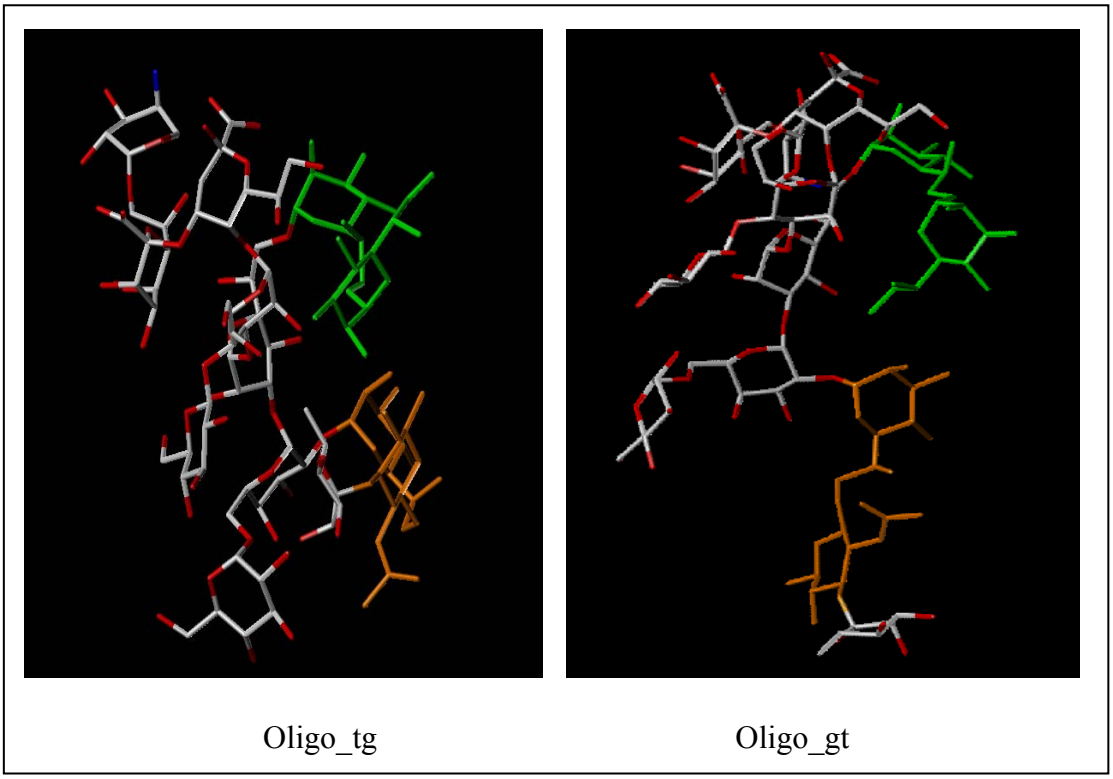

Figure 35. Most representative snapshots from MD simulation. Orange and green representations are respectively for β-D-QuiNac-7-α-L,D-Hep and α-L,D-Hep-7-α-L,D-Hep disaccharides (see discussion).

7.2 Discussion

Herein it has been elucidated a novel approach aimed to the conformational study, in a water explicit model using AMBER package, of a core oligosaccharide moiety isolated from a LPS molecule. The analysis was carried out on the core oligosaccharide of *B. cenocepacia* J2315 considering two different structures arising from the two possible orientations, *gt* or *tg*, of hydroxyl groups of C5-C6 linkage of galactose residue. Slight differences were observed about the two models analyzed, mostly concerning little inversions in relative abundance of conformers population among preferential Φ/Ψ torsion angles values. Thus, there were no simulation data evidencing that one conformer was

preferred to the other. Further, from MD analysis *inter*-proton distances were back-calculated and compared to those experimentally collected from 2D NMR experiments. The NMR derived data were obtained analyzing a *B. cenocepacia* K56-2 mutant, XOA3, since the obtained oligosaccharide was less heterogeneous than wild type ET-12 strain.[2,7] Even though spectra from this mutant core oligosaccharide did not give key NOE contacts evidencing a preferred *gt* or *tg* orientation, a good agreement was found between experimental and calculated *inter*-proton distances. As for core oligosaccharide behavior in three-dimensional space, from MD data were carried out interesting results. A very high flexibility was found for the glycosidic linkage of β-D-QuiNAc-7-α-L,D-Hep disaccharide, depicted in figure 35. In a recent study, it has been showed that this site contains the adaptor sugar to which the reminder of the O-antigen repeating units become attached in *B. cenocepacia*. QuiNAc is found to be the adaptor sugar whereas the terminal Rha residue, that is linked to QuiNAc through a α(1→3) linkage, is the first sugar of the repeating O-chain unit (Rha-GalNAc-GalNAc). Thus, probably, the slight rigidity of this portion is helpful for the recognition by the ligase. In addition, during the whole simulation of both structures considered, it was evident that the terminal branch constituted by the disaccharide α-L,D-Hep-(1→7)-α-L,D-Hep was not folded on the core backbone but it was exposed toward the external space. Perhaps this represent a molecular signal recognized and linked by a putative ligand, as lectins, since it has been found for *B. cenocepacia* that a soluble lectin, BC2A-L, recognizes oligomannose motifs and analogs.[8] Remarkable results were also obtained for the analysis of the inner core region. As evidenced from both the analysis run, there is an high rigidity of the mostly conservative region of the core, Hep-(1→3)-[β-Glc-(1→4)]-α-Hep-(1→5)-[α-Ko-(1→4)]-α-Kdo, if compared to the other portions of the molecule. It is noteworthy that this region is intrinsically rigid since experiments were run on molecule as it is without lipid A portion and without considering the proximity to cellular membrane. Thus, it can be hypothesized that this portion, containing structural motifs essential for bacterial surviving, markedly contributes to the strength stability and rigidity of the cellular membrane.

References

1. De Soyza A, Ellis CD, Khan CMA, Corris PA, Demarco de Hormaeche R. *Burkholderia cenocepacia* lipopolysaccharide, lipid A, and proinflammatory activity. *Am. J. Respir. Crit. Care Med* (2004). 170: 70-77.

2. Silipo A, Molinaro A, Ieranò T, De Soyza A, Sturiale L, Garozzo D, Aldridge C, Corris PA, Khan, CMA, Lanzetta R, Parrilli M. The complete structure and pro-inflammatory activity of the lipooligosaccharide of the highly epidemic and virulent Gram-negative bacterium *Burkholderia cenocepacia* ET-12 (Strain J2315). *Chem. Eur. J.* (2007) 13: 3501– 3511.

3. Brisson JR, Rawford E, Uhrin D, Khieu NH, Perry MB, Severn WB, Richards JC. The core oligosaccaride component from *Mannehimia (Pasteurella) haemolytica* serotype A1 lipopolysaccharide contains L-*glycero*-D-*manno*- and D-*glycero*-D-*manno*-heptoses: analysis of the structure and conformation by high resolution NMR spectroscopy. *Can. J. Chem.* (2002) 80: 949-963

4. Birnbaum GI, René R, Brisson JR, Jennings HJ. Conformation of ammonium 3-deoxy-D-manno-2-octulosonate (Kdo) and methyl alpha- and beta- ketopyranosides of Kdo : X-Ray structure and 1H NMR analysis. *Carbohydr. Chem.* (1987) 6: 17-39

5. Allinger NL, Yuh YH, Lii JH. Molecular mechanics. The MM3 force field for hydrocarbons. *J. Am. Chem soc.* (1989) 111: 8551-8566.

6. Kirschner KN, Yongye AB, Tschampel SM, Gonzalez-Outerino J, Daniels CR, Foley BR, Woods RJ. Glycam06. a generalizable biomolecular force field. Carbohydrates. *J. Comput. Chem.* (2008) 29: 622-655.

7. Ortega X, Silipo A, Saldìas MS, Bates CC, Molinaro A, Valvano MA. Biosynthesis and structure of the *Burkholderia cenocepacia* K56-2 lipopolysaccharide core oligosaccharide. Truncation of the core oligosaccharide leads to increased binding and sensitivity to polymyxin B. *J. Biol. Chem.* (2009) 284: 21738-21751.

8. Lameignere E, Shiao TC, Roy R, Wimmerova M, Dubreuil F, Varrot A, Imberty A. Structural basis of the affinity for oligomannosides and analogs displayed by BC2L-A, a *B. cenocepacia* soluble lectin. Glycobiology (2009) accepted for publication.

Chapter 8

PSEUDOMONAS AERUGINOSA STRATEGY TO LOWER INNATE IMMUNITY DURING CHRONIC LUNG INFECTION IN CYSTIC FIBROSIS DISEASE.

The last part of this work has the purpose of investigating whether and how *Pseudomonas aeruginosa* LPS is involved in bacterial strategy to evade the host immune sensing. *P. aeruginosa* can establish life-long airways chronic infection in CF patients causing persistent respiratory symptoms and decline of the lung functions. It has been noticed that there are pathogenic variants distinguished from initially acquired strain.

With the aim of understanding how this pathogen could establish deleterious but stable relationship with the patients, herein chemical and biological activity of *P. aeruginosa* LPS in clonal strains are investigated.[1] These structures were purified by *P. aeruginosa* strains, mucoid and non-mucoid phenotypes, isolated from acute and chronic infection during a period of up to 7.5 years from a unique CF patient. Chemical structure of lipid A was defined by MS spectrometry. Moreover, significantly higher NF-κB activation, IL-8 expression and production were detected in HEK293hTLR4/MD2-CD14 after stimulation with LPS purified from early *P. aeruginosa* strain as compared to late strains. Similar results were obtained in IB3-1 cells of CF origin and their isogenic corrected cells (C38). This findings provide relevant information with respect to chronic infections in CF since there will be discovered how *P. aeruginosa* has evolved the capacity to evade immune system detection promoting survival and establishing favourable conditions for chronic persistence.

8.1 *P. aeruginosa* lipid A chemical and genetic modifications in clonal strains of early colonization and late chronic infection of CF patient.

The LPS of *P. aeruginosa* clonal strains AA2, AA43 (mucoid) and AA44 (figure 36) was extracted by conventional methods (see section III) and showed the typical ladder like pattern by SDS-PAGE electrophoresis. The O-repeating unit resulted identical in all three strains and the structure was already reported elsewhere.[2]

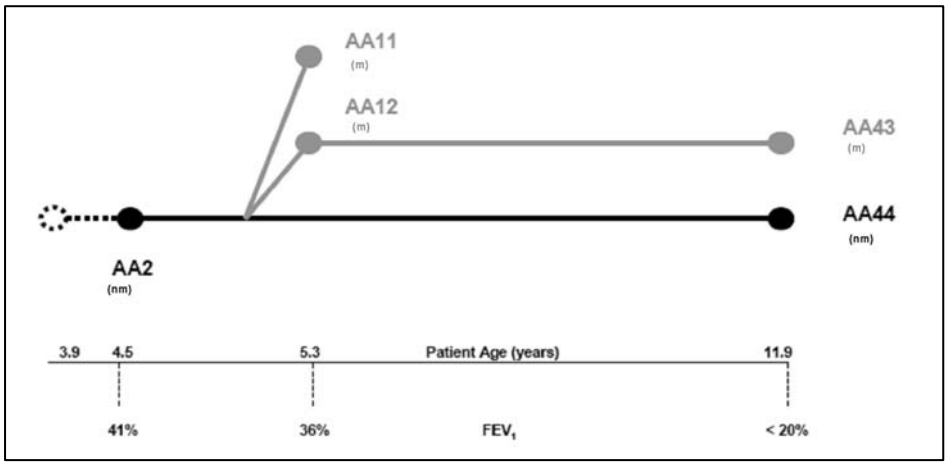

Figure 36. *P. aeruginosa* A2, AA43 and AA44 clones from airways of a CF patient during a period of 7.5 years were selected

The structure of lipid A of the three *P. aeruginosa* strains (figure 37) was determined by chemical analyses and MS spectrometry (see section III). As shown in figure 37, MALDI negative ion spectra revealed that LPS extracted from AA2 and AA43 presented the same lipid A species even though with a different relative abundance. In both cases, MALDI mass spectra showed a main peak that matched with a penta-acylated lipid A constituted by a *bis*-phosphorylated disaccharide backbone carrying a 10:0 (3-OH) in ester linkage on GlcN II and two 12:0 (3-OH) in amide linkage on both GlcN residues. Furthermore, both 12:0 (3-OH) were substituted by a secondary fatty acid, a 12:0 on GlcN II and a 12:0 (2-OH) on the GlcN I. Both lipid A blend also contained a tetra-acylated lipid A deriving from the previous by loss of the only 10:0 (3-OH) in ester linkage on GlcN II. An asymmetric hexa-acylated lipid A bearing the extra 16:0 that esterifies the 10:0 (3-OH) on GlcN II was present almost exclusively in the lipid A blend of strain AA43. Minor species carrying two secondary 12:0 (2-OH) fatty acids and others lacking a phosphate group were also present.

As for AA44, completely different lipid A were found, in which the main difference with those above was the presence of a further 10:0 (3-OH) on GlcN I. The most prevalent one was a symmetric hexa-acylated lipid A constituted by a *bis*-phosphorylated disaccharide backbone carrying two 10:0 (3-OH) in ester linkage and two 12:0 (3-OH) in amide linkage. Further, both amide chains were substituted by a secondary fatty acid, a 12:0 and a 12:0 (2-OH) on the GlcN II and I, respectively. In addition, hepta-acylated lipid A bearing the additional 16:0 on GlcN II species was present.

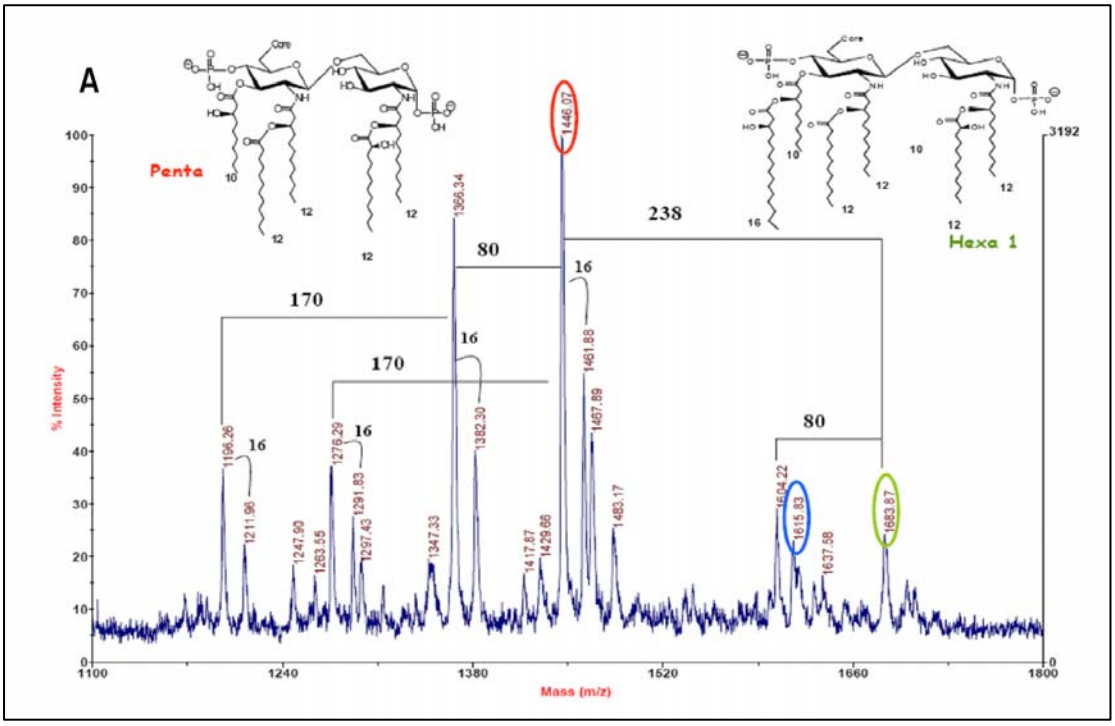
A
Penta
Hexa 1
Core
1446.97
3192
1366.34
238
80
16
170
16
170
16
1461.88
1467.89
80
1276.29
16
1382.30
1291.83
1297.43
1196.26
16
1211.96
1247.90
1263.55
1347.33
1417.67
1429.66
1483.17
1634.22
1615.83
1637.58
1683.87
% Intensity
Mass (m/z)
1100
1240
1380
1520
1660
1800

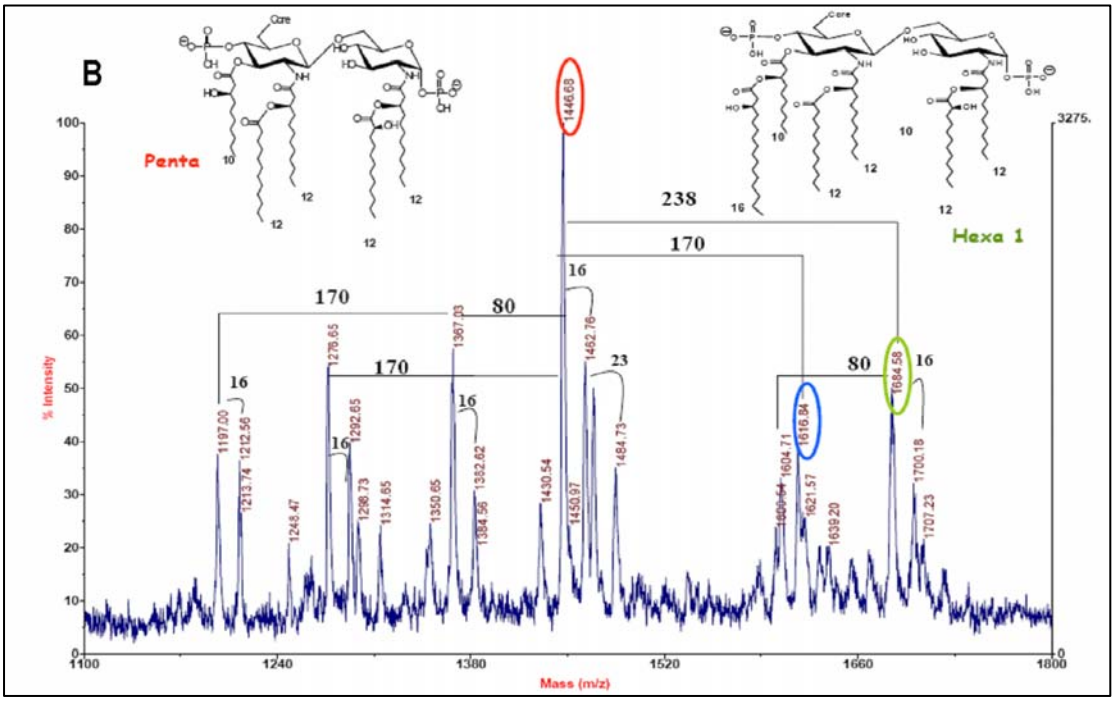
B
Penta
Hexa 1
Core
1446.68
3275.
238
170
16
170
80
16
1452.76
23
170
80
16
1684.58
1278.65
1367.03
16
1292.65
16
1197.00
1212.56
1213.74
1248.47
1298.73
1314.65
1350.65
1382.62
1384.56
1430.54
1450.97
1484.73
1604.71
1616.84
1621.57
1639.20
1700.18
1707.23
% Intensity
Mass (m/z)
1100
1240
1380
1520
1660
1800

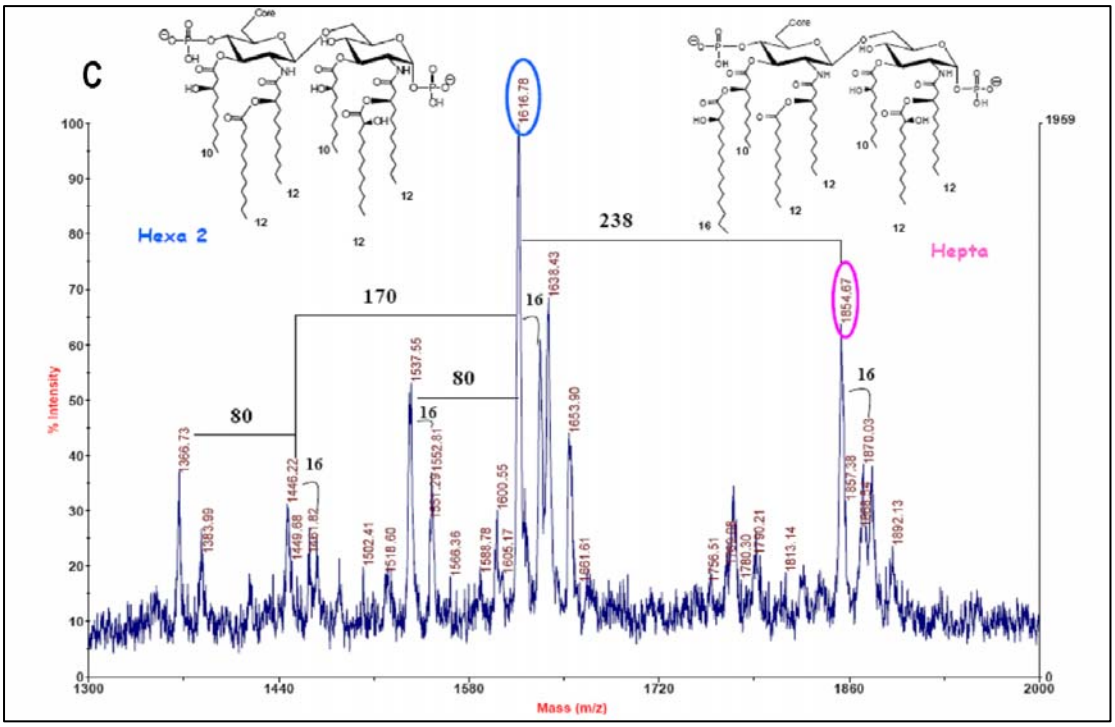

Figure 37. MALDI MS spectra of lipid A blend obtained by acid hydrolysis of LPS from *P. aeruginosa* clinical strains isolated at the onset of chronic colonization (AA2) (**A**) and after years of chronic infection (AA43 and AA44) from a CF patient (**B** and **C**). A difference of 238 Da corresponds to a 16:0 fatty acid residue whereas 170 corresponds to a 10:0 (3-OH) residue and 80 Da are indicative of a phosphate group. The 16 Da different is relative to the presence of a hydroxyl group at C-2 of the secondary 12:0 fatty acids. The non indicated ion peaks are relative to the species already indicated and bearing sodium or potassium counter-ions.

Lipid A modifications in AA2, AA43 and AA44 were stable, as they were not lost after serial passages *in vitro*, suggesting presence of gene mutation. Sequence analysis and multiple alignment of *pagL*, *phoP*, *phoQ*, *lpxO1* and *lpxO2* genes responsible for modifying lipid A, revealed *pagL* mutation in AA44 but not in AA2 and AA43 strains.[1]

8.2 Biological activity of LPS from *P. aeruginosa* clinical isolates tested on human cells (HEK 293-hTLR4/MD2-CD14 and C38) including those of CF origin (IB3-1).

HEK 293-hTLR4/MD2-CD14 were exposed to different LPS concentration (10, 50 and 100 ng/mL) of *P. aeruginosa* AA2, AA43, AA44 and PAO1 for 4 h and NF-κB activation was evaluated through the assessment of luciferase activity (figure 38a). LPS of *P. aeruginosa* AA2 induced a significantly higher NF-κB activation with respect to cells exposed to LPS of AA43 and AA44 (AA2 vs AA43 and AA44 LPS $p<0.01$) in a dose

dependent manner. IL-8 expression was measured through real time quantitative (q)-PCR after 4 h stimulation (figure 38b). In accordance with NF-κB activity, the level of IL-8 expression increased higher after stimulation with LPS of AA2 while LPS of AA43 and AA44 induced lower increase when compared to AA2 LPS (AA2 vs AA43 and AA44 LPS $p<0.01$). For ELISA assay, HEK 293-hTLR4/MD2-CD14 were stimulated for 24 h with *P. aeruginosa* LPS (figure 38c). The level of IL-8 release induced by AA2 LPS was significantly higher than that induced by AA43 and AA44 LPS (AA2 vs AA43 and AA44 LPS $p<0.05$). Under all conditions, stimulation with PAO1 LPS was considerably higher than those induced by the clinical isolates (PAO1 vs AA2, AA43 and AA44 LPS $p<0.05$) (figure 38**)**.

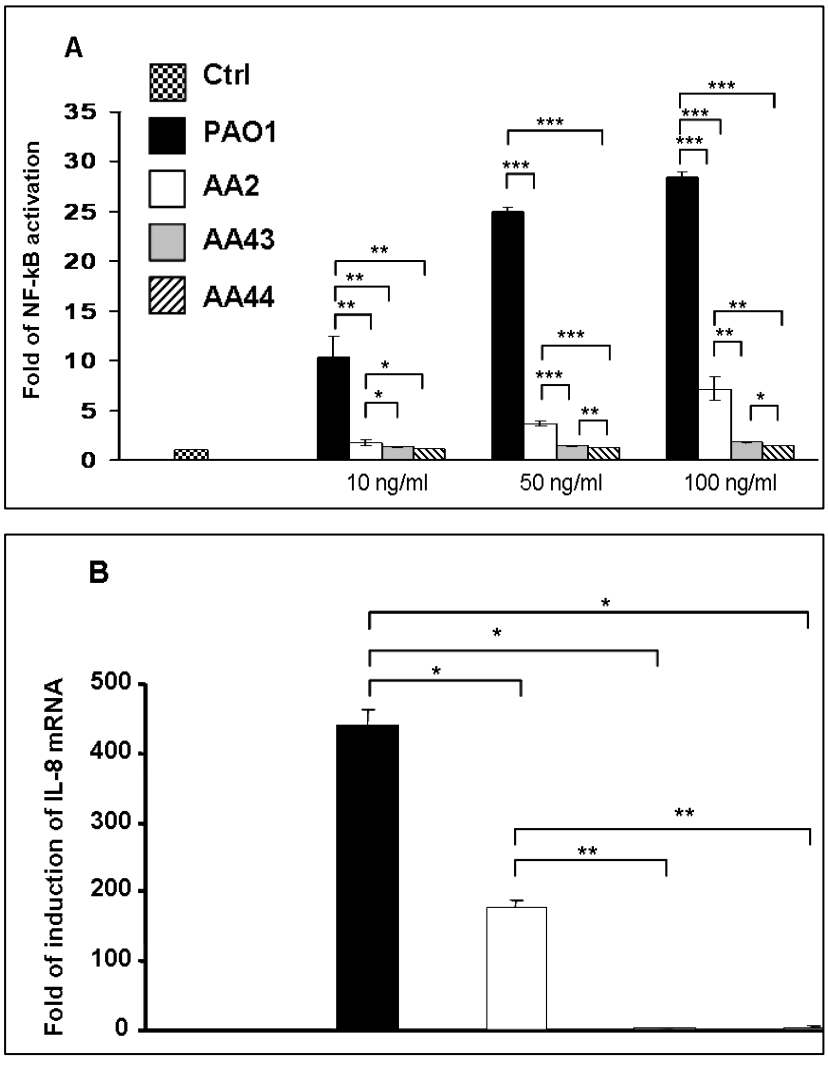

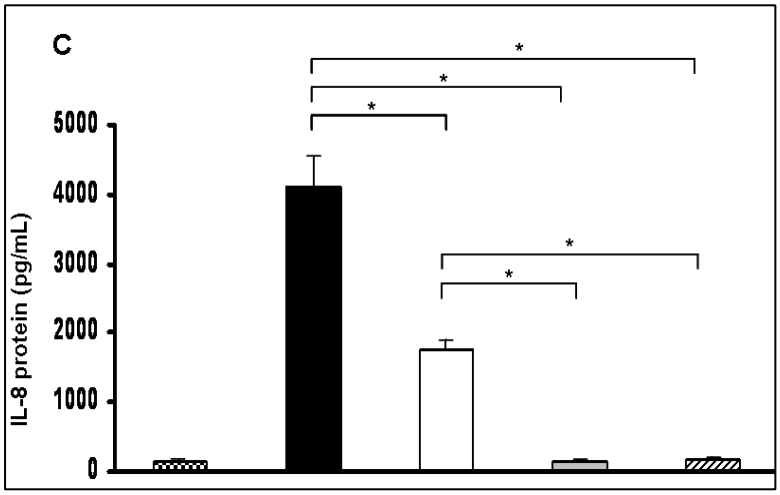

Figure 38. Stimulation of HEK 293-hTLR4/MD2-CD14 with LPS derived from the three clinical isolates of *P. aeruginosa* AA2, AA43 and AA44. a) Fold of activation of NF-kB after 4 h of stimulation with different concentrations of LPS; commercial LPS of *P. aeruginosa* was used as a control. b) IL-8 mRNA induction after stimulation with 100 ng/mL of LPS for 4 h. c) IL-8 secretion after stimulation with 100 ng/mL of LPS for 24 h. Commercial LPS of PAO1 was used as a control. *p<0.05, **p<0.01, ***p<0.001

Next, CF respiratory cells (IB3-1) and the isogenic corrected cells (C38) were tested after LPS stimulation. IB3-1 cells stimulated with AA2 LPS induced significantly more TNF-α and IL-8 expression, assessed by real time q-PCR, when compared with AA44 and AA43 LPS (AA2 vs AA43 and AA44 LPS $p<0.05$) (figure 39a and 39b). IL-8 protein release, measured by ELISA, was consistent with expression (AA2 vs AA43 and AA44 LPS $p<0.05$) (figure 39c). Similar results were obtained in C38 cells, even though these cells were generally less responsive when compared to IB3-1. PAO1 LPS was used as positive control and stimulated both IB3-1 and C38 cells (figure 39).

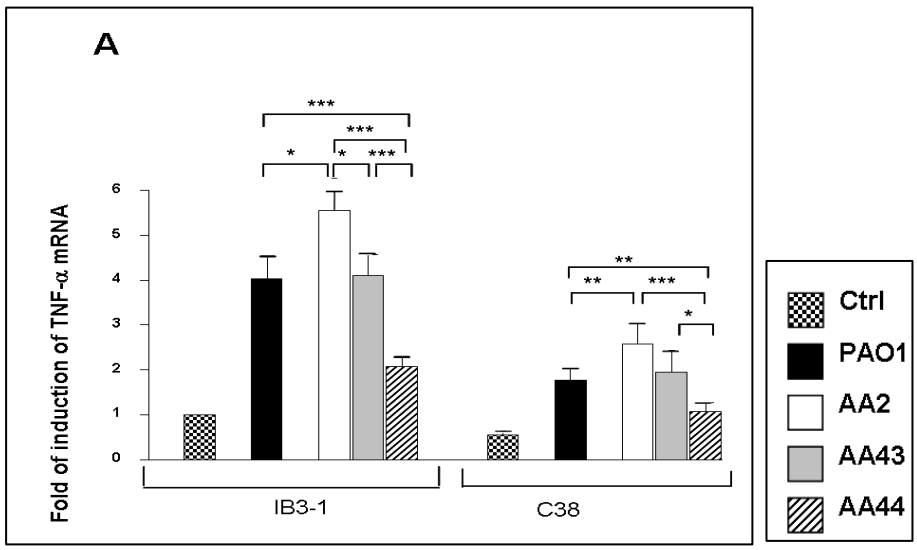

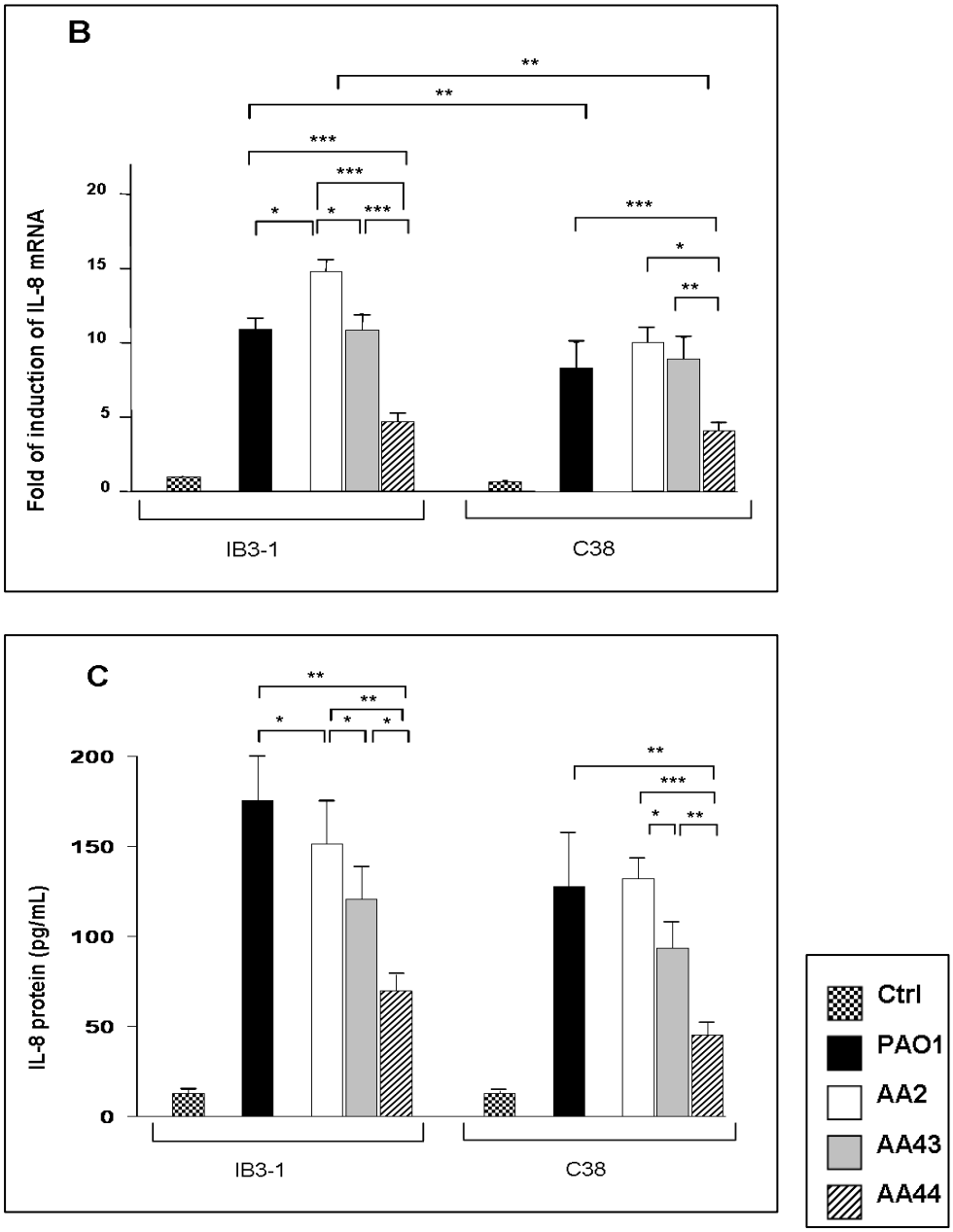

Figure 39. Response of IB3-1 and C38 cells after stimulation with LPS derived from the three clinical isolates of *P. aeruginosa* AA2, AA43 and AA44.a) Fold of induction of TNF-α and (b) IL-8 mRNA after stimulation with 100 ng/mL of LPS for 4 h. Commercial LPS of PAO1 was used as control. The values represent the expression levels relative to untreated IB3-1 (means±SD). c) IL-8 secretion after stimulation with 100 ng/mL of LPS for 24 h. *p<0.05, **p<0.01, ***p<0.001 in the Student's t-test.

8.3 Discussion

Persistence is normally established after an acute period of infection involving activation of both the innate and acquired immune system. Chemical structure of LPS were determined for three *P. aeruginosa* clones isolated from airways of a CF patient during a

period of 7.5 years. Among the three strains lipid A diversity was observed in the number and location of fatty-acid side chains. Early AA2 and AA43 late mucoid *P. aeruginosa* strains synthesized a lipid A blend essentially composed by a tetra-, penta- and hexa-acylated species lacking 10:0 (3-OH) primary fatty acid on GlcNI. In contrast, the late non-mucoid AA44 strain was constituted by homologue lipid A species which further carried a 10:0 (3-OH) residue, i.e., a hexa-acylated and hepta-acylated moieties. These findings are in accordance with previous observations that *P. aeruginosa* synthesizes more highly acylated (hexa- and hepta-acylated) LPS structures during adaptation to the CF airways.[3-5] Furthermore, major structural changes observed exclusively in lipid A extracted from the non mucoid AA44 strain seem to reveal bacterial camouflage of its outward directed molecular PAMP, i.e., endotoxin not protected by capsular polysaccharide. Otherwise, the mucoid AA43 showed minor changes in the lipid A when compared to early strain AA2. As shown recently for *Klebsiella pneumoniae*,[6] presence of capsule in mucoid AA43 could hinder the LPS molecules by acting as bacterial products to elicit the host's immune system.

As previously described, *P. aeruginosa* strains with severe CF lung disease lacked deacylated lipid A structures, suggesting that loss of deacylase enzymatic activity (PagL) can occur during long-term adaptation to the CF airway.[3,7] Here, sequence analysis and alignment of the three clonally related *P. aeruginosa* strains demonstrated for the first time pathoadaptive mutation in *pagL* of late AA44 strain. These results indicate that *P. aeruginosa* modified lipid A by *pagL* inhibition to reduce TLR4-signalling following a mechanism previously demonstrated for *Salmonellae* and *Bordetella pertussis*.[8,9]

In contrast to AA44, the early AA2 and the late AA43 strains were equipped essentially by penta- and hexa-acylated lipid A but differed in their ratio. The lipid A isoforms have profound implications for human disease, owing to altered recognition by the TLR4 complex.[10] In particular, penta-acylated lipid A of *P. aeruginosa* could antagonize TLR-4 dependent responses of the human cells to hexa-acylated lipid A from *E. coli*.[11]

In this study LPS of the late AA43, harbouring a mixture of hexa- and under-acylated lipid A and AA44, presenting hexa-acylated and hepta-acylated lipid A moieties, displayed a reduced immunomodulatory TLR4-mediated activity compared to early AA2. In particular, the LPS of AA43 and AA44 showed weak NF-κB and IL-8 inflammatory response when tested in HEK293 cells expressing TLR-4. Similar results were confirmed in C38 cells, even though these cells were reported as generally less responsive to stimuli when compared to IB3-1.[12] Altogether these results emphasize the reduced immunopotential of

LPS extracted from late colonizer *P. aeruginosa* strains, in line with other reports that demonstrated the lost of large arsenal of virulence factors during chronic infection.[13]

References

1. Cigana C, Curcuru' L, Leone MR, Ieranò T, Lorè NI, Bianconi I, Silipo A, Cozzolino F, Lanzetta R, Molinaro A, Bernardini ML, Bragonzi A. "*Pseudomonas aeruginosa* exploits lipid A and muropeptides modification as a strategy to lower innate immunity during chronic lung infection in cystic fibrosis" *Plos Pathogen* (2009), accepted for publication.
2. Knirel YA, Kocharova NA, Zähringer U, Pier GB Conserved and variable structural features in the lipopolysaccharide of Pseudomonas aeruginosa. *J Endotox Res* (2006)12: 324-336.
3. Ernst RK, Emerson JC, Kraig GM, Adams KN, Harvey MD, Ramsey B, Speert DP, Burns JL, Miller SI. Unique lipid a modifications in *Pseudomonas aeruginosa* isolated from the airways of patients with cystic fibrosis. J Infect Dis (2007)196: 1088-1092.
4. Hajjar AM, Tsai JH, Wilson CB, Miller SI. Human Toll-like receptor 4 recognizes host-specific LPS modifications. Nat Immunol (2002)3: 354-359.
5. Ernst RK, Guo L, Lim KB, Burns JL, Hackett M, Miller SI. Specific Lipopolysaccharide Found in Cystic Fibrosis Airway *Pseudomonas aeruginosa*. Science (1999) 286: 1561-1565.
6. Wu MF, Lin TL, Wang JT, Yang FL, Wu SH, Hu BS, Chou TY, Tsai MD, Lin CH, Hsieh SL. Humoral immunity against capsule polysaccharide protects the host from magA+ *Klebsiella pneumoniae*-induced lethal disease by evading Toll-like receptor 4 signaling. *Infect Immun* (2009) 77: 615-621.
7. Ernst RK, Moskowitz SM, Kraig GM, Kawasaki K, Stead CM, Trent MS, Miller SI. The *Pseudomonas aeruginosa* lipid A deacylase: selection for expression and loss within the cystic fibrosis airway. *J Bacteriol* (2006)188: 191-201.
8. Kawasaki K, Miller SI. 3-O-deacylation of lipid A by PagL, a PhoP/PhoQ-regulated deacylase of *Salmonella typhimurium*, modulates signalling through Toll-like receptor 4. *J Biol Chem* (2004) 279: 20044-20048.
9. Geurtsen J, Hamstra HJ, Ten Hove J, de Haan A, Kuipers B, Tommassen J, van der Ley P. Expression of the lipopolysaccharide-modifying enzymes PagP and PagL modulates the endotoxic activity of *Bordetella pertussis*. *Infect Immun* (2006) 74: 5574-5585.
10. Miller SI, Bader MW. LPS, TLR4 and infectious disease diversity. *Nat Rev Microbiol* (2005) 3: 36-46.
11. Bäckhed F, Elke K, Schwedab H, Oscarsonc S, Richter-Dahlforsa A. Structural requirements for TLR4-mediated LPS signalling: a biological role for LPS modifications. *Microbes and Infection*. (2003) 5: 1057-1063.

12. Di Mango E, Bryan R, Tabibi S, Prince A. Activation of NF-kappaB by adherent *Pseudomonas aeruginosa* in normal and cystic fibrosis respiratory epithelial cells. *J Clin Invest* (1998)101: 2598-2605.
13. Smith EE, Wu Z, Saenphimmachak C, Hoffman LR, D'Argenio DA, Miller SI, Ramsey BW, Speert DP, Moskowitz SM, Burns JL, Kaul R, Olson MV. Genetic adaptation by *Pseudomonas aeruginosa* to the airways of cystic fibrosis patients. *Proc Natl Acad Sci* U S A (2006) 30: 8487-8492.

SECTION III

EXPERIMENTAL SECTION

Chapter 9

LPS STRUCTURAL ANALYSIS

9.1 Bacterial growth and LPS extraction from *B. multivorans, B. vietnamiensis* and *B. cenocepacia* clonal strains.

Bacterial clonal strains of *B. multivorans* and *B. vietnamiensis* isolated pre and post lung transplantation (chapter 3 and 4), and *B. cenocepacia* ET-12 strain collected post lung transplantation (chapter 5) were stored on microbeads. These were streaked on to LB-agar. Standard hot phenol/water LPS extraction was undertaken.[1] For large volume extraction strains were grown in 5 x one-litre cultures of nutrient broth containing 0.5% yeast extract (DIFCO, Oxford, UK) 37°C to late log phase. This growth was harvested by centrifugation at 1000g and resuspended in minimal volume of distilled water and freeze dried. The pellets were then resuspended in distilled water and sonicated on ice. The resulting sonicated suspension was then subjected to DNAse II digestion (final concentration 200ug/ml) at 37°C for 2 hours. A final digest with proteinase K, final concentration 2mg/ml, was undertaken at 60°C for 2 hours prior to boiling. This was then mixed with hot phenol for 20 minutes at 70°C, cooled on ice then centrifuged at 800g. The water soluble phase was then removed and dialysed against repeated changes of fresh distilled water for 72 hours. Ultracentrifugation at 39,500g for 16 hours at 13°C was then undertaken and the supernatant was subsequently removed. The remaining pellet was dissolved in a minimal volume of distilled water and then freeze dried. Extracted LPS was reconstituted and protein contamination assessed using a BCA protein kit (Perbio Science, UK). The level of DNA contamination was assessed using the method of Warburg and Christian using absorption ratios at E280/260. Repeat DNAse and proteinase K digestion followed by ultracentrifugation were conducted until satisfactory LPS purity levels of less than 5% contamination were obtained. LPS fractions were analyzed by SDS-polyacrylamide gel electrophoresis on 16% gels, which were stained with silver nitrate.

9.2 Bacterial growth and LPS extraction from *B. multivorans* C1576 and from *P. aeruginosa* AA2, AA43 and AA44 clonal strains.

Burkholderia multivorans strain C1576 (chapter 6) was cultivated in liquid Luria Bertani medium enriched with 0.2% glucose for three days at 30°C with shaking. The broth culture was centrifuged, the cells were washed with 0.5% NaCl and freeze-dried.

P. aeruginosa clones from airways of a CF patient during a period of 7.5 years were selected (chapter 8). This patient was homozygous for the most common CF-causing *CFTR* mutation, ΔF508. Clinical data indicated that he belonged to the subgroup with a severe course of the *P. aeruginosa* airways infection with chronic leukocytosis, elevated serum immunoglobulins and high titers of antipseudomonal IgG in peripheral blood and experienced the most rapid decline of lung function amongst all the more than 600 individuals with CF who had been regularly seen at the CF clinic Hannover since 1980.[2]

LPS was extracted according to hot phenol-water procedure at 68°C as described.[1] Briefly, dried cells were suspended in hot distilled water and hot phenol 90% (1:1, by vol.) and stirred at 68°C for 1h. The mixture is then centrifuged at 4°C at 8500g for 45', water phase is recovered and phenol phase is again extracted with hot water (three total extractions). The two phases recovered were then extensively dialysed. LPS was revealed by sodium dodecyl sulfate polyacrylamide gel electrophoresis (SDS-PAGE 12%). The gel was stained with silver nitrate for detection of LPSs. In order to get rid of all the cell contaminants, the LPS fraction was further subjected to enzymatic hydrolysis with RNAse, DNAse and proteinase K followed by a size-exclusion chromatography on Sephacryl S-300 in 50 mM NH_4CO_3.

9.3 Chemical analysis

Determination of sugars residues and of their absolute configuration through GC-MS analysis, were all carried out as described.[3,4] Monosaccharides were identified as acetylated *O*-methyl glycosides derivatives. After methanolysis (2M HCl/MeOH, 85°, 24 h) and acetylation with acetic anhydride in pyridine (85°, 30 min) the sample was analyzed by GC-MS. The absolute configuration of sugar residues has been determined by GC-MS analysis of the acetylated *O*-(+)-Oct-2yl glycosides derivatives and comparison with authentic standards. Linkage analysis was carried out by methylation of the complete core region and of the complete O-chain region for *B. multivorans* C1576 as described:[5] the sample was methylated with iodomethane, hydrolyzed with 2 M trifluoroacetic acid (100°C, 2 h), carbonyl-reduced with $NaBD_4$, acetylated with acetic anhydride and pyridine, and analyzed by GC-MS.

Total fatty acid content was obtained by acid hydrolysis. LOS was first treated with HCl 4M (4h, 100°C) and then neutralized with NaOH 5M (30 min, 100°C). Fatty acids were then extracted in $CHCl_3$, methylated with diazomethane and analyzed by GLC-MS. The ester bound fatty acids were selectively released by base-catalyzed hydrolysis with NaOH 0.5M/MeOH (1:1 v/v, 85°, 2h), then the product was acidified, extracted in $CHCl_3$, methylated with diazomethane and analyzed by GLC-MS. The absolute configuration of fatty acids was determined as described.[6]

9.4 Isolation of oligosaccharides and lipid A from *B. multivorans, B. vietnamiensis* LOSs pre- and post-transplantation and from *B. cenocepacia* LOS isolated post lung transplantation.

Lipid A and core oligosaccharides fractions were obtained by SDS promoted acetate buffer hydrolysis (100 mM AcONa, pH 4.5, 0.1% SDS) adding 1mL to 10 mg of purified LOS (100°C, 4 h). Lyophilized samples were then treated with EtOH/HCl 2M in order to remove SDS. Lipid A fractions were precipitated by adding water to dried samples and centrifuging at 4°C at 8500g for 1h. Recovered supernatants containing oligosaccharide fractions, were purified by gel-permeation chromatography using a column (1.5 x 94 cm, total volume 166 ml) of Biogel P-6 in H_2O (flow: 13 ml/h).

9.5 Isolation lipid A and O-chain moieties from *B. multivorans* C1576

The O-chain moiety was isolated performing a mild acid hydrolysis. About 15 mg of purified LPS were dissolved in 1 mL of acetate buffer (pH=4.4) adding SDS (1mg/mL) and the hydrolysis was run for 3 hours at 100°C. After Lipid A removal by centrifugation, the water-soluble product was then purified on gel filtration chromatography on a Sephacryl S-100 column. The obtained precipitate (free lipid A) was washed with water. Lipid A was partially *O*-deacylated by treatment with 12% NH_4OH at 25 °C for 18 h[7] whereas it was completely *O*-deacylated by anhydrous hydrazine.

9.6 Isolation of lipid A samples from *P. aeruginosa* AA2, AA43 and AA44 clonal strains .

Free lipid A was obtained by treatment of LPS (10 mg) with 0.1 M sodium acetate buffer (pH 4.4) containing 1% SDS (100°C, 3 h). The solution was then lyophilized, treated with 2 M HCl : EtOH (1:100, v:v) to remove the SDS, evaporated, dissolved in water and ultracentrifuged (100.000 × *g*, 4°C, 90 min). The obtained precipitate (free lipid A) was washed with water.

9.7 NMR analysis

All the structural assignments of core oligosaccharides moieties characterized (chapters 3-5) and of O-chain portion isolated from *B. multivorans* C1576 (chapter 6) were carried as follows. 1D and 2D ^{1}H-NMR spectra were recorded in D_2O, at 300 K, at pD 7; on Bruker 600 DRX equipped with a cryo probe. Spectra were calibrated with internal acetone [δ_H 2.225, δ_C 31.45]. ROESY and NOESY experiments were recorded using data sets ($t_1 \times t_2$) of 4096 × 256 points with mixing times between 100 ms and 400 ms. Double quantum-filtered phase-sensitive COSY experiments were performed using data sets of 4096 × 256 points. TOCSY experiments were performed with spinlock times of 100 ms, using data sets ($t_1 \times t_2$) of 4096 × 256 points. In all homonuclear experiments the data matrix was zero-filled in both dimensions to give a matrix of 4K × 2K points and was resolution enhanced in both dimensions by a cosine-bell function before Fourier transformation. Coupling constants were determined by 2D phase sensitive DQF-COSY.[8,9] HSQC and HMBC experiments were measured in the ^{1}H-detected mode via single quantum coherence with proton decoupling in the ^{13}C domain, using data sets of 2048 × 256 points. Experiments were carried out in the phase-sensitive mode.[10] A 60 ms delay was used for the evolution of long-range connectivities in the HMBC experiment. In all heteronuclear experiments the data matrix was extended to 2048× 1024 points using forward linear prediction extrapolation.

9.8 MALDI TOF mass spectrometry.

MALDI-TOF mass spectra were recorded in negative or in positive polarity on a Perseptive (Framingham, MA, USA) Voyager STR instrument equipped with delayed extraction technology. High resolution mass spectra were acquired in reflector mode on a 4800 Proteomics analyzer MALDI TOF/TOF mass spectrometer (Applied Biosystems,

Framingham, MA, USA). In this case mass spectra, resulting from the sum of 1250 laser shots, were obtained with a resolution higher than 10000 (as the ratio between the mass of the peak and its full width at half maximum intensity) and with mass accuracy below 100 ppm. Lipid A samples were dissolved in $CHCl_3/CH_3OH$ (50:50, v/v) at a concentration of about 25 $pmol\mu L^{-1}$. Matrix solution was prepared by dissolving 2,4,6-trihydroxyacetophenone (THAP) in CH_3OH/0.1% trifluoroacetic acid/CH_3CN (7:2:1, v/v) at a concentration of 75 $mgmL^{-1}$. A 1:1, v/v sample/matrix solution mixture (< 1 μl) was deposited onto a stainless-steel MALDI sample plate , and left to dry at room temperature.

The R-type LPS sample required a more laborious preparation as recently reported.[11] Briefly, a small amount of the intact R-type LPS was first suspended in a mixture of methanol/water (1:1) containing 5mM ethylenediaminetetraacetic acid (EDTA) and allowed to dissolve by a brief ultrasonication. A few microliters of the obtained mixture were then desalted on a small piece of Parafilm™ with some grains of cation-exchange beads (Dowex 50WX8-200, Sigma–Aldrich), previously converted into the ammonium form; 0.3 μL of this sample solution was finally deposited, together with the same volume of 20mM dibasic ammonium citrate, in a thin layer of homogeneous matrix film obtained from a solution whose components were 2,4,6- trihydroxyacetophenone (THAP), 200mg/mL in methanol, and nitrocellulose (Trans-blot membrane, BioRad), 15mg/mL in acetone/propan-2-ol (1:1 v/v), mixed in a 4:1 v/v ratio.

MS analysis of the oligosaccharide sample was performed utilising a matrix solution of dihydroxybenzoic acid (DHB) 50 mg/ml in TFA 0.1%-ACN 80/20, by the classic dried drop method: 1 μl of a sample/matrix solution mixture (1:1, v/v) was deposited onto the MALDI sample plate and left to dry at room temperature.

As for ***B. multivorans*** C1576 lipid A, ESI mass spectra were recorded on a Bruker Esquire 4000 ion trap mass spectrometer connected to a syringe pump for the injection of the samples. The instrument was calibrated using a tune mix given by Bruker. Before MS analysis, a small amount of lipid A was resuspended in 400 μL of water, stirred on a vortex and centrifuged. The pellet was treated again in the same manner, freeze-dried and used for MS analysis. Samples were dissolved in a chloroform : methanol = 2 : 1 mixture in a suitable concentration, injected at 180 μL/hr, and detected in the negative ion mode. When the spectra were recorded in the positive ion mode, 3 μL of a 0.75 M ammonium acetate solution were added to 200 μL of sample dissolved in chloroform : methanol = 2 : 1.

9.9 Conformational analysis and MD simulations on *B. multivorans* C1576 O-chain

Molecular mechanics calculations on B. multivorans O-chain (chapter 6), were performed using the MM3* force field as included in MacroModel 8.0. A dielectric constant of 80 was used. For each disaccharide structure, both Φ and Ψ were varied incrementally using a grid step of 18°, each (Φ, Ψ) point of the map was optimized using 2000 P.R. conjugate gradients. The molecular dynamic simulations were run by using the MM3* force field; bulk water solvation was simulated by using MacroModel generalized Born GB/SA continuum solvent model. All simulations were performed at 300 K, structures were initially subjected to an equilibration time of 300 ps, then a 10000 ps molecular dynamic simulation was performed with a dynamic time-step of 1.5 fs, a bath constant t of 0.2 ps and the SHAKE protocol to the hydrogen bonds. Trajectory coordinates were sampled every 2 ps, and a total of 5000 structures were collected for every simulation.[12-14] Ensemble average-interproton distances were calculated using the NOEPROM program[15] by applying the isolated spin pair approximation as described.[16] Coordinate extractions were performed with the program SuperMap, supplied with the NOEPROM package, and data visualized with ORIGIN software. Solvent-accessible surfaces were calculated with the Surface utility of Macromodel and with Molecular Surface displays of Chem3D package.

9.10 Conformational analysis and MD simulations on *B. cenocepacia* J2315 core oligosaccharide

This study was started by performing a conformational search on all the disaccharidic moieties constituting the examined oligosaccharide. *SYBYL* program was used to build all monosaccharides. The partial charge on their atoms was also calculated (using MOPAC force field and MNDO method) considering that all residues are neutral except Kdo, Ko and Ara4N that are charged in physiological conditions. Then each residue was minimized considering the current local charges.

Disaccharides were build exploring all the possible conformers for each monomer unit, that is to say that were considered all the possible orientations of the hydroxymethyl group around the C5-C6 bond (***g****auche*-***g****auche* and ***g****auche*-***t****rans* for *gluco* and *manno* conformers; ***t****rans*-***g****auche* and ***g****auche*-***t****rans* for *galacto* conformers, and all the orientation of hydroxyl ring groups (clock, **c**, and counter clock, **r**). The only exceptions were for C5-C6 bond of L-*glycero*-D-*manno* heptose (L,D-Hep) residue, that was always considered in a

gg conformation, and for C6-C7 bond of 3-deoxy-D-*manno*-oct-2-ulopyranosonic acid (D-Kdo), and D-*glycero*-D-*talo*-oct-2-ulopyranosonic acid (D-Ko) that were instead considered in *tg* conformation as reported.[17,18] Then each disaccharide was minimized using a dielectric constant of 78.5 in order to reproduce an aqueous environment.

Structures obtained by *SYBYL* were converted into *mm3* files trough *mol2-mm3* and with *CRYSTAL* programs. After that a conformational search was performed through the *mm3-scan* program with a scan step of 20°. At each step of the conformational search, geometry optimization of disaccharides was performed applying the MM3 force field,[19] typically used for carbohydrates.[20] Finally, for each disaccharide, all the simple energy maps obtained were superposed in order to get an adiabatic map that was visualized with Xfarbe program.[21]

Twenty-nanosecond MD simulations of oligo_gt and oligo_tg (chapter 7) were performed using AMBER 8 package (University of California). Oligosaccharide sequences were build using *SYBYL* considering the lowest energy conformations either for oligo_gt or for oligo_tg starting structures. The Xleap module of AMBER was run in order to obtain *prmtop* (topology) and *incprd* (coordinates) input files. Glycam database[22] was used in order to get the pdb file of each monosaccharide. Since not all monomers present in the oligosaccharidic sequence analyzed were included in Glycam database, *antechamber* program was used for 2-acetamido-2,6-dideoxy-D-glucose (D-QuiNAc), 4-amino-4-deoxy-L-arabinose (L-Ara4N), L-*glycero*-D-*manno*-heptose (L,D-Hep), 3-deoxy-D-*manno*-oct-2-ulopyranosonic acid (D-Kdo), D-*glycero*-D-*talo*-oct-2-ulopyranosonic acid (D-Ko). The partial charges of this five residues were calculated with Gaussian and then processed through *antechamber* with RESP fitting. Real oligosaccharide coordinates were then insert in each pdb file and loaded on Xleap re-calling Glycam_06 force field.[23] In both oligo_gt and oligo_tg, a Na^+ ion was added in order to neutralize the molecule. The whole system was immersed in an octahedral box of water TIP3PBOX using a cut-off of 12 angstroms. *Xleap* added 3699 and 3822 water molecules respectively to *tg*- and *gt*- oligosaccharides.

Both systems considered were minimized (500 steps of deepest descendent and 500 steps of conjugate gradient algorithms) holding the solute fixed. Then both systems were entirely minimized using more minimization steps for oligo_gt. Systems were then warmed from 0K up to 300K with a 100ps MD simulations with a weak restrain on the solute. The following 100ps of equilibration phase were characterized by an energy minimization of the entire systems without restrains, fixing the temperature (300K) and the pressure (1 atm). The MD production phase was run for 20ns for both the oligosaccharides considered, using

a time step of 2 fs, under constant pressure (1 atm) and temperature (300K) controlled by Langevin dynamics with a collision frequency of 1.0 ps $^{-1}$. SHAKE algorithm[24] was turned on in order to constrain bonds involving hydrogen, constant volume periodic boundaries were employed. SANDER module was used for minimization, equilibration and production phases while Ptraj program was employed for simulations analysis. Trajectories were visualized through VMD software[25] and data were processed using Scilab and Xmrg programs.

References

1. Westphal O, Jann K. Bacterial lipopolysaccharides: extraction with phenol-water and further applications of the procedure. *Methods Carbohydr. Chem.* (1965) 5**:** 83–91.
2. Bragonzi A, Nonis A, Cramer N, Montanari S, Rejman J, Di Serio C, Döring G and Tümmler B Pseudomonas aeruginosa microevolution during cystic fibrosis lung infection establishes clones with adapted virulence AJRCCM (2009)180:138-45.
3. Leontein K, Lönngren J. Determination of the absolute configuration of sugars by Gas-Liquid Chromatography of their acetylated 2-octyl glycosides. *Methods Carbohydr. Chem.* (1978) 62: 359-362.
4. Molinaro A, De Castro C, Lanzetta R, Evidente A, Parrilli M, Holst O. Lipopolysaccharides possessing two L-glycero-D-manno-heptopyranosyl-alpha -(1-->5)-3-deoxy-D-manno-oct-2-ulopyranosonic acid moieties in the core region. The structure of the core region of the lipopolysaccharides from *Burkholderia caryophylli*. *J. Biol. Chem.* (2002) 277: 10058-10063.
5. Hakomori S. A rapid permethylation of glycolipid, and polysaccharide catalyzed by methylsulfinyl carbanion in dimethyl sulfoxide. *J. Biochem.* (1964) 55: 205-208.
6. Rietschel ET. Absolute configuration of 3-hydroxy fatty acids present in lipopolysaccharides from various bacterial groups. *Eur. J. Biochem.* (1976) 64: 423-428.
7. Silipo A, Lanzetta R, Amoresano A, Parrilli M, Molinaro A.. Ammonium hydroxide hydrolysis: a valuable support in the MALDI-TOF mass spectrometry analysis of lipid A fatty acid distribution. *J. Lipid Res.* (2002) 43: 2188-2195.
8. Piantini U, Sørensen OW, Ernst RR.. Multiple quantum filters for elucidating NMR coupling networks. *J. Am. Chem. Soc.* (1982) 104: 6800-6801.
9. Rance M, Sørensen OW, Bodenhausen G, Wagner G, Ernst RR, Wuthrich K. Improved spectral resolution in COSY ^{1}H NMR spectra of proteins via double quantum filtering. *Biochem. Biophys. Res. Commun.* (1983). 117: 479-485.
10. States DJ, Haberkorn RA, Ruben DJ. A Two-Dimensional Nuclear Overhauser Experiment with Pure Absorption Phase in Four Quadrants. *J. Magn. Reson.* (1982) 48: 286-292.

11. Sturiale L, Garozzo D, Silipo A, Lanzetta R, Parrilli M, Molinaro A. New conditions for matrix-assisted laser desorption/ionization mass spectrometry of native bacterial R-type lipopolysaccharides. *Rapid. Commun. Mass Spectrom.* (2005) 19: 1829-1834.

12. Mari S, Sánchez-Medina I, Jimenez-Barbero J, Bernardi A. Synthesis and conformational analysis of an alpha-D-mannopyranosyl-(1-->2)-alpha-D-mannopyranosyl-(1-->6)-alpha-D-mannopyranose mimic. *Carbohydr. Res*. (2007) 342: 1859-1868.

13. Asensio JL, Canada FJ, Cheng X, Khan N, Mootoo DR, Jimenez-Barbero J. Conformational differences between O- and C-glycosides: the alpha-O-man-(1-->1)-beta-Gal/alpha-C-Man-(1-->1)-beta-Gal case--a decisive demonstration of the importance of the exo-anomeric effect on the conformation of glycosides. *Chem. Eur. J*. (2000) 6: 1035-1041.

14. Bernardi A, Potenza D, Capelli AM, Garcia-Herrero A, Canada FJ, Jimenez-Barbero J. Second-generation mimics of ganglioside GM1 oligosaccharide: a three-dimensional view of their interactions with bacterial enterotoxins by NMR and computational methods. *Chem. Eur. J*. (2002) 8: 4598-4612.

15. Asensio JL, Jiménez-Barbero J. The use of the AMBER force field in conformational analysis of carbohydrate molecules: determination of the solution conformation of methyl alpha-lactoside by NMR spectroscopy, assisted by molecular mechanics and dynamics calculations. *Biopolymers* (1995) 35: 55-75

16. Corzana F, Cuesta I, Freire F, Revuelta J, Bastida A, Jiménez-Barbero J, Asensio JL. The pattern of distribution of amino groups modulates the structure and dynamics of natural aminoglycosides: implications for RNA recognition. *J. Am. Chem. Soc.* (2007) 129: 2849-2865

17. Brisson JR, Rawford E, Uhrin D, Khieu NH, Perry MB, Severn WB, Richards JC. The core oligosaccaride component from *Mannehimia (Pasteurella) haemolytica* serotype A1 lipopolysaccharide contains L-glycero-D-manno- and D-glycero-D-manno-heptoses: analysis of the structure and conformaion by high resolution NMR spectroscopy. *Can. J. Chem.* (2002) 80: 949-963

18. Birnbaum GI, René R, Brisson JR, Jennings HJ. Conformation of ammonium 3-deoxy-D-manno-2-octulosonate (Kdo) and methyl alpha- and beta- ketopyranosides of Kdo : X-Ray structure and 1H NMR analysis. *Carbohydr. Chem.* (1987) 6: 17-39

19. Allinger NL, Yuh YH, Lii JH. Molecular mechanics. The MM3 force field for hydrocarbons. *J. Am. Chem soc.* (1989) 111: 8551-8566.

20. Pérez S, Imberty A, Engelsen SB, Gruza J, Mazeau K, Jimenez-Barbero J, Poveda A, Espinosa JF, van Eyck BP, Johnson G, French AD, Kouwijzer MLCE, Grootenius PDJ, Bernardi A, Raimondi L, Senderowitz H, Durier V, vergoten G, Rasmussen K. A comparison and chemometric analysis of several molecular mechanics force fields and parameter set applied to carbohydrates. *Carbohydr. Res.* (1998) 314: 141-155.

21. Preusseur A. Algorithm 671: FARB-E-2D: fill area with bicubics on rectangles- a contour plot program. ACM Trans. Math. Software (1989) 15: 79-89

22. Woods RJ, Dwek RA, Edge CJ, Fraser-Reid B. Molecular Mechanical and Molecular Dynamic simulations of Glycoproteins and oligosaccharides. 1. GLYCAM_93 parameters development. *J. Phys. Chem.* (1995) 99: 3832-3836.

23. Kirschner KN, Yongye AB, Tschampel SM, Gonzalez-Outerino J, Daniels CR, Foley BR, Woods RJ. Glycam06. a generalizable biomolecular force field. Carbohydrates. *J. Comput. Chem.* (2008) 29: 622-655.

24. Rickaert JP,Cicotti G, Berendsen HJC. Numerical integration of the Cartesian equations of motion of a system with constraints: molecular dynamic of *n*- alkanes. *J. Comp. Chem.* (1977) 23.

25. Humphrey W, Dalke A, Schulten K. VMD-Visual Molecular Dynamics. *J. Mol. Graphics* (1996) 14: 33-38.

Conclusions

The entire item of this project was focused on the establishment of LPS role in a rapid bacterial adaptation to a new host environment. Clonal strains of *B. multivorans* and *B. vietnamiensis* were recovered pre and post lung transplantation from CF patients and their endotoxin characterized. It has been showed a deep involvement of bacterial LPS in pathogen adaptation to a lung allograft that does not bear CF epithelium. Even though the tendency is not the same for the two species considered, purified endotoxins isolated pre and post lung transplantation showed a different biological activity either for *B. multivorans* or for *B. vietnamiensis* paired clonal strains. This biological differences are caused by a modulation of lipid A primary structure for the strains isolated post lung transplantation. Lipid A contributes to the majority of endotoxic activity of LPS. A group of factors influences the lipid A biological activity including the number and the distribution of acyl chains, the phosphorylation pattern and the presence of charged groups on the polar heads: these changes are recognised at the human TLR-4 receptor. However, even though data reported herein attested which type of structural changes occured in bacterial virulence factors during the adaptation, they did not explain why members of the Bcc exhibit different biological characteristics following transplantation. Results showed that while *B. vietnamiensis* increased acylation (moving towards a pentaacylated LOS and a generally more inflammatory phenotype), *B. multivorans* decreased LOS acylation following transplantation (less inflammatory phenotype). Moreover, as for *B. multivorans* clonal strains analyzed, an additional difference was given by the presence of an Ara4N residue to the outer core Ko residue of post-transplantation LOS, helpful in increasing bacterial resistance to cationic antimicrobial compounds. Understanding if these different behaviours reflect divergent biological responses between bacteria in host environment requires more study.

Interesting insights were also offered from data obtained from the structural analysis of *B. cenocepacia* LOS isolated from a CF recipient after lung transplantation. This study evidenced the significant role assumed by the core oligosaccharide portion in bacterial pathogenesis. A comparison between the virulent LOS isolated from the lethal J2315 strain and the endotoxin herein characterized, both belonging to *B. cenocepacia* ET-12 clonal lineage, showed that structural differences were exclusively limited to core region, in particular to the outer core, e.g. the most exposed part.

The attempt to explain the biological activity of bacterial endotoxin with chemical structures was also the aim of the work dealing with the LPS analysis from *B. multivorans* C1576, the most virulent strain of Bcc genomovar II. Results obtained from this study showed that this pathogenic strain produced a smooth type LPS where the O-chain portion was constituted by two different coexisting polysaccharides. Besides some common peculiar features, as the presence of rhamnose residues that increased the hydrophobic character of the O-antigen moiety, the two polysaccharides presented a different primary structure that originated two different supramolecular arrangements. It is well known that in smooth type LPS the O-chain portion is important for bacterial survival and pathogenesis and that many bacteria can change the structure of their outer membrane, increasing their variability and virulence, depending on the host reaction. It has been proved that bacteria can adopt a strategy during host invasion when they undergo "phase variation" that involves structural modifications in antigenic determinants. Here, it can be speculated that the presence of two different O-polysaccharide chains is the result of a phase variation that the bacterium uses to augment immunological specificity of the antigenic portion of its LPS. As for *B. multivorans* C1576 lipid A, in contrast with lipid A isolated from *B. multivorans* LOS also characterized in the present thesis, this is mostly constituted by a mono-phosphorylated tetra-acylated lipid A species which may bear (or not) a further Ara4N residue. Thus, it can be hypothesized that lipid A dephosphorylation, a post-biosynthetic modification, could be influenced by endotoxin size, i.e. the presence of a LOS or a LPS.

Biological activity of LPS is strictly dependent to the three-dimensional arrangement assumed by these molecules. Thus, it has been performed a conformational study on the most virulent strain (J2315) of *B. cenocepacia* ET-12 clonal lineage. The analysis was conducted on LOS core oligosaccharide exploring all the possible adopted conformations in an aqueous environment, in order to mimic *in vivo* conditions. MD simulations study showed that molecular behavior is dictated by the oligosaccharidic sequence of core portion. It has been found an intrinsic rigidity of the mostly conserved inner core region that exclusively arises from the primary structure of this LOS moiety. The highest flexibility was found in the outer core region which is also the more variable component of the molecule studied. The most flexible points of this section were the outer core disaccharide containing the residue recognized as "primer" by the O-chain ligase, and the terminal heptoses branch, that is not folded on the core oligosaccharide backbone but is constantly exposed toward the external environment, maybe because is a binding site for a

putative ligand.

The last part of this project was centred on LPS involvement in bacterial slow adaptation to host environment during the installation of chronic infection. *P. aeruginosa* could establish life-long chronic infections in CF hosts after an acute period of inflammation involving activation of both the innate and acquired immune system. While the acute infection is usually fully resolved by eliminating the invading bacteria, persistent life-long infection is caused by some bacteria that evade immune surveillance. Herein it has been characterized chemical structure of LPS for three *P. aeruginosa* clones isolated from airways of a CF patient during the acute and the chronic phases of infection for a period of up to 7.5 years. Among the three strains lipid A diversity was observed in the number and location of fatty-acid side chains. More specifically, late strains are characterized by a lost of virulence in bacterial endotoxins induced either by the presence of secreted polysaccharides, that mask bacterial virulence factors, or by an over-acylation of lipid A moiety that generates less inflammatory lipid A phenotypes. The latter was explained by sequence analysis and alignment of the three clonally related *P. aeruginosa* strains that demonstrated, for the first time, pathoadaptive mutation in deacylase coding gene, *pagL*, of late strain. The concept that arises from this study is that bacteria, during chronic infection, has the necessity to evade the immune surveillance through the lost of its arsenal of virulence factors.

Results obtained from the projects constituting this thesis work, attested the importance of LPS in bacterial life and pathogenesis. Moreover, deep structural analyses conducted showed which LPS molecular components are mostly involved in endotoxin biological activity. The knowledge of molecular structures determinant in inflammatory process or the comprehension of mechanisms adopted by bacteria to escape host immune surveillance during its adaptation to host environment, offer novel pharmacological targets for the development of new aimed biomedical therapies.